INFORMATION TO USERS

This manuscript has been reproduced from the microfilm master. UMI films the text directly from the original or copy submitted. Thus, some thesis and dissertation copies are in typewriter face, while others may be from any type of computer printer.

The quality of this reproduction is dependent upon the quality of the copy submitted. Broken or indistinct print, colored or poor quality illustrations and photographs, print bleedthrough, substandard margins, and improper alignment can adversely affect reproduction.

In the unlikely event that the author did not send UMI a complete manuscript and there are missing pages, these will be noted. Also, if unauthorized copyright material had to be removed, a note will indicate the deletion.

Oversize materials (e.g., maps, drawings, charts) are reproduced by sectioning the original, beginning at the upper left-hand corner and continuing from left to right in equal sections with small overlaps. Each original is also photographed in one exposure and is included in reduced form at the back of the book.

Photographs included in the original manuscript have been reproduced xerographically in this copy. Higher quality 6" x 9" black and white photographic prints are available for any photographs or illustrations appearing in this copy for an additional charge. Contact UMI directly to order.

UMI®

Bell & Howell Information and Learning
300 North Zeeb Road, Ann Arbor, MI 48106-1346 USA
800-521-0600

Kinematics of General Planar Stewart-Gough Platforms

Matthew John David Hayes

M.Eng., McGill University, 1996

B.Eng., McGill University, 1995

B.F.A., Concordia University, 1986

Department of Mechanical Engineering and

Centre for Intelligent Machines

McGill University

Montréal, Québec, Canada

September, 1999

A Thesis submitted to the Faculty of Graduate Studies and Research

in partial fulfilment of the requirements for the degree of

Doctor of Philosophy

ABSTRACT

This thesis presents a detailed kinematic analysis of three degree-of-freedom planar parallel manipulator platforms possessing topological symmetry, called general planar Stewart-Gough platforms (PSGP). A specific super-set of topologically asymmetric platforms and one with actuated holonomic higher pairs are included in the analysis.

After PSGP are described and classified, the remainder of the first portion is devoted to the review of the geometric and mathematical tools used in the analysis.

A single univariate polynomial is derived which yields the solutions to the forward kinematics problem of every PSGP platform. Kinematic mapping is used to represent distinct displacements of the platform as discrete points in a three-dimensional projective image space. Separate motions of each leg map to skew one-sheet hyperboloids, or hyperbolic paraboloids, depending on the kinematic architecture of the leg. After two elimination steps the three quadric surfaces are reduced to a sixth order univariate. The roots of this polynomial reveal all solutions to the forward kinematics problem. The procedure leads to a robust algorithm which can be applied to the abovementioned super-set.

The inverse kinematics problem of these platforms is solved, in closed form, using the same kinematic mapping. The procedure can be applied to any three-legged planar platform with lower pairs, regardless of symmetry.

A workspace analysis and simple criteria for the determination of the existence of a dextrous workspace are presented. Finally, a geometric singularity and self-motion detection method, which does not employ Jacobian matrices, is discussed.

RÉSUMÉ

Cette thèse présente une analyse cinématique détaillée des manipulateurs parallèles planaires à trois degrés de liberté et topologiquement symétriques, appelés *plate-formes planaires générales de Stewart-Gough* (PSGP). De plus, un sur-groupe de plate-formes topologiquement asymétriques, et un manipulateur parallèle muni de trois articulations supérieures holonomiques et motorisées, sont inclus dans l'analyse.

Après la description et la classification des PSGP, nous rappelons les outils mathématiques et géométriques nécessaires à l'analyse cinématique.

Les solutions de la cinématique directe de toutes les PSGP sont obtenues grâce à un polynôme de degré six. Ce polynôme est obtenu après deux étapes de calcul en utilisant une transformation cinématique. Les racines de ce polynôme sont les points d'intersection des trois surfaces quadratiques dans l'espace cinématique. Cette procédure conduit à un algorithme robuste qui peut être également utilisé pour le sur-groupe mentioné ci-dessus.

Nous obtenons une solution explicite de la cinématique inverse de ces plate-formes en utilisant la même transformation cinématique. La procédure peut être utilisée pour toute plate-forme planaire à trois segments avec des articulations inférieures, quelle que soit la symétrie.

Nous présentons une analyse de l'espace de travail et un critère simple pour l'existence d'un espace de dextérité. Finalement, en utilisant des considérations géométriques, une méthode de detection des singularités géométriques et de mouvement propre, qui n'utilise pas les matrices jacobiennes, est examinée.

ACKNOWLEDGEMENTS

There are a great many people to thank for their help, support and encouragement during the writing of this thesis. To start, Paul Zsombor-Murray, Manfred Husty and William Moser invested countless hours patiently teaching me the "basics" and held my hand as I stumbled through the "hard" parts. Paul Zsombor-Murray also helped to ensure my electrolyte balance was kept finely tuned. I also want to thank Abdul Ahmed and Stuart Price for the tremendous level of confidence they placed in my abilities. Mojtaba Amhadi helped me prepare for my preliminary oral examination by thinking-up lots of difficult questions. Many thanks to Pierre Montagnier and my dear friends Véronique Barthet and Nathalie Goyette for correcting my French.

I must acknowledge the financial support of Brian Collier, Alan Tenenhouse, Margaret Warner, José Trifaro, and Claudio Cuello and, oh yes, of the Natural Sciences and Engineering Research Council. Anna McNicoll made sure I never missed a paycheque and Shyam Ramchandani made sure I never missed a laugh. Brian and Anna saw me through all four of my degrees!!!!

Then there are those who found the time for lengthy discussions, among other things, at Thomson House "Geometry Seminars" on Thursday afternoons. They include Valentin Guenov, Andrzej Cebula, Vladimir Karakusevic, Pasquale Gervasi, Venkat Krovi, Luca Cortelezzi, again Paul Zsombor-Murray and Manfred Husty, but especially Brenda Barklay! Her legendary draughting skill ensured that anyone who ever attended one of these seminars was well fortified to make insightful commentary and otherwise participate with giddy abandon.

Extra-special thanks are owed to Mike (Mouse) Parker and Jan Binder for their technical assistance with Árpád, patience and good company. Hats off to Mouse for figuring out some of John Conway's rope tricks. Without the help of Kathleen VanderNoot I would never have been able to cope with the photocopy machine. A doff of the cap to Marlene Gray for her insightful help in my dealings with the high

muckey-mucks and for getting my air conditioner fixed ... cooler heads do indeed prevail; to Irène Cartier for keeping me in pens, pencils and coloured chalk, not to mention expense reports and making sure I got paid on-time; to Ornella Cavaliere just for being Ornella. Kathleen, Marlene, Ornella and Irène were also really good sports whenever my young son, William came for a visit.

My friends who put up with my antics during this particular adventure: Véronique Barthet, Kim High, Alain Morin, Nathalie Goyette, Tracy Folster, Terence (Taz) Ozolins, Nabil Elkouh, Sheila Cragg, Simone Sebben, Peter Hedberg, Magda Arciszewski, Geoff McDowell and Robert Burns. I enjoyed the mornings Taz slowed his pace so I could run with him on the mountain. Thanks to Beryl and Clinton MacKay for their unwavering support, cucumbers and "Beryl jam". Richard Kerr taught me that a tune is more lasting than the voice of the birds; a word is more lasting than the riches of the world; a really good road-bicycle can't be beat; and stay away from *Mongolian fire-oil*! Anne, Marc and Andy Comeau always made sure I got my apple pie for Thanksgiving dinner and visits from the Simone fairy on New Year's eve.

Without the pioneering work of Fredrick Banting and Charles Best this thesis would, quite literally, never have been completed. I especially acknowledge the contribution made by their canine subjects. I am also profoundly indebted to Mark Sherman, Francine Emian, Saki Koutelias, Marian Lowry, Eva Prandekas, and the rest of the staff at the Royal Victoria Hospital's Metabolic Day Centre. I have never seen such a remarkable group of dedicated professionals: without-fail, they find ways to put on sincere smiles despite these trying times.

Then there's my mother, Mary Margaret Watson, and step-father, Donald Burns. Their wise council helped to keep me focused and on track. My sister Megan looked after William on Sundays, giving me extra time for my thesis. Thanks, I think.

The greatest thanks of all are for Susan Smith and William Hayes. They helped me to learn that the lake is not encumbered by the swan; nor I by the love in my heart for them.

... Let's go for a skate!

NOMENCLATURE

PSGP	*Planar Stewart-Gough platform.*
DOF	*Degree-of-freedom.*
FK	*Forward kinematics.*
IK	*Inverse kinematics.*
R, P, U, S, G	*Revolute*, *prismatic*, *universal*, *spherical* and *gear* joints (kinematic pairs, Section 2.3).
RRG	Example of a succession of three joints in a simple kinematic chain beginning with the joint connecting the first link to the fixed base.
$R\underline{P}R$	Example of a *characteristic chain* (Section 2.6.1). The underscore indicates the actuated joint. Such chains are used to identify a three-legged platform with topological symmetry among legs.
F_A, F_B, F_C	*Fixed-base* joint point coordinates (Section 2.7).
K_A, K_B, K_C	*Knee-joint* point coordinates (Section 2.7).
M_A, M_B, M_C	*Moving-platform* joint point coordinates (Section 2.7).
x, y, z	Point coordinates in a moving reference frame (Section 2.7).
X, Y, Z	Point coordinates in a non-moving reference frame (Section 2.7).
X_1, X_2, X_3, X_4	Image space point coordinates (Section 3.6.3).
$\mathcal{K}_0$, $\mathcal{K}_1$, $\mathcal{K}_2$, $\mathcal{K}_3$	*Circle* coordinates (Section 4.2).
CKG	*Chebyshev-Grübler-Kutzbach* formula (Section 2.4.1).

TABLE OF CONTENTS

LIST OF FIGURES

LIST OF TABLES

CLAIM OF ORIGINALITY

Certain aspects of planar three-legged fully-parallel platforms and their kinematic analysis are presented herein for the first time. The following contributions are of particular interest:

(1) The 3-legged holonomic higher pair architecture.

(2) The geometric properties of the above-mentioned platform.

(3) The general constraint surface equation.

(4) The observation that there are two distinct types of constraint surface:

  (a) an hyperboloid of one sheet,

  (b) an hyperbolic paraboloid containing a generator on the intersection of hyper-planes $X_3 = X_4 = 0$.

(5) The general univariate polynomial to solve the FK problem of every *general planar Stewart-Gough platform* (PSGP), as herein defined, as well as the FK problem of some topologically asymmetric platforms and PSGP with active holonomic higher pairs.

(6) Closed form solutions for the IK problem of all PSGP, together with the additional architectures mentioned in (5).

(7) Some general observations concerning the workspace of PSGP, together with a novel and simple way to detect certain singularities.

Parts of these results have appeared in six refereed publications: [**63, 64, 66, 67, 69, 70**].

CHAPTER 1

Introduction

This thesis is an investigation of the kinematics of planar three-legged fully-parallel platform manipulators in general, and a topologically[1] symmetric sub-class in particular. Those belonging to this sub-class are called general *planar Stewart-Gough platforms* (PSGP). Moreover, a novel architecture is introduced where the end effector is a circular disk which rolls without slip along the straight lines of the non-grounded links of each of three serial legs. The kinematic analysis presented turns out to be general enough to handle this architecture containing higher-pairs.

1.1. Thesis Subject Development

The steps leading to the procedures developed herein will be summarised below so as to put this research in a *state-of-the-art* perspective. First, a few introductory words on *serial* and *parallel* manipulators are in order.

[1]The term *topology* is used to indicate a specific kinematic architecture, not in the mathematical sense where it would be concerned with those properties of geometric configurations, taken as point sets, which are invariant under elastic deformations that are homeomorphisms [47].

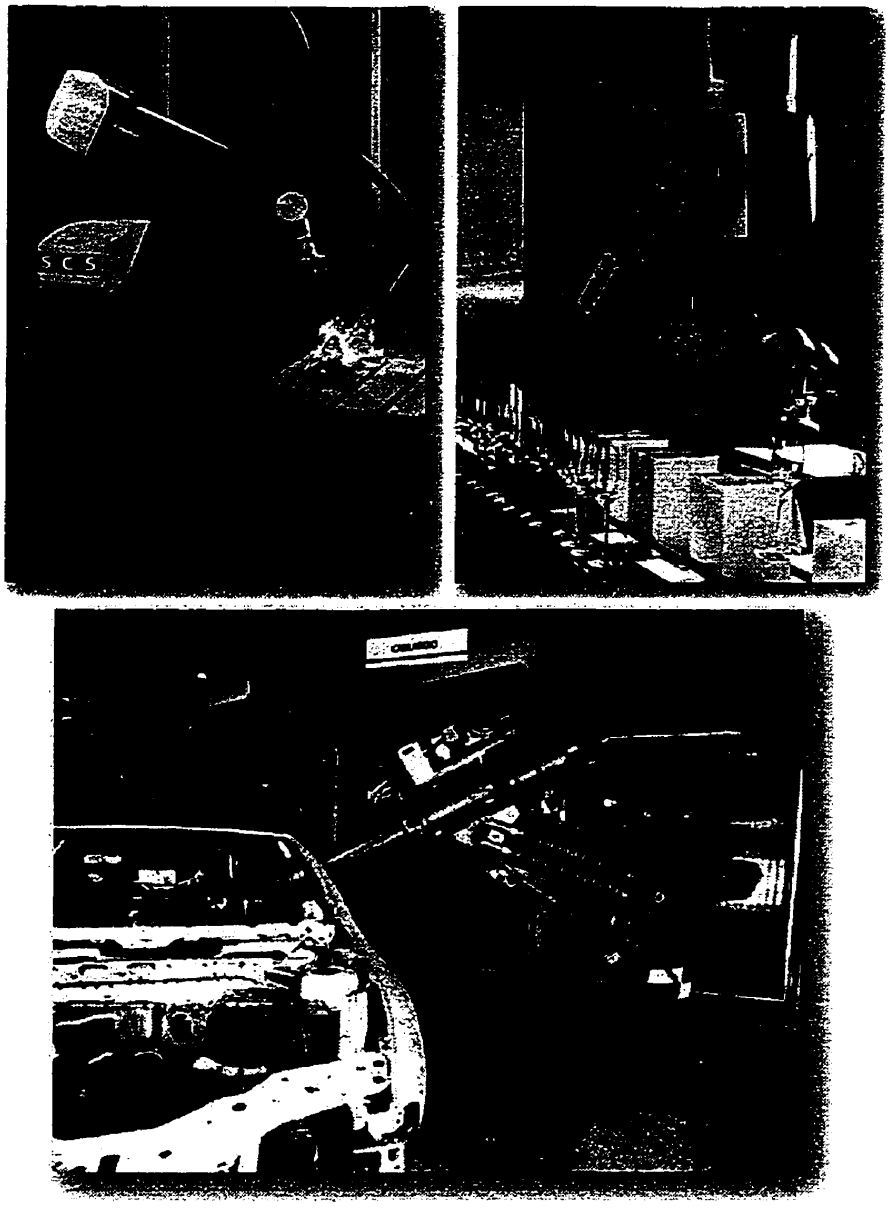

FIGURE 1.1. Typical industrial serial robot applications: welding; packaging; assembly.

1.1.1. Serial and Parallel Manipulators. Research and development of robotic systems in general is motivated by several major factors. Obviously, the subject is rich from a theoretical standpoint because there are many unresolved problems. A more important factor is, perhaps, economic. Production methods must be continuously improved in order to enhance the prosperity of any society, *i.e.*, to

reconcile the apparent contradiction between rising costs and diminishing returns. It is widely believed that processes which make use of robotic manipulators must contribute substantially to these methods aimed at producing an ever-widening variety of goods and services: quantity and quality are ever-increasing, meanwhile incurring ever-decreasing production costs. Clearly, all this must involve continual improvements of the manipulators themselves.

Currently, most industrial robotic manipulators have anthropomorphic architecture [**8, 34, 102**]. These *robot arms* typically consist of an open, or *serial* chain of articulated rigid links connecting the manipulator hand, or end effector to a rigidly fixed base. Figure 1.1 shows industrial serial robots engaged in various activities: welding, packaging and assembly tasks are commonly assigned to robotic manipulators.

In general they are satisfactory to designers and users because they enjoy the following advantages [**8, 34, 49, 60, 97**]:

(1) Their kinematic design is relatively simple.

(2) They generally have large workspaces.

(3) Human operators can readily identify with an open loop kinematic chain which may be compared with the human arm. This is a strong advantage in programming the arm, training operators, *etc.*.

(4) Each joint actuator enjoys complete independence.

(5) The forward and inverse kinematics are well known and the dynamics have been thoroughly analysed for many cases.

However, it is broadly acknowledged that they generally suffer from the following disadvantages [**8, 34, 49, 60, 97**]:

(1) Serial manipulators require an actuator for each joint. If the actuators are located at the intermediate joints, their added mass contributes to the total inertia of the robot, leading to unwelcome dynamic characteristics.

(2) In the case of joint mounted actuators, the design of the links must take into account their cantilever-like structure. Flexibility and balance are also of concern. The links must be 'over-designed' to compensate and the vicious circle of still more massive links continues to grow [**60**].

(3) Because of the cantilever loading of links, serial manipulators have a small pay-load to manipulator weight ratio.

(4) If positional accuracy and precision are required, the velocity of the end-effector is limited by the above considerations as well.

(5) The alternative to joint mounted actuators is to have a set mounted at the base, driving the distal joints through a transmission system. However, the drive-train must be long, and is equally prone to undesired effects of flexibility.

A tray of filled beer glasses can always be carried by a waiter with one hand if the goal is simply to move the tray. However, if the goal is to carry it through a crowded room without spilling any beer then the waiter may consider using two hands. The load is distributed and greater stability is provided. This suggests that the drawbacks associated with serial architecture can be mitigated by providing the end effector with more than one serial connection to the fixed base. This alternative architecture is termed *parallel.*

In parallel manipulators the end-effector is attached to the base, or ground, by more than one kinematic chain; an architecture with closed-loops. Perceived advantages of parallel architectures are cited in [**34, 60, 97**]:

(1) It is not necessary for each joint to be actuated directly by individual motors, hence a smaller contribution to the mass of the links. The links, in turn, can be made lighter.

(2) By allowing at least some motors to be base-fixed, they can be larger and more powerful. Thus, the load-carrying capacity versus the mass of the robot can be increased, along with the speed of operation.

(3) The ensuing reduction in gear drives and transmission systems increases the inherent accuracy of the robot while simultaneously lowering the component cost to make one.

A few of the shortcomings of parallel manipulators are [**97**]:

(1) The workspace is small.

(2) The workspace may be densely packed with a variety of singularities[2].

(3) Simultaneous control is required for some or all of the drive motors.

(4) Long slender legs, particularly for large flight simulators, produce undesirable flexibility and kinematic instabilities [**34**].

For serial manipulators the load-to-weight ratio is typically on the order of 5%, whereas for parallel manipulators it is not unusual to be on the order of 500% [**34, 97**]. Figure 1.2 shows the CAE Electronics *Airbus A310-200* flight simulator used by KLM Airlines for pilot training. It can shake its 10000 kg pay-load at a frequency of 20 Hz with an amplitude of 50 mm [**34**], an unimaginable task for a serial manipulator. Because of the improved dynamic characteristics, parallel platforms can move with greater velocity and acceleration than serial counterparts [**114**].

[2]A singularity is a configuration of relative positions and orientations among the links where the manipulator becomes uncontrollable, or the articular forces (or torques) required to balance an externally applied wrench are infinite. In the vicinity of a singularity the actuators, and the manipulator itself, are vulnerable to damage.

FIGURE 1.2. Airbus A310-200 flight simulator (courtesy of CAE Electronics Ltd.).

A prototype for a parallel manipulator, with an architecture similar to the flight simulator, is shown in Figure 1.3. It was developed in a collaborative effort between the Institut National de Recherche en Informatique et en Automatique (INRIA) in France and the European Synchrotron Radiation Facility (ESRF). The moving platform is used to manipulate a heavy X-ray apparatus with great accuracy. The total weight of the of the manipulator is 35 kg while the experimental apparatus is carries represents a load of 230 kg. This platform manipulator has a load-to-weight ratio of 650%, while its positioning accuracy is better than 0.1μm [**102**]!

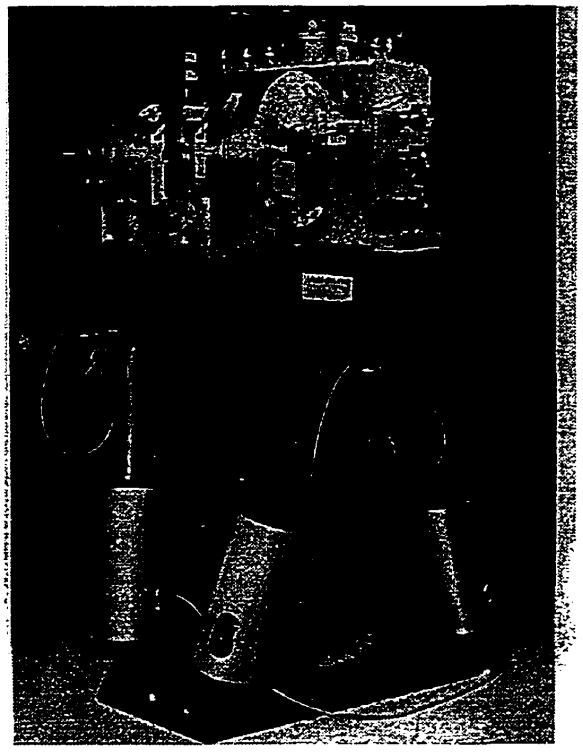

FIGURE 1.3. The ESRF platform (courtesy of INRIA).

However, parallel architecture is not without its drawbacks. Some investigators have tried to develop ideas that address various aspects of these shortcomings. The undesirable flexibility associated with slender legs and small workspace volume is virtually eliminated with designs for planar, spherical and spatial double-triangular manipulators put forward by Daniali [**34**]. This feature is achieved by pairs of planar, spherical and spatial triangles that can move relative to each other, hence the three legs connecting the moving triangle to the relatively fixed triangle have nearly zero-length. Earlier examples of this type of parallel architecture are those of a double-tetrahedral mechanism [**140, 147**]. A working prototype was constructed by Zsombor-Murray and Hyder in 1992 [**147**]. Movable pairs of platonic solid outlines have been investigated as long ago as 1813, when Cauchy investigated an articulated octahedron [**20**].

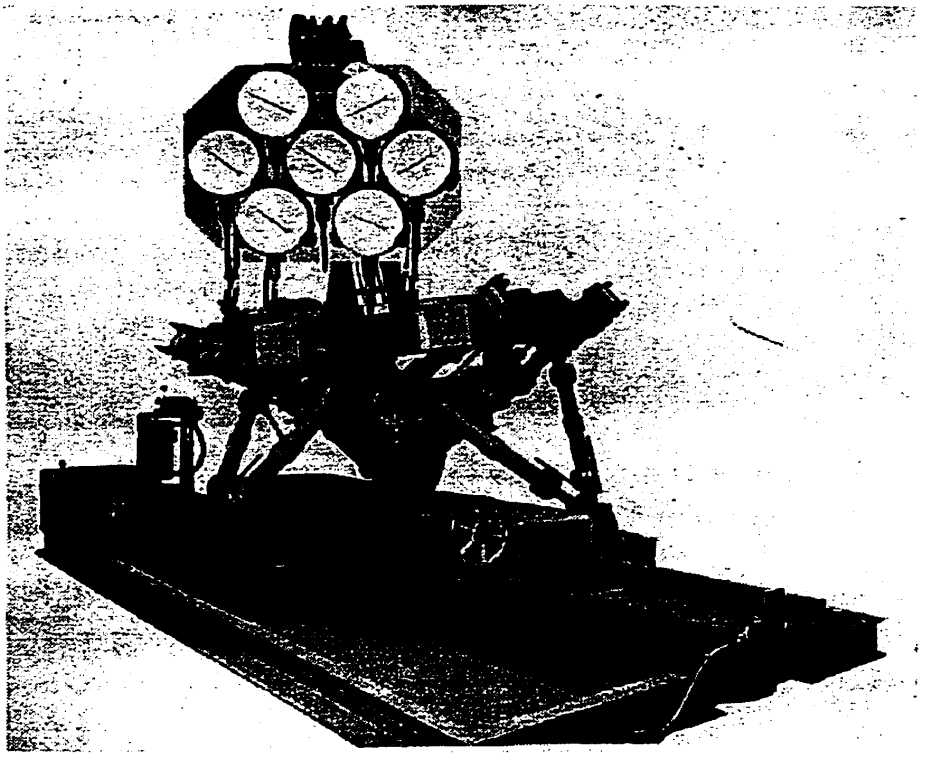

FIGURE 1.4. The Gough *universal rig* [**53**]. A tire test-stand from 1956!

1.1.2. Stewart-Gough Platforms. In 1965 D. Stewart [**137**] first suggested that flight simulators, like the one shown in Figure 1.2, could be built on fully-parallel platform type manipulators with six DOF. In subsequent years such manipulators came to be known as *Stewart platforms*. However, a design for a tire test-stand shown in Figure 1.4, with the same architecture of a modern flight simulator, virtually identical to that proposed by Stewart, had already been contributed by V.E. Gough and staff at Cornell nine years earlier [**53**]. Indeed, the development for Gough's *universal rig* began in 1949 [**102**]. The term *Stewart-Gough platform* (SGP) is therefore used in an attempt to correct this historical oversight. It is quickly becoming standard terminology in the literature, see Angeles [**8**], Dietmaier [**40**], Husty [**81**], Merlet [**101**], and Nielsen and Roth [**108**], for example. Indeed, some propose that the term *Gough platform* is more appropriate [**102**].

Although interesting, and possibly critical, theoretical problems connected with SGP remain unsolved, the current state-of-the-art has enabled prototypes and commercial manipulators to be designed, built and sold. For instance, the flight simulator architecture has been adapted for a wide variety of uses. The ESRF platform is but one example. A couple of others include a *virtual reality platform* shown in Figure 1.5 used to train athletes in equestrian skills, and an antenna positioning device for satellite tracking, also shown in Figure 1.5. Both prototypes were developed at INRIA [**102**]. There are, however, risks attached to patenting designs while related theoretical problems are unresolved. For example, there is a 1993 patent for a parallel manipulator [**55**], intended for use as a flight simulator. Subsequent investigation [**85**] shows that every assembly configuration within its workspace is singular and permits uncontrollable platform motions.

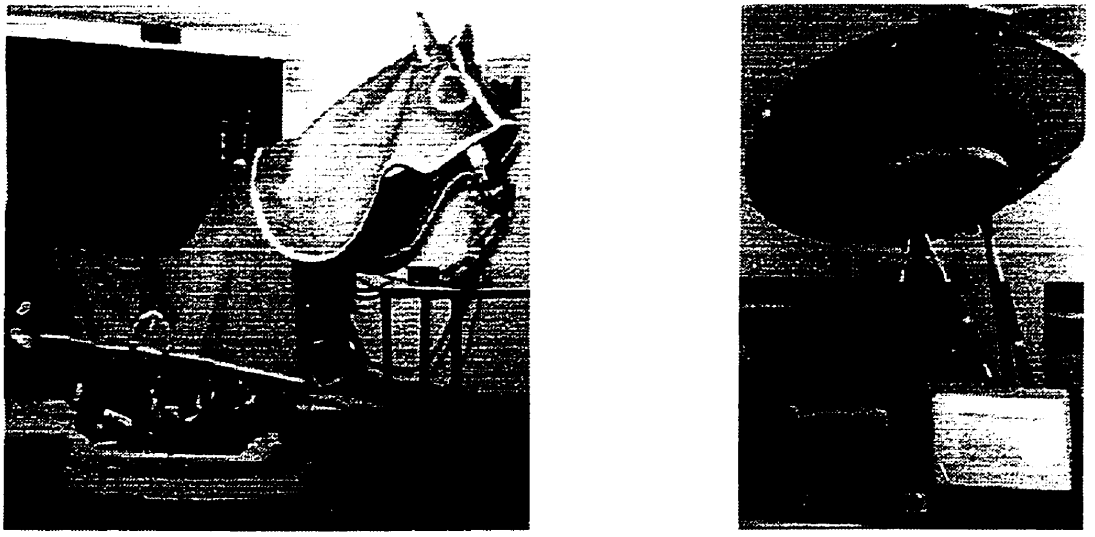

FIGURE 1.5. Equestrian simulator and antenna positioning device (courtesy of INRIA).

The platforms possessing topological symmetry considered in this thesis can be considered as three DOF planar versions of the six DOF SGP. We therefore call them *planar Stewart-Gough platforms* (PSGP). Figure 1.6 shows a typical example.

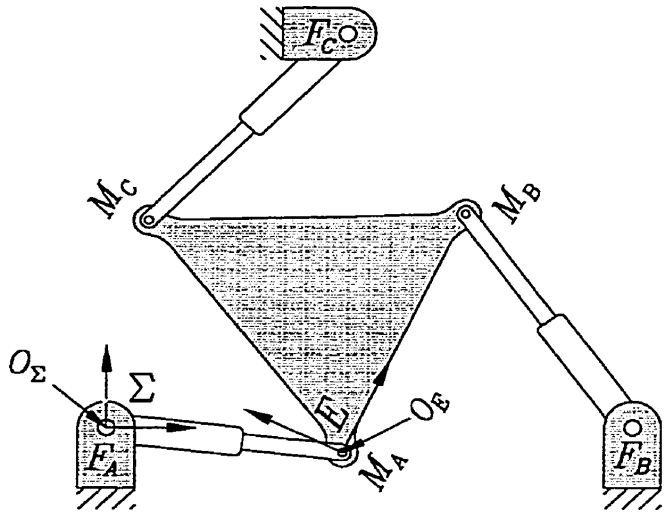

FIGURE 1.6. A typical planar parallel manipulator.

1.2. Motivation

The body of literature is thick with many kinematic analyses of SGP. In particular, the FK problem of PSGP has received attention. Due to the nature of the FK problem, much of the earlier research concentrated on numerical solutions [**122, 123, 124, 133**]. While numerical methods are often useful, they yield no insight into theoretical issues, such as the size of the solution space, i.e., the number of assembly modes. Furthermore, these methods rely on an initial guess which must be fairly close to the solution in order to converge [**124, 50**].

Many efforts have been made to provide some theoretical insight by viewing the problem from a different perspective. It was established by Hunt [**76**] that PSGP with 3 RRR (or, when the middle joint is activated, the kinematically equivalent RPR)[3] legs admit at most six real assembly configurations for a given set of activated joint inputs. General solution procedures using elimination theory to derive a 6^{th} degree univariate polynomial, which leads to all assembly configurations, were developed by Gosselin and Sefrioui [**50**] and Wohlhart [**142**]. The FK problem is solved for

[3] R stands for *revolute* joint; P stands for *prismatic* joint, see Section 2.3.

all permutations of three-legged planar lower-pair-jointed SGP in Merlet [**100**]. The univariate polynomial was again derived by Pennock and Kassner [**111**], but the work was extended to include an investigation of the workspace [**112**]. Earlier work by Gosselin [**49**] provides a useful workspace optimisation scheme for planar, spherical and spatial platform-type parallel manipulators. A detailed enumeration of assembly configurations of planar SGP can be found in Rooney and Earle [**122**]. Synthesis issues are addressed using a straightforward geometric approach by Shirkhodaie and Soni [**133**], while Murray and Pierrot [**107**] give an extremely elegant n-position synthesis algorithm, based on quaternions, for the design of PSGP with three RPR legs. What appears to be lacking is a derivation of the general univariate to solve the FK of any lower pair jointed PSGP. This, then, is the primary goal of this thesis. But, it did not start out that way. The original research proposal was for an investigation of planar three-legged parallel platforms with active holonomic higher pairs.

The success of most of the methods mentioned above depends largely on the fact that the platforms are jointed with lower pairs. This allows the platform geometry to be readily determined. This is a critical point, since all the above methods require knowledge of the platform geometry. However, when the end-effector is replaced with a disk (pinion gear) and the three revolutes joining the end-effector to the legs are replaced with racks which remain engaged with the pinion, the geometry suddenly becomes difficult, making the level of complexity of the IK and FK problems equal. This is in contrast to the general observation that the IK problem for lower pair jointed parallel problems is trivial [**49**], while the same problem for serial manipulators is typically complicated. Similarly, the FK problem of parallel platforms is generally more complex than that of serial manipulators. In fact there is a strange duality between parallel and serial manipulators: a difficult problem for one is usually a simple problem for the other. This duality has yet to be fully explained, although several attempts have been made [**141, 146**].

The literature, however, appears to be all but devoid of work investigating fully-parallel platforms whose joints include holonomic higher kinematic pairs. This omission is unfortunate because such platforms offer distinct advantages over their lower-pair-jointed cousins in two respects. First, the locations of the attachment points connecting each of the three legs to the platform are continuously variable with respect to each other during platform motions, *i.e.*, the platform has a continuously variable geometry. This means that a general procedure for the kinematic analysis of this type of platform can be applied to multiple-arm cooperating robots because any such procedure is necessarily dependent on the initial assembly configuration (IAC) of the platform [**3, 4, 63**]. This leads directly to the second advantage, in that these platforms can be designed as fully parallel, cooperating, or hybrid devices.

A good deal of attention has been given to rolling-without-slip in the context of grasp and fine control. Mimura and Funahashi [**104**] looked at grasping and fine-motion manipulation by multi-fingered robotic hands, the Utah/MIT dextrous hand being an example. Hui and Goldenberg [**74**] considered a hybrid control architecture using rolling constraints between a dextrous hand and the rigid object it manipulates. Yun *et al.* [**145**] investigated control issues of multiple arms with pure rolling contacts. Various types of contact between hand and object have been studied extensively by Salisbury and Roth [**128**]. But, even here the robotic hands are jointed with lower pairs only. The rolling contact is merely an approximation of contact between the end-effector and workpiece. Particular attention is given to grasp and its effect on the workspace by Chen and Kumar [**23**]. Continuing in this vein, the kinematics of rolling contact for two surfaces of arbitrary shape were examined by Cole *et al* [**25**]. Rolling systems are not peculiar to robotic hands. Automatic Guided Vehicles (AGV) are an important class for industrial applications, dangerous materials handling, *etc.*. The kinematics and dynamics of a three wheeled 2 DOF AGV were studied in great detail in [**127**]. However, in the case of the AGV, continuous rolling contact is a by-product

of constraints imposed by the operating environment. It is not a design parameter affecting control (except to detect wheel slip) or kinematic synthesis.

The common thread in the multiple arm and AGV literature cited above is that the contact between robot and object, or environment, is pure rolling. Grasp and fine-motion manipulation by multi-fingered robotic hands are issues closely connected to contact type. Work in this area is still open, hence we feel justified in examining the kinematic analysis of a three-legged PSGP with holonomic higher pairs. However, to maintain a reasonable scope for this thesis, the device will be treated as a fully-parallel planar manipulator.

Recently, it has been shown that kinematic mapping has important applications in planar robot kinematics. A particular mapping [**14, 57**] is used by De Sa [**36**] and De Sa and Roth [**37, 38**] to classify one parameter planar algebraic motions. Ravani [**119**] and Ravani and Roth [**120, 121**] employed it to to study planar motion synthesis. Husty [**79**] used the same mapping in a novel FK solution procedure for planar three-legged SGP. He then used it to analyse the workspace of the same type of platform [**80**]. The particular mapping used is well suited to manipulators with holonomic higher pairs, as in Figure 1.7, since it is independent of the geometry of the platform [**79**]. However, it has never, to the best of our knowledge, been applied with complete success to the FK problem of our platform. Indeed, no practical solution procedure for the IK nor FK problems can be found in the literature. Thus the secondary goal of this thesis, but one of primary interest, is to present a practical solution procedure that employs kinematic mapping for the IK and FK problem of planar three-legged platforms with holonomic higher pairs.

It appears that all previous work directly related to fully-parallel PSGP with holonomic higher pairs is contained in two publications, by the same authors [**3, 4**].

Because of the serendipitous way in which the main theme of the thesis developed from the study of these two papers, its chronology shall now be presented.

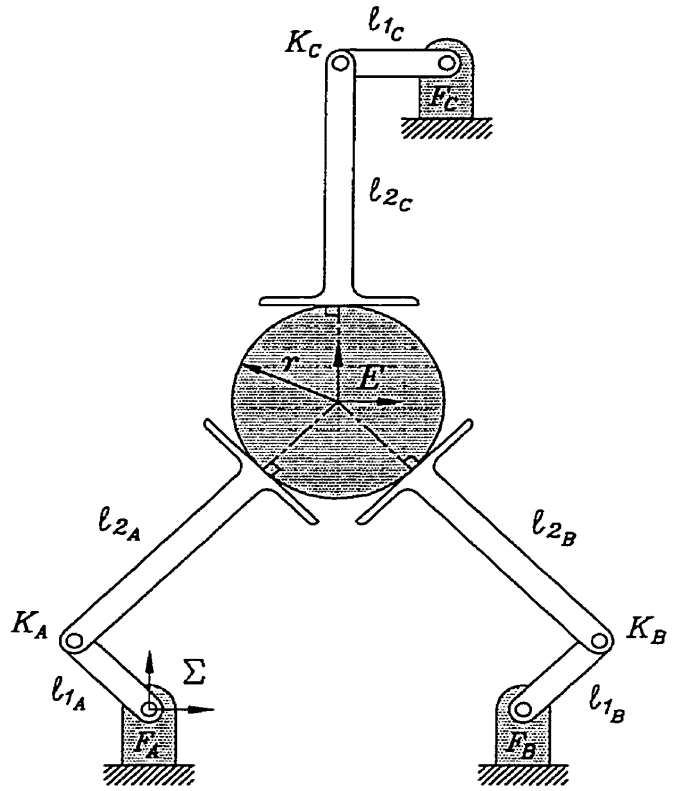

FIGURE 1.7. An $RR\underline{G}$ platform.

1.2.1. Variation on a Theme. The research trail began in 1995 with my M.Eng. thesis [**65**] which aimed to correct a conceptual flaw found in a procedure [**3**] for solving the inverse kinematics (IK) problem of a novel planar parallel manipulator suggested by Vijay Kumar at the University of Pennsylvania. The manipulator consists of a circular disk which rolls without slip along the straight lines of the non-grounded rigid links of two $2R$ serial legs. Its kinematics are deceptively complicated because of the rolling contact. A three legged version is illustrated in Figure 1.7. The points of contact between each leg and the disk are holonomic higher pairs. These G-pairs are modelled as a pinion gear meshing with three racks. With the exception of cams and gears, which are not considered to be robotic mechanical devices,

research on mechanisms containing higher pairs is rare. Gears are common, efficient and reliable machine elements but they are unusual as robotic joints.

The IK procedure, developed by Agrawal and Pandravada [**3**], used the relative angle between the two rack-pinion normals to indicate the absolute orientation of the pinion. If the pinion undergoes a pure translation there is obviously no change in its absolute orientation, yet the angle between the normals must change. This means the output of the IK algorithm has limited applications.

A thorough literature review revealed only one other paper, by the same authors, dealing with the kinematics of fully parallel planar platforms with holonomic higher pairs. The second paper [**4**] dealt with the workspace analysis of the same two-legged platform. However the analysis was based on the earlier, flawed IK algorithm. Absolutely no other publications dealing with this type of fully parallel platform were found. The initial motivation, then, was to solve the IK and FK problem for a three legged version of the manipulator. The third leg was added to make the platform topologically symmetric. That is, the pinion has three degrees of freedom (DOF) and therefore needs three motors to fully control it. The two-legged version requires one leg to have at least two activated joints.

The problem common to all three legged planar platforms with 3 DOF is that, unless redundant actuators are used, only three joint inputs can be specified. The problem unique to the pure rolling contact platform is how the change in location of the contact point between each rack and the pinion effects the displacement. If the pinion remains stationary while a rack moves, it must be that the rack rolls on the disk. Conversely, the pinion can roll on a stationary rack. In the above situations, if the change in location of the contact point along the rack is identical, the displacement of the disk centre will be different. In the first case, the location of the pinion centre remains fixed. In the second case, it translates along a line parallel to the stationary

rack. Most displacements, however, require a combination of the two types of relative rolling. Keeping track of the proportions is critical to both the IK and FK problems. It also appears to be a formidable task.

Our first attempt at solving the the IK problem [**63, 65**] made use of the loop closure equations and the fact that arbitrary pinion displacements can be decomposed into the commutative product of a single translation and a single rotation about the pinion centre. Given the desired pose and initial assembly configuration (IAC), a set of intermediate joint variables are calculated for the pure translation component. Then, using this intermediate set as a new IAC, solutions are generated for a fixed axis rotation. Unfortunately, the direct algebraic result of the displacement decomposition is that the upper bound on the number of IK solutions is 64. It is well known that for a three-legged, three DOF planar platform with passive lower pairs there can be at most 8 [**49, 97**]. The 56 spurious solutions indicate the procedure is not optimal. Nonetheless, it was the first published *correct* IK solution procedure for this type of platform. Moreover, since the algorithm solves for one leg at a time, it can be used on platforms with any number of closed kinematic loops.

The next step was to develop an FK solution procedure. This proved to be somewhat more challenging than expected. Again, this was due to the unexpected complications imposed by the holonomic higher pairs. It was decided to use Husty's kinematic mapping procedure [**79**] because it is independent of the geometry of the platform. This feature is very useful because the platform attachment points (i.e., the contact points between the pinion and racks), which really define the platform geometry, change their relative positions continuously during platform motions.

The procedure that was first developed [**64**] relied on the position of the non-grounded R-pairs (called *knee joints* K_i, $i \in \{A, B, C\}$, see Figure 1.7) in the pinion-fixed reference frame, E, as inputs to the kinematic mapping procedure. They were

called *pseudo inputs* because the *actual inputs* are the change in rack tangent angle. This was rather an academic exercise because there was no obvious way to relate the knee joint positions to the change in rack tangent angles until the pinion orientation was known. Since the FK problem involves the determination of the position and orientation of the platform given the active joint inputs, this was a cart-before-horse scenario, to be sure. Even-though it was not entirely practical, it was a start: it was the first attempt at solving the FK problem of this type of manipulator. Indeed, reworking the IK and FK solution procedures formed the basis of my Ph.D. research proposal.

In September 1996 Manfred Husty made the incisive observation that if the pinion is considered to be fixed then contact points on the rack move on involutes of the pinion [**82**]. This means there is a bijective (one-to-one and onto) correspondence between the change in rack tangent angle, which determines the change in location of any rack point on a pinion involute and the location of the corresponding knee joint in the pinion-fixed frame, E. Employing these *involute inputs* and some additional coordinate transformations the kinematic mapping procedure can be used [**66, 69**].

Next, the IK problem was revisited. Using the involute inputs, mentioned above, a simple procedure was developed to extract the active joint inputs from the *pre-image* of a point in the kinematic mapping image space (which abstractly represents a platform pose as a point in a three-dimensional (3-D) homogeneous projective space) [**67**].

It was then decided to attempt to obtain a symbolic univariate, in terms of an image space coordinate, whose roots would reveal all FK solutions for any arbitrary three-legged platform with active holonomic higher pairs. With the aid of the symbolic computer algebra software *Maple V*, it turned out to be quite simple to derive the univariate. It is a sixth order polynomial, confirming the results of Hunt [**76**],

Gosselin [49], and Merlet [97]. Its coefficients contain 5201 sums of products of design constants and joint inputs.

Finally, in another communication with Husty [84], it was realised that the univariate polynomial could be used on *any* topologically symmetric planar three-legged platform with three DOF. In fact, the univariate turned out to be applicable to the FK (and IK) problem of a wide range of topologically asymmetric platforms as well. With some clever substitutions [84] the number of terms for the general case drops from 5201 to 3613. When the platform architecture is fully specified the number drops to 694 for one sub-class, and drops again to 30 for the remaining two sub-classes. A detailed derivation of the univariate and enumeration of the coefficient terms is given in Chapter 4. This is, in essence, the story to be played out in the following pages.

1.3. Thesis Overview

Optimal trajectory planning and obstacle avoidance in a crowded workspace requires fast computation of FK solutions. Control of the robot requires the availability of IK solutions. Hence, the main goal of this thesis is to address these issues in detail. The solution procedures developed are general, and can be used to solve the IK and FK problems of *any* topologically symmetric PSGP, including planar platforms with active holonomic higher pairs.

In Chapter 2 some elementary concepts are recalled and necessary definitions and nomenclature are stated. Planar three-legged fully-parallel manipulators with 3 DOF are classified and those possessing topological symmetry are defined to be PSGP. The manipulators of this class are described together with the holonomic higher pair architecture. Geometric properties and applications of the higher pair platforms are discussed. A mobility analysis is presented.

Chapter 3 is a discussion of the geometric and algebraic tools and concepts used in the subsequent kinematic analysis of PSGP. It commences with a brief summary of the projective extension of the Euclidean plane and space. Then Klein's *Erlangen Programme* is detailed leading to a discussion of geometry from the *Cayley-Klein* perspective. Various representations of planar displacements are reviewed. Lastly, kinematic mapping is discussed.

The FK problem of PSGP and those with holonomic higher pairs is the focus of Chapter 4. The kinematic constraints in the displacement space are examined. Then, in order to apply the kinematic mapping, the image of these constraints must be studied. After establishing the nature of these constraints, it is a simple matter to derive the general univariate. Finally, upper bounds on the number of FK solutions are given and rationalised in terms of the constraints.

Chapter 5 details application of the univariate to the FK problem. Procedures for determining the coefficients for all PSGP are described. The solution procedure for the higher pair platform is included. In addition, procedures for topologically asymmetric platforms are discussed.

The IK problem is considered in Chapter 6. Closed form solutions, in terms of the coordinates of the kinematic mapping image space, are given. These solutions are valid for every three-legged, three DOF planar platform jointed with lower pairs. The kinematic mapping IK solution procedure for the higher pair platform is developed in detail.

Chapter 7 presents a workspace analysis as well as simple criteria for the determination of the existence of a dextrous workspace. Singularity and self-motion detection are also discussed.

Finally, Chapter 8 contains conclusions and suggestions for future research.

CHAPTER 2

General Planar Stewart-Gough Platforms

General planar three-legged fully-parallel manipulators with three degrees-of-freedom are described and classified in this chapter. Those possessing topological symmetry, including position of activated joints, are defined to be general planar Stewart-Gough platforms (PSGP). First, some elementary concepts are recalled and some necessary definitions and nomenclature stated.

2.1. Kinematic Chains

A *kinematic chain* is a set of *rigid bodies* coupled by mechanical constraints such that there can be relative motion between them [8]. The individual rigid bodies are called *links* in the chain. The chains are classified according to how the links are connected.

2.1.1. Simple Kinematic Chains. A kinematic chain is *simple* if each link in the chain is coupled to *at most* two other links [7]. The *degree of connectivity* (DOC) [7] of a link indicates the number of rigid bodies joined to it. If all the links are binary, having a DOC of two, the chain is *closed*. For example, a four-bar

mechanism. Alternately, the chain is *open* with the first and last links having a DOC of one.

2.1.2. Complex Kinematic Chains. A kinematic chain is *complex* if at least one of its links has a DOC greater-than-or-equal to three [7]. A complex chain may always be decomposed into simple kinematic sub-chains. Due to the three connection points between their base and platform, PSGP are complex chains [49]. The analysis presented subsequently relies on decomposing complex chains into simple ones.

2.2. Degree-of-Freedom

The degree-of-freedom (DOF) of a kinematic chain is defined to be an integer value corresponding to the minimum number of independent coordinates required to fully describe, geometrically, an arbitrary configuration of the chain [6]. There is one coordinate, usually defined on the field of real numbers, associated with each DOF. Since any one of these coordinates can change without necessitating a change in the others they are all independent. Such coordinates are historically called *generalised coordinates* [10]. For the study of robot kinematics, generalised coordinates usually represent measures of distance and angle. A kinematic chain constitutes a mechanism if its DOF is a positive value; a statically determinate structure if the DOF is zero; a hyper-static (statically under-determined, or over-constrained) structure if the DOF is a negative value [6].

A rigid body free to move in three dimensional space has six DOF. The DOF are generally taken to be three translations parallel to three linearly independent basis directions and three rotations about three linearly independent axes, although any system of six generalised coordinates is sufficient. That is, the six numbers need not be three distances and three angles [75]. While it is not necessary that the

rotation axes be the same as the translation directions, it is usually convenient to use a three-dimensional orthogonal reference frame to describe the space of the motion, the rotation axes being respectively parallel to the coordinate axes [**136**]. Mechanical constraints are imposed on rigid bodies to limit their motion as required. In this sense, constraints are the complements of DOF. For instance, if a rigid body has two DOF in Euclidean space, indicated by E_3, four constraints must be imposed.

2.3. Kinematic Pairs

The term kinematic *pair* indicates a joint between two links, hence the use of the word pair [**7**]. They are mechanical constraints imposed on the links. Joints involving surface contact are called *lower pairs*. Those involving nominal point, line, or curve contact are *higher pairs*. Lower pairs enjoy innate practical advantages over higher pairs. First, applied loads are spread continuously over the contacting surfaces. Second, they can be, in general, easily and accurately manufactured.

2.3.1. Lower Pairs. There are six types of lower pair [**75**], classified as follows:

1. ***S*-pair:** The spherical S-pair consists of a convex, or solid sphere which exactly conforms with a spherical shell of identical radius. In other words, a ball-joint. S-pairs permit three rotational DOF.
2. ***E*-pair:** The planar E-pair (E stands for the German word *Ebene*, which means plane) is a special S-pair comprising two concentric spheres of infinite radius. To fix one plane relative to the other requires three generalised coordinates, usually determined by two translations and one rotation. Regardless, the E-pair allows three DOF.

3. ***C*-pair:** The cylindrical C-pair consists of mating convex and concave circular cylinders. They can rotate relative to one another, about their common axis, and they can translate relative to each other in a direction parallel to the axis. Hence, there are two DOF: one rotational and the other translational.
4. ***R*-pair:** The revolute R-pair is made up of two congruent mating surfaces of revolution. It has one rotational DOF about its axis.
5. ***P*-pair:** The prismatic P-pair comprises two congruent non-circular cylinders, or prisms. It has one translational DOF.
6. ***H*-pair:** The helical H-pair, or screw, consists of two congruent helicoidal surfaces whose elements are a convex screw and a concave nut. For an angle θ of relative rotation about the screw axis there is a translation of distance h in a direction parallel to the screw axis. The sense of the translation depends on the *hand* of the screw threads and on the sense of the rotation. The distance h is the pitch. When $h = 0$, the H-pair becomes an R-pair; when $h = \infty$ it becomes a P-pair. The H-pair has one DOF which is either specified as a translation or a rotation, coupled by the pitch, h.

Only planar platforms are considered herein. The only relevant lower pairs are P- and R-pairs. Moreover, all six of the lower pairs listed above can be produced from combinations of these two [8]. Figure 2.1 (*i*) and (*ii*) show bodies joined by R- and P-pairs, respectively.

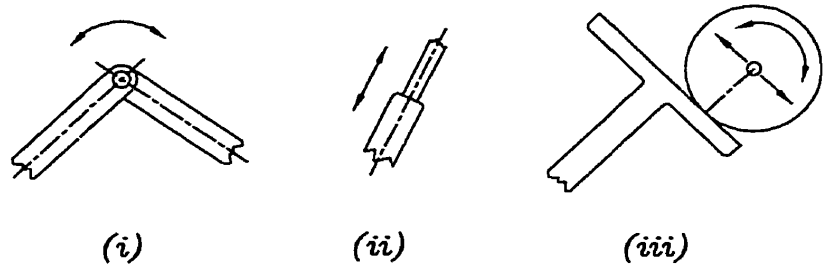

FIGURE 2.1. The three pairs used: (*i*) R-pair; (*ii*) P-pair; (*iii*) G-pair.

2.3.2. Higher Pairs. Higher pairs are important because they often offer the most direct means of achieving complex motions. The main drawback is that they are typically more complicated, implying that they are more expensive to design and manufacture. A few examples are mating spur gears, rack and pinion, cam and follower. The higher pairs may be classified according to the nature of the relative motion between the jointed links:

1. **Pure sliding:** The relative motion is pure translation as in, for example, a reciprocating cam activating a knife-edge or mushroom head follower, or the finger tip of a robot hand sliding along a flat surface.
2. **Pure rolling:** The relative motion involves rolling without slip. Such as the tangential pitch circles of mating sets of spur gears, or rack and pinion systems.
3. **Combination of sliding and rolling:** In rotating cam and follower systems the tip of the follower slides along any constant radius of curvature portions of the cam surface. As the cam rotates and, relative to the follower, its radius of curvature changes, the follower rotates about some axis. As this occurs, the follower tip will also roll on the cam surface.

2.3.3. Holonomic and Non-holonomic Constraints: *G*-Pairs. The term *holonomic* is derived from the Greek word *holos* meaning *integer*. It describes constraints that may be expressed in *integral form*, *i.e.*, in terms of displacements, as opposed to *differential form*, *i.e.*, in terms of linear and angular velocities [**7**]. Differential form kinematic constraints involving link angular velocities are *non-holonomic* unless the motion is planar and occurs without slip [**7, 48**].

The subject of this thesis includes the kinematic analysis of PSGP with holonomic higher pairs that involve rolling without slip on a straight line, like rack and pinion gear sets. This type of higher pair, illustrated in Figure 2.1 (*iii*), is abbreviated as

a G-pair (G for gear). Since the platforms examined herein, including the special architectures, are all planar and there is no slip between the higher pairs, all the kinematic constraints in this thesis are holonomic.

A very detailed discussion of relevant conditions that make a constraint holonomic can be found in [48], which is briefly summarised now for reference. The constraint equations confining the motion of a rigid body can be written as functions

$$f_i(q_1, q_2, \ldots, q_m, t) = 0, \tag{2.1}$$

where the q's are constrained *generalised coordinates*, t stands for time and the subscript i denotes a particular constraint equation. Any limitation placed on the generalised coordinates restricts the position of the rigid body, and hence these are called *position constraints*[1]. Position constraints impose restrictions on the velocity as well. The *velocity constraints* are obtained by differentiating Equation (2.1) with respect to time:

$$\dot{f}_i = \sum_{j=1}^{m} \left[\frac{\partial}{\partial q_j} f_i(q_1, q_2, \ldots, q_m, t)\right] \dot{q}_j + \left[\frac{\partial}{\partial t} f_i(q_1, q_2, \ldots, q_m, t)\right] = 0, \tag{2.2}$$

where the $\dot{q}$'s are called *generalised velocities.* Equations (2.1) and (2.2) are equivalent in the limitations they impose as long as the initial position is specified.

A more general form for the velocity constraint equations is obtained by replacing the derivatives by arbitrary coefficients that are functions of only the generalised coordinates and time:

$$\sum_{j=1}^{m} a_{ij}(q_1, q_2, \ldots, q_m, t)\dot{q}_j + b_i(q_1, q_2, \ldots, q_m, t) = 0. \tag{2.3}$$

Equations (2.2) and (2.3) represent equivalent constraints if the corresponding coefficients of each generalised velocity and of the velocity-independent term are the

[1] In [48] these are termed *configuration constraints.*

same up to a multiplicative factor, which may itself be a function of the generalised coordinates and time, $g_i = g_i(q_1, q_2, \ldots, q_m, t)$. A velocity constraint is derivable from a position constraint, and vice-versa, if, and only if

$$a_{ij} g_i = \frac{\partial f_i}{\partial q_j}, \qquad b_i g_i = \frac{\partial f_i}{\partial t}. \tag{2.4}$$

The velocity constraint equations are holonomic (meaning integrable) if they satisfy Equation (2.4), otherwise they are non-holonomic.

This terminology actually refers to the differential form, called the *Pfaffian form*, of a constraint equation [**56**]. The Pfaffian form is obtained from Equation (2.3) by multiplying it through by dt, giving:

$$\sum_{j=1}^{m} a_{ij}(q_1, q_2, \ldots, q_m, t) dq_j + b_i(q_1, q_2, \ldots, q_m, t) dt \;=\; 0. \tag{2.5}$$

When Equation (2.4) is satisfied, multiplying Equation (2.5) by the function g_i transforms the Pfaffian form to a perfect differential of the function f_i. This leads to the following definition [**48**]:

DEFINITION 2.3.1. *A velocity constraint is* holonomic *if there exists an integrating factor g_i for which the Pfaffian form of the constraint equation becomes a perfect differential. In this case, it may be integrated yielding the position constraint on the generalised coordinates.*

The concept of a holonomic constraint may be viewed from a geometric perspective. The generalised coordinates, q_i, may be taken to be the basis $(q_1, q_2, \ldots, q_m)$ of an m-dimensional (m-D) *constraint* space. The constrained motion in the constraint space is the locus of points as the motion evolves in time. Consider a holonomic constraint $f(q_1, q_2, \ldots, q_m, t) = 0$. At any instant t the position of the rigid body is confined to some surface in the constraint space. The corresponding Pfaffian form of

the velocity constraint states that infinitesimal displacements must be in the corresponding tangent plane to the constraint surface [**109**].

When the constraint is non-holonomic, the constraint surface cannot be defined. Hence, the velocity constraint cannot be integrated. In this case the Pfaffian form of the constraint equation restricts infinitesimal displacements to lie on a tangent plane that can only be defined by the current state of the motion [**48**].

2.4. Rigid Body Displacements: The Isometry Group

A rigid body displacement can be described geometrically as an *isometry*: a bijective mapping of Euclidean space E_3 onto itself which leaves the distance between any two points invariant. Although a motion is clearly associated with an isometry, the isometry does not represent the motion: it is the correspondence between an initial and a final position of a set of points. A motion is a continuous series of infinitesimal displacements. Because an isometry maps collinear points into collinear points, it transforms lines into lines, and hence is a *collineation*. The invariance of distance also ensures that triangle vertices are transformed into congruent triangle vertices. Thus, isometries preserve angle and are also *conformal transformations* [**71**].

The word *set* has so far been used to mean a collection of geometric objects, such as points, or lines. It may, however, be used more broadly to mean a collection of any sort. The set of isometries includes the following transformations: rotation; translation; screw; reflection (in a plane); central inversion (reflection in a point) [**30**]. It is easy to show that the set of isometries, together with a binary operator which combines them, called *product*, defined on the set, constitutes a group, $\mathcal{G}$. The elements of $\mathcal{G}$, $\{x, y, z, \dots\}$ and the product operator satisfy the following axioms [**13**]:

i.	[closure]	$xy \in \mathcal{G}$	$\forall\, x, y \in \mathcal{G}$
ii.	[associativity]	$(xy)z = x(yz)$	$\forall\, x, y, z \in \mathcal{G}$
iii.	[identity]	$\exists\, I \in \mathcal{G}:$	$Ix = xI = x, \forall\, x \in \mathcal{G}$
iv.	[inverse]	$\exists\, x^{-1} \in \mathcal{G}:$	$xx^{-1} = x^{-1}x = I, \forall\, x \in \mathcal{G}$

The isometry group of the Euclidean plane E_2 is a sub-group of the isometry group of E_3. Every isometry is the product of at most four reflections, in E_2 four is replaced by three [**30**]. Since a reflection reverses sense, an isometry is direct or opposite according to whether it is the product of an even or odd number of reflections. The set of direct isometries form a sub-group. This is because any product of direct isometries is another direct isometry. Whereas, the same does not hold for the set of opposite isometries: the product of two opposite isometries is a direct isometry, violating the closure axiom. This is why opposite isometries do not form a sub-group. The sub-group of direct isometries is also known as the *group of Euclidean displacements*, $\mathcal{G}_6$ [**30, 71, 90**]. The subscript 6 refers to the number of generalised coordinates required to specify a displacement. In turn, the isometries are a sub-group of the *Euclidean similarity transformations*, also termed the principal group, $\mathcal{G}_7$ [**30, 71, 90**]. Seven parameters determine a similarity transformation, the additional one being a magnification factor to uniformly scale distances. The $\mathcal{G}_7$ transformations are also conformal collineations, but the distance between two points is not, in general, invariant.

2.4.1. DOF by Group: Chebyshev-Grübler-Kutzbach Formula. The relative motion associated with each of the lower pairs listed in Section 2.3 constitute a sub-group of $\mathcal{G}_6$ under the binary product operator (*i.e.*, the composition of two displacements). The *dimension* of these sub-groups is defined to be the DOF of the relative motion permitted by the lower pair [**7**]. It is indicated by $\dim(\mathcal{G}_S)$,

where $\mathcal{G}_S \subset \mathcal{G}_6$. These sub-groups, together with their corresponding dimension, are identified in Table 2.1.

Lower pair	$\mathcal{G}_S$	$\dim(\mathcal{G}_S)$
S	$\mathcal{S}$	3
E	$\mathcal{E}$	3
C	$\mathcal{C}$	2
R	$\mathcal{R}$	1
P	$\mathcal{P}$	1
H	$\mathcal{H}$	1

TABLE 2.1. Lower pair sub-groups and their dimension.

Let the *product* of two sub-groups, indicated by $\mathcal{G}' = \mathcal{G}_1 * \mathcal{G}_2$, be the composition of the displacements they represent. If the product is also a sub-group of $\mathcal{G}_6$ then the dimension of this new sub-group will be $\dim(\mathcal{G}') \leq 6$. Let the product of the sub-groups of a *trivial* [2] kinematic chain with l links be $\mathcal{G}' \subset \mathcal{G}_6$. Furthermore, let $\dim(\mathcal{G}') = d$. The i^{th} kinematic pair imposes u_i constraints on the two links it couples. Clearly, l unconstrained rigid links have $d(l-1)$ relative DOF, given that one of the rigid links is designated as a non-moving reference link. Any joint connecting two neighbouring rigid bodies removes at least one relative DOF. If the joint removes no DOF then the bodies are not connected. If the joint removes three DOF in the plane, or six DOF in space the two bodies are a rigid structure. Summarising this discussion, the DOF of a trivial chain can be expressed as

$$d(l-1) - \sum_{i=1}^{j} u_i - m \;=\; \text{DOF}, \tag{2.6}$$

where $d = \dim(\mathcal{G}')$, l is the number of links, u_i is the number of constraints imposed by the i^{th} joint, j is the number of joints, and m represents the number of *idle* DOF[3]

[2]Trivial kinematic chains are those whose kinematic pairs have associated sub-groups whose product is a sub-group of $\mathcal{G}_6$ [7]. For example, the S-, E-, C-, R-, P- and H-pairs are all trivial.

[3]The *idle* DOF of a chain are the number of independent single DOF motions that do not affect the transmission of motion from the input to output links of the chain. However, idle DOF have no

of the chain. This equation is known as the Chebyshev-Grübler-Kutzbach (CGK) formula [7].

2.5. General Planar Stewart-Gough Platforms Defined

A general planar Stewart-Gough platform (PSGP) is defined to be a moving planar platform connected to a fixed base by three *identical* open kinematic chains, called *legs*. Each of the three legs is connected by three independent one DOF joints, one of which is actuated. Therefore, each independent chain has three DOF. Since all three legs are *identical* the actuated joint must be the same one and the same type in each leg. This definition is the logical reduction to the plane of the following definition of the general six DOF spatial SGP.

These six DOF platforms consist of a mobile platform connected to a fixed rigid base by six articulated legs of variable length [**81**], see Figure 2.2. Each of the P-pair legs, see Figure 2.3, is joined to the base by a *universal joint*[4] (U-pair) and to the moving platform by an S-pair [**8**]. This architecture is described topologically by the sequence of joints of one of six legs connecting the fixed base to the moving platform: *universal-prismatic-spherical*, indicated by UPS. While this architecture is arguably the most *well known*, it is not the most general [**83**]. From a geometric perspective, the *general* SGP consists of six arbitrary points in a particular reference frame that can move in constrained relative motion with respect to six arbitrary points in another. The one condition is that the points of connection between the mobile platform and each leg move on fixed spheres [**81**].

---

direct bearing on the material presented herein and need not be discussed further. The interested reader is referred to [**6, 7**] where this concept is discussed in great detail.

[4]There are a number of types of *universal joint*, the one used on SGP is but one of the lot. It comprises two R-pairs whose axes intersect at a fixed angle, see Figure 2.3. The term has its origin in the ability of a joint to transmit motion between two intersecting, but non-collinear shafts. Such a universal joint is called a *Hooke*, or a *Cardan joint*, although neither Hooke nor Cardan invented it [**61**].

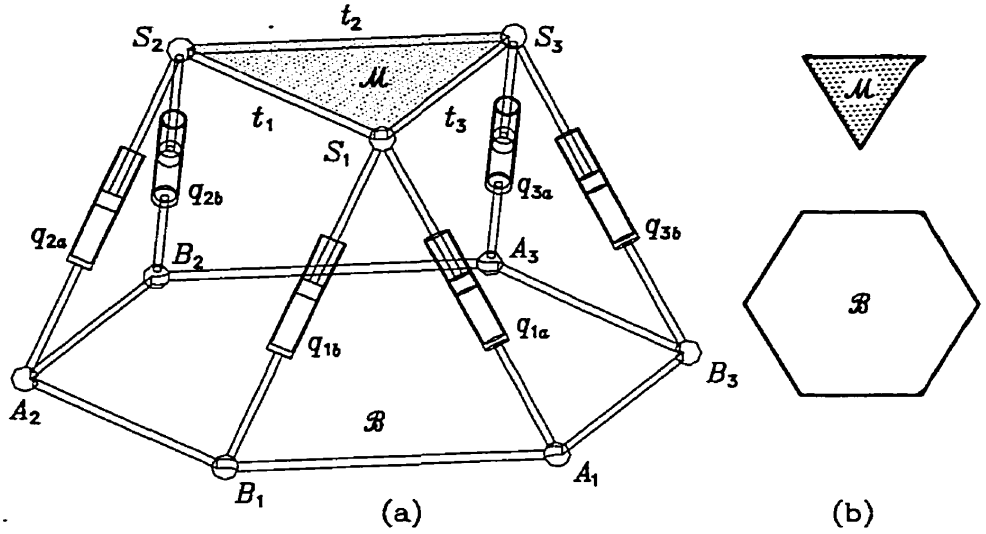

FIGURE 2.2. A *UPS*-SGP: (a) layout; (b) platform and base geometry (courtesy of Prof. J. Angeles).

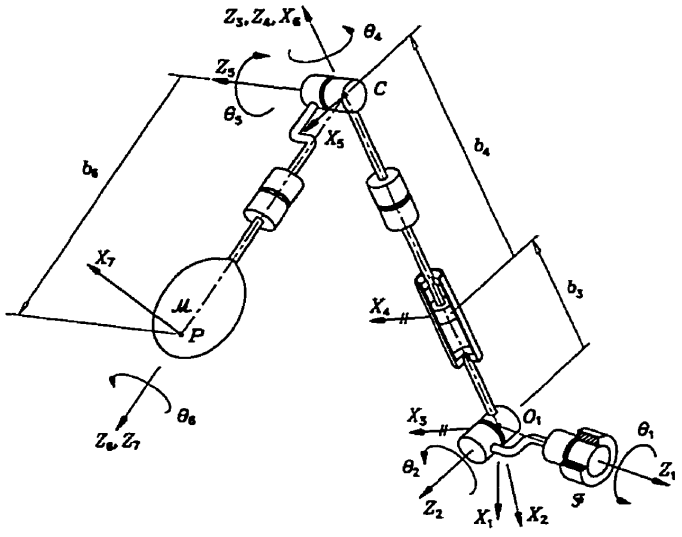

FIGURE 2.3. Leg architecture of the *UPS*-SGP (courtesy of Prof. J. Angeles).

If the platform and base points are all coplanar and if the motion is restricted to the plane of these points, the SGP loses at least three DOF. Three of the legs, and hence, three pairs of platform-base points, along with three joints in each of the legs become redundant. Thus, the general PSGP can be viewed as three arbitrary points in a particular plane that move relative to three arbitrary points in another plane,

parallel to the first. For the planar analogue of the UPS-SGP, the base U-pairs and platform S-pairs become R-pairs whose rotation axes are perpendicular to the plane of motion. The moving platform can be connected to the fixed base by three variable length legs. Each leg can be modelled as a simple kinematic chain.

Indeed, the only lower pairs used in planar mechanisms are R- and P-pairs. This, together with the fact that PSGP have only three legs with three joints each, suggests that the complexity of the kinematic analysis of these platforms should be, more or less, independent of architecture. This is not the case, as yet, for SGP. For instance, the FK problem of a SGP type platform with six 6-R legs is computationally prohibitive [**8**].

It is to be seen in the literature, [**43, 76, 77, 81, 101**] for example, that general SGP are topologically symmetric. That is, the platform is connected to the base by six identical kinematic chains. Moreover, the actuated joint in each chain is the same. In this sense the *general* PSGP shall be considered as topologically symmetric, but with three legs of arbitrary though identical architecture. This symmetry, however, does not necessarily include link lengths and offset angles.

2.6. Classifying Lower Pair PSGP Using Characteristic Chains

2.6.1. Characteristic Chains. The possible combinations of R- and P-pairs constraining the independent open kinematic chains, consisting of successions of three joints starting from the fixed base, in a PSGP are [**34, 100**]:

$$RRR,\ RPR,\ RRP,\ RPP,\ PRR,\ PPR,\ PRP,\ PPP.$$

We must, however, exclude the PPP chain because no combination of pure planar translations can cause a change in orientation. Moreover, there are a maximum of two independent translations in the plane, hence a PPP chain has at most two DOF.

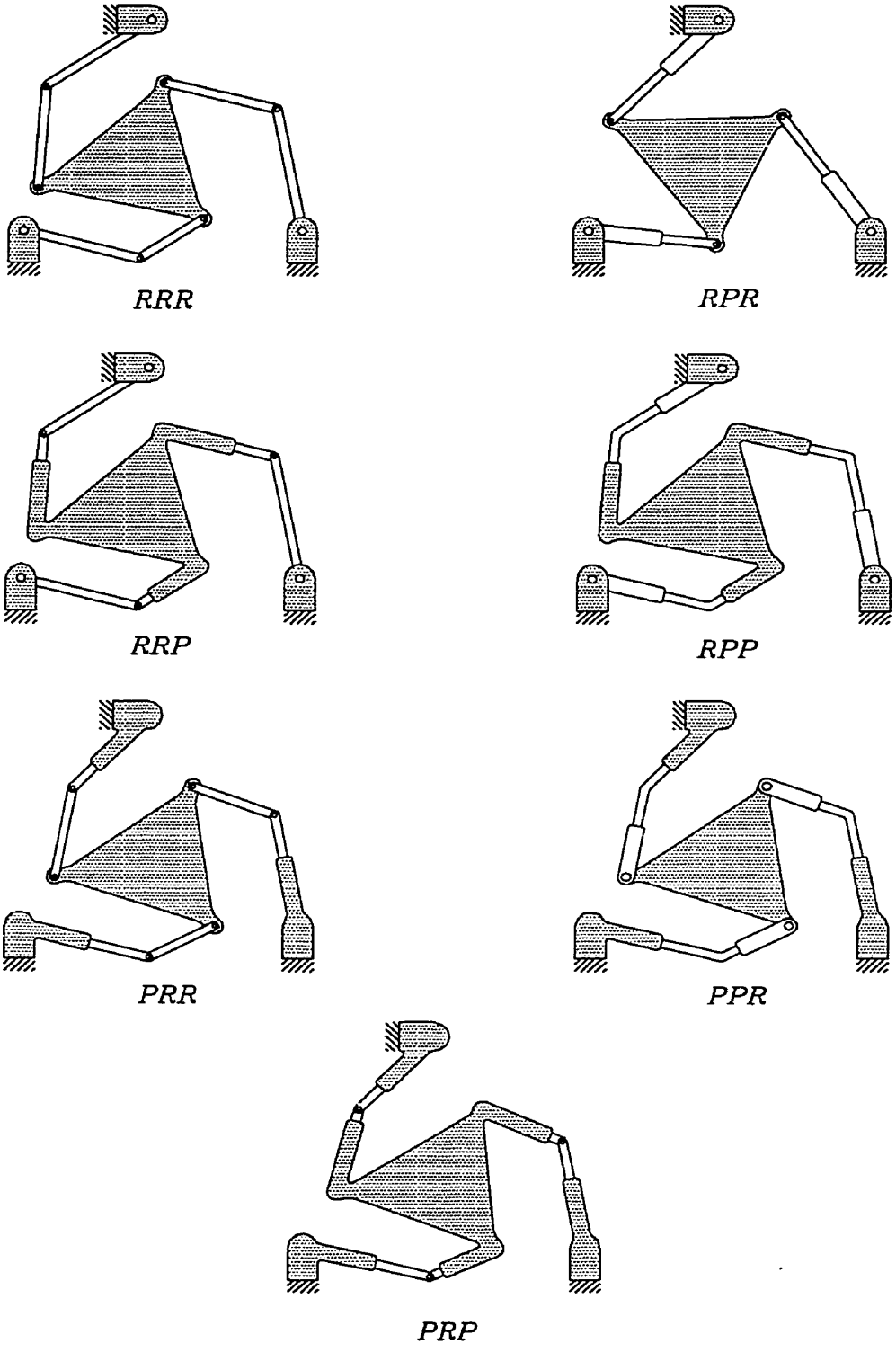

FIGURE 2.4. The seven possible topologies for the PSGP.

Since this is less than the required three, a symmetric platform consisting of three PPP legs can not be considered as a PSGP by our definition. Thus, there are seven possible PSGP topologies, illustrated in Figure 2.4, each characterised by one of the seven allowable simple chains. They are referred to as *characteristic chains.*

It is important to note that in order for legs containing two P-pairs to possess three DOF it is necessary for the two translation directions to be non-parallel.

2.6.2. Characteristic Passive Sub-chains. The leg actuation scheme controls the three DOF of the moving platform. The active joint in a leg shall be identified with an underscore. Since any one of the three joints in any of the seven characteristic chains may be actuated there are twenty-one possible topologically symmetric PSGP.

When the value of the activated joint coordinate is specified, the joint is locked and may be effectively removed from the characteristic chain. Examining Figure 2.4 it is to be seen that the resulting passive sub-chain is one of only four types: either RR, PR, RP, or PP. These are called *characteristic passive sub-chains.* However, PP-type architecture must be rejected as not useful [**100**] because such a platform either moves uncontrollably or is not assemblable when the actuated joint variables are specified, see Section 7.2.3. This reduces the number of possible PSGP to eighteen. They are listed, according to characteristic passive sub-chain, in Table 2.2.

RR-type	PR-type	RP-type
$\underline{R}RR$	$\underline{R}PR$	$\underline{R}RP$
$R\underline{R}R$	$P\underline{R}R$	$R\underline{R}P$
$RR\underline{R}$	$PR\underline{R}$	$RP\underline{R}$
$\underline{P}RR$	$\underline{P}PR$	$\underline{P}RP$
$R\underline{P}R$	$P\underline{P}R$	$R\underline{P}P$
$RR\underline{P}$	$PR\underline{P}$	$RP\underline{P}$

TABLE 2.2. The 18 possible PSGP.

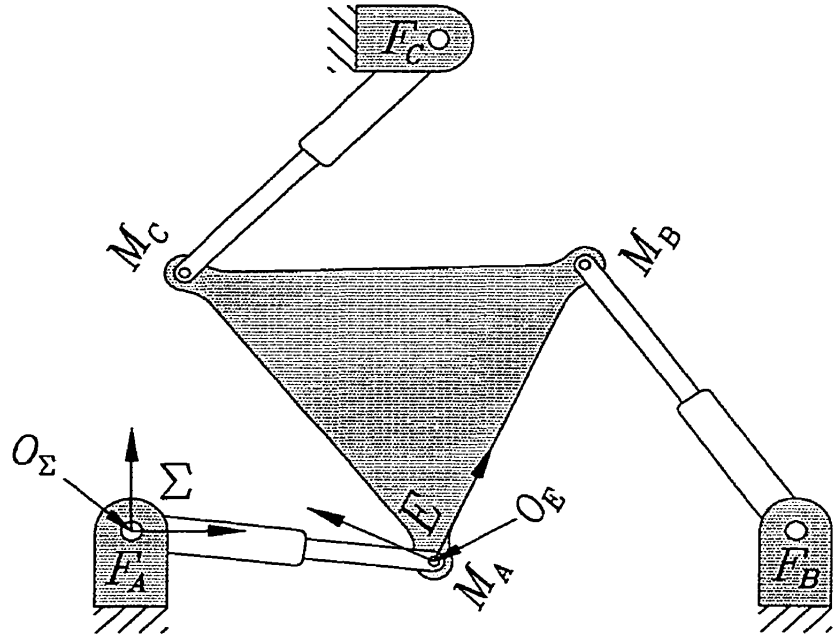

FIGURE 2.5. Reference frames and points if base and platform joints are R-pairs.

2.7. Manipulator Descriptions

The planar platforms considered in this thesis can be represented as complex kinematic chains consisting of three closed sub-chains (F_AF_B, F_AF_C, F_CF_B), as in Figure 2.5, for instance. In general, they consist of seven articulated rigid elements which move with constrained relative motion, all grounded to a rigid fixed base. These eight members are joined by combinations of nine lower R- and P-pairs. The three simple kinematic sub-chains connecting the base to the platform, here termed *legs*, each contain two intermediate links. No PSGP leg is joined exclusively with P-pairs.

2.7.1. Lower-Pair PSGP Reference Frames and Points. To geometrically describe a PSGP six arbitrary points, three in each of two arbitrary reference frames, must be defined. It is convenient to represent the displacements of the moving platform with respect to the base by describing the pose of a reference frame attached to the platform in a stationary reference frame fixed to the base. Referring to Figure

2.5 the fixed base and the moving platform frames are orthogonal and right-handed. They are labelled Σ and E, respectively. Each of the three legs are identified as A, B and C. Figure 2.5 illustrates an RPR platform, but the reference frames together with the fixed and moving points are labelled identically for all eighteen PSGP. The moving platform is defined by the triangle whose vertices are M_i, $i \in \{A, B, C\}$, while the fixed base is defined by the triangle whose vertices are F_i, $i \in \{A, B, C\}$. Figure 2.6 illustrates both triangles, the sides of the fixed one shown as dashed lines. The three fixed base points are coupled to the three moving platform points by identical kinematic sub-chains.

The manipulator parameters[5] that are independent of topology are the locations of the origins of frames Σ and E, indicated by O_Σ and O_E, along with those of the three fixed base points and those of the three moving platform points. Selection of these origins and points requires some elaboration. Each of the three legs are connected to the base by either revolute or prismatic joints. If the base joints are revolutes, as in Figure 2.5, the three fixed base points are selected to be the centres of the three base R-pairs. These are the piercing points of the revolute axes with the platform plane of motion. Then O_Σ is chosen to be incident on F_A so that the Cartesian coordinates of $F_{A/\Sigma}$, *i.e.*, the coordinates of F_A in frame Σ, are $(0, 0)$. The basis directions of reference frame Σ are chosen such that $F_{B/\Sigma} = (B_1, 0)$. That is, the orientation of Σ is selected so that F_B is on the positive x_Σ-axis. The Cartesian coordinates of $F_{C/\Sigma} = (C_1, C_2)$ are then, generally, nonzero.

Normally the F_i are expressed in terms of the coordinates in Σ. Points in Σ have Cartesian coordinates represented symbolically by the uppercase letter pairs (X, Y) and homogeneous coordinates by the triples of ratios $(X : Y : Z)$. Platform points

[5]It is important to emphasise that the kinematic analysis used herein is completely *independent of platform geometry*. Therefore, the choice of coordinate reference frames is irrelevant. We select the ones that simplify the computations.

M_i are typically expressed in both frames, Σ and E. Their coordinates in E are indicated symbolically by lowercase letter pairs (x, y) and homogeneous coordinates by the triples of ratios $(x : y : z)$. It is worthwhile to point out that the forward kinematics problem reduces to finding $M_{i/\Sigma}$ given $M_{i/E}$, $F_{i/\Sigma}$ and the active joint inputs. Moreover, the inverse kinematic problem involves determining the active joint inputs given the $M_{i/\Sigma}$.

If the platform joints are R-pairs, an identical procedure is followed to select the location for O_E, the orientation of E and the coordinates of $M_{i/E}$, $i \in \{A, B, C\}$. The centre of the platform R-pair in leg A is taken to be both O_E and M_A. The remaining two points, M_B and M_C, are chosen analogously to F_B and F_C, giving: $M_{A/E} = (0, 0)$; $M_{B/E} = (b_1, 0)$; $M_{C/E} = (c_1, c_2)$.

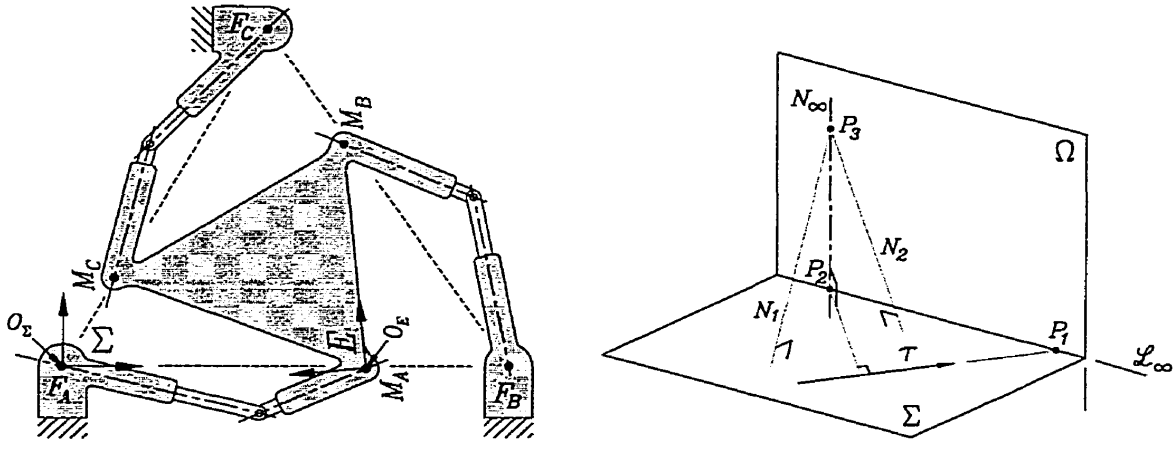

FIGURE 2.6. Reference frames and points where platform joints are P-pairs; axis associated with a particular P-pair.

Considering the alternate situation, if the base joints and/or platform joints are P-pairs, as illustrated by Figure 2.6, the procedure seems to become less straightforward. This is partly because it does not make sense, from a mechanical engineering point of view, to speak of the axis of a prismatic joint. These joints permit translations parallel to one direction. One such translation, indicated by τ, is shown in Figure

2.6. Mathematically, the axis of a prismatic joint could be described as the line at infinity, N_∞, of all planes normal to the direction of τ. This is illustrated in Figure 2.6, where Σ is the plane containing the P-pair, τ is a particular translation effected by the P-pair, N_1 and N_2 are normals to Σ, and Ω is the plane at infinity. The two planes Σ and Ω intersect in $\mathcal{L}_\infty$. Lines in the direction of τ intersect $\mathcal{L}_\infty$ in the point P_1. Lines normal to τ in plane Σ, indicated by η, intersect $\mathcal{L}_\infty$ in the point P_2. The line N_∞ is the intersection of all planes normal to Σ and parallel to η. Moreover, all normals to Σ, N_1 and N_2 being two of them, intersect N_∞ in the point P_3. The join of P_2 and P_3 is N_∞, which is the axis of the particular prismatic joint. In other words, the axis of a P-pair is the absolute polar line to the point at infinity of the direction of translation.

Regardless, P-pairs would be impossible to manufacture if they had no longitudinal axis of symmetry to establish the direction of translation, *i.e.*, no longitudinal centre line. We will use these centre lines to establish relevant F_i (ankle), K_i (knee) and M_i (hip) points. One must not confuse this centre line with the joint axis, which is, for mechanical reasons, inaccessible.

The process for selecting the origins and reference points is identical to the R-pair case with the exception that O_Σ and O_E are selected to be *any* convenient points on the appropriate centre lines. The basis directions of Σ and respective base points are selected so that their coordinates are : $F_{A/\Sigma} = (0, 0)$; $F_{B/\Sigma} = (B_1, 0)$; $F_{C/\Sigma} = (C_1, C_2)$. Meanwhile, the basis directions of E and respective platform points are selected so that their coordinates are : $M_{A/E} = (0, 0)$; $M_{B/E} = (b_1, 0)$; $M_{C/E} = (c_1, c_2)$. Figure 2.6 illustrates a PRP platform showing the centre lines and the respective reference frames and points. For topologically asymmetric fully-parallel three-legged planar manipulators the appropriate procedure is followed leg-by-leg depending on whether the relevant joints are revolutes or prismatics.

2.7.2. PSGP with Holonomic Higher Pairs. A novel RR-type platform containing active holonomic G-pairs shall now be introduced. It is described by an $RR\underline{G}$ characteristic chain, illustrated in Figure 2.7. Because of the special topology extra attention is given to its description. It is based on the design proposed by Agrawal and Pandravada in [**3, 4**], wherein the kinematics of two $2R$ links manipulating a disk in the plane are examined. When tangential contact is maintained between the disk and legs it is an $RRGGRR$ single loop platform. When a third $2R$ leg is added and the G-pairs are active, the result is a special RR-type platform, provided tangential contact is maintained.

The circular disk rolls without slip on each of the three lines tangent to it. This rolling system is modelled as a pinion meshing with three racks. Each of the three legs, A, B and C, connect a rack to a base point via two R-pairs. A rack is rigidly attached to the disk end of each second link. The racks are constrained to remain in contact with the pinion. Tangential contact can be maintained mechanically using passive joints [4], the higher pairs can then be activated via a transmission with no additional active joints. The group of motions associated with G-pairs has the same dimension as those of R- and P-pairs: $\dim(\mathcal{G}) = 1$.

What really distinguishes this manipulator from PSGP, which are jointed exclusively with lower pairs, is that the initial assembly configuration (IAC) of the platform *must* be included in the analysis due to the roll-without-slip condition. If only displacements are considered, then any IAC may be used as the *reference position.* Activating the higher pairs gives some control over the relative rolling which is essential for the kinematic analysis presented herein. Moreover, this means it may be considered as an RR-type PSGP, although a special one.

The R-pairs connecting two links in a leg are referred to as *knee joints* K_A, K_B, K_C, and are constrained to move on circles centred on the three fixed points F_A, F_B, F_C.

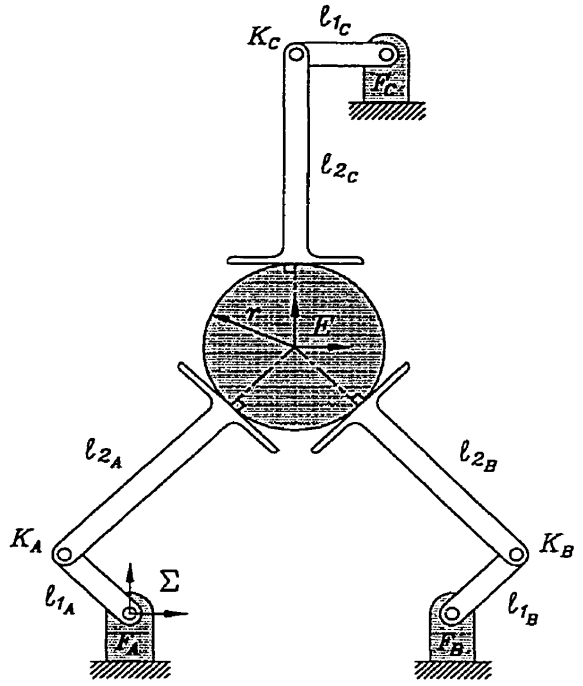

FIGURE 2.7. A PSGP with holonomic higher pairs.

The position and orientation of the pinion are described by reference frame E, which has its origin on the disk centre and moves with it. Frame Σ has its origin at the base of leg A and is fixed. In the reference position shown in Figure 2.7, the basis directions of E and Σ are identical.

The three fixed base points are the centres of the three base R-pairs (see Figure 2.7). However, the three platform points are the points of contact between the pinion and racks. The platform points are not fixed relative to each other, but change from pose to pose. It will be seen that the variable platform points are not problematic and that the kinematic analysis is essentially the same as for any RR-type platform.

2.7.3. Special Geometric Properties. This mechanical system has some interesting geometric properties which lead to some unique practical applications. The general motion of the disk in the plane involves relative motion between the disk and each serial 2R leg. Each rack can roll on the pinion, the pinion can roll on the

racks, or there can be a combination of the two motions. For general planar motion the system, illustrated in Figure 2.7, has the following properties:

(1) If the pinion rolls on one rack, then it must roll on all.

(2) As a consequence of (1) if one of the higher G-pairs is locked the pinion can not rotate about its centre.

(3) Any, or all of the racks may roll on the pinion.

(4) Consider leg A, for example. Suppose that its higher pair is locked but the other two are not. During a general motion, the pinion will be stationary with respect to rack A while the other racks are free to roll on the pinion. Then there are two possibilities:

   (a) If the relative angle between ℓ_{1_A} and ℓ_{2_A} changes, the motion of the pinion is either a translation, or a rotation about a centre other than its own axis by an angle equal to the change in angle of ℓ_{2_A} measured in Σ.

   (b) If the relative angle between ℓ_{1_A} and ℓ_{2_A} is constant during the motion, then the pinion rotates about the leg base by an angle equal to the change in the angle between ℓ_{1_A} and Σ. Regardless, in both cases there can be no rotation of the disk about its centre, since one of the higher pairs is locked. Such a motion would violate (2).

(5) Let $\Delta\tau_i$, $i \in \{A, B, C\}$, be the change in rack tangent angle in a particular leg with counter clock-wise rotation considered positive. If $\Delta\tau_A$ has the same magnitude but opposite sense as either $\Delta\tau_B$ or $\Delta\tau_C$, then the motion of the pinion is pure rectilinear translation of its centre. Pure curvilinear translation can also occur if the magnitude condition is violated however, the opposite sense condition must be met.

(6) If $\Delta\tau_A$, $\Delta\tau_B$, and $\Delta\tau_C$ have the same magnitude and sense, then the motion of the pinion is pure fixed axis rotation about its centre.

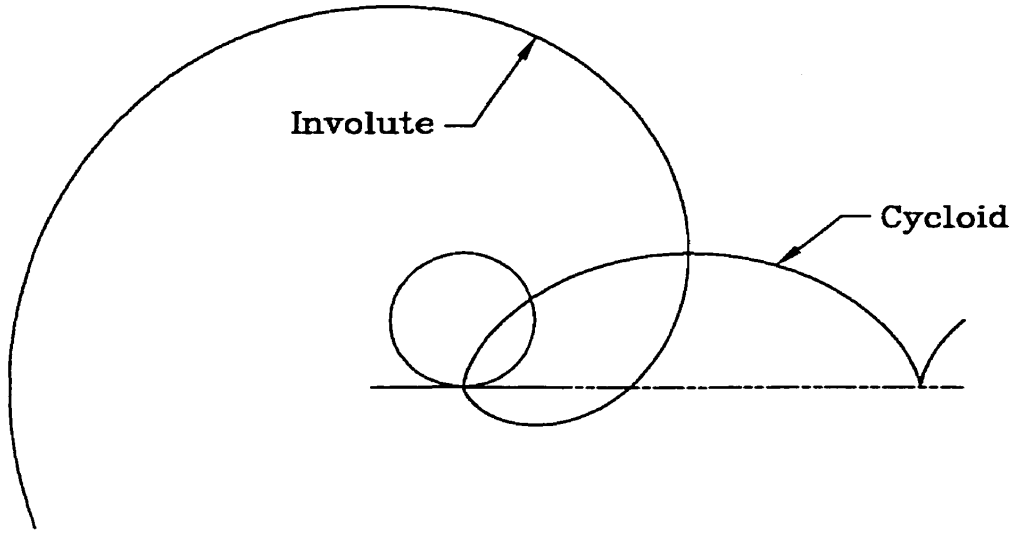

FIGURE 2.8. A cycloid and an involute of a disk.

The the relative rolling between rack and pinion pairs also leads to an interesting observation. Consider the following two curve definitions, see Figure 2.8:

(1) **Cycloid:** Locus of a point on a circle that rolls without slip on a line.

(2) **Involute:** Locus of a point on a line that rolls without slip on a circle.

These two definitions tell us that the circle and line are kinematic inversions, or duals, since each definition can be obtained from the other simply by exchanging the words *circle* and *line*. This may seem like a trivial observation, but it turns out to be of some importance for the classification of constraint-related surfaces in a quasi-elliptic geometry, to be discussed later, in the following sense: a model of the elliptic plane is the surface of a sphere on which straight lines are taken to be great circles.

2.7.4. Tangency Condition. By virtue of the pure rolling constraints, the straight lines along which the disk rolls must always remain tangent to the disk. Consider a line and a circle in the Euclidean plane. The equation of the line can be

represented by the linear equation

$$ax + by + c = 0, \tag{2.7}$$

for constant coefficients a, b, c, and variable points (x, y). A circle with centre (x_c, y_c) and radius r is given by

$$(x - x_c)^2 + (y - y_c)^2 - r^2 = 0. \tag{2.8}$$

Equation (2.7) can be solved for y to give the familiar slope-intercept form of the line, and the expression is substituted into Equation (2.8). The result is expanded in powers of x which yields a quadratic:

$$Ax^2 + Bx + C = 0, \tag{2.9}$$

where:

$$\begin{aligned} A &= \frac{a^2}{b^2} + 1, \\ B. &= 2\left(-x_c + \frac{ac}{b^2} + \frac{ay_c}{b}\right), \\ C &= x_c^2 - r^2 + ((c/b) + y_c)^2. \end{aligned}$$

To satisfy the tangency condition, the discriminant of the quadratic must vanish:

$$\sqrt{B^2 - 4AC} = 0.$$

The discriminant itself is a quadratic in terms of the constant a:

$$(x_c^2 - r^2)a^2 + (c + by_c)2x_c a + (b^2 y_c^2 - b^2 r^2 + 2bcy_c + c^2) = 0. \tag{2.10}$$

This condition is necessary, but not sufficient to guarantee pure rolling contact. However, all solutions to the FK and IK problems must satisfy this condition. FK and IK algorithms can use this condition as a check on the validity of solutions.

2.8. Applications for *RRG*-Type Platforms

The applications for *RRG*-type platforms are a super-set of those of the lower pair jointed PSGP. That is, they are essentially the same with some notable additions. Because of its ability to grasp objects while rotating them it can be used for accurate centring operations. For example, it could be designed to replace a standard four-jaw chuck in lathe turning operations, thus eliminating costly set-up time. The details of the forced tangential contact could be set such that rack could disengage from the pinion in a controlled manner allowing for a reachable workspace with dynamic boundaries. The *RRG*-type platform could also be used in situations requiring adjustable, variable coupler length four-bar mechanisms that can be changed to Grashof, change-point, or non-Grashof kinematics. Not only can the coupler curve shape parameters be adjusted, the curve itself can be made uni- or bicursal, to suit the needs of the design at hand. This makes for some welcome flexibility regarding function generation, rigid body guidance and path generation synthesis problems [**68**].

Changing the rack tangent angles changes the assembly configuration of the platform. Each distinct set of inputs yields a distinct set of distances between the knee joints. Referring to Fig. 2.7, we can lock the racks in two legs so that there is a desired distance between corresponding knee joints. With no loss in generality we can select legs A and B. Since two of the actuators are locked, the platform loses 2 DOF. Furthermore, the ungrounded links in legs A and B, together with the pinion are a temporary rigid body with an effective length corresponding to the distance between the two knee joints K_A and K_B. The resulting four-bar mechanism (see Figure 2.9) can be driven with rack C. If the link lengths are suitably chosen, it will be a *convertible Grashof-Change-Point-Non-Grashof* mechanism.

Fig. 2.9 illustrates the most general situation, where the grounded links in legs A and B have different lengths. Cases (*i*) through (*iii*) show the mechanisms that

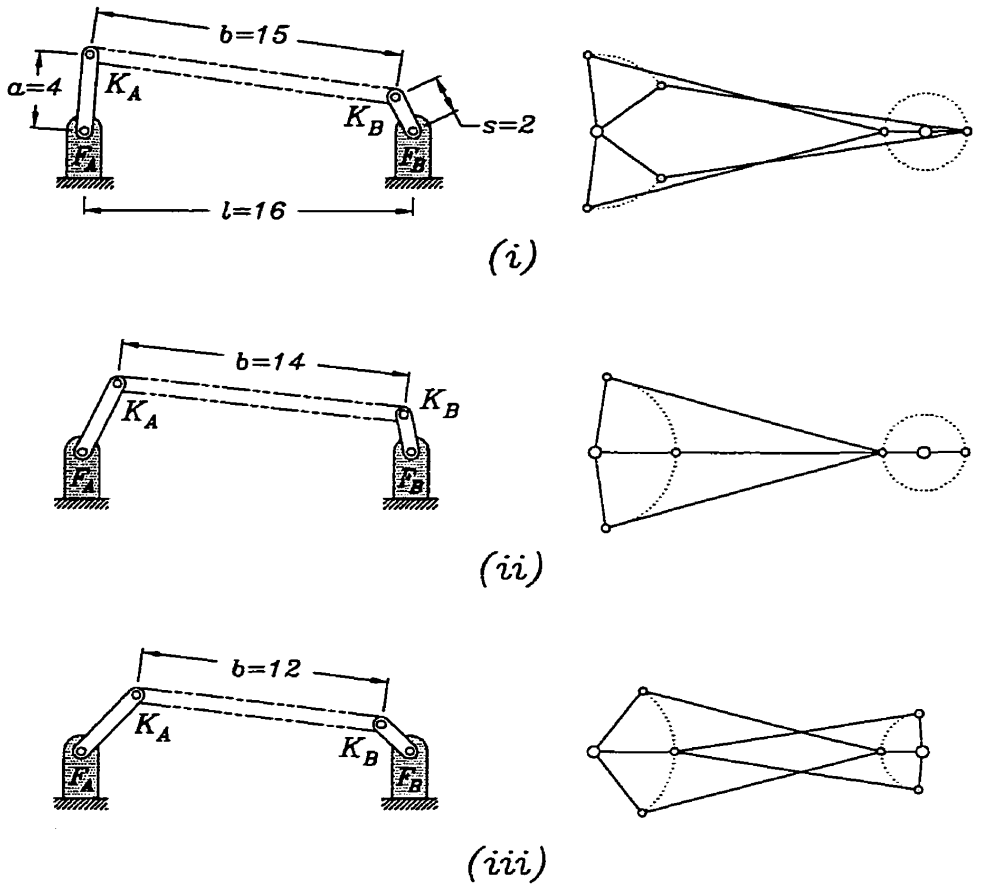

FIGURE 2.9. Application to planar four-bar mechanisms: (*i*) Grashof; (*ii*) change-point; (*iii*) non-Grashof. The excursion arcs and singular positions of the small and large arm crank pins for each of the three cases are shown on the right.

result as the effective coupler length, b, given in generic units, varies between 15, 14, and 12. The other lengths are constant: $\ell = 16$, $s = 2$, and $a = 4$. The sum of the longest (ℓ) and shortest (s) link lengths is less than, equal to, and greater than the sum of the other two (a and b) giving Grashof, change-point, and non-Grashof mechanisms, respectively [**110**].

(*i*) Lengths: $\ell = 16$, $s = 2$, $a = 4$, $b = 15$

$$l + s = 18 \quad < \quad a + b = 19$$

$$\Rightarrow \text{ Grashof crank-rocker.}$$

(*ii*) Lengths: $l = 16$, $s = 2$, $a = 4$, $b = 14$

$$l + s = 18 \quad = \quad a + b = 18$$

$$\Rightarrow \text{ Change Point.}$$

(*iii*) Lengths: $l = 16$, $s = 2$, $a = 4$, $b = 12$

$$l + s = 18 \quad > \quad a + b = 16$$

$$\Rightarrow \text{ Non-Grashof double rocker.}$$

Recall the characteristics of these three variants of a four-bar mechanism: a Grashof mechanism can be a crank-crank, crank-rocker, or double-rocker mechanism, depending on which link is fixed; whereas all inversions of a non-Grashof mechanism are double-rockers. As a reminder, the excursion arcs and singular positions of the small and large arm crank pins for each of the three cases are shown on the right of Figure 2.9. For this application the link lengths in the driving leg, C, and the disk radius are unimportant provided they allow for the desired coupler lengths and output error tolerance.

2.9. Nomenclature and Link Reference Frames

One of the main contributions of this thesis is the derivation of a single univariate polynomial whose zeros represent the solutions to the FK problem for every PSGP, as defined in Section 2.5. The single variable is a special displacement parameter in a certain kinematic image space. The coefficients of the polynomial are products of the design constants and input variables, which have a fixed, constant value for any given pose of the manipulator. Care must be taken to use *portable* notation. That is, notation that can be unambiguously used to fully describe *any* PSGP, regardless of topology, in order that the univariate can be used in the kinematic analysis.

2.9.1. Position Vectors. Position vectors shall, in general, be described with lowercase bold letters. The points they represent shall be described with the corresponding uppercase letter. For instance, consider the knee joint:

- Point: K.
- Homogeneous point coordinates: $(K_x : K_y : K_z)$.
- Position vector: $\boldsymbol{k}$.

2.9.2. Platform Pose Variables. The *pose* of the platform is described by the position of the moving frame E, together with its orientation, all expressed in the fixed frame Σ, see Figure 2.10.

- (a, b) are the Cartesian coordinates of the origin of E in Σ, $O_{E/\Sigma}$.
- φ is the orientation expressed as the angle between the x- and X-axis, the positive sense being counterclockwise.

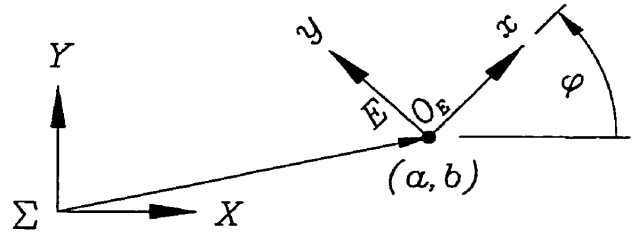

FIGURE 2.10. Platform pose variables.

2.9.3. Link Reference Frames. Link reference frames are, with the exception of Σ, E and R (discussed below), in the case of $RR\underline{G}$ platforms, assigned using the well known procedure developed by Denavit and Hartenberg [**39**] and elaborated on by Angeles [**8**] and Craig [**33**]. These frames are usually called D-H reference frames. D-H frames are usually assigned so that D-H parameters can be used to characterise a manipulator. Since all platforms dealt with herein are planar, neither are really required. Regardless, the D-H frames are assigned because the procedure

is well defined, systematic and well known. Moreover, if this work is to be extended to non-planar platforms, the D-H frames will likely be used. For all PSGP, the fixed base, and the fixed frame at the leg attachment point (the fixed base point F_i) are enumerated as link 0 and frame 0, respectively. The orientation of frame 0 in each leg is arbitrary, and is selected to be parallel to the fixed base frame Σ. Thus, the base reference frame in each leg is indicated simply by Σ. The platform, and the moving frame at the attachment point (the moving platform point M_i) are enumerated as link 3 and frame 3, respectively. The orientation of these frames is selected to be parallel to the moving platform frame E. Similarly, the platform reference frame in each leg is indicated by E. The intermediate links, and their frames, are enumerated as 1 and 2 in each leg. The frames are, of course, fixed relative to the link they represent. The D-H frames for leg A in an RRR manipulator are shown in Figure 2.11 (i).

Figure 2.12 (i) shows the D-H reference frames for leg B in an RPR platform. Frames 0 (Σ) and 3 (E) have their origins on the base and platform R-pairs. The origin of frame 1 is incident with the origin of frame 0 (indicated by Σ), but moves with the base revolute. The origin of frame 2 is incident with the origin of frame 3 (indicated by E), but moves with the platform revolute.

When the base joints are prismatic the basis directions of frame 1 depend on the angle between the X-axis and the direction of translation (represented as the centre line of the P-pair). This is called the *angular offset* of the particular frame with respect to frame 0 (Σ). A similar angular offset occurs when the platform joints are P-pairs, except they are described in terms of the platform frame E. The angular offsets are shown for leg B of a PRP manipulator in Figure 2.13.

The D-H reference frame assignment procedure is only valid for kinematic chains whose joints are all lower pairs [**39**]. To define the G-pair reference frames a variation on the procedure in [**65**] is used. This involves taking the *axis* of the G-pair to

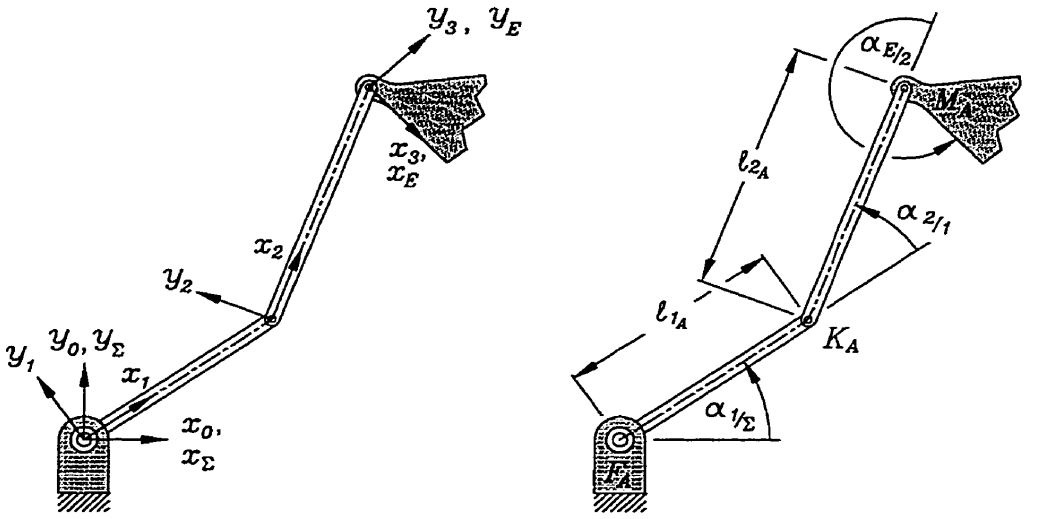

FIGURE 2.11. (*i*) D-H reference frames in an *RRR* platform: leg *A*; (*ii*) joint parameters.

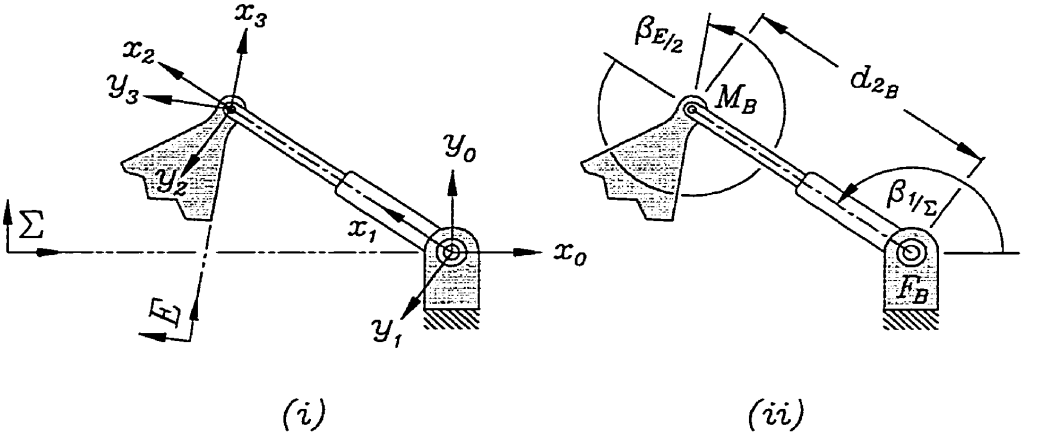

FIGURE 2.12. (*i*) D-H reference frames in an *RPR* platform: leg *B*; (*ii*) joint parameters.

be normal to both the direction of translation of the pinion centre relative to the corresponding rack and to the plane of motion. The positive sense of this axis, defined as the z-axis of a three dimensional Cartesian reference frame, is out of the page. If the y-axis points towards the pinion centre, the x-axis direction is assigned to complete a right-handed reference frame. Two frames are assigned in this way: the *rack-fixed* frame R and the rack frame 3 that translates with the contact point along

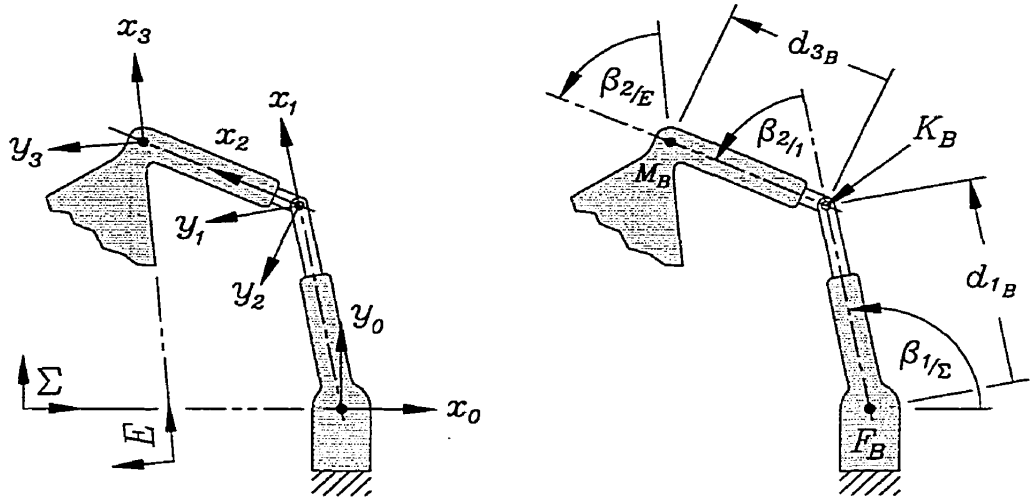

FIGURE 2.13. (*i*) D-H reference frames in an PRP platform: leg B; (*ii*) joint parameters.

the rack. The origin of R, indicated by O_R, is on the contact point between rack and pinion when the platform is in its *reference position* (see Figure 2.14 *(i)* and 2.7 showing the reference position used throughout this thesis), which can always be used as a feasible IAC. Thus, it is selected to be that position where the distance between O_E and O_2 is minimum in each leg. Figure 2.14 shows the frame assignments for leg C in an $RR\underline{G}$ manipulator. It is important to note that for the $RR\underline{G}$ platforms the basis directions of E and Σ are parallel in the reference position shown in Figure 2.7, but reference frame 3_i is, in general, not parallel to E.

2.9.4. Fixed Link Design Parameters.

- ℓ_{i_j} is the length of link i, $i \in \{1,2\}$, in leg j, $j \in \{A,B,C\}$. See Figures 2.7 and 2.11 *(ii)*, for example.
- $\alpha_{i/j}$, $\beta_{i/j}$, $\gamma_{i/j}$, $i,j \in \{\Sigma,1,2,E\}$ $i \neq j$, are the angular offsets of P-pair reference frame i with respect to reference frame j for legs A, B, C, respectively. See Figure 2.13.

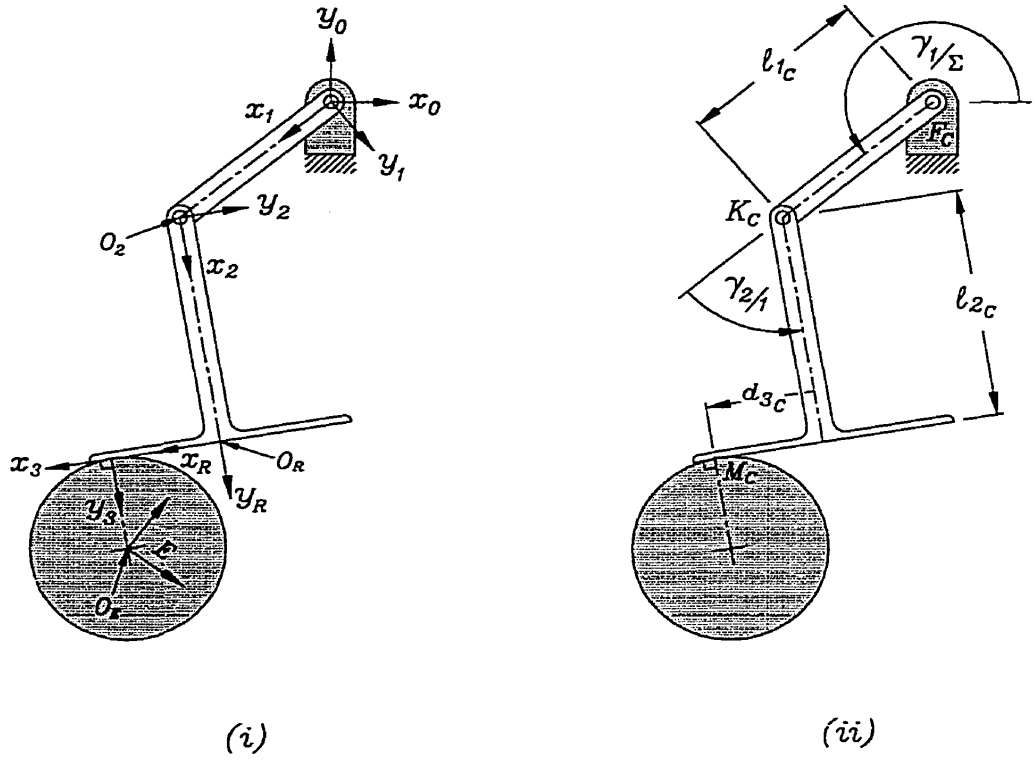

FIGURE 2.14. (*i*) D-H reference frames in an $RR\underline{G}$ platform: leg C; (*ii*) joint parameters.

- r is the radius of the disk in $RR\underline{G}$ platforms, see Figure 2.7.

2.9.5. Joint Variables.

- d_{i_j} is the length of prismatic joint i, $i \in \{1,2,3\}$, in leg j, $j \in \{A,B,C\}$, examples are illustrated in Figures 2.12 and 2.13. It is also used to describe the change in contact point along the rack for the higher pairs in $RR\underline{G}$ platforms, see Figure 2.14 .
- $\alpha_{i/j}$, $\beta_{i/j}$, $\gamma_{i/j}$ are the joint angles of link i with respect to reference frame j, $i,j \in \{\Sigma,1,2,E\}$, $i \neq j$, for legs A, B, C, respectively. Examples are shown in Figures 2.11-2.14. These are the same symbols used to describe fixed joint angular offsets, however both the context (*i.e.*, leg type) and the subscripts should eliminate any confusion.

The three variable joint angles for leg A of an RRR manipulator are illustrated in Figure 2.11 (*ii*). The angles shown are $\alpha_{1/\Sigma}$ (which is identical to $\alpha_{1/0}$), $\alpha_{2/1}$ and $\alpha_{E/2}$ (which is identical to $\alpha_{3/2}$), which represent the relative angles that the x_1-, x_2- and x_E-axes (or x_3-axes) make with the x_Σ- (or x_0-), x_1- and x_2-axes, respectively.

Figure 2.12 (*ii*) shows the three variable joint parameters for leg B of an RPR platform. The length d_{2_B} gives the distance between the origin of frame 2 and the origin of frame 1. The angles $\beta_{1/\Sigma}$ and $\beta_{E/2}$ give the relative angles of the x_1- and x_E-axes measured against the x_Σ- and x_2-axes, respectively. The PRP platform, shown in Figure 2.13 *(ii)*, illustrates the variable prismatic lengths d_{1_B} and d_{2_B} together with the variable revolute angle, $\beta_{2/1}$, and the two P-pair angular offsets, $\beta_{1/\Sigma}$ and $\beta_{2/E}$. The $RR\underline{G}$ platform, in Figure 2.14 *(ii)*, shows the two variable angles, $\gamma_{1/\Sigma}$ and $\gamma_{2/1}$. Also shown is the position of the contact point between the pinion and rack measured relative to its reference position.

If a leg possesses an intermediate R-pair it will be called a *knee joint* and labelled K_i, $i \in \{A, B, C\}$. Completing the anthropomorphism, the M_i platform points will occasionally be referred to as *hip* points, and the F_i as *ankle* points.

2.10. Mobility Analysis

Any planar platform connected to three grounded legs, each joined with three independent 1 DOF joints can be characterised in the following way: each leg contains two intermediate links between the base and platform, giving a total of 8 links. The 9 joints are either R- or P-pairs (or G-pairs for the $RR\underline{G}$-type legs), each imposing 2 constraints. Under the condition that no one leg is joined exclusively with P-pairs, it can be shown that the dimension of the associated sub-group is $d = 3$. Using the CGK formula, Equation (2.6), gives

$$3(8-1) - 9(2) - 0 \;=\; 3 \text{ DOF}. \tag{2.11}$$

It is worthwhile to note that the platform has 3 DOF regardless of the number of grounded 2-link legs to which it is connected by R- and P-pairs (or G-pairs, as the case may be). The proof is obtained by showing the left hand side (LHS) of Equation (2.6) is always equal to 3.

For ℓ links and j joints Equation 2.6 may be re-expressed as:

$$3(l-1)-2j = \text{DOF}, \tag{2.12}$$

since each joint removes two DOF. The base and platform always count as two links and each of the n legs contains two intermediate links. Thus for n legs the number of links is

$$l = 2n+2. \tag{2.13}$$

Furthermore, each leg has three joints, so:

$$j = 3n. \tag{2.14}$$

Substituting Equations (2.13) and (2.14) into the LHS of Equation (2.12) gives

$$3(2n+2-1)-2(3n) \;=\; 6n+3-6n \;=\; 3 \tag{2.15}$$

Therefore, n can be any integer. Moreover, this result is valid for any arbitrary architecture of combinations of the 18 types of characteristic chains plus the $RR\underline{G}$-type.

CHAPTER 3

Kinematic Mappings of Displacements

In this chapter the geometric and algebraic tools used in the kinematic analysis of PSGP shall be discussed. Collectively, they are a fabric woven from fine threads contained in the great classic works of Plücker [**115, 116, 117, 118**], Grassmann [**54**], Klein [**89, 90**], Study [**138**], Grünwald [**57**], Blaschke [**14**], Sommerville [**135, 136**], and the relatively new, but nonetheless landmark, contributions of Bottema and Roth [**17**], De Sa [**36**], Ravani [**119**], Husty [**81, 83**].

It may be argued that the study of robot kinematics is essentially the study of isometry. Both are primarily concerned with the *group of Euclidean displacements*: $\mathcal{G}_6$ in E_3 and $\mathcal{G}_3$ in E_2. Since these concepts form the backbone of this thesis, some discussion is in order. The aim is to begin with general 3-D *Euclidean* displacements, and treat planar displacements as a special case of the former. Thus, it is to be hoped that the techniques employed in this thesis may then be generalised to spatial six DOF parallel platforms. The Isometry group was described in Section 2.4. The following sections will build on that discussion by recalling some pertinent concepts regarding projective, metric and non-metric geometries.

3.1. Homogeneous Coordinates

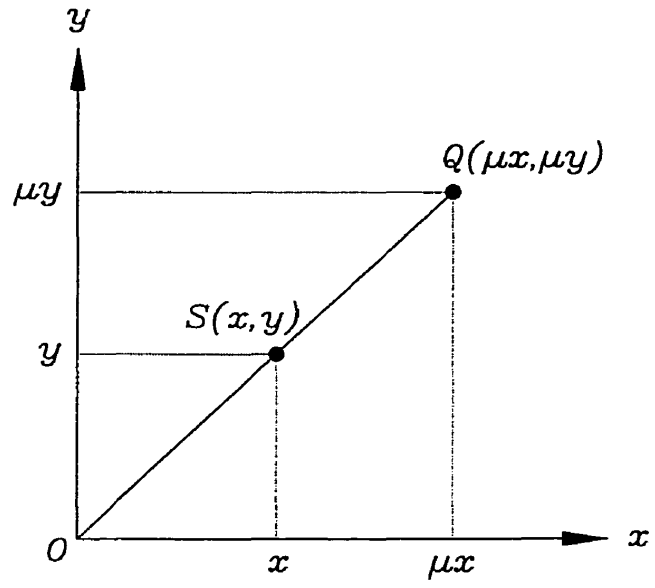

FIGURE 3.1. Cartesian coordinates in E_2.

Let O be the origin of the Cartesian coordinate system, shown in Figure 3.1. Let S be a distinct point in the plane. The ray passing through O and S is described by the coordinate pair (x, y). Another distinct point $Q \neq O$, on ray OS is described by the pair $(\mu x, \mu y)$, where $\mu \in \mathcal{R}$ (ie., a real number). As $\mu \to \pm\infty$ the seemingly meaningless pair (∞, ∞) is obtained [**126**].

To remedy this representational problem, the point pairs may be represented by two ratios, given by ordered triples (x_0, x_1, x_2). If $x_0 \neq 0$, then the point S can be uniquely described as:

$$x = \frac{x_1}{x_0} \quad , \quad y = \frac{x_2}{x_0}. \tag{3.1}$$

Then any triple of the form $(\lambda x_0, \lambda x_1, \lambda x_2)$ (for $\lambda \neq 0$) describes exactly the same point S. In other words, two real points are equal if the triples representing them are

proportional. This is because

$$\frac{\lambda x_1}{\lambda x_0} = \frac{x_1}{x_0} = x, \quad \text{and} \quad \frac{\lambda x_2}{\lambda x_0} = y.$$

The coordinates $(x_0 : x_1 : x_2)$ are called *homogeneous coordinates.* When $x_0 = 1$ the Cartesian coordinate pair (x, y) is recovered.

The Cartesian coordinates $(\mu x, \mu y)$, $\mu \neq 0$, of the family of points on the ray through Q in Figure 3.1 can be expressed in homogeneous coordinates as ratios:

$$(\mu x, \mu y) = (x_0 : \mu x_1 : \mu x_2) = (\frac{x_0}{\mu} : x_1 : x_2).$$

In E_2, as $\mu \to \pm\infty$ the homogeneous coordinates $(0 : x_1 : x_2)$ are obtained. There is no point on the line OS to which this triple can correspond because E_2 is unbounded. However, in the projective extension of the Euclidean plane[1] the triple $(0 : x_1 : x_2)$ describes the *point at infinity (ideal point)* on the line OS. Since the same triple is obtained regardless if $\mu \to +\infty$ or $\mu \to -\infty$, a unique point at infinity is associated with the line OS in E_2. Hence, an ordinary line adjoined by its point at infinity is a closed curve [**31**].

The triple $(0 : 0 : 0)$ describes neither an ideal point nor a real point on OS. $(x : y : 0) = (0 : 0 : 0)$ seems to imply that $S = O$, which is a contradiction in the construction of the ray OS. The trivial triple $(0 : 0 : 0)$ is therefore not included in the point set comprising the projective extension of E_2.

All lines in E_2 which are extended to their points at infinity have the homogenising coordinate $x_0 = 0$. The totality of all the existing points at infinity (with the exception of $(0 : 0 : 0)$) are described by $x_0 = 0$. The extended Euclidean plane which includes

[1]The *projective plane*, P_2, can be thought of as the Euclidean plane, E_2, to which the *line at infinity* has been added. The generalisation of this concept of *extension* is attributed to Herman Grassmann [**54**].

all the points at infinity is called the *projective plane* P_2. Since $x_0 = 0$ is a linear equation, it represents the *line at infinity.*

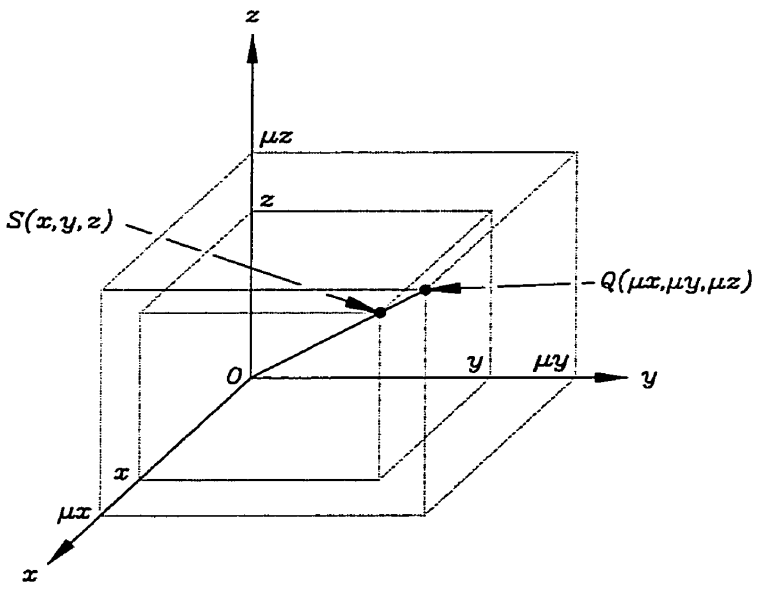

FIGURE 3.2. Cartesian coordinates in E_3.

Entirely analogous statements can be made for the 3-D Euclidean space, E_3. This space is covered by a Cartesian coordinate system with origin O and axes x, y, z. The axes are usually defined as orthogonal. Such an orthogonal Cartesian system is illustrated in Figure 3.2. The homogeneous coordinates $(x_0 : x_1 : x_2 : x_3)$ of the point $S \in E_3$ are defined as:

$$x = \frac{x_1}{x_0}, y = \frac{x_2}{x_0}, z = \frac{x_3}{x_0} \quad , \quad x_0 \neq 0. \tag{3.2}$$

As in two dimensional projective space, when $x_0 = 1$ the Cartesian coordinate triple (x, y, z) is recovered.

It should be noted that in general the choice of homogenising coordinate is arbitrary. Over the course of time the following conventions have developed.

(1) In North America and the British Commonwealth the homogenising coordinate is taken to be the last one. The coordinate indices begin with 1. In the plane, $(x_1 : x_2 : x_3)$ represent the coordinates of a point, with x_3 the homogenising coordinate. In space, a point is described with $(x_1 : x_2 : x_3 : x_4)$, x_4 being the homogenising coordinate. In general, the homogenising coordinate in an n-D space has the index $n + 1$.

(2) In Europe the first coordinate, given the index 0, is taken to be the homogenising one. Thus, x_0 represents the homogenising coordinate regardless of the dimension of the coordinate space.

Both conventions shall be employed henceforth. This is to underscore the idea that such a restriction is arbitrary and unnecessary in the context of projective geometry, discussed in Section 3.4. However, where required the homogenising coordinate shall be explicitly identified.

3.2. Duality

In the Euclidean plane a general line has the equation

$$Ax + By + C = 0, \tag{3.3}$$

where A, B and C are arbitrary constants defining the slope and intercepts with the coordinate axes. The x and y that satisfy the equation are points on the line. Using homogeneous coordinates this linear equation becomes

$$X_1x_1 + X_2x_2 + X_3x_3 = 0, \tag{3.4}$$

where the X_i characterise lines (*i.e.*, $X_1 = A$, $X_2 = B$, $X_3 = C$) and the x_i characterise points. Now Equation (3.3) is represented by an equation that is linear in the X_i as well as the x_i. Every term in Equation (3.4) is *bilinear*, or *homogeneously*

linear. This should explain the etymology of the term *homogeneous coordinates*. The X_i are substituted for the A, B and C to underscore the bilinearity and symmetry.

Equation (3.4) may be viewed as a locus of variable points on a fixed line, or as a pencil of variable lines on a fixed point. The X_i define the line and are hence termed *line coordinates*, indicated by the ratios $[X_1 : X_2 : X_3]$; whereas the x_i define the point and bear the name *point coordinates*, indicated by the ratios $(x_1 : x_2 : x_3)$. Note the distinction that line coordinates are contained in square brackets, [ ], while point coordinates have parentheses for delimiters, ( ). Equation (3.4) is a *bilinear* equation describing the mutual incidence of point and line in the plane. Thus, point and line are considered as *dual* elements in the *projective plane* P_2. The importance of this concept is that any valid theorem concerning points and lines yields another valid theorem by simply exchanging these two words [**11**]. For example, the proposition

(1) *Any two distinct points determine one and only one line*

is dualised by exchanging the words point and line giving a different proposition,

(2) *Any two distinct lines determine one and only one point.*

In space the mutual incidence of point and plane is given by the bilinear equation

$$X_1x_1 + X_2x_2 + X_3x_3 + X_4x_4 \;=\; 0, \tag{3.5}$$

where the x_i remain point coordinates, however the X_i are now *plane coordinates*, the dual elements of 3-D *projective space* P_3 being point and plane. Because of the duality, the roles of coefficient and variable are interchangeable. For instance, Equation (3.5) can represent the family points on a fixed plane, or the family planes on a fixed point.

The importance of the principle of duality as a conceptual tool can not be over-emphasised. It shall be employed frequently in the analysis presented in subsequent chapters.

3.3. Line, Point and Plane Coordinates

A necessary and sufficient condition that three distinct points in the plane, represented by the homogeneous coordinates as $(x_1 : x_2 : x_3)$, $(y_1 : y_2 : y_3)$ and $(z_1 : z_2 : z_3)$, be collinear is that [**11, 19, 28, 44**]

$$\begin{vmatrix} x_1 & x_2 & x_3 \\ y_1 & y_2 & y_3 \\ z_1 & z_2 & z_3 \end{vmatrix} = 0.$$

It then follows that the line determined by two distinct points $(y_1 : y_2 : y_3)$ and $(z_1 : z_2 : z_3)$ has an equation that is easily obtained employing the *Grassmannian expansion* [**54, 90, 150**]:

$$\begin{vmatrix} x_1 & x_2 & x_3 \\ y_1 & y_2 & y_3 \\ z_1 & z_2 & z_3 \end{vmatrix} = \begin{vmatrix} y_2 & y_3 \\ z_2 & z_3 \end{vmatrix} x_1 + \begin{vmatrix} y_3 & y_1 \\ z_3 & z_1 \end{vmatrix} x_2 + \begin{vmatrix} y_1 & y_2 \\ z_1 & z_2 \end{vmatrix} x_3 = 0,$$

where a variable point on a fixed line has *point coordinates* $(x_1 : x_2 : x_3)$ and, dually, a variable line on a fixed point has *line coordinates*

$$\left[\begin{vmatrix} y_2 & y_3 \\ z_2 & z_3 \end{vmatrix} : \begin{vmatrix} y_3 & y_1 \\ z_3 & z_1 \end{vmatrix} : \begin{vmatrix} y_1 & y_2 \\ z_1 & z_2 \end{vmatrix} \right] = [X_1 : X_2 : X_3]. \tag{3.6}$$

Comparing the coordinates, it is to be seen that equation (3.4) represents this exact duality.

A similar relation exists when the equation of a plane is written using homogeneous coordinates. In E_3 a necessary and sufficient condition that four points, whose homogeneous point coordinates are $(x_1 : x_2 : x_3 : x_4)$, $(y_1 : y_2 : y_3 : y_4)$, $(z_1 : z_2 : z_3 : z_4)$ and $(w_1 : w_2 : w_3 : w_4)$, be coplanar is that [**11, 31**]

$$\begin{vmatrix} x_1 & x_2 & x_3 & x_4 \\ y_1 & y_2 & y_3 & y_4 \\ z_1 & z_2 & z_3 & z_4 \\ w_1 & w_2 & w_3 & w_4 \end{vmatrix} = 0.$$

It follows that the plane determined by three distinct points has an equation, again obtained with the Grassmannian expansion, given by Equation (3.5). A variable point on a fixed plane has *point coordinates* $(x_1 : x_2 : x_3 : x_4)$, while the principle of duality means that a variable plane on a fixed point has *plane coordinates*

$$\left[\begin{vmatrix} y_2 & y_3 & y_4 \\ z_2 & z_3 & z_4 \\ w_2 & w_3 & w_4 \end{vmatrix} : \begin{vmatrix} y_3 & y_4 & y_1 \\ z_3 & z_4 & z_1 \\ w_3 & w_4 & w_1 \end{vmatrix} : \begin{vmatrix} y_1 & y_2 & y_4 \\ z_1 & z_2 & z_4 \\ w_1 & w_2 & w_4 \end{vmatrix} : \begin{vmatrix} y_3 & y_1 & y_2 \\ z_3 & z_1 & z_2 \\ w_3 & w_1 & w_2 \end{vmatrix} \right]$$

$$= [X_1 : X_2 : X_3 : X_4].$$

3.4. Geometry

Every geometry of space whose group of transformations are *collineations* which contain the sub-group $\mathcal{G}_7$ can be derived from *projective geometry.* This geometry has the smallest set of invariants. It is also the most general. This means that every theorem valid in projective geometry is also valid in the sub-geometries defined by less general collineations. The sub-geometries usually have a larger set of invariants. It was Arthur Cayley who first realised that "projective geometry is all geometry" [**21**] however, it was Felix Klein who provided the means to systematically derive the sub-geometries [**90**].

3.4.1. The Erlangen Programme. In 1872 Felix Klein gave his famous inaugural address at the Friedrich-Alexander University in Erlangen, Germany, the text of which is now known as the *Erlangen Programme* [**89**]. Relying on the earlier work of Arthur Cayley [**21**], it was intended to show how Euclidean and non-Euclidean geometry could be established from projective geometry. However, Klein's contributions turned out to be more general, leading to a whole series of new geometries. Today, they are known as *Cayley-Klein*[2] *geometries* and the spaces in which they are valid are *Cayley-Klein spaces* [**143**] (discussed in Section 3.4.5). The following summary of the Erlangen Programme was provided by Klein, himself, in [**90**]:

> Given any group of transformations[3] in space which includes the principal group, $\mathcal{G}_7$, as a sub-group, then the invariant theory of this group gives a definite kind of geometry, and every possible geometry can be obtained in this way.

According to the Erlangen Programme, the following *dual* propositions are always valid [**36**]:

(1) A geometry on a space defines a group of linear transformations[4] in that space.

(2) A group of linear transformations in a space defines a geometry on that space.

---

[2]This term is attributed to Sommerville[**134, 144**].

[3]The terms *transformation* and *linear transformation* shall be used interchangeably throughout this thesis. This is because all transformations used in this work are linear.

[4]The modern understanding of *linear transformation* is limited to those defined on metric vector spaces. However, in this thesis the term *linear transformation* refers to any non-singular injective collineation (*i.e.*, a one-to-one transformation that maps collinear points onto collinear points), in any space. We use the transformations as $n \times n$ matrix operators, but care must be taken because they operate on $n \times 1$ matrices, and not vectors. For instance, a vector space can not be defined on P_3 using 4-D vectors, whose elements are composed of homogeneous coordinates, because there is no $\mathbf{0}$ element, which, when added to any other element $\mathbf{v}$ leaves $\mathbf{v}$ unchanged: $\mathbf{v} + \mathbf{0} = \mathbf{v}$. In P_3 the point $(0:0:0:0)$ is not defined. Hence, the more general definition must be used. The interested reader is directed to [**45, 130, 136**].

Moreover, the character of a geometry is determined by the relations which remain invariant under the associated group of linear transformations.

These linear transformations are of the form

$$\mathbf{Ax} = k\mathbf{b}, \tag{3.7}$$

where $\mathbf{x}$ and $\mathbf{b}$ are the $n+1$ homogeneous coordinates of two points in an n dimensional space, $\mathbf{A}$ is a nonsingular $(n+1) \times (n+1)$ matrix and k is a proportionality constant arising from the use of the homogeneous coordinates.

An *invariant* is defined [**73, 90, 130**] as a function of the coordinates under the transformation such that

$$\phi(b_1, \ldots, b_{n+1}) = \Delta^p \phi(x_1, \ldots, x_{n+1}), \tag{3.8}$$

where Δ is the determinant of the matrix $\mathbf{A}$ (which is, by definition, nonsingular) and p is a weighting factor. If $p = 0$ then ϕ is an *absolute invariant*, otherwise it is a *relative invariant* with weight p [**130**]. Klein's definition of a geometry involves absolute invariants, *i.e.*, functions of the coordinates which remain unchanged by the associated group of transformations [**36**].

3.4.2. Transformation Groups. The *projective transformations* in projective space P_3 may be thought of as 4×4 matrix operators that are collineations (it is important to note that an $(n+1)$-D homogeneous coordinate space is required to analytically describe the elements of an n-D projective space). These matrices are non-singular by definition. They are sometimes referred to as *structure matrices* [**22**] since changing the structure of the matrix changes the character of the geometry it

represents. A transformation of P_3 may be written as

$$\mathbf{P} = \begin{bmatrix} a_1 & a_2 & a_3 & a_4 \\ b_1 & b_2 & b_3 & b_4 \\ c_1 & c_2 & c_3 & c_4 \\ d_1 & d_2 & d_3 & d_4 \end{bmatrix}, \tag{3.9}$$

where the 16 elements are arbitrary, but all contain a common factor owing to the use of homogeneous coordinates. Because there are no restrictions on the elements, with the exception that the determinant of the matrix never vanishes, they are the most general geometric transformations in 3-D space. Hence, the *projective group* of all collineations in P_3 has fifteen parameters, and is termed $\mathcal{G}_{15}$ [**90**]. The fundamental invariant of $\mathcal{G}_{15}$ in particular, and n-dimensional projective geometry in general, is the *cross ratio* of four collinear points.

The concept of cross ratio is one of the oldest now known to be part of projective geometry. It is believed that the theory was known to Pappus of Alexandria (AD 290-350) [**29, 44, 135**]. It is defined as follows [**44**]:

DEFINITION 3.4.1. *If the collinear points A, B, C, and D, at least three of which are distinct, on a projective line have coordinates* $(a_1 : a_2)$, $(b_1 : b_2)$, $(c_1 : c_2)$ *and* $(d_1 : d_2)$, *respectively, then the real number*

$$R(A,B,C,D) = \frac{\begin{vmatrix} a_1 & a_2 \\ c_1 & c_2 \end{vmatrix} \begin{vmatrix} b_1 & b_2 \\ d_1 & d_2 \end{vmatrix}}{\begin{vmatrix} b_1 & b_2 \\ c_1 & c_2 \end{vmatrix} \begin{vmatrix} a_1 & a_2 \\ d_1 & d_2 \end{vmatrix}} \tag{3.10}$$

if it exists is the cross ratio *of the four points in the order A, B, C, D. If the number does not exist, the cross ratio is said to be* infinite.

The equations of general affine transformations in affine space A_3 contain twelve arbitrary coefficients. Thus, the *affine group* is indicated by $\mathcal{G}_{12}$. It should be apparent that $\mathcal{G}_{12} \subset \mathcal{G}_{15}$. This transformation group of A_3 is typically expressed as:

$$\mathbf{A} = \begin{bmatrix} a_1 & a_2 & a_3 & a_4 \\ b_1 & b_2 & b_3 & b_4 \\ c_1 & c_2 & c_3 & c_4 \\ 0 & 0 & 0 & 1 \end{bmatrix}. \tag{3.11}$$

Affine geometry can be considered as more *rich* than projective geometry because its set of invariants includes more than just the cross ratio. For example, affine transformations leave the plane at infinity, $x_4 = 0$, invariant, which is not the case for projective transformations, in general.

The group of Euclidean transformations of E_3, also a subgroup of $\mathcal{G}_{15}$, are represented by

$$\mathbf{E} = \begin{bmatrix} a_1 & a_2 & a_3 & a_4 \\ b_1 & b_2 & b_3 & b_4 \\ c_1 & c_2 & c_3 & c_4 \\ 0 & 0 & 0 & 1 \end{bmatrix}. \tag{3.12}$$

However, $\mathbf{E}$ contains a 3×3 proper orthogonal sub-matrix (*i.e.*, having a determinant of $+1$) [**33**]. The principal group, $\mathcal{G}_7$, represents the most general Euclidean collineations [**45**]. The Euclidean displacement group $\mathcal{G}_6$ is characterised by the property that both distance and sense are invariant under $\mathcal{G}_6$ [**30**].

3.4.3. Invariants. Recall that an absolute invariant is defined to be a function of the coordinates of an element in the given geometry which remains invariant under the associated linear transformation group [**44, 90**]. The Euclidean displacement group $\mathcal{G}_6$ is defined in a metric space (see Section 3.4.4). In addition to the

preservation of distance and sense, its set of invariants contains a special imaginary quadratic form. First consider $\mathcal{G}_3 \subset \mathcal{G}_6$. The equation of an arbitrary circle, k, in E_2 with radius r and centre $C(x_c, y_c)$ is:

$$(x - x_c)^2 + (y - y_c)^2 \;=\; r^2. \tag{3.13}$$

Expressing Equation (3.13) using homogeneous coordinates $x = \frac{x_1}{x_3}$, $y = \frac{x_2}{x_3}$ produces

$$(x_1 - x_c x_3)^2 + (x_2 - y_c x_3)^2 \;=\; r^2 x_3^2. \tag{3.14}$$

The intersection with the line at infinity $x_3 = 0$ is given by the equations

$$x_1^2 + x_2^2 = 0, \quad x_3 = 0. \tag{3.15}$$

The constants r, x_c and y_c which characterise the circle do not appear in the result. Thus, every circle in the plane intersects the line at infinity in exactly the same two points, namely,

$$I_1(1 : -i : 0), \quad I_2(1 : i : 0). \tag{3.16}$$

They are widely called the *imaginary*, or *absolute circle points* [**17, 31, 90, 136**]. It can be shown, in the same way, that every sphere cuts the plane at infinity in the imaginary conic:

$$x_1^2 + x_2^2 + x_3^2 = 0, \quad x_4 = 0, \tag{3.17}$$

which is called the *imaginary*, or *absolute sphere circle.*

These absolute quantities account for the apparent deficiency of Bezout's theorem [**75, 130**] for the intersections of algebraic curves and surfaces. That is, two curves of order n and m will intersect in at most nm points ; similarly, two surfaces of order n and m will intersect in a curve of, at most, order nm. Clearly, two circles intersect in at most two points, while two spheres intersect in a circle (a second order curve).

Since every circle contains I_1 and I_2, two circles intersect in at most four points, and Bezout's theorem is seen to be true. The same applies for spheres; they intersect in a curve which splits into a real and an imaginary conic.

To summarise, the invariants of $\mathcal{G}_3$ include those of the projective and affine planes, but additionally include the line at infinity and two imaginary conjugate points on it, namely I_1 and I_2. The invariants of $\mathcal{G}_6$ include those of projective and affine 3-D space, including the plane at infinity and an imaginary conic on it: the imaginary sphere circle.

3.4.4. Metric Spaces. Metric and non metric geometries may be looked upon as *special cases* of projective geometry. Before continuing, some definitions are required.

DEFINITION 3.4.2. *The* **Cartesian Product** *of any two sets, $\mathcal{S}$ and $\mathcal{T}$, denoted $\mathcal{S} \times \mathcal{T}$, is the set of all ordered pairs (s,t) such that $s \in \mathcal{S}$ and $t \in \mathcal{T}$.*

DEFINITION 3.4.3. *Let $\mathcal{S}$ be any set. A function d mapping $\mathcal{S} \times \mathcal{S}$ into $\mathcal{R}$ (the set of real numbers) is a* **metric** *on $\mathcal{S}$ iff* [58]

(1) $d_{s_1 s_2} = 0$ *iff* $s_1 = s_2$;

(2) $d_{s_1 s_2} \geq 0, \quad \forall\, s_i \in \mathcal{S}$;

(3) $d_{s_1 s_2} = d_{s_2 s_1}, \quad \forall\, s_i \in \mathcal{S}$;

(4) $d_{s_1 s_2} + d_{s_2 s_3} \geq d_{s_1 s_3}, \quad \forall\, s_1, s_2, s_3 \in \mathcal{S}$.

A *metric space* is a set $\mathcal{S}$, together with a metric d defined on $\mathcal{S}$. A *metric geometry* on that space is defined by the group of linear transformations which leave the metric invariant. For example, Euclidean space is a metric space because it contains the set $\mathcal{P}$ of all points. The metric defined on $\mathcal{P}$ is Euclidean distance,

$$d \;=\; \sqrt{(x_2 - x_1)^2 + (y_2 - y_1)^2 + (z_2 - z_1)^2}, \tag{3.18}$$

which is an invariant of $\mathcal{G}_6$. Thus, Euclidean geometry is a metric geometry. It is important to note that a rule to measure distance in a space is not sufficient to make the space metric. All four conditions in Definition 3.4.3 must be satisfied. An example of a geometry containing a distance rule and distinct points with zero distance between them is *Isotropic Geometry*. The transformations associated with the isotropic plane are [**5**]

$$\begin{bmatrix} 1 \\ X \\ Y \end{bmatrix} = \begin{bmatrix} 1 & 0 & 0 \\ a & 1 & 0 \\ b & c & 1 \end{bmatrix} \begin{bmatrix} 1 \\ x \\ y \end{bmatrix}. \tag{3.19}$$

Distance in this geometry is measured by the difference of the x-coordinates of two points: $d = x_2 - x_1$. The distance between two points is clearly invariant under the transformation in Equation 3.19, but it is also clear that there exist an infinite number of distinct points possessing the same x-coordinate and therefore have zero distance between them. The complete enumeration of all such *degenerate geometries* was given by Sommerville in [**134**].

3.4.5. Cayley-Klein Spaces and Geometries. Projective geometry can be developed from the fundamental elements of point, line, plane and Hilbert's axioms [**72**] of incidence, order and continuity independently of the concept of metric. Thus, in projective geometry there is no rule to measure and the only absolute invariant is the cross ratio of four points [**29**]. In defining a *Cayley-Klein* space one could start with projective geometry and define a *rule* to measure distance. Usually this is done by introducing a quadratic form. For instance, Euclidean geometry can be developed from projective geometry by building upon the foundation of *Cayley's principle* [**21**] that *projective geometry is all geometry* using Klein's Erlangen Programme, *i.e.*, the theory of algebraic invariants. Euclidean geometry can be obtained by adjoining, or

constraining, P_3 with the special quadratic form [**90**]

$$x_1^2 + x_2^2 + x_3^2 = 0, \tag{3.20}$$

which represents the absolute sphere circle. It is an imaginary quadric containing all points with a vanishing norm. This quadratic form is induced by the Euclidean distance function between the homogeneous coordinates of points $(x_1 : x_2 : x_3 : x_4)$ and $(y_1 : y_2 : y_3 : y_4)$

$$d = \frac{\sqrt{(x_1y_4 - y_1x_4)^2 + (x_2y_4 - y_2x_4)^2 + (x_3y_4 - y_3x_4)^2}}{x_4y_4}. \tag{3.21}$$

The quadratic form, or *norm*, belonging to this rule is

$$x_1^2 + x_2^2 + x_3^2.$$

Equations (3.20) and (3.21) are fundamental invariants of $\mathcal{G}_6$. However, Equation (3.20) is independent of x_4. An entirely different quadratic form in P_3 can be obtained by adding x_4^2 to Equation (3.20):

$$x_1^2 + x_2^2 + x_3^2 + x_4^2 = 0. \tag{3.22}$$

Changing the quadratic form changes the rule for measuring magnitudes. For instance, the signs could be changed as follows:

$$x_1^2 - x_2^2 - x_3^2 - x_4^2 = 0. \tag{3.23}$$

Each new rule gives a different form of *space*. These are the *Cayley-Klein* spaces. The first quadratic form, equation (3.20) gives Euclidean, or *parabolic* space. Equation (3.22) gives *Riemann* non-Euclidean, or *elliptic* space, while Equation (3.23) gives *Lobachevskii* non-Euclidean, or *hyperbolic* space [**90, 143**]. In each of these spaces there is a group of transformations that leaves the norm invariant. These characterise the corresponding geometries [**46**].

Equation (3.20) may be viewed as sphere with no volume. The distance between two distinct points on this virtual quadric vanishes. The term *virtual* means that only complex points lie on it. Similarly, equation (3.22) may be viewed as a virtual ellipsoid. Whereas, Equation (3.23) represents a real hyperboloid of two sheets.

The non-Euclidean geometries were serendipitously discovered by efforts to prove Euclid's parallel axiom: *given a line g and a point P, not on g, there is one, and only one line p through P that does not intersect g.* The Euclidean model of Riemann's elliptical plane is a unit sphere. Straight lines on a sphere are geodesics, *i.e.*, great circles. All great circles intersect in two anti-podal points. If the they are taken to be the same point, then there are no parallel lines in the elliptic plane, because all lines intersect in a point [**71**].

The Euclidean model for Lobachevskii's hyperbolic plane is the points contained in a unit circle, excluding points on the circumference. Straight lines are chords of the circle, the end points excluded. Thus, given a line g and a point P not on g in the hyperbolic plane there are an infinite number of lines through P that do not intersect g [**71**].

Klein was the first to make use of the terms elliptic, parabolic and hyperbolic to classify these geometries [**90**]. The use of these names implies no direct connection with the corresponding conic sections, rather they mean the following. A central conic is an ellipse or hyperbola according as it has no asymptote or two asymptotes. Analogously, a non-Euclidean plane is elliptic or hyperbolic according as each of its lines contains no point at infinity, or two [**30**].

However, many other possibilities exist. For instance 4-D Minkowskian geometry [**103**] is well known for its application to Einstein's *Special Theory of Relativity* [**29**]. It differs from the other geometries in that time differentials are among its set of

elements. In the following hierarchy, each geometry can be derived from the one above it by some kind of condition imposed on the transformation group [**29**].

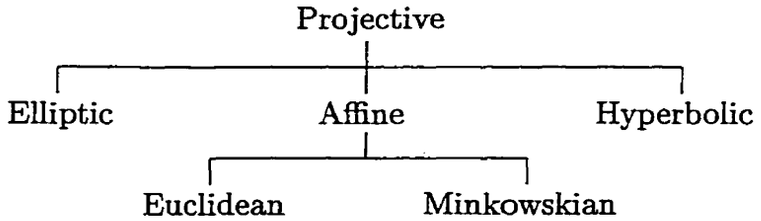

3.5. Representations of Displacements

As mentioned in Chapter 2, it is convenient to think of the relative displacement of two rigid-bodies in E_3 as the displacement of a Cartesian reference coordinate frame E attached to one of the bodies with respect to a Cartesian reference coordinate frame Σ attached to the other [**17**]. Without loss of generality, Σ may be considered as fixed while E is free to move. Then the position of a point in E in terms of the basis of Σ can be expressed compactly as

$$\mathbf{p}' = \mathbf{A}\mathbf{p} + \mathbf{d}, \tag{3.24}$$

where, $\mathbf{p}$ is the 3×1 position vector of a point in E, $\mathbf{p}'$ is the position vector of the same point in Σ, $\mathbf{d}$ is the position vector of the origin of frame E in Σ, and $\mathbf{A}$ is a 3×3 proper orthogonal rotation matrix (*i.e.*, its determinant is $+1$).

It is clear from Equation (3.24) that a general displacement can be decomposed into a pure rotation and a pure translation. The representation of the translation is straightforward: it is given by the position vector in Σ of 0_E. However, there are many ways to represent the orientation. For example *fixed angle* or *Euler angle* representations may be used. There are twelve distinct ways to specify an orientation in each representation. This is because the rotation is decomposed into the product

of three rotations about the coordinate axes in a certain order, with twelve distinct permutations. The axes of the fixed frame are used in the fixed angle representation (also called *roll, pitch, yaw* angles [**33**]), while the axes of the moving frame are used for the Euler angle representation.

3.5.1. Orientation: Euler-Rodrigues Parameters. An invariant representation for rotations is given by the *Euler-Rodrigues parameters* [**8**]. Using *Cayleys formula for proper orthogonal matrices* [**17, 33**], matrix **A** in equation (3.24) can be rewritten in the following form [**17**]:

$$\mathbf{A} = \Delta^{-1} \begin{bmatrix} c_0^2 + c_1^2 - c_2^2 - c_3^2 & 2(c_1c_2 - c_0c_3) & 2(c_1c_3 + c_0c_2) \\ 2(c_1c_2 + c_0c_3) & c_0^2 - c_1^2 + c_2^2 - c_3^2 & 2(c_2c_3 - c_0c_1) \\ 2(c_1c_3 - c_0c_2) & 2(c_2c_3 + c_0c_1) & c_0^2 - c_1^2 - c_2^2 + c_3^2 \end{bmatrix}, \quad (3.25)$$

where

$$\Delta = c_0^2 + c_1^2 + c_2^2 + c_3^2,$$

and the c_i, called *Euler-Rodrigues parameters* [**7, 17**], are defined as

$$\begin{aligned} c_0 &= \cos\tfrac{\varphi}{2}, \\ c_1 &= s_x \sin\tfrac{\varphi}{2}, \\ c_2 &= s_y \sin\tfrac{\varphi}{2}, \\ c_3 &= s_z \sin\tfrac{\varphi}{2}. \end{aligned}$$

The c_i may be *normalised* such that $\Delta = 1$, in which case $\mathbf{s} = [s_x, s_y, s_z]^T$ is a unit direction vector parallel to the axis and φ is the angular measure of a given rotation. The Euler-Rodrigues parameters are *quadratic invariants* of a given rotation [**7**].

Since **s** is a unit vector, it is immediately apparent that the c_i are not independent, but related by

$$c_0^2 + c_1^2 + c_2^2 + c_3^2 \;=\; 1.$$

The geometric interpretation of the four Euler-Rodrigues parameters is that an orientation may be viewed as a point on a unit hyper-sphere in a four-dimensional space. Assembled into a 4×1 array, the Euler-Rodrigues parameters are the *unit quaternions* invented by Sir William Hamilton [**8**]. The group of spherical displacements, $SO(3)$, are elegantly represented with unit quaternions.

3.5.2. Displacements as Points in Study's Soma Space. In 1903 Eduard Study showed [**139**] that Euclidean displacements may be represented by eight parameters, or coordinates in a seven dimensional homogeneous projective space. Thus, displacements can be represented as points; fundamental elements in this space. His work was undoubtedly inspired by that of Julius Plücker and Felix Klein. Klein's Erlangen Programme gave rise to a systematic method for constructing new geometries based on the algebraic invariants of the associated transformation groups. However, it was Plücker who first suggested the idea of taking the line as the fundamental element of space [**117**]. Various types of line coordinates were introduced by Cayley and Grassmann [**87**]; Plücker adopted a coordinate system which is a special form of these. The success of Plücker's work was hindered by the Cartesian analysis that he employed [**115, 116, 117**]. Klein, Plücker's student, introduced the system of coordinates determined by six linear complexes in mutual involution: on any line common to two linear complexes a one-to-one correspondence of points is determined by the planes through the line by taking the poles of each plane for the complexes. If a certain condition is satisfied connecting the coefficients of the two complexes, then these

pairs of points form an involution [**87**]. Moreover, Klein's observation that the line geometry of Plücker is point geometry on a quadric contained in a five dimensional space was of critical importance in the conceptualisation of the soma space [**144**].

Plücker and soma coordinates are analogous in that the set of all lines, in the case of Plücker coordinates, and the set of all displacements, in the case of soma coordinates both exist as the set of points covering special quadric surfaces in higher dimensional spaces. Points not on the respective quadrics represent neither lines nor displacements. Since both quadrics have identical forms, it is instructive to first examine how Plücker coordinates come about, and the nature of their constraint surface, before moving on to Study's soma.

3.5.3. Plücker Coordinates. Plücker developed line coordinates [**115, 116**] to address the need of describing lines as the fundamental elements of his *neue Geometrie* [**117**]. Line coordinates may be obtained from Cartesian coordinates by considering the following: a line on the intersection of two planes, or dually the ray on two points. In the former case, the Plücker coordinates specify the linear pencil of planes and are generally called *axial Plücker coordinates.* In the latter case, they are called *ray Plücker coordinates.* If $X(x_0 : x_1 : x_2 : x_3)$ and $Y(y_0 : y_1 : y_2 : y_3)$ are the homogeneous coordinates of two different points on a line, the *Grassmannian sub-determinants* [**90**] of the associated 2×4 matrix composed of the point coordinates, comprise the homogeneous Plücker coordinates of the line [**83**]:

$$p_{ik} = \begin{vmatrix} x_i & x_k \\ y_i & y_k \end{vmatrix} \qquad i, k \in \{0, \ldots, 3\},\ i \neq k.$$

Of the twelve possible Grassmannians, only six are independent, since $p_{ik} = -p_{ki}$. Traditionally, the following six are used

$$p_{01} : p_{02} : p_{03} : p_{23} : p_{31} : p_{12}.$$

These six coordinates collected in a 6×1 matrix are called the *Plücker array.*

A line, however, is uniquely determined by a point and three direction cosines. The Plücker coordinates are super-abundant by two, hence there are two constraints on the six parameters. First, because the coordinates are homogeneous, there are only five independent ratios. It necessarily follows that

$$(p_{01} : p_{02} : p_{03} : p_{23} : p_{31} : p_{12}) \neq (0 : 0 : 0 : 0 : 0 : 0).$$

Second, the six numbers must obey the following quadratic condition:

$$p_{01}p_{23} + p_{02}p_{31} + p_{03}p_{12} = 0. \tag{3.26}$$

The quadric condition represented by Equation (3.26) is called the *Plücker identity* [**87**]. Geometrically, it represents a four-dimensional quadric hyper-surface in a five-dimensional projective homogeneous space, called *Plücker's quadric*, $\mathcal{P}_4^2$ [**29, 135**]. Distinct lines in Euclidean space are distinct points on $\mathcal{P}_4^2$.

The Plücker quadric can be derived in the following way [**83**]. Consider the following determinant, Δ, of a matrix composed of the homogeneous coordinates of two points $X(x_i)$ and $Y(y_i)$, $i \in \{0, 1, 2, 3\}$, counted twice. Obviously, the determinant vanishes because of the linear dependence between rows 1, 3 and 2, 4. This determinant can be expanded using 2×2 sub-determinants (Grassmannians) along the first two rows, according to the *Laplacian expansion theorem* [**45**]. That is, multiply the compliment of the minor by $(-1)^h$, where h is the sum of the numbers denoting the

rows and columns in which the minor appears. This gives

$$0 = \Delta = \begin{vmatrix} x_0 & x_1 & x_2 & x_3 \\ y_0 & y_1 & y_2 & y_3 \\ x_0 & x_1 & x_2 & x_3 \\ y_0 & y_1 & y_2 & y_3 \end{vmatrix} = (-1)^{3+(1+2)} \begin{vmatrix} x_0 & x_1 \\ y_0 & y_1 \end{vmatrix} \begin{vmatrix} x_2 & x_3 \\ y_2 & y_3 \end{vmatrix} +$$

$$(-1)^{3+(1+3)} \begin{vmatrix} x_0 & x_2 \\ y_0 & y_2 \end{vmatrix} \begin{vmatrix} x_1 & x_3 \\ y_1 & y_3 \end{vmatrix} + (-1)^{3+(1+4)} \begin{vmatrix} x_0 & x_3 \\ y_0 & y_3 \end{vmatrix} \begin{vmatrix} x_1 & x_2 \\ y_1 & y_2 \end{vmatrix} +$$

$$(-1)^{3+(2+3)} \begin{vmatrix} x_1 & x_2 \\ y_1 & y_2 \end{vmatrix} \begin{vmatrix} x_0 & x_3 \\ y_0 & y_3 \end{vmatrix} + (-1)^{3+(2+4)} \begin{vmatrix} x_1 & x_3 \\ y_1 & y_3 \end{vmatrix} \begin{vmatrix} x_0 & x_2 \\ y_0 & y_2 \end{vmatrix} +$$

$$(-1)^{3+(3+4)} \begin{vmatrix} x_2 & x_3 \\ y_2 & y_3 \end{vmatrix} \begin{vmatrix} x_0 & x_1 \\ y_0 & y_1 \end{vmatrix} = 2(p_{01}p_{23} - p_{02}p_{13} + p_{03}p_{12}) \qquad (3.27)$$

Since $p_{13} = -p_{31}$, Equation 3.27 simplifies to Equation 3.26.

Now attention is turned towards determining the structure of the quadric hypersurface $\mathcal{P}_4^2$. The important observation is that Equation (3.26) contains only bilinear cross-terms. This implies that the quadric has been rotated out of its *standard position*, or *normal form* [**42**]. The quadratic form associated with $\mathcal{P}_4^2$, can be represented using a 6×6 symmetric matrix, $\mathbf{M}$ [**9**]:

$$\mathbf{p}^T\mathbf{M}\mathbf{p} = [p_{01} \ldots, p_{12}] \begin{bmatrix} 0 & 0 & 0 & 1/2 & 0 & 0 \\ 0 & 0 & 0 & 0 & 1/2 & 0 \\ 0 & 0 & 0 & 0 & 0 & 1/2 \\ 1/2 & 0 & 0 & 0 & 0 & 0 \\ 0 & 1/2 & 0 & 0 & 0 & 0 \\ 0 & 0 & 1/2 & 0 & 0 & 0 \end{bmatrix} \begin{bmatrix} p_{01} \\ \vdots \\ p_{12} \end{bmatrix}.$$

This quadratic form can be orthogonally diagonalised with another 6×6 matrix $\mathbf{P}$, constructed with the eigenvectors of $\mathbf{M}$. The matrix $\mathbf{P}$ is easily found to be

$$\mathbf{P} = \frac{\sqrt{(2)}}{2} \begin{bmatrix} 1 & 0 & 0 & -1 & 0 & 0 \\ 0 & 1 & 0 & 0 & -1 & 0 \\ 0 & 0 & 1 & 0 & 0 & -1 \\ 1 & 0 & 0 & 1 & 0 & 0 \\ 0 & 1 & 0 & 0 & 1 & 0 \\ 0 & 0 & 1 & 0 & 0 & 1 \end{bmatrix}.$$

Now, pre-multiplying $\mathbf{M}$ with the transpose of $\mathbf{P}$ and post-multiplying with $\mathbf{P}$ itself gives the diagonalised matrix, $\mathbf{D}$, *i.e.*, $\mathbf{P}^T\mathbf{M}\mathbf{P} = \mathbf{D}$:

$$\mathbf{D} = \frac{1}{2} \begin{bmatrix} 1 & 0 & 0 & 0 & 0 & 0 \\ 0 & 1 & 0 & 0 & 0 & 0 \\ 0 & 0 & 1 & 0 & 0 & 0 \\ 0 & 0 & 0 & -1 & 0 & 0 \\ 0 & 0 & 0 & 0 & -1 & 0 \\ 0 & 0 & 0 & 0 & 0 & -1 \end{bmatrix}.$$

Matrix $\mathbf{D}$ reveals the normal form of $\mathcal{P}_4^2$ in *canonical form* [**42**] from the matrix multiplication $\mathbf{p}^T\mathbf{D}\mathbf{p} = \mathbf{p}^T(\mathbf{P}^T\mathbf{M}\mathbf{P})\mathbf{p}$:

$$p_{01}^2 + p_{02}^2 + p_{03}^2 - p_{23}^2 - p_{31}^2 - p_{12}^2 = 0. \tag{3.28}$$

Observing the signs on these six pure quadratic terms, one immediately sees that the Plücker quadric, $\mathcal{P}_4^2$, has the form of an hyperboloid in the five dimensional space. In this space, only the points on $\mathcal{P}_4^2$ represent lines.

3.5.4. Study's Soma. A general Euclidean displacement of reference frame E with respect to Σ, as given by equation (3.24), depends on six independent parameters: three are required for the orientation of E and three for the position of O_E. Regarding this situation geometrically, distinct Euclidean displacements of E may be represented as distinct points in a six-dimensional space. Hence, a displacement is an element of a six-dimensional geometry. However, Study showed [**139**] that a coordinate space of dimension eight is necessary to ensure that all the relations among the entries of equation (3.25) are fulfilled. Thus, an array of eight numbers can represent a displacement as a fundamental element in a seven dimensional homogeneous projective space. These eight numbers were termed *soma* by Study [**138**]. Similar to the Plücker array, Study's soma are

$$(c_0 : c_1 : c_2 : c_3 : g_0 : g_1 : g_2 : g_3).$$

The first four of Study's soma coordinates are the Euler parameters, c_i, defined in Section 3.5.1. The remaining four, g_i $i \in \{0, \ldots, 3\}$, are linear combinations of the elements of $\mathbf{d}$, from Equation (3.24), and the c_i such that the following quadratic condition is satisfied:

$$c_0 g_0 + c_1 g_1 + c_2 g_2 + c_3 g_3 = 0. \tag{3.29}$$

Study defined these four parameters to be

$$\begin{aligned} g_0 &= d_1 c_1 + d_2 c_2 + d_3 c_3, \\ g_1 &= -d_1 c_0 + d_3 c_2 - d_2 c_3, \\ g_2 &= -d_2 c_0 - d_3 c_1 + d_1 c_3, \\ g_3 &= -d_3 c_0 + d_2 c_1 - d_1 c_2. \end{aligned} \tag{3.30}$$

Owing to the homogeneity of the Euler-Rodrigues parameters there is an additional quadratic constraint on the soma, stemming from the denominator of Equation (3.25), which is similar to the non-zero condition for the Plücker coordinates:

$$c_0^2 + c_1^2 + c_2^2 + c_3^2 \neq 0. \tag{3.31}$$

Thus, of the eight soma coordinates only six are independent, but all eight are required to uniquely describe a displacement [**139**].

Equation (3.29) represents a six-dimensional quadric hyper-surface in a seven-dimensional space. It is called *Study's quadric*, S_6^2 [**81**]. Its form can be determined in a way analogous to that used for $\mathcal{P}_4^2$. After applying the same procedure, the normal form of S_6^2 is revealed to be:

$$c_0^2 + c_1^2 + c_2^2 + c_3^2 - g_0^2 - g_1^2 - g_2^2 - g_3^2 = 0.$$

We see immediately that S_6^2 has the form of an hyperboloid in the soma space. Of all the points in the soma space, only those on S_6^2 represent displacements.

3.5.5. Vectors in a Dual Projective Three-Space. Another way of looking at the eight soma coordinates is to consider them as two sets of four parameters, each of which can represent a vector in a four-dimensional coordinate space [**119, 121**]. A spatial Euclidean displacement can then be mapped into the set of two *Study vectors* in the four-dimensional space in an analogous way that a line in Euclidean space can be mapped to sets of two *Plücker vectors*. Employing this concept, Ravani [**119**] introduced the idea of representing a Euclidean displacement as a point in a dual projective three-space. This, however, leads directly to the representation of displacements in terms of dual quaternions, see Blaschke [**15**], Bottema and Roth [**17**], or McCarthy [**95**] for example.

Although this representation and that of Study are analytically identical, they represent completely different geometric interpretations. In the latter case, displacements are represented by points on Study's quadric in its seven-dimensional projective space, while the former represents displacements by two vectors in a dual projective three-space.

3.5.6. Transfer Principle. A representation identical to the one discussed in the last section can be obtained using the *transfer principle* (Bottema and Roth [**17**], Ravani and Roth [**121**]). Spherical displacements are readily represented using the four Euler-Rodrigues parameters. That is, if a spherical displacement is mapped into the points of a real three-dimensional projective space where the coordinates are four-tupples of Euler-Rodrigues parameters, then spatial displacements can be mapped into a similar, but dual, space. In other words, the representation of a spatial displacement is obtained simply by dualising the corresponding spherical displacement (Ravani and Roth [**121**]).

3.6. Kinematic Mappings of Displacements

So far in this chapter we have discussed various ways to represent displacements. In all of them, at least six independent numbers are required. This led Study, in 1903 [**138**], to the idea of mapping distinct displacements in Euclidean space to the points of a seven-dimensional projective image space. The homogeneous coordinates of the image space are the eight soma. As mentioned earlier, these eight coordinates are not independent. They are super-abundant by two. However, two quadratic constraints must be satisfied. The non-zero condition, equation (3.31), and the displacement must be a point on S_6^2, Equation (3.29). It is natural to expect that a six-dimensional image space would suffice. However, as previously mentioned, Study [**139**] showed that an 8-D coordinate space is required.

3.6.1. General Euclidean Displacements. Study's kinematic mapping of general Euclidean displacements is given by the following equations in terms of the eight Study soma $\{c_i : g_i\}$

$$(x_1 : x_2 : x_3 : x_4 : y_1 : y_2 : y_3 : y_4) = (c_1 : c_2 : c_3 : c_0 : \frac{g_1}{2} : \frac{g_2}{2} : \frac{g_3}{2} : \frac{g_0}{2}). \quad (3.32)$$

Equation (3.24) can always be represented as a linear transformation by making it *homogeneous* (see McCarthy [**95**], for example). Let the homogeneous coordinates of points in the fixed frame Σ be the ratios $[X : Y : Z : W]$, and those of points in the moving frame E be the ratios $[x : y : z : w]$. Then Equation (3.24) can be rewritten as

$$\begin{bmatrix} X \\ Y \\ Z \\ W \end{bmatrix} = \mathbf{Q} \begin{bmatrix} x \\ y \\ z \\ w \end{bmatrix}, \quad (3.33)$$

where

$$\mathbf{Q} = \Delta^{-1} \begin{bmatrix} c_0^2 + c_1^2 - c_2^2 - c_3^2 & 2(c_1c_2 - c_0c_3) & 2(c_1c_3 + c_0c_2) & d_1 \\ 2(c_1c_2 + c_0c_3) & c_0^2 - c_1^2 + c_2^2 - c_3^2 & 2(c_2c_3 - c_0c_1) & d_2 \\ 2(c_1c_3 - c_0c_2) & 2(c_2c_3 + c_0c_1) & c_0^2 - c_1^2 - c_2^2 + c_3^2 & d_3 \\ 0 & 0 & 0 & \Delta \end{bmatrix}, \quad (3.34)$$

with $\Delta = c_0^2 + c_1^2 + c_2^2 + c_3^2$, and the d_i are the components of the position vector of $O_{E/\Sigma}$.

Let the transformation matrix $\mathbf{T}$ be the *image* of the elements of $\mathbf{Q}$ under the kinematic mapping. Since $\Delta \neq 0$ by one of the quadratic constraints, it's value is arbitrary and represents a scaling factor whose value is meaningless in a projective space. Recall, the homogeneous coordinates of $[\lambda x : \lambda y : \lambda z]$ and of $[\gamma x : \gamma y : \gamma z]$

represent the same point in the projective plane for any non-zero scalar constants λ and γ. Then we may write

$$\mathbf{T} = \begin{bmatrix} x_1^2-x_2^2-x_3^2+x_4^2 & 2(x_1x_2-x_3x_4) & 2(x_1x_3+x_2x_4) & 2(y_4x_1-y_3x_2+y_2x_3-y_1x_4) \\ 2(x_1x_2+x_3x_4) & -x_1^2+x_2^2-x_3^2+x_4^2 & 2(x_2x_3-x_1x_4) & 2(y_3x_1+y_4x_2-y_1x_3-y_2x_4) \\ 2(x_1x_3-x_2x_4) & 2(x_2x_3+x_1x_4) & -x_1^2-x_2^2+x_3^2+x_4^2 & 2(-y_2x_1+y_1x_2+y_4x_3-y_3x_4) \\ 0 & 0 & 0 & x_1^2+x_2^2+x_3^2+x_4^2 \end{bmatrix}. \tag{3.35}$$

This transforms the coordinates of points in frame E to coordinates of the same points in frame Σ (assuming that the two frames are initially coincident) after a given displacement in terms of the coordinates of a point on S_6^2.

3.6.2. Planar Displacements. The transformation matrix $\mathbf{T}$ simplifies considerably when we consider displacements that are restricted to the plane. Three DOF are lost and hence four Study parameters vanish. The displacements may be restricted to any plane. Without loss in generality, we may select one of the principal planes in Σ. Thus, we arbitrarily select the plane $Z = 0$. Since E and Σ are assumed to be initially coincident, this means

$$\begin{bmatrix} X \\ Y \\ 0 \\ W \end{bmatrix} = \mathbf{T} \begin{bmatrix} x \\ y \\ 0 \\ w \end{bmatrix}. \tag{3.36}$$

This requires that $d_3 = 0$ (since $Z = z = 0$, E can translate in neither the Z nor z directions), $s_x = s_y = 0$, and $s_z = 1$ (the equivalent rotation axis is parallel to the Z

and z axes). This, in turn, means

$$\begin{aligned} c_1 &= 0, \\ c_2 &= 0, \\ c_3 &= \sin\varphi/2, \\ c_0 &= \cos\varphi/2, \\ g_1 &= -d_1c_0 - d_2c_3, \\ g_2 &= -d_2c_0 + d_1c_3, \\ g_3 &= 0, \\ g_0 &= 0. \end{aligned}$$

This leaves us with only four soma coordinates to map:

$$(x_3 : x_4 : y_1 : y_2) = (c_3 : c_0 : \frac{g_1}{2} : \frac{g_2}{2}). \tag{3.37}$$

The homogeneous linear transformation matrix reduces to

$$\mathbf{T} = \begin{bmatrix} x_4^2 - x_3^2 & -2x_3x_4 & 0 & 2(y_2x_3 - y_1x_4) \\ 2x_3x_4 & x_4^2 - x_3^2 & 0 & -2(y_1x_3 + y_2x_4) \\ 0 & 0 & x_3^2 + x_4^2 & 0 \\ 0 & 0 & 0 & x_3^2 + x_4^2 \end{bmatrix}. \tag{3.38}$$

We may eliminate the third row and column because they only provide multiples of the trivial equation

$$Z = z = 0. \tag{3.39}$$

Thus, $\mathbf{T}$ reduces to a 3×3 matrix,

$$\mathbf{T} = \begin{bmatrix} x_4^2 - x_3^2 & -2x_3x_4 & 2(y_2x_3 - y_1x_4) \\ 2x_3x_4 & x_4^2 - x_3^2 & -2(y_1x_3 + y_2x_4) \\ 0 & 0 & x_3^2 + x_4^2 \end{bmatrix}. \tag{3.40}$$

Planar displacements still map to points on S_6^2, but we need only consider a special sub-set of these points. In fact, we may change our geometric interpretation altogether. We see that planar displacements can be represented by points in a three-dimensional projective homogeneous image space. The coordinates of the points are the four Study parameters $(x_3 : x_4 : y_1 : y_2)$. In this sub-space, the points are not restricted to a special quadric. They can take on any value with the exception that x_3 and x_4 are not simultaneously zero. Points on the real line defined by $x_3 = x_4 = 0$ are not the images of real planar displacements because this sub-space is still contained in the soma space, where the non-zero quadratic condition requires $x_1^2+x_2^2+x_3^2+x_4^2 \neq 0$. It is easy to see that if $x_1 = x_2 = 0$ the quadratic non-zero condition can only be violated if $x_3 = x_4 = 0$. This condition is of little interest since we are only interested in *real* displacements.

3.6.3. The Grünwald-Blaschke Mapping of Plane Kinematics. Another mapping of planar displacements, which is seen to be isomorphic to the Study mapping, can be derived in a somewhat more intuitive way. Very detailed accounts may be found in Bottema and Roth [**17**], De Sa [**36**] and Ravani [**119**]. It was introduced in 1911 simultaneously, and independently, by Grünwald [**57**] and Blaschke [**14**].

The idea is to map the three independent quantities that describe a displacement to the points of a 3-D image space called Σ'. A general displacement in the plane requires three independent parameters to fully characterise it. The position of a point

in E relative to Σ can be given by the homogeneous linear transformation

$$\begin{bmatrix} X \\ Y \\ Z \end{bmatrix} = \begin{bmatrix} \cos\varphi & -\sin\varphi & a \\ \sin\varphi & \cos\varphi & b \\ 0 & 0 & 1 \end{bmatrix} \begin{bmatrix} x \\ y \\ z \end{bmatrix}, \tag{3.41}$$

where the ratios $(x : y : z)$ represent the homogeneous coordinates of a point in E, $(X : Y : Z)$ are those of the same point in Σ. The Cartesian coordinates of the origin of E measured in Σ are (a, b), while φ is the rotation angle measured from the X-axis to the x-axis, the positive sense being counter-clockwise. Clearly, in Equation (3.41) the three characteristic displacement parameters are (a, b, φ). Image points (points in the 3-D homogeneous projective image space) are defined in terms of the displacement parameters (a, b, φ) as

$$\begin{aligned} (X_1 : X_2 : X_3 : X_4) \;=\; & ((a\sin(\varphi/2) - b\cos(\varphi/2) : \\ & (a\cos(\varphi/2) + b\sin(\varphi/2) : \\ & 2\sin(\varphi/2) : 2\cos(\varphi/2))\,. \end{aligned} \tag{3.42}$$

By virtue of the relationships expressed in Equation (3.42), the transformation matrix from Equation (3.41) may be expressed in terms of the homogeneous coordinates of the image space, Σ'. This yields a linear transformation to express a displacement of E with respect to Σ in terms of the image point:

$$\begin{bmatrix} X \\ Y \\ Z \end{bmatrix} = \begin{bmatrix} (X_4^2 - X_3^2) & -2X_3X_4 & 2(X_1X_3 + X_2X_4) \\ 2X_3X_4 & (X_4^2 - X_3^2) & 2(X_2X_3 - X_1X_4) \\ 0 & 0 & (X_4^2 + X_3^2) \end{bmatrix} \begin{bmatrix} x \\ y \\ z \end{bmatrix}. \tag{3.43}$$

Comparing the elements of the 3×3 transformation matrix in Equation (3.43) with the one in Equation (3.40) it is a simple matter to show that the homogeneous coordinates of the image space Σ' and those of the soma space are related in the

following way:

$$(X_1 : X_2 : X_3 : X_4) \;=\; (y_2 : -y_1 : x_3 : x_4). \tag{3.44}$$

Comparing Equation (3.42) with Equation (3.37) it is evident that the two transformations are isomorphic.

Since each distinct displacement described by (a, b, φ) has a corresponding unique image point, the inverse mapping can be obtained from Equation (3.42): for a given point of the image space, the displacement parameters are

$$\begin{aligned} \tan(\varphi/2) &= X_3/X_4, \\ a &= 2(X_1X_3 + X_2X_4)/(X_3^2 + X_4^2), \\ b &= 2(X_2X_3 - X_1X_4)/(X_3^2 + X_4^2). \end{aligned} \tag{3.45}$$

Equations (3.45) give correct results when either X_3 or X_4 is zero. Caution is in order, however, because the mapping is injective, not bijective: *there is at most one pre-image for each image point* [**24**]. Thus, not every point in the image space represents a displacement. It is easy to see that any image point on the real line $X_3 = X_4 = 0$ has no pre-image and therefore does not correspond to a real displacement of E. From Equation (3.45), this condition renders φ indeterminate and places a and b on the line at infinity.

3.7. Geometry of the Image Space

As mentioned in Section 3.4.5, the group of collineations leaving the absolute quadric invariant gives rise to hyperbolic and elliptic geometry. The geometry is hyperbolic when the absolute quadric is real and elliptic when it is complex. The kinematic mapping image space is determined by a group of linear transformations,

and hence collineations, having the form of Equation (3.43). It is shown in [**17, 36**] that the invariants of this transformation group are

(1) Two complex conjugate planes: $V_{1,2} = X_3 \pm iX_4 = 0$.

(2) The real line ℓ given by the equations $X_3 = X_4 = 0$, which is the intersection of V_1 and V_2: $\ell = V_1 \cap V_2$.

(3) The complex conjugate points $J_1 = (1 : i : 0 : 0)$ and $J_2 = (1 : -i : 0 : 0)$, which are contained on ℓ: $\{J_1, J_2\} \in \ell$.

Note that J_1 and J_2 are on the (real) line ℓ, and the planes V_1 and V_2 intersect in ℓ. The planes V_1 and V_2 comprise a degenerate imaginary quadric given by the equation

$$(X_3 - iX_4)(X_3 + iX_4) \;=\; X_3^2 + X_4^2 \;=\; 0, \tag{3.46}$$

Blaschke [**14**] observed that this is really a special limiting case of the elliptic absolute quadric expressed by

$$\rho(X_1^2 + X_2^2) + X_3^2 + X_4^2 \;=\; 0. \tag{3.47}$$

As $\rho \to 0$ the degenerate invariant quadric of the image space is obtained. Since this is a limiting case, the geometry of the image space is termed *quasi-elliptic* [**14, 36**]. The term quasi-elliptic owes its existence to Blaschke [**5**].

Furthermore, the metric concepts of the distance between two points, the angle between two planes, and the parallelism of two lines are defined [**14, 36**]. Finally, sets of transformations in Σ' are comparable to rotations and translations of Euclidean geometry. Of interest are two special cases:

(1) $X_3 \neq 0$, $X_4 = 0 \Rightarrow \phi = \pi$: These are the 180° half-turns in the Euclidean plane.

(2) (a) $X_3 = 0$, $X_4 \neq 0 \Rightarrow \phi = 0$: These are the pure *rectilinear* and *curvilinear* translations in the Euclidean plane.

(b) $X_3 =$ constant, $\Rightarrow X_4 =$ constant: These are also rectilinear and curvilinear translations in the Euclidean plane, but the moving frame E maintains a constant angle non-zero angle with respect to the fixed frame Σ.

CHAPTER 4

The Forward Kinematics Problem

The *forward kinematics* (FK) problem, also termed the *direct kinematics* [**8**], or *direct position analysis* [**81**] involves determining all possible poses of the moving platform when the actuated joints are locked with specific input values. Referring to Fig. 4.1, the FK problem of a general PSGP can be stated in the following way: given three base points F_A, F_B, F_C in an arbitrary fixed coordinate system, Σ, together with three platform points M_A, M_B, M_C in an arbitrary moving platform coordinate system, E, and given the three actuated joint input values that effectively represent line segment lengths F_AM_A, F_BM_B, F_CM_C, find the positions of E so that the points M_A, M_B, M_C can be joined to the points F_A, F_B, F_C by line segments whose lengths and directions are related to the specified input values.

This subject has been the focus of a tremendous volume of research. A brief sampling of the main contributions, as far as PSGP go, is represented by Peysah [**113**], Gosselin, *et al.* [**49, 50, 51**], Hunt [**76**], Hunt and Primrose [**77**], Husty [**79**] and Merlet [**97, 100**]. With the exception of the method put forward by Husty in [**79**], all of the analysis depends on the geometry and architecture of the platform. Only Merlet [**100**] addresses the FK problem of all possible three-legged lower-pair-jointed planar platforms. However, because plane trigonometry is used to formulate the

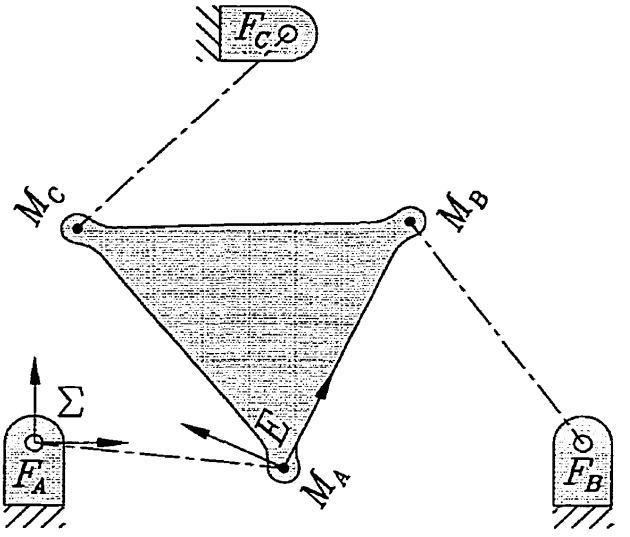

FIGURE 4.1. The FK problem.

constraint equations, distinct architectures require distinct sets of equations, which are further dependent on the platform geometry. While Merlet's approach can be used for every architecture employing lower pairs, it fails for $RR\underline{G}$ types because the platform geometry is not constant.

How many distinct three-legged lower-pair-jointed planar platforms with three DOF are there? This number is arrived at by considering that there are 18 possible kinematic chains to choose from for each leg. A selection of r different elements taken from a set of n elements, without regard to order, is a *combination* of the n elements taken r at a time [**41**]. If the elements are allowed to be counted more than once the number of possible combinations is given by

$$C(n,r) = \frac{(n+r-1)!}{r!(n-1)!}, \tag{4.1}$$

$$C(18,3) = 1140. \tag{4.2}$$

When topological symmetry is a requirement, the number is, of course, 18, those enumerated in Table 2.2, reproduced here in Table 4.1.

Husty's approach [**79**] is independent of the platform geometry. He formulates the FK problem using geometric conditions of the kinematic constraints rather than the platform geometry. The main contribution of this thesis is the generalisation of that approach. That is, a single univariate sextic polynomial is derived and used to solve the FK problem for *all* PSGP, as well as some platforms with certain mixed leg types, and including some special topologies incorporating holonomic higher G-pairs. The coefficients of the univariate are products of given design parameters and the single variable is a coordinate in the kinematic mapping image space. It turns out the image space coordinates corresponding to the six roots of the univariate are linear functions of each root, yielding the solutions to the FK problem. This should prove to be an important tool for designers because the general univariate gives symbolic, not numeric solutions. This means the effects of changing design parameters on the platform kinematics, and by extension dynamics, can be directly evaluated.

RR-type	PR-type	RP-type
$\underline{R}RR$	$\underline{R}PR$	$\underline{R}RP$
$R\underline{R}R$	$P\underline{R}R$	$R\underline{R}P$
$RR\underline{R}$	$PR\underline{R}$	$RP\underline{R}$
$\underline{P}RR$	$\underline{P}PR$	$\underline{P}RP$
$R\underline{P}R$	$P\underline{P}R$	$R\underline{P}P$
$RR\underline{P}$	$PR\underline{P}$	$RP\underline{P}$

TABLE 4.1. The 18 characteristic chains.

As mentioned above, the application of the univariate is not restricted to PSGP. Some mixed leg types can be accommodated. Due to a limitation imposed by the derivation of the univariate, discussed in Section 4.3, leg combinations must all belong to one of the three types in Table 4.1. This being the case, the univariate may be applied to the FK problem of $3[C(6,3)] = 3(56) = 168$ different platforms. Additionally, some architectures containing higher pairs can be analysed, which appears to be missing in all existing literature.

We can solve the FK for some mixed leg type platforms by using the kinematic mapping procedure, determining the intersections of the three quadrics numerically. However, even this approach can not be used for platforms containing any mix of PR- and RP-type legs. The FK problem formulation becomes computationally singular because the fixed and moving frames for each of these leg types are different. To put a number on those we can solve, we first compute the number of combinations there are choosing one leg from each type, *i.e.*, one RR-, one PR- and one RP-type leg:

$$6^3 = 216.$$

Next, determine the forbidden PR-RP-type combinations taken three at a time:

$$C(12,3) - 2[C(6,3)] = 356 - 112 = 252.$$

The $2[C(6,3)]$ pure PR-types and RP-types are allowed, as are RR-PR-types and RR-RP-types. We can exchange the roles of E and Σ in RR-type legs without changing the physical description of the kinematic constraints. Hence, there are $216 + 252 = 468$ forbidden combinations. This means that the FK problem of the 672 remaining combinations can be solved: 168 platforms by using the univariate; 504 by finding the intersection points of their associated constraint surfaces. This process amounts to numerically computing the univariate. However, the univariate with numerical coefficients is architecture and input specific and can only be used for one specific platform and input set, whereas the general univariate has symbolic coefficients and is not so restricted.

From a basic research point-of-view, the solution procedure presented here is incomplete. All 1140 different architectures must be included in a completely general algorithm for solving the FK problem which, regretfully, shall not be found directly in the contents of these pages. For now, the claim of *generality* can only be applied to PSGP as herein defined.

4.1. Kinematic Constraints

Husty observed that $R\underline{P}R$ platform motions are governed by the geometric condition that points with fixed positions in E are bound to move on fixed circles in Σ [**79**]. This kinematic constraint is represented by a quadratic condition in the image space which is a surface whose points are the possible poses of the platform. In order to generalise his approach to all PSGP similar kinematic constraints must be found for all 18 RR-, PR- and RP-type platforms.

Consider an arbitrary RR-type PSGP. The characteristic chain can be any of the six listed in Table 4.1. When the active joint in each leg is locked the sub-chain that remains has two passive R-pairs, this is obviously always the case. Regardless of the characteristic chain, once the active joint is locked one of the remaining R-pairs is fixed in Σ and the other moves on a circle of fixed radius centred on the stationary R-pair. Thus, the motions of an RR-type platform are constrained by the fact that three points with fixed positions in E move on the circumferences of three constant radii, fixed-centred circles in Σ.

Now, consider an arbitrary PR-type platform. When the active joint in each leg is locked the passive R-pair is constrained to move on a line with fixed line coordinates in Σ. This linear constraint may, however, be thought of as one that is a degenerate quadratic, *i.e.*, a circle whose centre lies on a point on the line at infinity. In a projective sense the three lines are three degenerate circles. In this sense the RR- and PR-type platform displacements are governed by the same constraint.

Finally, consider an arbitrary RP-type platform. When the active joint in each leg is locked the passive P-pair is constrained to move on a point with fixed point coordinates in Σ. The kinematic constraint is represented by a planar pencil of lines on a point. When considered projectively, this constraint is nothing but the *dual* of

the constraint for PR-type platforms: a planar pencil of points on a line. Moreover, if E is considered as the fixed and Σ as the moving frame, the kinematic constraints for RP-type platforms are identical to those of PR- and RR-type. In this sense RP-type legs can be considered as kinematic inversions of corresponding PR-type legs. Hence, the displacements of all PSGP are governed by projectively identical kinematic constraints. The next goal is to find a useful algebraic representation of the corresponding constraint surface in the image space.

4.2. Equation of the Image Space Constraint Manifold

Moving points bound to the circumference of a fixed circle represent the most general displacement constraint for all PSGP because the line constraints are degenerate cases of the former. For this reason the general image space constraint manifold of displacements for individual legs of a PSGP can be derived by considering circle-bound points in the displacement space.

The ungrounded R-pair in an RR-type leg is forced to move on a circle with a fixed centre. Meanwhile, the platform can rotate about the moving R-pair. This two parameter family of displacements corresponds to a two parameter family of image points. The family of image points constitute a hyper-surface [**17**]. Its expression can be obtained in the following way: Consider the motion of a fixed point in E that is constrained to move on a fixed circle in Σ, with radius r, centred on the homogeneous coordinates $(X_c : Y_c : Z)$ and having the equation

$$(X - X_c Z)^2 + (Y - Y_c Z)^2 - r^2 Z^2 = 0, \tag{4.3}$$

which, when expanded becomes

$$X^2 + Y^2 - 2XX_c Z - 2YY_c Z + X_c^2 Z^2 + Y_c^2 Z^2 - r^2 Z^2 = 0. \tag{4.4}$$

It is convenient to express Equation 4.4 in the following *homogeneous form*:

$$\mathcal{K}_0(X^2+Y^2) - 2\mathcal{K}_1 XZ - 2\mathcal{K}_2 YZ + \mathcal{K}_3 Z^2 = 0, \tag{4.5}$$

where

$$\begin{aligned} \mathcal{K}_0 &= \text{arbitrary homogenising constant,} \\ \mathcal{K}_1 &= X_c, \\ \mathcal{K}_2 &= Y_c, \\ \mathcal{K}_3 &= \mathcal{K}_1^2 + \mathcal{K}_2^2 - r^2. \end{aligned}$$

Equation (4.5) is homogeneously quadratic in the *variables* X, Y, Z, and homogeneously linear in the *constants* $\mathcal{K}_i$, $i \in \{0,1,2,3\}$ (with $\mathcal{K}$ standing for *kreis*, the German word for *circle*). There is then a dual relationship between the constants and the variables, in that Equation (4.5) could represent the locus of variable points $(X : Y : Z)$ on a fixed circle with *circle coordinates* $[\mathcal{K}_0 : \mathcal{K}_1 : \mathcal{K}_2 : \mathcal{K}_3]$, or dually as a family of variable circles on a fixed point with point coordinates $(X : Y : Z)$. Thus, the four $\mathcal{K}_i$, $i \in \{0,1,2,3\}$ are defined to be homogeneous *circle coordinates*, while X, Y, Z are the homogeneous *point coordinates* of the circle's point locus. Note that four circle coordinates are required since three independent ratios are necessary to uniquely determine a circle, whereas two independent ratios uniquely determine a point in the same plane of the circle. If $\mathcal{K}_0 = 0$ Equation (4.5) represents a line, which is a real degenerate circle, with *line coordinates*[1]

$$[\mathcal{K}_1 : \mathcal{K}_2 : \mathcal{K}_3] \;=\; [-\tfrac{1}{2}L_1 : -\tfrac{1}{2}L_2 : L_3], \tag{4.6}$$

where the L_i are defined to be planar-point duals, as in equation (3.6), and *not* as Plücker line coordinates.

[1]Here we have changed the coordinates from $[X_1 : X_2 : X_3]$, as defined in Equation (3.6), to $[L_1 : L_2 : L_3]$ so they will no be confused with the image space coordinates $[X_1 : X_2 : X_3 : X_4]$.

Recall Equation (3.43) from the previous chapter, reproduced here for reference:

$$\begin{bmatrix} X \\ Y \\ Z \end{bmatrix} = \begin{bmatrix} (X_4^2 - X_3^2) & -2X_3X_4 & 2(X_1X_3 + X_2X_4) \\ 2X_3X_4 & (X_4^2 - X_3^2) & 2(X_2X_3 - X_1X_4) \\ 0 & 0 & (X_4^2 + X_3^2) \end{bmatrix} \begin{bmatrix} x \\ y \\ z \end{bmatrix}. \quad (4.7)$$

This linear transformation gives the coordinates of points in the fixed frame Σ in terms of the points in the moving frame E and the kinematic mapping image points corresponding to a particular displacement. An algebraic expression of the image space constraint manifold emerges when the expressions for $(X : Y : Z)$ from Equation (4.7) are substituted into Equation (4.5):

$$\begin{aligned} &(\mathcal{K}_0 z^2(X_1^2 + X_2^2) + (1/4)\left[\mathcal{K}_0(1 - z^2)(x^2 + y^2) + 2z(\mathcal{K}_1 x + \mathcal{K}_2 y) + Rz^2\right] X_3^2 + \\ &(1/4)\left[Rz^2 + \mathcal{K}_0(1 - z^2)(x^2 + y^2) - 2z(\mathcal{K}_1 x + \mathcal{K}_2 y)\right] X_4^2 - (\mathcal{K}_1 z^2 + \mathcal{K}_0 xz)X_1X_3 + \\ &(\mathcal{K}_2 z^2 - \mathcal{K}_0 yz)X_1X_4 - (\mathcal{K}_0 yz + \mathcal{K}_2 z^2)X_2X_3 + (\mathcal{K}_0 xz - \mathcal{K}_1 z^2)X_2X_4 + \\ &(\mathcal{K}_1 yz - \mathcal{K}_2 xz)X_3X_4)\left[(1/4)(X_3^2 + X_4^2)\right] = 0, \end{aligned} \quad (4.8)$$

where the substitution $\mathcal{K}_3 = R - \mathcal{K}_0(x^2 + y^2)$, $R = \mathcal{K}_1^2 + \mathcal{K}_2^2 - r^2 + \mathcal{K}_0(x^2 + y^2)$ has been made. The R term is used as an ingenious collection of constants, proposed by Husty [84], which reduces the number of flops required to solve the FK problem by about 30%. Equation (4.8) is a quartic in the image space variables X_i, $i \in \{1, 2, 3, 4\}$, but dually linear in the circle (or line) coordinates $\mathcal{K}_i$, $i \in \{0, 1, 2\}$. Note that if $\mathcal{K}_0 = 0$, then R is simply $\mathcal{K}_3$.

Closer inspection of this quartic reveals that it contains two quadratic factors in X_i. The factor $1/4(X_3^2 + X_4^2)$ is exactly the non-zero condition of the planar kinematic mapping, which must be satisfied for a point to be the image of a real displacement. Since only the images of real displacements are considered, this factor is non-zero and may be safely eliminated. What remains is a quadratic in the X_i. The quantities x, y, z, R, and $\mathcal{K}_i$, $i \in \{0, 1, 2, 3\}$ are all design constants. Hence, the first factor in

Equation (4.8) is the point Equation of a quadric surface in the 3-D projective image space. This general quadric is the geometric image of the kinematic constraint that a point in E moves on either a circle, or a line, in Σ.

4.2.1. Identifying the Quadric Constraint Manifold. After the non-zero condition factor is eliminated, equation (4.8) becomes

$$\begin{aligned}
&\mathcal{K}_0 z^2(X_1^2 + X_2^2) + (1/4)\left[\mathcal{K}_0(1-z^2)(x^2+y^2) + 2z(\mathcal{K}_1 x + \mathcal{K}_2 y) + Rz^2\right] X_3^2 + \\
&(1/4)\left[Rz^2 + \mathcal{K}_0(1-z^2)(x^2+y^2) - 2z(\mathcal{K}_1 x + \mathcal{K}_2 y)\right] X_4^2 - (\mathcal{K}_1 z^2 + \mathcal{K}_0 xz)X_1X_3 + \\
&(\mathcal{K}_2 z^2 - \mathcal{K}_0 yz)X_1X_4 - (\mathcal{K}_0 yz + \mathcal{K}_2 z^2)X_2X_3 + (\mathcal{K}_0 xz - \mathcal{K}_1 z^2)X_2X_4 + \\
&(\mathcal{K}_1 yz - \mathcal{K}_2 xz)X_3X_4 \;=\; 0, \qquad (4.9)
\end{aligned}$$

This general equation is greatly simplified under the following assumptions:

(1) No platform of practical significance will have a point at infinity, so it is safe to set $z = 1$.

(2) Platform rotations of $\phi = \pi$ (half-turns) have images in the plane $X_4 = 0$. It is easy to verify that three constraint surfaces intersect the plane $X_4 = 0$ in the complex conjugate points $(1 : \pm i : 0 : 0)$. Because the X_i are implicitly defined by Equation (3.42), setting $\phi = \pi$ gives

$$\begin{aligned}
X_1 &= a, \\
X_2 &= b, \\
X_3 &= 2, \\
X_4 &= 0. \qquad (4.10)
\end{aligned}$$

The displacement parameters can be determined by substituting the quantities from Equation (4.10) into Equation (4.9) giving three constraint equations in terms of a and b. After checking for these solutions, the image space coordinates may be normalised by setting $X_4 = 1$.

(3) Without loss of generality the special coordinate systems of Figure 4.6 can be used because our approach does not depend on platform geometry (this assumption will be applied in section 4.3).

Applying the first two assumptions to Equation (4.9) gives the simplified constraint surface (CS) equation:

$$\begin{aligned} CS: \quad & \mathcal{K}_0(X_1^2 + X_2^2) + (1/4)\left[2(\mathcal{K}_1 x + \mathcal{K}_2 y) + R\right] X_3^2 + (1/4)\left[R - 2(\mathcal{K}_1 x + \mathcal{K}_2 y)\right] - \\ & (\mathcal{K}_1 + \mathcal{K}_0 x) X_1 X_3 - (\mathcal{K}_0 y + \mathcal{K}_2) X_2 X_3 + (\mathcal{K}_2 - \mathcal{K}_0 y) X_1 (\mathcal{K}_0 x - \mathcal{K}_1) X_2 + \\ & (\mathcal{K}_1 y - \mathcal{K}_2 x) X_3 \; = \; 0. \end{aligned} \tag{4.11}$$

The constraint surface can be identified in many ways. For instance, the quadratic form could be diagonalised using well established methods from linear algebra [**9**], to remove the cross terms, then remove the linear offsets. Another, somewhat more elegant, approach is to employ the *Grassmannian method* found in Zsombor-Murray and Hayes [**150**]. A third way is to proceed in a less obvious, but intuitive way by employing some careful *geometric thinking* [**148**]. In what follows, this third approach shall be used to identify the quadrics. There are two cases to consider: 1) if the platform is RR-type, the $\mathcal{K}_i$ are circle coordinates and one may set $\mathcal{K}_0 = 1$; and 2) if the platform is PR- or RP-type, the $\mathcal{K}_i$ are line coordinates and it is necessary to set $\mathcal{K}_0 = 0$.

4.2.2. *RR*-type: Hyperboloid of One Sheet. Setting $\mathcal{K}_0 = 1$ in Equation (4.11) gives the following:

$$\begin{aligned} H: \quad & X_1^2 + X_2^2 + (1/4)\left[2(\mathcal{K}_1 x + \mathcal{K}_2 y) + R\right] X_3^2 - (\mathcal{K}_1 + x) X_1 X_3 - (y + \mathcal{K}_2) X_2 X_3 + \\ & (\mathcal{K}_2 - y) X_1 + (x - \mathcal{K}_1) X_2 + (\mathcal{K}_1 y - \mathcal{K}_2 x) X_3 + (1/4)\left[R - 2(\mathcal{K}_1 x + \mathcal{K}_2 y)\right] \\ & = 0. \end{aligned} \tag{4.12}$$

This surface is seen to be an hyperboloid of one sheet, hence indicated by H, after the subsequent arguments are considered. Equation (4.12) resembles a circle in that it contains the squares of two variables with identical coefficients, X_1^2 and X_2^2, together with a constant term when the value of X_3 is held constant. This suggests investigating intersections of the quadric with planes where X_3 =constant. Collect X_1 and X_2 terms on the left and constant terms, including X_3 terms, on the right-hand side of the equation, then complete the squares in X_1 and X_2 [**129**]. After some algebra, the following equation is obtained:

$$\begin{aligned}\left(X_1 - \tfrac{1}{2}(y - \mathcal{K}_2 + (\mathcal{K}_1 + x)X_3)\right)^2 + \left(X_2 - \tfrac{1}{2}(\mathcal{K}_1 - x + (\mathcal{K}_2 + y)X_3\right)^2 \\ = \tfrac{r^2}{4}(1 + X_3^2).\end{aligned} \tag{4.13}$$

Equation (4.13) represents a circle in the planes where X_3 is a constant. The circle centre has coordinates

$$\left(\frac{1}{2}(y - \mathcal{K}_2 + (\mathcal{K}_1 + x)X_3) \ : \ \frac{1}{2}(\mathcal{K}_1 - x + (\mathcal{K}_2 + y)X_3) \ : \ X_3\right), \tag{4.14}$$

and radius

$$R_{X_3} \ = \ \frac{r}{2}\sqrt{(1 + X_3^2)}. \tag{4.15}$$

As X_3 is varied, the locus of circle centres defines a curve whose parametric equation can be obtained as follows. Take an arbitrary circle in the plane $X_3 = t$ and set its radius to $R_{X_3} = 0$:

$$\frac{r}{2}\sqrt{(1 + t^2)} \ = \ 0. \tag{4.16}$$

Since the term $1 + t^2$ can never vanish for real values of X_3, zero can only be obtained by setting $r = 0$, *i.e.*, the constraint circle upon which the platform point moves

must collapse to the fixed revolute centre so that the fixed and moving points are coincident. Making these substitutions in Equation (4.13) gives

$$\left[X_1 - \frac{1}{2}(y - \mathcal{K}_2 + (\mathcal{K}_1 + x)t)\right]^2 + \left[X_2 - \frac{1}{2}(\mathcal{K}_1 - x + (\mathcal{K}_2 + y)t\right]^2 = 0. \quad (4.17)$$

Because the two terms are squared and added the only way to satisfy Equation (4.17) over the real field is if the quantities within the square brackets vanish. This immediately gives the parametric equation

$$\begin{bmatrix} X_1 \\ X_2 \\ X_3 \end{bmatrix} = \frac{1}{2}\begin{bmatrix} y - \mathcal{K}_2 \\ \mathcal{K}_1 - x \\ 0 \end{bmatrix} + \frac{t}{2}\begin{bmatrix} \mathcal{K}_1 + x \\ \mathcal{K}_2 + y \\ 2 \end{bmatrix}. \quad (4.18)$$

Equation (4.18) is linear in the single parameter t and is clearly the equation of a line. This leads to the conclusion that the quadric surface is a family of generally non-concentric circles whose centre points are all collinear. Furthermore, it is apparent from Equation (4.13) that the smallest circle of the family occurs when $X_3 = 0$. As X_3 increases in value the circles become larger regardless of the sign of X_3. The only possible quadric surface that fits this geometric description is an hyperboloid of one sheet. The hyperboloid axis is given by Equation (4.18). Note that the axis is not necessarily perpendicular to the circles. The axis belongs to the hyperboloid and the curves to which it is perpendicular are, in general, ellipses. However, the hyperboloid always intersects the planes parallel to $X_3 =$ constant in circles. Thus, the X_3-axis is perpendicular to the circles. If, however, $\mathcal{K}_1 = \mathcal{K}_1 = x = y = 0$ the axis of the hyperboloid is the X_3-axis, and the circles, one in each plane $X_3 =$ a constant, are coaxial. Note if X_3 is a constant then X_4 must also be a constant (recall $X_3 = 2\sin\varphi/2$ and $X_4 = 2\cos\varphi/2$). Points in the planes $X_3 =$ constant represent positions of the platform having the same orientation. Curves in these planes represent curvilinear planar motions.

4.2.3. Parametric Equation of the Constraint Hyperboloid. If computer generated images of the constraint hyperboloid are required then a parametrisation is necessary. The parametric equation of a second order surface requires two parameters. The implicit form of the constraint hyperboloid, Equation (4.12), represents a circle in the projection of the intersection of the two hyper-planes X_3 =constant and $X_4 = 1$. An arbitrary hyperboloid circle can be parametrised with an angle ζ, see Figure 4.2. The radius of the circle can then be changed by varying the parameter t. Referring to Figure 4.2, the hyperboloid circle equation may be written as

$$(X_1 - X_{1c})^2 + (X_2 - X_{2c})^2 - R_{X_3}^2 \;=\; 0, \tag{4.19}$$

where (X_{1c}, X_{2c}) are the coordinates of the circle centre and R_{X_3} is its radius.

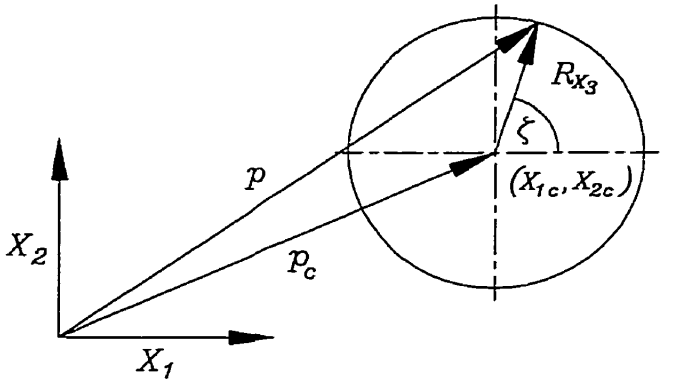

FIGURE 4.2. An arbitrary hyperboloid circle.

The locus of points satisfying Equation (4.19) can be generated parametrically with the angle ζ such that the following vector equation, illustrated in Figure 4.2, is fulfilled:

$$\boldsymbol{p} \;=\; \boldsymbol{p}_c + \boldsymbol{R}_{X_3}(\zeta). \tag{4.20}$$

Writing Equation (4.20) in component form gives

$$\begin{bmatrix} X_1 \\ X_2 \end{bmatrix} = \begin{bmatrix} X_{1c} + R_{X_3}\cos\zeta \\ X_{2c} + R_{X_3}\sin\zeta \end{bmatrix}. \tag{4.21}$$

Using the expressions in Equation (4.13) with $X_3 = t$, Equation (4.21) can be rewritten, giving the parametric form of the constraint hyperboloid in terms of the two parameters t and ζ:

$$\begin{bmatrix} X_1 \\ X_2 \\ X_3 \end{bmatrix} = \frac{1}{2}\begin{bmatrix} [(\mathcal{K}_1 + x)t - \mathcal{K}_2 + y] + (r\sqrt{t^2+1})\cos\zeta \\ [(\mathcal{K}_2 + y)t + \mathcal{K}_1 - x] + (r\sqrt{t^2+1})\sin\zeta \\ 2t \end{bmatrix}, \quad \begin{array}{l} \zeta \in \{0, \ldots, 2\pi\}, \\ t \in \{-\infty, \ldots, \infty\}. \end{array} \tag{4.22}$$

Figure 4.3 is a parametric representation of a constraint hyperboloid where $\mathcal{K}_1 = \mathcal{K}_2 = 0$, $r = 4$, and the moving platform points have the coordinates $x = y = 0$.

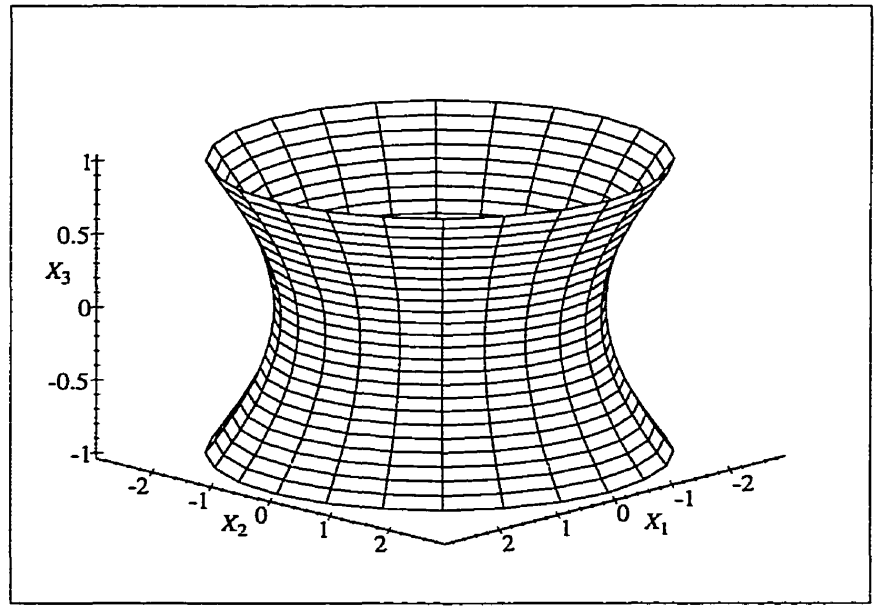

FIGURE 4.3. A projection of H in the hyper-plane $X_4 = 1$.

4.2.4. *PR*- and *RP*-type: Hyperbolic Paraboloid. A very different constraint manifold is obtained when the displacement condition is changed so that a fixed point in the moving frame E is constrained to move on a fixed line in the non-moving frame Σ. This condition requires the $\mathcal{K}_i$ to represent planar line coordinates. Hence, it is necessary to set $\mathcal{K}_0 = 0$. Equation (4.5) becomes

$$Z(-2\mathcal{K}_1 X - 2\mathcal{K}_2 Y + \mathcal{K}_3 Z) \;=\; 0. \tag{4.23}$$

The factor $Z = 0$ represents the line at infinity in P_2, while the factor in parentheses is the equation of a line where the first two line coordinates are multiplied by -2. The fact that the second degree equation splits into two linear factors is the rationalisation for saying that the line is a degenerate circle. The -2 can be treated as a proportionality factor arising from the original circle formulation of the equation of constraint. The *trivial* factor $Z = 0$ can be ignored because only ordinary lines (non-ideal lines) need be considered for practical designs. The circle coordinates, $K_{\tilde{z}}$, are simply obtained from the line coordinates L_i, see Equation (4.6).

Transforming the point coordinates $(X : Y : Z)$ in Equation (4.23) using Equation (4.7), and setting $X_4 = z = 1$ gives an hyperbolic paraboloid, indicated by HP:

$$\begin{aligned} HP:\ (\mathcal{K}_2 - \mathcal{K}_1 X_3)X_1 - (\mathcal{K}_1 + \mathcal{K}_2 X_3)X_2 + \frac{1}{4}\left[\mathcal{K}_3 + 2(\mathcal{K}_1 x + \mathcal{K}_2 y)\right] X_3^2 + \\ (\mathcal{K}_1 y - \mathcal{K}_2 x)X_3 + \frac{1}{4}\left[\mathcal{K}_3 - 2(\mathcal{K}_1 x + \mathcal{K}_2 y)\right] \;=\; 0. \end{aligned} \tag{4.24}$$

This is seen to be true after the following argument is considered. Equation (4.24) is a quadric in the X_i, but very different in form from Equation (4.12). To compare them, Equation (4.24) too, may be intersected by planes where X_3 is a constant, together with $X_4 = 1$. As X_3 is varied, a family of mutually skew lines is obtained wherein all common normals between line pairs are parallel. This means that Equation (4.24) describes a family of mutually skew lines that are all parallel to

a plane, but not to each other. Thus, the family of lines is a regulus of an hyperbolic paraboloid.

Clearly, a line is not a circle. However, lines in P_2 are *closed* by a point at infinity just as a circle is closed by any finite point on it. In a projective sense, lines and circles are both closed curves (all circles contain J_1 and J_2, but the circle itself is continuous). In this way, a line may be considered a degenerate circle whose centre is on the line at infinity. Given this projective geometric connection between these kinematic constraints, it is not unreasonable to expect similar connections between the corresponding constraint manifolds in the kinematic mapping image space.

The hyperboloid of one sheet (as well as the cylinder and cone, which, are degenerate hyperboloids) and the hyperbolic paraboloid are the only quadrics ruled with real lines. These are *doubly ruled* while cones and cylinders, which appear *singly ruled*, contain degenerate double rulings [**71**]. In the same way that a line can be considered a degenerate circle, the hyperbolic paraboloid may be considered a degenerate hyperboloid. This is due to the geometric distinction between the two quadrics: three mutually skew lines, not parallel to any plane, determine an hyperboloid of one sheet; whereas, three mutually skew lines that are parallel to some plane determine an hyperbolic paraboloid [**136**]. Furthermore, there is no special case of the hyperbolic paraboloid which is a surface of revolution [**71**], unless one argues that a plane is a degenerate cylinder of revolution closed by a line at infinity. Still, there is no dilatation[2] that can transform an hyperbolic paraboloid into a surface of revolution [**27**]. It is apparent on inspection that every real plane intersects the hyperbolic paraboloid in either a parabola or an hyperbola. Both types of curve are closed only by the line at infinity so that the intersection can never be an ellipse or circle without real

[2]A dilatation is a similarity transformation that applies a positive, non-zero scaling factor with respect to an invariant point, or line in such a way that all points in space change in a fixed ratio. These transformations change circles into ellipses (or circles), lines into lines, planes into planes, and all second-order curves and surfaces into second-order curves and surfaces, respectively [**30**].

points at infinity. Consequently the hyperbolic paraboloid cannot be obtained from any surface of revolution by a dilatation because there are circles on every surface of revolution. These circles would be transformed into ellipses by a dilatation [**71**].

4.2.5. Parametric Equation of the Constraint Hyperbolic Paraboloid.

The general hyperboloid of one sheet, *i.e.*, not one of revolution, can be constructed geometrically by rotating a line which joins pairs of points with constant difference of eccentric angle on two equal and similarly placed ellipses in parallel planes [**136**]. The hyperbolic paraboloid can also be constructed with a moving line. Let $ABA'B'$ be the vertices of a regular tetrahedron; Q and Q' are variable points on AB and $A'B'$ such that $AQ = A'Q'$. The moving line QQ' generates an hyperbolic paraboloid [**136**]. The quadric surface is covered by two systems of generating lines. Each system is called a *regulus*. In this construction two distinct lines in one regulus are used to generate the lines in the other. Using this approach, Equation (4.24) can be parametrised. However, knowing the plane equation to which the lines of one regulus are parallel, only one line in the opposite regulus is required. This line can be used as the directrix of the opposite regulus.

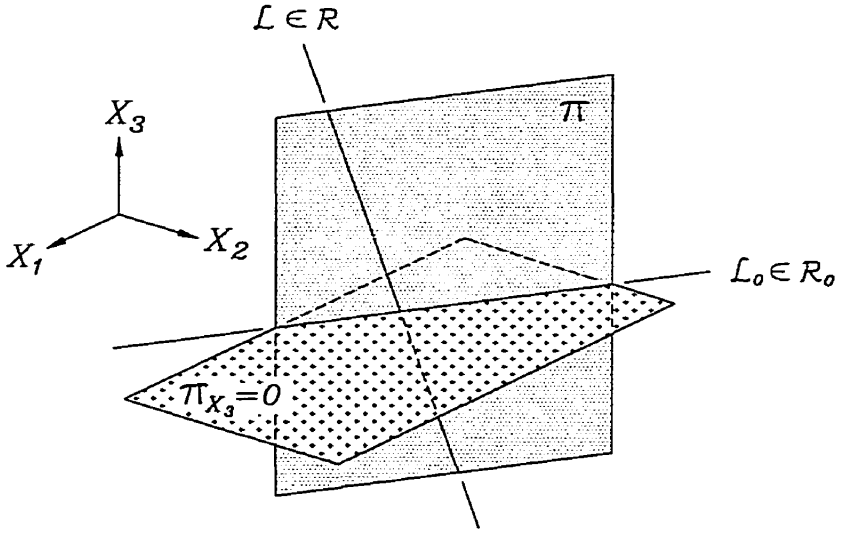

FIGURE 4.4. Construction of the hyperbolic paraboloid.

When $X_3 = 0$ then Equation (4.24) represents a line, $\mathcal{L}_0$, which is contained in the plane $X_3 = 0$, indicated by $\pi_{X_3} = 0$. Now, consider the plane π that also contains $\mathcal{L}_0$, but is perpendicular to $\pi_{X_3} = 0$, see Figure 4.4. The X_3-axis is parallel to π. Each line in one regulus, $\mathcal{R}$, intersects every line in the *opposite* regulus, $\mathcal{R}_0$. Let the line $\mathcal{L}_0$ be one line in regulus $\mathcal{R}_0$. There is one and only one line $\mathcal{L}$ contained in the intersection of regulus $\mathcal{R}$ and plane π: $\mathcal{L} \in \mathcal{R} \in \pi$. Clearly, $\mathcal{L}$ intersects $\mathcal{L}_0$: $\mathcal{L} \cap \mathcal{L}_0$. Moreover, it intersects every line in $\mathcal{R}_0$: $\mathcal{L} \cap \mathcal{R}_0$. The two lines $\mathcal{L}_0$ and $\mathcal{L}$ are unique in their respective planes, $\pi_{X_3} = 0$ and π.

Every distinct point on $\mathcal{L}$ represents an intersection with a distinct line in $\mathcal{R}_0$. For the parametrisation we observe that unique values of X_3 give unique points on $\mathcal{L}$. Every different line in $\mathcal{R}_0$, which can be called $\mathcal{L}_i$ since it is uniquely determined by the plane $X_3 = C_i$, has a direction different from all other lines in $\mathcal{R}_0$ because all lines in this regulus are parallel to the plane $\pi_{X_3} = 0$ but not to each other. Furthermore, $\mathcal{L}_i$ intersects $\mathcal{L}$ in a point that must also be contained in $X_3 = C_i$, because the quadric is covered by the intersection points of the generating lines in opposite reguli.

The locus of points on $\mathcal{L}$ is a function of the parameter $X_3 = t$. This is because there is one and only one distinct line contained in each plane $X_3 = t$ that is contained in $\mathcal{R}_0$ and intersects $\mathcal{L}$ in a point. The points of $\mathcal{L}$ are determined by the piercing points of $\mathcal{L}_i \in \mathcal{R}_0 \cap \pi$. This family of piercing points trace $\mathcal{L} \in \mathcal{R}$. Thus, $\mathcal{L}$ may be expressed parametrically in terms of $X_3 = t$ by the three simultaneous equations:

$$\mathcal{L} = \begin{bmatrix} f(t) \\ g(t) \\ t \end{bmatrix}. \tag{4.25}$$

A general line in space can be described by a fixed point on the line along with a direction. For every value of t there is a a unique point on $\mathcal{L}$, which is a point on the

corresponding line $\mathcal{L}_i \in \mathcal{R}_0$. The direction of $\mathcal{L}_i$ is also a function of t since it must be parallel to $\pi_{X_3} = 0$ which is, itself, parallel to $\pi_{X_3} = t$, but to no other line in $\mathcal{R}_0$. The locus of points on $\mathcal{L}_i$ can be obtained by stepping in the direction of $\mathcal{L}_i$ on a line through the unique point on $\mathcal{L}$, which is obtained by varying a second parameter, s:

$$\mathcal{L}_i \;=\; HP \;=\; \begin{bmatrix} f(t) \\ g(t) \\ t \end{bmatrix} + s \begin{bmatrix} a(t) \\ b(t) \\ 0 \end{bmatrix}. \tag{4.26}$$

This collection of lines is a quadric by virtue of the mixed second order quantities $sa(t)$ and $sb(t)$. It is, in fact, the parametric equation of the constraint hyperbolic paraboloid (HP). Determining the functions $f(t)$, $g(t)$, $a(t)$ and $b(t)$ will yield the parametrisation.

The first step is to determine the plane π. The condition is that π is perpendicular to $\pi_{X_3} = 0$. This being the case, the variable X_3 can have any value in π. After setting $X_3 = 0$ in Equation (4.24), the equation for $\mathcal{L}_0$ is obtained:

$$\mathcal{L}_0 :\; \mathcal{K}_2 X_1 - \mathcal{K}_1 X_2 + \frac{1}{4}\left(\mathcal{K}_3 - 2(\mathcal{K}_1 x + \mathcal{K}_2 y)\right) \;=\; 0. \tag{4.27}$$

The line $\mathcal{L}_0$ is the line of intersection of the two planes: $\pi_{X_3} = 0 \cap \pi$. The plane π is perpendicular to $\pi_{X_3} = 0$ and must also contain $\mathcal{L}_0$. Due to this, π can be described by solving Equation (4.27) for either X_1 or X_2 and allowing X_3 to take on any value. Solving for X_1 we obtain

$$\pi \;=\; \begin{cases} X_1 \;=\; \frac{1}{\mathcal{K}_2}\left(\mathcal{K}_1 X_2 - \frac{1}{4}\left(\mathcal{K}_3 - 2(\mathcal{K}_1 x + \mathcal{K}_2 y)\right)\right) \\ X_3 \;=\; X_3 \end{cases}. \tag{4.28}$$

If $\mathcal{K}_2$ is less than some predetermined tolerance, *i.e.*, close to zero, then Equation (4.27) is solved for X_2, giving

$$\pi \;=\; \begin{cases} X_2 \;=\; \frac{1}{\mathcal{K}_1}(\mathcal{K}_2 X_1 + \frac{1}{4}(\mathcal{K}_3 - 2(\mathcal{K}_1 x + \mathcal{K}_2 y))) \\ X_3 \;=\; X_3 \end{cases} . \tag{4.29}$$

Note that $\mathcal{K}_1$ and $\mathcal{K}_2$ cannot both vanish since $\mathcal{K}_1 = k \sin\theta$ and $\mathcal{K}_2 = k\cos\theta$, with k being a non-zero real number.

In what follows either representation of the plane π, Equation (4.28) or Equation (4.29), may be used yielding identical results. Without loss in generality $\mathcal{K}_2$ can be assumed sufficiently large for this derivation. Equations (4.28) mean that any point $[X_1 : X_2 : X_3] \in \pi$ is given by choosing values for X_2 and X_3 and then solving Equation (4.27) for X_1 (*i.e.*, the first of equations (4.28)). Thus, the plane π, which is perpendicular to $\pi_{X_3} = 0$, is completely described by the first of equations (4.28), since X_2 and X_3 are arbitrary, and independent.

The next step is to find an expression for $\mathcal{L} \in \mathcal{R}$. This is done by finding the line of intersection of π and the implicit equation of the hyperbolic paraboloid, Equation (4.24). This is the unique line in $\mathcal{R}$ contained in π which intersects $\mathcal{L}_0 \in \mathcal{R}_0$. This equation is obtained by substituting the first of first of equations (4.28) into Equation (4.24), yielding

$$\pi \cap HP: \\ \frac{X_3}{\mathcal{K}_2}\left[-(\mathcal{K}_1^2 + \mathcal{K}_2^2)X_2 + \left(\frac{1}{2}(\mathcal{K}_2^2 y + \mathcal{K}_1\mathcal{K}_2 x) + \mathcal{K}_2\mathcal{K}_3\right) X_3 + \mathcal{K}_1\mathcal{K}_3 + (\mathcal{K}_2^2 - \frac{1}{2}\mathcal{K}_1^2)x\right] = 0, \tag{4.30}$$

assuming $\mathcal{K}_2$ is sufficiently large. This intersection contains two factors, $X_3 = 0$, and the line

$$\mathcal{L}: \; -(\mathcal{K}_1^2 + \mathcal{K}_2^2)X_2 + \left(\tfrac{1}{2}(\mathcal{K}_2^2 y + \mathcal{K}_1\mathcal{K}_2 x) + \mathcal{K}_2\mathcal{K}_3\right) X_3 + \mathcal{K}_1\mathcal{K}_3 + (\mathcal{K}_2^2 - \tfrac{1}{2}\mathcal{K}_1^2)x = 0. \tag{4.31}$$

This agrees with the fact that a plane intersecting with a quadric must produce a second order curve. Here the conic degenerates into two lines. This second factor *must* be an expression for $\mathcal{L}$, since it is a line contained in the intersection of π and HP that is *not* $\mathcal{L}_0$. Since $\mathcal{L}_0$ and $\mathcal{L}$ intersect, and because they are both in HP, these lines are in the opposite reguli $\mathcal{R}_0$ and $\mathcal{R}$.

Now, solve Equation (4.31) for X_2. After setting $X_3 = t$ the following expression is obtained:

$$g(t) = \frac{\left[\left(\frac{1}{2}(\mathcal{K}_1\mathcal{K}_2 x + \mathcal{K}_2^2 y) + \mathcal{K}_2\mathcal{K}_3\right) t - \frac{1}{2}(\mathcal{K}_1^2 + \mathcal{K}_2^2)x + \frac{1}{2}\mathcal{K}_1\mathcal{K}_2 y + \mathcal{K}_1\mathcal{K}_3\right]}{\mathcal{K}_1^2 + \mathcal{K}_2^2}. \tag{4.32}$$

$g(t)$ represents the X_2 coordinate of a point on the line $\mathcal{L} \in \mathcal{R}$ for a particular value of t. The X_1 coordinate is obtained by substituting the expression for $X_2 = g(t)$ into Equation (4.28) which yields another function of only t:

$$f(t) = \frac{\left[\left(\frac{1}{2}(\mathcal{K}_1\mathcal{K}_2 y + \mathcal{K}_1^2 x) + \mathcal{K}_1\mathcal{K}_3\right) t + \frac{1}{2}(\mathcal{K}_1^2 + \mathcal{K}_2^2)y - \frac{1}{2}\mathcal{K}_1\mathcal{K}_2 x - \mathcal{K}_2\mathcal{K}_3\right]}{\mathcal{K}_1^2 + \mathcal{K}_2^2}. \tag{4.33}$$

This gives Equation (4.25), which is the desired parametric equation for $\mathcal{L}$ in terms of $X_3 = t$. Note that the denominators of the rational functions $f(t)$ and $g(t)$ are identical: $\mathcal{K}_1^2 + \mathcal{K}_2^2$. Moreover, the denominator is non-vanishing because $\mathcal{K}_1^2$ and $\mathcal{K}_2^2$ are, for the linear kinematic constraints, line coordinates and cannot simultaneously be zero. All distinct lines in $\mathcal{R}_0$ must contain a point on $\mathcal{L}$. Furthermore, every distinct plane $\pi_{X_3} = t$ contains a distinct line of $\mathcal{R}_0$ and every unique plane $\pi_{X_3} = t$ intersects $\mathcal{L}$ in a unique point.

Now, direction vectors for the $\mathcal{L}_i$ are required. The coefficients in Equation (4.24) are constants, and may be collected giving

$$aX_1 + bX_2 + cX_3^2 + dX_3 + e \;=\; 0, \tag{4.34}$$

where a and b are both functions of $X_3 = t$. In an arbitrary plane $\pi_{X_3} = t$ the direction of the corresponding line is given by the coefficient ratio $-b/a$, *i.e.*, the slope of the line in the given plane. In other words, the line $\mathcal{L}_i$ is parallel to the direction given by

$$a(t)X_1 + b(t)X_2 = 0, \tag{4.35}$$

where $a(t) = \mathcal{K}_2 - \mathcal{K}_1 t$ and $b(t) = -(\mathcal{K}_1 + \mathcal{K}_2 t)$. Non-trivial solutions of Equation (4.35) require

$$a(t) = X_2,\ b(t) = -X_1 \tag{4.36}$$

or,

$$a(t) = -X_2,\ b(t) = X_1, \tag{4.37}$$

which are equivalent conditions because the linear sum vanishes. Thus, the locus of points on a line in the direction of $\mathcal{L}_i$ is

$$\begin{bmatrix} X_1 \\ X_2 \\ X_3 \end{bmatrix} = s \begin{bmatrix} -b(t) \\ a(t) \\ 0 \end{bmatrix}, \tag{4.38}$$

where $-\infty \leq s \leq \infty$. These are the projections of the lines in $\mathcal{R}_0$ onto the plane $\pi_{X_3} = 0$.

Combining equations (4.25) and (4.38) gives the desired parametrisation of the constraint hyperbolic paraboloid (HP):

$$HP: \begin{bmatrix} X_1 \\ X_2 \\ X_3 \end{bmatrix} = \begin{bmatrix} f(t) \\ g(t) \\ t \end{bmatrix} + s \begin{bmatrix} -b(t) \\ a(t) \\ 0 \end{bmatrix}, \quad \begin{array}{l} -\infty \leq t \leq \infty, \\ -\infty \leq s \leq \infty. \end{array} \tag{4.39}$$

Figure 4.5 illustrates a parametric representation of a constraint hyperbolic paraboloid with circle coordinates $\mathcal{K}_0 = 0$, $\mathcal{K}_1 = 1$, $\mathcal{K}_2 = \mathcal{K}_3 = 0$, and fixed platform point coordinates $x = y = 0$.

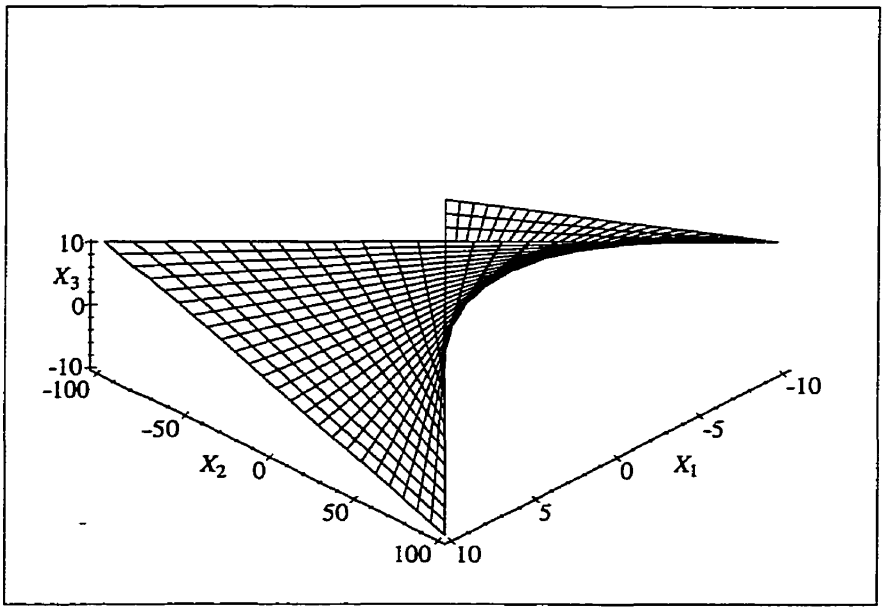

FIGURE 4.5. A projection of HP in the hyper-plane $X_4 = 1$.

4.3. Obtaining the General Univariate Polynomial in X_3

The constraint manifold for PSGP is determined by the circle coordinate $\mathcal{K}_0$. If $\mathcal{K}_0 = 1$ the projection of the manifold into the image sub-space $X_4 = 1$ is an hyperboloid of one sheet; on the other hand, if $\mathcal{K}_0 = 0$ it is an hyperbolic paraboloid. Expressions for both are embedded in the general constraint surface (CS) equation given in Equation (4.11), reproduced below as Equation (4.40):

$$\begin{aligned} CS: \quad & \mathcal{K}_0(X_1^2 + X_2^2) + (1/4)\left[2(\mathcal{K}_1 x + \mathcal{K}_2 y) + R\right] X_3^2 + (1/4)\left[R - 2(\mathcal{K}_1 x + \mathcal{K}_2 y)\right] - \\ & (\mathcal{K}_1 + \mathcal{K}_0 x) X_1 X_3 - (\mathcal{K}_0 y + \mathcal{K}_2) X_2 X_3 + (\mathcal{K}_2 - \mathcal{K}_0 y) X_1 (\mathcal{K}_0 x - \mathcal{K}_1) X_2 + \\ & (\mathcal{K}_1 y - \mathcal{K}_2 x) X_3 \; = \; 0. \end{aligned} \tag{4.40}$$

The points on this constraint surface represent all possible displacements of the platform when two of the three legs are disconnected from the platform. In other words, they represent the possible displacements of E about the base point to which the platform is still connected. Three such constraint surfaces are obtained, one corresponding to each leg, CS_A, CS_B and CS_C.

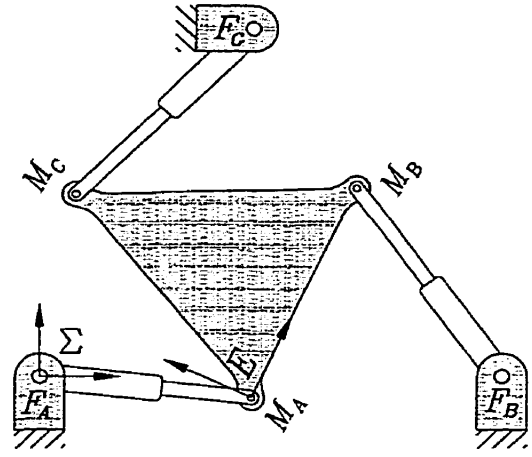

FIGURE 4.6. Convenient reference frames.

Without loss in generality, the special coordinate frames in Figure 4.6 can be used (see assumption 3 from subsection 4.2.1). In the most general case (*i.e.*, for any PSGP, regardless of leg type) the fixed points in the frame Σ have the homogeneous coordinates

$$\begin{aligned} F_{A/\Sigma} &= (0:0:1), \\ F_{B/\Sigma} &= (X_{B_1}:0:1), \\ F_{C/\Sigma} &= (X_{C_1}:X_{C_2}:1); \end{aligned}$$

while those of the points fixed in the frame E are

$$\begin{aligned} M_{A/E} &= (0:0:1), \\ M_{B/E} &= (b_1:0:1), \\ M_{C/E} &= (c_1:c_2:1). \end{aligned}$$

Note that we have not explicitly stated which frame is fixed since they are different for PR-types and RP-types. The circle coordinates determined from the F_i are:

$$\begin{aligned} \mathcal{K}_{A_i} &= (\mathcal{K}_0 : A_1 : A_2 : A_3), \\ \mathcal{K}_{B_i} &= (\mathcal{K}_0 : B_1 : B_2 : B_3), \\ \mathcal{K}_{C_i} &= (\mathcal{K}_0 : C_1 : C_2 : C_3), \end{aligned}$$

where the $\mathcal{K}_0$ coordinate is the same in all legs. Here it is important to state the current limitation of this approach: the $\mathcal{K}_0$ coordinate must be the same value for each of the three legs in any one PSGP. If this is not done the subsequent system of surface equations can not be reduced to a univariate because the number of computations involved becomes too large. There are two ways to resolve this problem: the first is to somehow simplify the constraint equations through better understanding of the geometry of the image space; the second is to wait until faster computers are available. This being the case, the use of the univariate is limited to PSGP and architectures comprising arbitrary legs, but all being either RR-, PR-, or RP-type. This is why the univariate is only applicable to the FK problem of $3[C(6,3)] = 168$ different platforms.

Substituting the $M_{i/E}$ and the $\mathcal{K}_i$ into Equation (4.40) gives the three specific constraint surfaces, CS_A, CS_B, CS_C:

$$CS_A : \mathcal{K}_0(X_1^2 + X_2^2) + \frac{1}{4}R_1X_3^2 + (A_2 - A_1X_3)X_1 - (A_1 + A_2X_3)X_2 + \frac{1}{4}R_1 = 0, \quad (4.41)$$

$$\begin{aligned} CS_B : \mathcal{K}_0(X_1^2 + X_2^2) &+ \frac{1}{4}(R_2 + 2B_1b_1)X_3^2 + (B_2 - (\mathcal{K}_0b_1 + B_1)X_3)X_1 + \\ &(\mathcal{K}_0b_1 - B_1 - B_2X_3)X_2 - B_2b_1X_3 + \frac{1}{4}(R_2 - 2B_1b_1) = 0, \end{aligned} \quad (4.42)$$

$$\begin{aligned} CS_C : \mathcal{K}_0(X_1^2 + X_2^2) &+ \frac{1}{4}(R_3 + 2C_1c_1 + 2C_2c_2)X_3^2 + (C_2 - \mathcal{K}_0c_2 - (\mathcal{K}_0c_1 + C_1)X_3)X_1 + \\ &(\mathcal{K}_0c_1 - C_1 - (C_2 + \mathcal{K}_0c_2)X_3)X_2 + (C_1c_2 - C_2c_1)X_3 + \frac{1}{4}(R_3 - 2C_1c_1 - C_2c_2) \\ &= 0. \end{aligned} \quad (4.43)$$

There are a wide variety of ways to obtain a univariate polynomial from these three surface equations using symbolic computer algebra systems. These include extension methods, such as *homotopy* or *polynomial continuation* [**106**] and elimination methods, such as *Sylvester's dialytic elimination* [**124, 130**]. Additionally, the *Buchberger algorithm* [**2**], which exploits David Hilbert's *Nullstellensatz*[3] and *Basis Theorem*[4], can be used to obtain the reduced minimal *Gröbner bases* [**2, 12, 27**]. For a particular ordering on the power products one of the Gröbner bases will be the univariate, if it exists. However, for this particular variety, the univariate in X_3 can be easily obtained in two elimination steps [**130**]. The first step is to subtract CS_B from CS_A and CS_C from CS_A, giving two equations, CS_{AB} and CS_{AC}, which are linear in X_1 and X_2:

$$\begin{aligned} CS_{AB}: \frac{1}{4}(R_1 - R_2 - 2B_1b_1)X_3^2 + [(\mathcal{K}_0 b_1 + B_1 - A_1)X_3) - B_2 + A_2]\,X_1 + \\ [(B_2 - A_2)X_3 - A_1 - \mathcal{K}_0 b_1 + B_1]\,X_2 + B_2 b_1 X_3 + \frac{1}{4}(R_1 - R_2 + 2B_1 b_1) = 0, \quad (4.44) \\ CS_{AC}: \frac{1}{4}(R_1 - R_3 - 2C_1c_1 - 2C_2c_2)X_3^2 + [(\mathcal{K}_0 c_1 + C_1 - A_1)X_3 + \mathcal{K}_0 c_2 - C_2 + A_2]\,X_1 + \\ [(\mathcal{K}_0 c_2 + C_2 - A_2)X_3 - \mathcal{K}_0 c_1 + C_1 - A_1]\,X_2 + (C_2 c_1 - C_1 c_2)X_3 + \\ \frac{1}{4}(R_1 - R_3 + 2C_1c_1 + 2C_2c_2) = 0. \quad (4.45) \end{aligned}$$

Equations (4.44) and (4.45) are solved simultaneously for X_1 and X_2. The resulting expressions are then substituted into Equation (4.43), yielding a univariate sextic polynomial in X_3. In this most general case, *i.e.*, leaving $\mathcal{K}_0$ arbitrary, the univariate has 3613 terms. Here the use of the word *term* requires some explanation. Of course,

[3]This theorem, which translates from German as the *Zero Theorem* [**1**], or *Zero-Point Theorem* [**27**], states that the polynomials of any non-unit ideal [**1**] whose coefficients are defined over an algebraically closed field [**59**] will always have common zeros, *i.e.* solutions.

[4]This theorem essentially guarantees that every polynomial ideal can be generated with a finite set of polynomials, which also means that the variety of the ideal can be expressed by a finite set of polynomial equations [**1, 2**]. In other words, the common solution for the infinite set of polynomials of a polynomial ideal can always be represented by a finite set of polynomials. This finite set actually generates the ideal. The Nullstellensatz and Basis Theorem were proved by Hilbert around 1890 [**1**].

a sextic univariate polynomial has 7 terms:

$$a_6 X_3^6 + a_5 X_3^5 + \ldots + a_1 X_3^1 + a_0 X_3^0 \;=\; 0. \tag{4.46}$$

Each term has a constant coefficient, but the a_i change as the inputs change. What 3613 *terms* means is that the 7 a_i are collectively composed of 3613 sums of products of design constants and inputs (see Appendix C).

When the circle coordinates are appropriately defined, the zeros, or roots, of this sextic represent the solutions to the FK problem of any PSGP together with the asymmetric and special architecture platforms mentioned at the outset of this chapter. The roots of the polynomial give the values of the image space coordinate X_3 with $X_4 = 1$. The remaining coordinates, X_1 and X_2 are linearly dependent on X_3. Their respective values are obtained from the simultaneous solution of equations (4.44) and (4.45). These coordinates are the points of intersection of the three constraint surfaces. Each point of intersection represents a pose of the moving platform such that the platform points are on their respective circles, or lines, representing solutions to the FK problem. Real intersections occur in pairs, because the complex solutions always come in conjugate pairs. Hence, there are 2, 4, 6, or 0 real solutions for a given FK problem.

Examining Figure 4.6, it is easy to see that RR-type platforms require three fixed points in E to move on three fixed non-degenerate real circles in Σ. Setting $\mathcal{K}_0 = 1$ in the constraint surface equations gives three hyperboloid equations, which reduces the number of terms in the univariate to 694, all listed in Appendix C.

The PR-types require fixed points in E to move on fixed lines in Σ, and the RP-types require fixed lines in E to move on fixed points in Σ. These two types are inversions: one can be obtained from the other by changing the roles of E and Σ. We set $\mathcal{K}_0 = 0$ and use $\mathcal{K}_1$, $\mathcal{K}_2$, $\mathcal{K}_3$ as images of the line coordinates $[L_1 : L_2 : L_3]$. The

number of terms in the univariate then reduces to 30. They are:

$$\left(\frac{1}{A_1B_2 - A_2B_1 - A_1C_2 + A_2C_1 + B_1C_2 - B_2C_1}\right)\sum_{i=6}^{0} a_i X_3^i \;=\; 0, \qquad (4.47)$$

where $a_6 = a_5 = a_4 = a_3 = 0$, leaving the rational factor and

$$\begin{aligned}
a_2 &= 2(A_1B_2C_1c_1 + A_1B_2C_2c_2 - A_1B_1b_1C_2 + A_2B_1b_1C_1 - A_2B_1C_1c_1 - A_2B_1C_2c_2) + \\
&\quad A_1B_2C_3 - A_1B_3C_2 + A_2B_3C_1 - A_2B_1C_3 + A_3B_1C_2 - A_3B_2C_1, \\
a_1 &= 4(A_1B_2C_1c_2 + A_1B_2b_1C_2 - A_1B_2C_2c_1 + A_2B_1C_2c_1 - A_2B_1C_1c_2 - A_2B_2b_1C_1), \\
a_0 &= 2(A_1B_1b_1C_2 - A_1B_2C_1c_1 - A_1B_2C_2c_2 + A_2B_1C_1c_1 + A_2B_1C_2c_2 - A_2B_1b_1C_1) + \\
&\quad A_1B_2C_3 - A_1B_3C_2 + A_2B_3C_1 - A_2B_1C_3 + A_3B_1C_2 - A_3B_2C_1.
\end{aligned}$$

Conditions for the vanishing of the rational factor, and what they mean, are discussed in Chapter 7, Section 7.2.4.

Finally, we must deal with the fact that the solution for RP-type platforms gives the pose (a', b', ϕ') of the *base* frame, Σ, with respect to the moving frame, E. However, we require the pose (a, b, ϕ) of E in Σ. It is easy to show that $\phi = -\phi'$. We then obtain (a, b) with a coordinate transformation using ϕ as the rotation angle. See Equation (5.8) in Chapter 5, Section 5.1.1.

4.4. Upper Bounds on the FK Solutions

The geometry of the image of the FK problem indicates that for each PSGP there should be a maximum of eight solutions. That is, three quadrics can intersect in, at most, eight real points. However, the general univariate, whose roots indicate coordinates of the images of all possible solutions is of degree six, which is in agreement with the broadly accepted findings of Hunt [**76**], Gosselin [**49**], Merlet [**97**], among others. The natural question is how to account for the missing intersection points?

4.4.1. *RR*-Type PSGP. This over-abundance is easily accounted for in the case of *RR*-type platforms. All constraint hyperboloids pass through the imaginary conjugate points $J_1(1 : i : 0 : 0)$ and $J_2(1 : -i : 0 : 0)$ on the line of intersection of the planes $X_3 = 0$ and $X_4 = 0$. This is so because of the special structure of these constraint surfaces: the planes described by $X_3 =$ constant intersect all the hyperboloids in circles; all circles contain J_1 and J_2. This is demonstrated by generating three arbitrary constraint hyperboloids using Equation (4.9) and intersecting them with the plane $X_4 = 0$. In that equation set $X_4 = 0$, $\mathcal{K}_0 = 1$ and $z = 1$. Then, H_A, H_B and H_B are obtained with the following substitutions: for H_A set $\mathcal{K}_1 = \mathcal{K}_2 = x = y = 0$ and $R = R_1$; for H_B set $\mathcal{K}_1 = B_1$, $x = b_1$, $\mathcal{K}_2 = y = 0$, and $R = R_2$; for H_C set $\mathcal{K}_1 = C_1$, $\mathcal{K}_2 = C_2$, $x = c_1$, $y = c_2$, and $R = R_3$. This gives the three hyperboloids intersected with the plane $X_4 = 0$:

$$H_A : \; X_1^2 + X_2^2 + \tfrac{1}{4}R_1 X_3^2 = 0, \tag{4.48}$$

$$H_B : \; X_1^2 + X_2^2 + \tfrac{1}{4}(R_2 + 2B_1 b_1)X_3^2 - (B_1 + b_2)X_3 X_1 = 0, \tag{4.49}$$

$$H_C : \; X_1^2 + X_2^2 + \tfrac{1}{4}(R_3 + 2(C_1 c_1 + C_2 c_2))X_3^2 - ((C_1 + c_1)X_1 - (C_2 + c_2)X_2)X_3 = 0. \tag{4.50}$$

Equations (4.48), (4.49) and (4.50) represent the intersections with $X_4 = 0$ of every possible set of constraint hyperboloids. It is easy to verify that these three surfaces and the plane $X_4 = 0$ intersect in the two imaginary conjugate points

$$\begin{aligned} J_1 &= (1 : i : 0 : 0), \\ J_2 &= (1 : -i : 0 : 0). \end{aligned}$$

These points have no pre-image and do not correspond to any possible displacement of the platform with respect to the base (see Section 3.6.3). Thus, two of the hyperboloids intersect in a fourth order curve which intersects the third hyperboloid in eight points. However, the two complex conjugate points J_1 and J_2 are common to every hyperboloid and account for two of the intersection points. Hence, there are,

at most, six real intersections each representing a solution to the FK problem. This explanation does not hold when the constraint surfaces are hyperbolic paraboloids, because these quadrics contain no circles that can lie evenly on them [**71**].

4.4.2. *PR*- and *RP*-Type PSGP. The following three constraint equations are obtained after setting $X_4 = 0$, $\mathcal{K}_0 = 0$ and $z = 1$ in Equation (4.9) then making the three sets of substitutions: for HP_A set $\mathcal{K}_1 = A_1$, $\mathcal{K}_2 = A_2$, $R = 0$, and $x = y = 0$; for HP_B set $\mathcal{K}_1 = B_1$, $\mathcal{K}_2 = B_2$, $R = B_3$, $x = b_1$, and $y = 0$; for HP_C set $\mathcal{K}_1 = C_1$, $\mathcal{K}_2 = C_2$, $R = C_3$, $x = c_1$, and $y = c_2$. This gives the intersection of every possible set of three constraint hyperbolic paraboloids with the plane $X_4 = 0$:

$$HP_A : A_1X_3X_1 + A_2X_3X_2 - \tfrac{1}{4}A_3X_3^2 = 0, \tag{4.51}$$

$$HP_B : B_1X_3X_1 + B_2X_3X_2 - \tfrac{1}{4}(B_3 + 2B_1b_1)X_3^2 = 0, \tag{4.52}$$

$$HP_C : C_1X_3X_1 + C_2X_3X_2 - \tfrac{1}{4}(C_3 + 2(C_1c_1 + C_2c_2))X_3^2 = 0. \tag{4.53}$$

It is easily verified that these equations are satisfied by the following image space point coordinates:

$$(X_1 : X_2 : X_3 : X_4) \;=\; (X_1 : X_2 : 0 : 0).$$

This means that every set of three constraint hyperbolic paraboloids contains the line of intersection of planes $X_3 = X_4 = 0$. In other words, this line is a generator for all possible constraint hyperbolic paraboloids. But, points on this line have no pre-image and, therefore, do not represent valid platform poses.

Consider the curve of intersection between any two constraint hyperbolic paraboloids. This curve must be a degenerate 4^{th} order curve that splits into the line $X_3 = X_4 = 0$ and a twisted cubic. The twisted cubic is the locus of common intersection points of every line in each regulus of both surfaces. Since the line $X_3 = X_4 = 0$ is a generator of both hyperbolic paraboloids, the twisted cubic must intersect it in two points. This stems from the fact that $X_3 = X_4 = 0$ is a projective

generator that *closes* each surface. As with a line in the opposite regulus, the twisted cubic will intersect the generator from two different directions. Taking any set of three distinct constraint hyperbolic paraboloids we can form three distinct twisted cubic curves of intersection together with the generator $X_3 = X_4 = 0$. The common intersections of the three surfaces will certainly be the points of intersection of the three twisted cubics and the line. Each cubic meets the line twice. This accounts for six points shared by the three surfaces. Every set of three distinct constraint hyperbolic paraboloids contains six such points on the line $X_3 = X_4 = 0$, none of which represents a valid platform pose. However, according to Bézout's theorem, there must be two additional intersection points which may, or may not, be valid poses. Thus, there are at most two real solutions to the FK problem for PR- and RP-type platforms.

This agrees with the fact that the univariate in this case is 2^{nd} order. It must be a 2^{nd} order curve for the following physical reason. Consider a PR-type PSGP with active base revolutes: locking the input joints and removing the platform connection of one of the legs gives a double-slider *elliptical trammel* mechanism. The coupler curve is, in general, elliptical. If the coupler point is the platform connection point of the third leg, the line of the third leg can intersect the elliptic coupler curve in at most two points.

CHAPTER 5

FK Solution Procedures

5.1. Application of the Univariate to the FK Problem

Solving the FK problem using the roots of the univariate polynomials developed in Chapter 4 requires three platform points with fixed positions in the moving frame that remain on curves with fixed coordinates in the non-moving frame. Detailed numerical examples of the procedures developed in this chapter can be found in Appendix A.

The FK problem can be expressed in geometric terms as follows:

***RR*-type:** Place the vertices of a rigid movable triangle on three non-moving circles respecting an initial pairing of vertex and circle.

***PR*-type:** Place the vertices of a rigid movable triangle on three non-moving lines respecting an initial pairing of vertex and line.

***RP*-type:** Place three movable, but relatively fixed lines on the vertices of a rigid non-moving triangle. If the triangle is considered as movable and the three lines as non-moving, the phrasing is identical to the that of the PR-type.

The points, *i.e.*, triangle vertices, are labelled M_i for $R\underline{R}R$, $R\underline{P}R$ and $\underline{R}PR$ platforms with Σ considered fixed and E as moving. These points are the F_i for $RP\underline{R}$ with Σ moving and E fixed. The curves for these four platforms are circles

centred on the base revolutes for the first two and the lines of the axes of symmetry of the intermediate prismatic for the last two. In order to establish these points and curves for some of the remaining 14 platform types some additional geometric specifications are required. These are the *virtual line* (VL), *virtual base* (VB) and the *virtual platform* (VP), discussed below. They allow the kinematic constraints to be described in exactly the same way for all PSGP, and hence the same univariate can be applied to the FK problem of all PSGP. This entire discussion is summarised in Tables 5.8, 5.9, 5.10. In addition, a detailed procedure for $RR\underline{G}$ platforms is given in Section 5.4.

5.1.1. Regular FK Solution Procedure. The following procedure is termed *regular* because the platform architecture allows either hip or ankle points to lie on the triangle vertices. The curves are excursion arcs of fixed length links connected to ground, or platform, by R-pairs, or they are the longitudinal axes of symmetry of P-pairs.

The regular solution procedure can be used for $R\underline{R}R$, $R\underline{P}R$, $\underline{R}PR$ and $RP\underline{R}$ platforms. The following discussion is an explanation of how this solution procedure works.

***R*$\underline{R}$*R* Platforms.** The hip points, M_i, with fixed positions in E, move on fixed circles centred on stationary ankle points, F_i, in Σ. The circle radii are determined by the intermediate R-pair angular inputs indicated by $\iota_{2/1}$, $\iota \in \{\alpha,\ \beta,\ \gamma\}$, see Figure 5.1 (i) showing leg A with $\iota = \alpha$. Figure 5.1 (i) illustrates the inputs which are required by the univariate, the pre-image of the output being the pose of frame E relative to frame Σ. Table 5.1 lists the input information required to evaluate the coefficients of the univariate. In general none of the coefficients vanish and the sixth order univariate must be solved numerically.

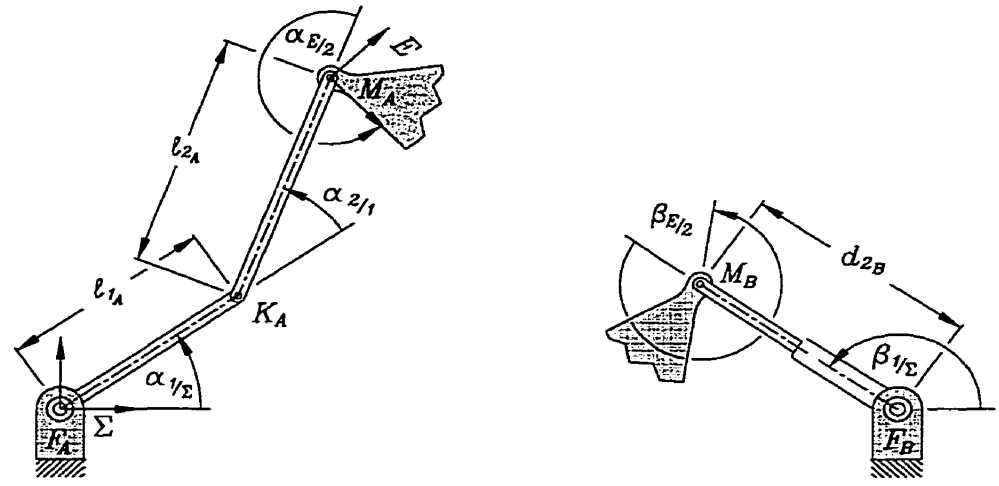

(i) RRR *(ii) RPR*

FIGURE 5.1. Parameters for *(i)* an *RRR* and *(ii)* an *RPR* platform.

Regular	$R\underline{R}R$ and $R\underline{P}R$ Platforms
Fixed frame	Σ
Moving frame	E
$R\underline{R}R$ Active joint inputs	$\iota_{2/1}$
$R\underline{P}R$ Active joint inputs	d_{2_i}
Moving points on circle	$M_{i/E}$
Circle centres	$F_{i/\Sigma}$
$R\underline{R}R$ Circle radii	$r_i = \left[(\ell_{1_i} + \ell_{2_i}\cos\iota_{2/1})^2 + (\ell_{2_i}\sin\iota_{2/1})^2\right]^{\frac{1}{2}}$
$R\underline{P}R$ Circle radii	$r_i = d_{2_i}$
Circle coordinates	$(\mathcal{K}_{0_i} : \mathcal{K}_{1_i} : \mathcal{K}_{2_i} : \mathcal{K}_{3_i}) = (1 : F_{x_i\Sigma} : F_{y_i\Sigma} : R_i - (x_i^2 + y_i^2))$, where $R_i = \mathcal{K}_{1_i}^2 + \mathcal{K}_{2_i}^2 - r_i^2 + \mathcal{K}_{0_i}(x_i^2 + y_i^2)$

TABLE 5.1. $R\underline{R}R$ and $R\underline{P}R$ reference frames and univariate constants. **Note:** $i \in \{A, B, C\}$ and $\iota \in \{\alpha, \beta, \gamma\}$

***R<u>P</u>R* Platforms.** These platforms are kinematically equivalent to the $R\underline{R}R$ ones from the previous paragraph, see Figure 5.1 *(ii)* showing leg B with $\iota = \beta$. The only difference in the input definitions is that the circle radii simplify to $r_i = d_{2_i}$. Table 5.1 lists the required input.

***$\underline{R}PR$* Platforms.** For these platforms the line coordinates of each leg are determined by the base R-pair inputs and the corresponding ankle point, F_i. For each leg the direction, given by the base R-pair inputs, together with the location of a point, the fixed ankle point F_i, on the line are known. The line equation is obtained from the Grassmannian expansion:

$$\begin{vmatrix} X & Y & Z \\ F_{x_{i/\Sigma}} & F_{y_{i/\Sigma}} & F_{z_{i/\Sigma}} \\ \cos\iota_{1/\Sigma} & \sin\iota_{1/\Sigma} & 0 \end{vmatrix} = (-F_{z_{i/\Sigma}}\sin\iota_{1/\Sigma})X + (F_{z_{i/\Sigma}}\cos\iota_{1/\Sigma})Y +$$

$$(F_{x_{i/\Sigma}}\sin\iota_{1/\Sigma} - F_{y_{i/\Sigma}}\cos\iota_{1/\Sigma})Z = 0. \quad (5.1)$$

The line coordinates $(L_{1_i} : L_{2_i} : L_{3_i})$, given by the coefficients of X, Y and Z respectively, are transformed, according to the relations and equations derived in Section 4.2, to circle coordinates as

$$(\mathcal{K}_0 : \mathcal{K}_{1_i} : \mathcal{K}_{2_i} : \mathcal{K}_{3_i}) = (0 : -\frac{1}{2}L_{1_i} : -\frac{1}{2}L_{2_i} : L_{3_i}). \quad (5.2)$$

The non-zero circle coordinates that determine the univariate coefficients are

$$(\mathcal{K}_{1_i} : \mathcal{K}_{2_i} : \mathcal{K}_{3_i}) = \quad (5.3)$$
$$\left(\frac{F_{z_{i/\Sigma}}}{2}\sin\iota_{1/\Sigma} : -\frac{F_{z_{i/\Sigma}}}{2}\cos\iota_{1/\Sigma} : (F_{x_{i/\Sigma}}\sin\iota_{1/\Sigma} - F_{y_{i/\Sigma}}\cos\iota_{1/\Sigma})\right).$$

Table 5.2 lists all the information required to evaluate the univariate coefficients.

***$RP\underline{R}$* Platforms.** These platforms are considered as inversions of the $\underline{R}PR$ platforms. Hence, the roles of E and Σ are reversed: the platform is fixed and the base moves relative to it. In this regard the FK problems of $\underline{R}PR$ and $RP\underline{R}$ platforms are isomorphic. Recall that the order of the joints is given starting from those fixed to the non-moving base and continues sequentially to the moving platform. Thus, the orders for $\underline{R}PR$ and $RP\underline{R}$ are identical, however the FK solution procedure requires some additional computations.

The FK solutions extracted from the intersections of the constraint surfaces in the image space give the pose of the base frame Σ with respect to the platform frame E. The resulting displacement parameters must be transformed to give the pose of the the platform frame E with respect to the base frame Σ. This is accomplished with a coordinate transformation which can be derived in the following way. The coordinate transformation of an arbitrary point from Σ to E is:

$$\boldsymbol{T}_{\Sigma/E} = \begin{bmatrix} \cos\varphi_{E/\Sigma} & \sin\varphi_{E/\Sigma} & -(a_{E/\Sigma}\cos\varphi_{E/\Sigma} + b_{E/\Sigma}\sin\varphi_{E/\Sigma}) \\ -\sin\varphi_{E/\Sigma} & \cos\varphi_{E/\Sigma} & a_{E/\Sigma}\sin\varphi_{E/\Sigma} - b_{E/\Sigma}\cos\varphi_{E/\Sigma} \\ 0 & 0 & 1 \end{bmatrix}. \quad (5.4)$$

The transformation in Equation (5.4) can be used to operate on any point in Σ. Certainly the origin of Σ, O_Σ, is a point in Σ. This point has coordinates $[0:0:1]^T$. The image of this point under $\boldsymbol{T}_{\Sigma/E}$ is

$$\begin{bmatrix} a_{\Sigma/E} \\ b_{\Sigma/E} \\ 1 \end{bmatrix} = \begin{bmatrix} -(a_{E/\Sigma}\cos\varphi_{E/\Sigma} + b_{E/\Sigma}\sin\varphi_{E/\Sigma}) \\ a_{E/\Sigma}\sin\varphi_{E/\Sigma} - b_{E/\Sigma}\cos\varphi_{E/\Sigma} \\ 1 \end{bmatrix}. \quad (5.5)$$

Note the subscripts indicate the following: $a_{\Sigma/E}$ and $b_{\Sigma/E}$ are the x- and y-coordinates of the origin of coordinate system Σ expressed in E; while the transformation $\boldsymbol{T}_{\Sigma/E}$ transforms coordinates *from* Σ to E. The system of equations represented by Equation (5.5) is linear in $a_{E/\Sigma}$ and $b_{E/\Sigma}$, which are the position of the platform frame expressed in the base frame, the two remaining quantities that are needed to complete the FK solution.

Solving the system gives, after making the substitution $\varphi_{\Sigma/E} = -\varphi_{E/\Sigma}$ (because the univariate reveals $\varphi_{\Sigma/E}$):

$$a_{E/\Sigma} = -(a_{\Sigma/E}\cos\varphi_{\Sigma/E} + b_{\Sigma/E}\sin\varphi_{\Sigma/E}) \quad (5.6)$$

$$b_{E/\Sigma} = a_{\Sigma/E}\sin\varphi_{\Sigma/E} - b_{\Sigma/E}\cos\varphi_{\Sigma/E}. \quad (5.7)$$

These relations can all be conveniently expressed as a special transformation used to operate on the univariate output giving the desired FK solutions:

$$\begin{bmatrix} a_{E/\Sigma} \\ b_{E/\Sigma} \\ \varphi_{E/\Sigma} \end{bmatrix} = \begin{bmatrix} -\cos\varphi_{\Sigma/E} & -\sin\varphi_{\Sigma/E} & 0 \\ \sin\varphi_{\Sigma/E} & -\cos\varphi_{\Sigma/E} & 0 \\ 0 & 0 & -1 \end{bmatrix} \begin{bmatrix} a_{\Sigma/E} \\ b_{\Sigma/E} \\ \varphi_{\Sigma/E} \end{bmatrix}. \tag{5.8}$$

The information required to evaluate the univariate coefficients for $RP\underline{R}$ platforms is compared with that of $\underline{R}PR$ in Table 5.2 *(i)*. Relevant parameters are illustrated in Figure 5.1 .

Regular	$\underline{R}PR$ Platforms	$RP\underline{R}$ Platforms
Fixed frame	Σ	E
Moving frame	E	Σ
Active joint inputs	$\iota_{1/\Sigma}$	$\iota_{2/E}$
Moving points on line	$M_{i/E}$	$F_{i/\Sigma}$
Fixed points on line	$F_{i/\Sigma}$	$M_{i/E}$
Circle coordinates:		
$\mathcal{K}_{0_i}$	0	0
$\mathcal{K}_{1_i}$	$\frac{1}{2}F_{z_{i/\Sigma}}\sin\iota_{1/\Sigma}$	$\frac{1}{2}M_{z_{i/E}}\sin\iota_{2/E}$
$\mathcal{K}_{2_i}$	$-\frac{1}{2}F_{z_{i/\Sigma}}\cos\iota_{1/\Sigma}$	$-\frac{1}{2}M_{z_{i/E}}\cos\iota_{2/E}$
$\mathcal{K}_{3_i}$	$F_{x_{i/\Sigma}}\sin\iota_{1/\Sigma} - F_{y_{i/\Sigma}}\cos\iota_{1/\Sigma}$	$M_{x_{i/E}}\sin\iota_{2/E} - M_{y_{i/E}}\cos\iota_{2/E}$

TABLE 5.2. $\underline{R}PR$ and $RP\underline{R}$ reference frames and univariate constants.

5.1.2. Virtual Line FK Solution Procedure. The virtual line (VL) is one that is parallel to the direction of the base-fixed or platform-fixed prismatic joints, but contains either the hip, M_i, or ankle point, F_i (see Figure 5.2). It is the line along which a reference point, of a PR- or RP-type platform with an active intermediate joint, moves with respect to the fixed frame. These lines replace the circular arcs of point motion. The VL is required for $P\underline{R}R$, $P\underline{P}R$, $R\underline{R}P$ and $R\underline{P}P$ type platforms.

Note that the VL is used only when intermediate joints are active and that it is not needed for any RR-type platform.

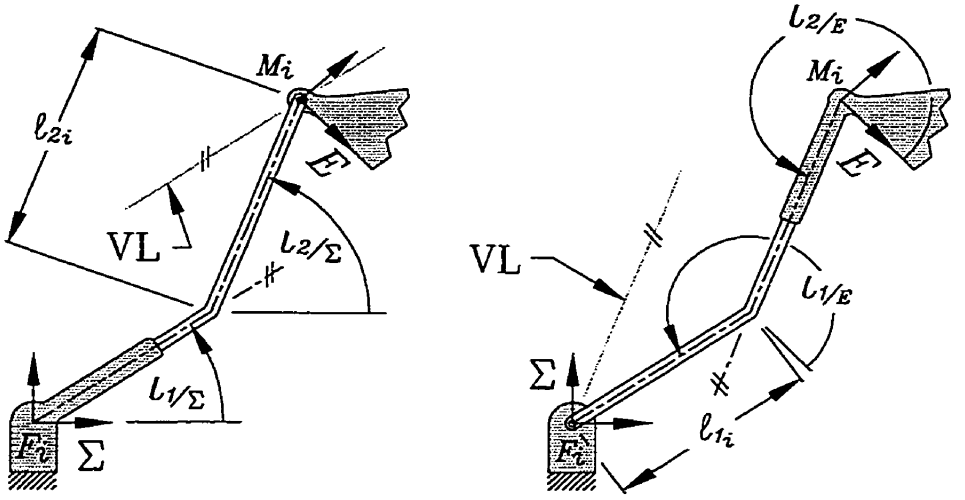

FIGURE 5.2. VL parameters for *(i)* a $P\underline{R}R$ and *(ii)* a $R\underline{R}P$ platform.

***P*$\underline{R}$*R* Platforms.** For these platforms the VL contains the M_i. However, the location of $M_{i/\Sigma}$ is not known *a priori*. Examining Figure 5.2, it is to be seen that a finite point on the VL can be determined from the known design constants and inputs ℓ_{2_i}, $\iota_{1/\Sigma}$, $\iota_{2/\Sigma}$ and $F_{i/\Sigma}$:

$$\begin{bmatrix} F_{i_{x/\Sigma}} + \ell_{2_i} \cos \iota_{2/\Sigma} \\ F_{i_{y/\Sigma}} + \ell_{2_i} \sin \iota_{2/\Sigma} \\ F_{i_{z/\Sigma}} \end{bmatrix}. \tag{5.9}$$

Because it is parallel to the direction of the corresponding base P-pair, the point at infinity on this VL has coordinates:

$$\begin{bmatrix} \cos \iota_{1/\Sigma} \\ \sin \iota_{1/\Sigma} \\ 0 \end{bmatrix}. \tag{5.10}$$

After determining the VL line coordinates with a Grassmannian expansion, then transforming them to the required circle coordinates, the following is obtained:

$$(\mathcal{K}_{0_i} : \mathcal{K}_{1_i} : \mathcal{K}_{2_i} : \mathcal{K}_{3_i}) = \Big(0 : \frac{1}{2}F_{i_{z/\Sigma}} \sin\iota_{1/\Sigma} : -\frac{1}{2}F_{i_{z/\Sigma}} \cos\iota_{1/\Sigma} : (F_{i_{x/\Sigma}} + \ell_{2_i} \cos\iota_{2/\Sigma}) \sin\iota_{1/\Sigma} - (F_{i_{y/\Sigma}} + \ell_{2_i} \sin\iota_{2/\Sigma}) \cos\iota_{1/\Sigma}\Big). \tag{5.11}$$

***PPR* Platforms.** For this platform the active pair is a prismatic. Thus, the active input is d_{2_i} and the angle $\iota_{2/\Sigma}$ is a design constant. The only difference is that $\ell_{2_i} = d_{2_i}$ in the VL line coordinates, and hence

$$(\mathcal{K}_{0_i} : \mathcal{K}_{1_i} : \mathcal{K}_{2_i} : \mathcal{K}_{3_i}) = \Big(0 : \frac{1}{2}F_{i_{z/\Sigma}} \sin\iota_{1/\Sigma} : -\frac{1}{2}F_{i_{z/\Sigma}} \cos\iota_{1/\Sigma} : (F_{i_{x/\Sigma}} + d_{2_i} \cos\iota_{2/\Sigma}) \sin\iota_{1/\Sigma} - (F_{i_{y/\Sigma}} + d_{2_i} \sin\iota_{2/\Sigma}) \cos\iota_{1/\Sigma}\Big). \tag{5.12}$$

Otherwise, the quantities listed in Table 5.3 apply to these platforms.

***RRP* and *RPP* Platforms.** These platforms are kinematic inversions of the $P\underline{R}R$ and $P\underline{P}R$ platforms. Thus, for computational purposes frame E is considered fixed and frame Σ as moving, and the design constants and variable inputs are labelled accordingly. The angular R-pair inputs for $R\underline{R}P$ platforms are $\iota_{2/1}$, with $\iota \in \{\alpha, \beta, \gamma\}$, while the P-pair inputs for $R\underline{P}P$ platforms are d_{2_i}, with $i \in \{A, B, C\}$. The angle $\iota_{1/E}$, required for computing the univariate coefficients, is determined easily enough from two known angles, the design constant $\iota_{2/E}$ and input angle $\iota_{2/1}$:

$$\iota_{1/E} = \iota_{2/E} - \iota_{2/1}. \tag{5.13}$$

The circle coordinates for these two platforms differ only in that the lengths of the intermediate links in each leg, ℓ_{2_i}, are fixed in $R\underline{R}P$ platforms and variable, d_{2_i}, in $R\underline{P}P$ platforms. Table 5.3 lists the quantities required to compute the univariate

coefficients for these platforms. Note that ℓ_{2_i} must be replaced with d_{2_i} for $R\underline{P}P$ platforms.

Virtual Line	$P\underline{R}R$ Platforms	$R\underline{R}P$ Platforms
Fixed frame	Σ	E
Moving frame	E	Σ
Active joint inputs	$\iota_{2/1}$	$\iota_{2/1}$
Moving points on VL	$M_{i/E}$	$F_{i/\Sigma}$
Circle coordinates:		
$\mathcal{K}_{0_i}$	0	0
$\mathcal{K}_{1_i}$	$\frac{1}{2}F_{z_{i/\Sigma}} \sin \iota_{1/\Sigma}$	$\frac{1}{2}M_{z_{i/E}} \sin \iota_{2/E}$
$\mathcal{K}_{2_i}$	$-\frac{1}{2}F_{z_{i/\Sigma}} \cos \iota_{1/\Sigma}$	$-\frac{1}{2}M_{z_{i/E}} \cos \iota_{2/E}$
$\mathcal{K}_{3_i}$	$(F_{x_{i/\Sigma}} + \ell_{2_i} \cos \iota_{2/\Sigma}) \sin \iota_{1/\Sigma} -$ $(F_{y_{i/\Sigma}} + \ell_{2_i} \sin \iota_{2/\Sigma}) \cos \iota_{1/\Sigma}$	$(M_{x_{i/E}} + \ell_{1_i} \cos \iota_{1/E}) \sin \iota_{2/E} -$ $(M_{y_{i/E}} + \ell_{1_i} \sin \iota_{1/E}) \cos \iota_{2/E}$

TABLE 5.3. $P\underline{R}R$ and $R\underline{R}P$ reference frames and univariate constants.

5.1.3. Virtual Base FK Solution Procedure. The virtual base (VB) is formed by the triangle whose vertices are the points of intersection of the links directly connected to the base and those directly connected to the platform. It is required to constrain points with fixed positions in a moving frame to fixed curves in a non-moving frame so the special coordinate systems, similar to those shown in Figure 2.5, can be used.

It is input specific: that is, for every distinct set of variable joint inputs there is a distinct VB. The VB reference frame, indicated by Σ_{VB} for RR- and PR-type platforms and E_{VB} for RP-platforms, may be considered as fixed for a given FK problem. It is used for the FK of $\underline{R}RR$, $\underline{P}RR$, $\underline{P}PR$ and $RP\underline{P}$ platforms. For a given set of joint inputs the virtual base points (VBP) are fixed points in the non-moving frame. For RR- and PR-type platforms the non-moving frame is Σ. The non-moving frame for RP-type platforms is frame E, since these are thought of as the kinematic inversion of PR-type platforms. The VB is used when certain *base*

joints are active. Figure 5.3 shows the various parameters, fixed and variable, for $\underline{P}PR$ and $RP\underline{P}$ platforms.

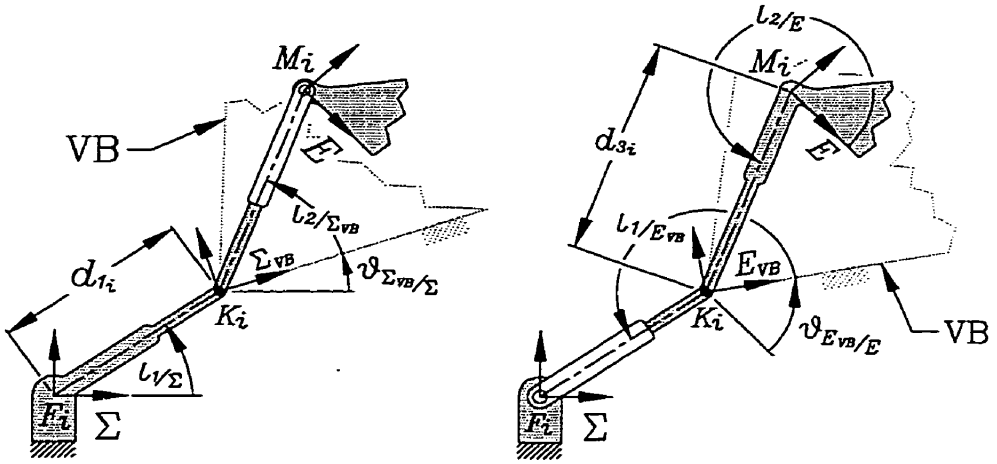

(i) $\underline{P}PR$ *(ii)* $RP\underline{P}$

FIGURE 5.3. VB parameters for *(i)* a $\underline{P}PR$ and *(ii)* an $RP\underline{P}$ platform.

***$\underline{R}RR$* and *$\underline{P}RR$* Platforms.** For these platforms the VB reference frame is Σ_{VB} because its pose is known in Σ. Recalling sub-section 2.9, the origin of Σ_{VB}, indicated by $O_{\Sigma_{VB}}$, is located on K_A. The orientation of Σ_{VB} is selected so that K_B is on the positive $x_{\Sigma_{VB}}$-axis. The variable joint inputs determine the locations of the knee joints in Σ, $K_{A/\Sigma}$, $K_{B/\Sigma}$ and $K_{C/\Sigma}$. A simple coordinate transformation reveals the coordinates $K_{A/\Sigma_{VB}}$, $K_{B/\Sigma_{VB}}$ and $K_{C/\Sigma_{VB}}$.

Performing the transformation requires the position and orientation of Σ_{VB} relative to Σ. The position, given by $O_{\Sigma_{VB}}$, is determined by the input of leg A. The orientation, $\vartheta_{\Sigma_{VB}/\Sigma}$, requires some manipulation. Referring to Figure 5.4, consider the quadrilateral defined by the four points F_A, K_A, K_B and F_B, from which the vector equation is easily obtained:

$$\overrightarrow{K_AK_B} = (\overrightarrow{F_AF_B} + \overrightarrow{F_BK_B}) - \overrightarrow{F_AK_A}. \tag{5.14}$$

The orientation can be determined using the components of Equation (5.14), yielding

$$\vartheta_{\Sigma_{VB}/\Sigma} = \operatorname{atan2}(y, x), \tag{5.15}$$

where

$$\begin{aligned} x &= F_{B_{x/\Sigma}} + \ell_{1_B} \cos\beta_{1/\Sigma} - \ell_{1_A} \cos\alpha_{1/\Sigma}, \\ y &= \ell_{1_B} \sin\beta_{1/\Sigma} - \ell_{1_A} \sin\alpha_{1/\Sigma}. \end{aligned}$$

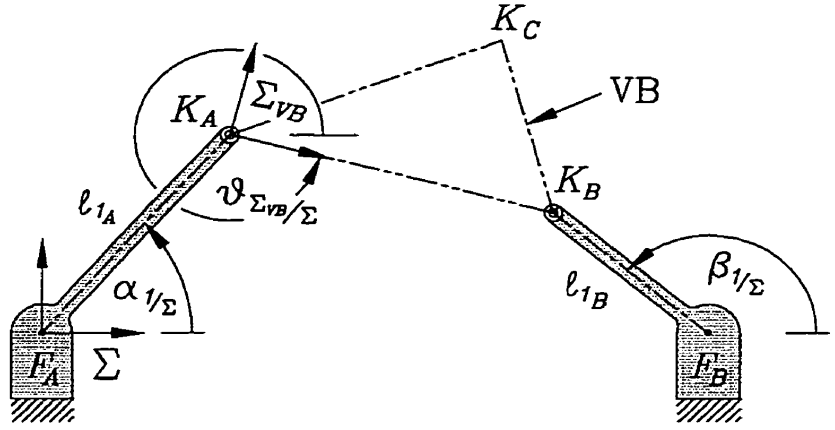

FIGURE 5.4. Determining the VB pose for *RR*- and *PR*-type platforms.

This information can be used to transform the coordinates of the knee joints from Σ to Σ_{VB}:

$$\boldsymbol{k}_{i/\Sigma_{VB}} = \boldsymbol{T}_{\Sigma/\Sigma_{VB}} \boldsymbol{k}_{i/\Sigma}, \tag{5.16}$$

where,

$$\boldsymbol{T}_{\Sigma/\Sigma_{VB}} = \begin{bmatrix} \cos\vartheta_{\Sigma_{VB}/\Sigma} & \sin\vartheta_{\Sigma_{VB}/\Sigma} & -(O_{x_{\Sigma_{VB}/\Sigma}} \cos\vartheta_{\Sigma_{VB}/\Sigma} + O_{y_{\Sigma_{VB}/\Sigma}} \sin\vartheta_{\Sigma_{VB}/\Sigma}) \\ -\sin\vartheta_{\Sigma_{VB}/\Sigma} & \cos\vartheta_{\Sigma_{VB}/\Sigma} & O_{x_{\Sigma_{VB}/\Sigma}} \sin\vartheta_{\Sigma_{VB}/\Sigma} - O_{y_{\Sigma_{VB}/\Sigma}} \cos\vartheta_{\Sigma_{VB}/\Sigma} \\ 0 & 0 & 1 \end{bmatrix}.$$

Virtual Base	$\underline{R}RR$ and $\underline{P}RR$ Platforms
Fixed frame	Σ_{VB}
Moving frame	E
$\underline{R}RR$ Active joint inputs	$\iota_{1/\Sigma}$
$\underline{P}RR$ Active joint inputs	d_{1_i}
Moving points on circle	$M_{i/E}$
Circle centres	$K_{i/\Sigma_{VB}}$
$\underline{R}RR$ Circle radii	$r_i = \ell_{2_i}$
$\underline{P}RR$ Circle radii	$r_i = \ell_{2_i}$
Circle coordinates	$(\mathcal{K}_{0_i} : \mathcal{K}_{1_i} : \mathcal{K}_{2_i} : \mathcal{K}_{3_i}) =$ $(1 : K_{x_i/\Sigma_{VB}} : K_{y_i/\Sigma_{VB}} : R_i - (x_i^2 + y_i^2))$, where $R_i = \mathcal{K}_{1_i}^2 + \mathcal{K}_{2_i}^2 - r_i^2 + \mathcal{K}_{0_i}(x_i^2 + y_i^2)$

TABLE 5.4. $\underline{R}RR$ and $\underline{P}RR$ reference frames and univariate constants.

After the inputs are suitably transformed the univariate coefficients can be determined and used to obtain the FK solutions. But, the solutions are expressed in the VB frame and must be transformed back to the fixed base frame Σ. That is, the univariate yields the pose of the platform as

$$\begin{bmatrix} a' \\ b' \\ \varphi' \end{bmatrix} = \begin{bmatrix} O_{x_{E/\Sigma_{VB}}} \\ O_{y_{E/\Sigma_{VB}}} \\ \varphi_{E/\Sigma_{VB}} \end{bmatrix}. \tag{5.17}$$

The orientation in Σ is easily determined:

$$\varphi_{E/\Sigma} = \varphi_{E/\Sigma_{VB}} + \vartheta_{\Sigma_{VB}/\Sigma}. \tag{5.18}$$

A quick examination of the VB geometry (see Figure 5.5 where $d_{1_A} = \ell_{1_A}$) reveals the following FK solutions in the fixed base frame Σ:

$$\begin{bmatrix} a \\ b \\ 1 \end{bmatrix} = \begin{bmatrix} O_{x_{E/\Sigma}} \\ O_{y_{E/\Sigma}} \\ 1 \end{bmatrix} = \begin{bmatrix} \cos\vartheta_{\Sigma_{VB}/\Sigma} & -\sin\vartheta_{\Sigma_{VB}/\Sigma} & O_{x_{\Sigma_{VB}/\Sigma}} \\ \sin\vartheta_{\Sigma_{VB}/\Sigma} & \cos\vartheta_{\Sigma_{VB}/\Sigma} & O_{y_{\Sigma_{VB}/\Sigma}} \\ 0 & 0 & 1 \end{bmatrix} \begin{bmatrix} a' \\ b' \\ 1 \end{bmatrix}, \tag{5.19}$$

where $O_{x_{\Sigma_{VB}/\Sigma}} = \ell_{1_A}\cos\alpha_{1/\Sigma}$ and $O_{y_{\Sigma_{VB}/\Sigma}} = \ell_{1_A}\sin\alpha_{1/\Sigma}$

***PPR* Platforms.** The *PPR* platforms need a little more work than the platforms discussed so far. Their constraint surfaces are hyperbolic paraboloids, hence $\mathcal{K}_{0_i} = 0$. The VB is determined as for *RRR* and *PRR* platforms. However, the intermediate joint in each leg is a P-pair. Determining the coordinates of the lines upon which the platform points move requires the summation of known angles. We proceed in a way that is similar to how the VL coordinates are determined. The lines that contain the knee joints are fixed relative to the base frame when a set of joint inputs are specified. Their directions are determined by the translation directions of the intermediate P-pairs. The line coordinates are

$$(L_{1_i} : L_{2_i} : L_{3_i}) = \tag{5.20}$$
$$(-K_{z_{i/\Sigma_{VB}}}\sin\iota_{2/\Sigma_{VB}} : K_{z_{i/\Sigma_{VB}}}\cos\iota_{2/\Sigma_{VB}} : K_{x_{i/\Sigma_{VB}}}\sin\iota_{2/\Sigma_{VB}} - K_{y_{i/\Sigma_{VB}}}\cos\iota_{2/\Sigma_{VB}}).$$

Examining Figure 5.5 one immediately sees that for any leg, the direction of the fixed line in the VB frame, Σ_{VB} is determined by the angle

$$\begin{aligned} \iota_{2/\Sigma_{VB}} &= (\iota_{1/\Sigma} + \iota_{2/1}) + \vartheta_{\Sigma/\Sigma_{VB}}, \\ &= \iota_{2/\Sigma} - \vartheta_{\Sigma_{VB}/\Sigma}. \end{aligned} \tag{5.21}$$

The line equation is obtained from two points on each line. The first is the knee joint centre of the corresponding leg, while the second is the point at infinity determined by the translation direction of the intermediate P-pair, all expressed in

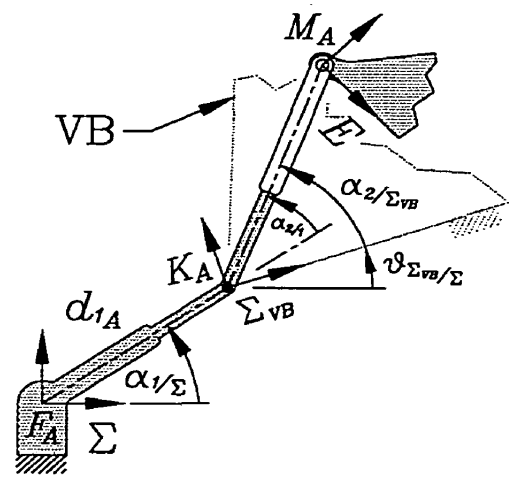

FIGURE 5.5. Determining the VB pose for $\underline{P}PR$ platforms.

Σ_{VB}. The Grassmannian expansion yields

$$-(K_{z_{i/\Sigma_{VB}}} \sin \iota_{2/\Sigma_{VB}})x + (K_{z_{i/\Sigma_{VB}}} \cos \iota_{2/\Sigma_{VB}})y + (K_{x_{i/\Sigma_{VB}}} \sin \iota_{2/\Sigma_{VB}} - K_{y_{i/\Sigma_{VB}}} \cos \iota_{2/\Sigma_{VB}})z = 0. \quad (5.22)$$

The corresponding circle coordinates are easily determined (using Equation (5.2)), and are listed, together with the other information required to evaluate the univariate coefficients in Table 5.5.

The roots of the univariate give the FK solutions relative to the VB frame, Σ_{VB}, which must be transformed back to the fixed base frame, Σ, with Equations (5.17), (5.18) and (5.19).

***RP*$\underline{P}$ Platforms.** This platform is simply the kinematic inversion of the $\underline{P}PR$ platform, however the FK solution procedure requires some additional computations, similar to those of the $RP\underline{R}$ platforms. These involve determining the pose of the VB, transforming the relevant parameters to that frame, computing the univariate coefficients and roots, then transforming the solutions to the fixed base frame, Σ. The complication arises from the assignment of E as the non-moving frame and

Virtual Base	$\underline{P}PR$ Platforms	$RP\underline{P}$ Platforms
Fixed frame	Σ_{VB}	E_{VB}
Moving frame	E	Σ
Active joint inputs	d_{1_i}	d_{3_i}
Moving points on line	$M_{i/E}$	$F_{i/\Sigma}$
Circle coordinates:		
$\mathcal{K}_{0_i}$	0	0
$\mathcal{K}_{1_i}$	$\frac{1}{2}K_{z_{i/\Sigma_{VB}}} \sin \iota_{2/\Sigma_{VB}}$	$\frac{1}{2}K_{z_{i/E_{VB}}} \sin \iota_{1/E_{VB}}$
$\mathcal{K}_{2_i}$	$-\frac{1}{2}K_{z_{i/\Sigma_{VB}}} \cos \iota_{2/\Sigma_{VB}}$	$-\frac{1}{2}K_{z_{i/E_{VB}}} \cos \iota_{1/E_{VB}}$
$\mathcal{K}_{3_i}$	$(K_{x_{i/\Sigma_{VB}}} \sin \iota_{2/\Sigma_{VB}} -$ $K_{y_{i/\Sigma_{VB}}} \cos \iota_{/\Sigma_{VB}})$	$(K_{x_{i/E_{VB}}} \sin \iota_{1/E_{VB}} -$ $K_{y_{i/E_{VB}}} \cos \iota_{1/E_{VB}})$

TABLE 5.5. $\underline{P}PR$ and $RP\underline{P}$ reference frames and univariate constants.

determining the pose of Σ relative to it. The required solution steps are discussed in the following paragraphs.

Referring to Figure 5.6, the active joints are the platform-fixed P-pairs, indicated by d_{3_i}. Once these three lengths are specified the vertices of the VB, the knee joint coordinates, are computed. The VB reference frame, E_{VB} is defined analogously to Σ_{VB}: the origin, $O_{E_{VB}}$, is located on K_A and the orientation is selected such that K_B is located on the positive $x_{E_{VB}}$-axis.

Next, consider the quadrilateral defined by the four points M_A, K_A, K_B and M_B, from which the following vector equation is obtained:

$$\overrightarrow{K_AK_B} = (\overrightarrow{M_AM_B} + \overrightarrow{M_BK_B}) - \overrightarrow{M_AK_A}. \tag{5.23}$$

The orientation of E_{VB} can be determined using the components of Equation (5.23), yielding

$$\vartheta_{E_{VB}/E} = \text{atan2}(y, x), \tag{5.24}$$

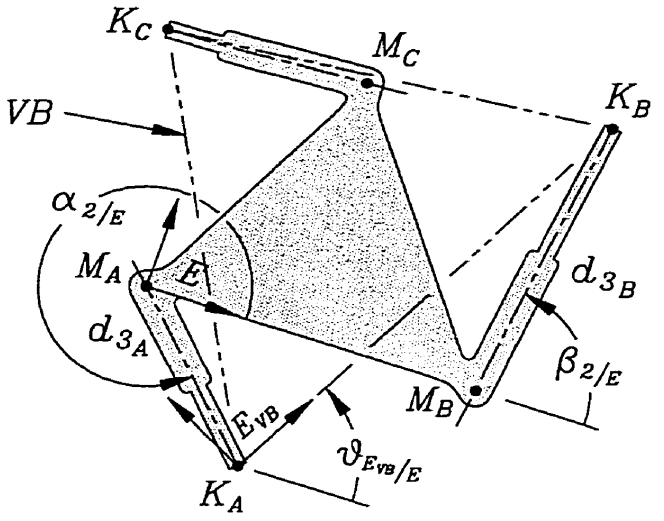

FIGURE 5.6. Determining the VB pose for $RP\underline{P}$ platforms.

where

$$\begin{aligned} x &= M_{B_{x/E}} + d_{3_B}\cos\beta_{2/E} - d_{3_A}\cos\alpha_{2/E}, \\ y &= d_{3_B}\sin\beta_{2/E} - d_{3_A}\sin\alpha_{2/E}. \end{aligned}$$

With this information the knee joints can be transformed from the platform frame E, in which they are known by virtue of the architecture, to the VB frame, E_{VB}, using

$$\boldsymbol{k}_{i/E_{VB}} = \boldsymbol{T}_{E/E_{VB}}\boldsymbol{k}_{i/E}, \tag{5.25}$$

where,

$$\boldsymbol{T}_{E/E_{VB}} = \begin{bmatrix} \cos\vartheta_{E_{VB}/E} & \sin\vartheta_{E_{VB}/E} & -(O_{x_{E_{VB}/E}}\cos\vartheta_{E_{VB}/E} + O_{y_{E_{VB}/E}}\sin\vartheta_{E_{VB}/E}) \\ -\sin\vartheta_{E_{VB}/E} & \cos\vartheta_{E_{VB}/E} & O_{x_{E_{VB}/E}}\sin\vartheta_{E_{VB}/E} - O_{y_{E_{VB}/E}}\cos\vartheta_{E_{VB}/E} \\ 0 & 0 & 1 \end{bmatrix}.$$

The lines that contain the knee joints are fixed relative to the platform frame when a set of joint inputs are specified. Their directions are determined by the translation

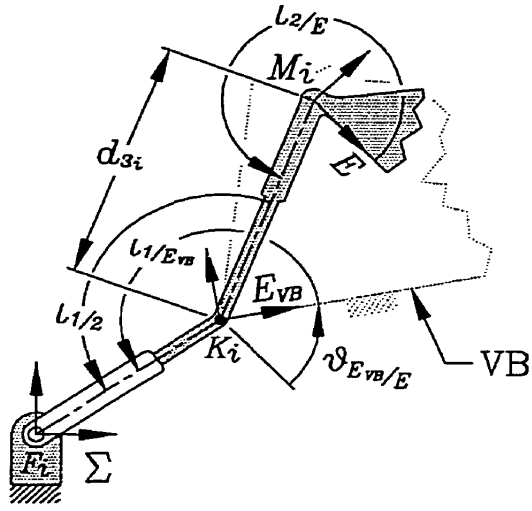

FIGURE 5.7. Determining the VB pose for $RP\underline{P}$ platforms.

directions of the platform-fixed P-pairs. The line coordinates are

$$(L_{1_i} : L_{2_i} : L_{3_i}) = \tag{5.26}$$
$$(-K_{z_{i/E_{VB}}} \sin \iota_{1/E_{VB}} : K_{z_{i/E_{VB}}} \cos \iota_{1/E_{VB}} : K_{x_{i/E_{VB}}} \sin \iota_{1/E_{VB}} - K_{y_{i/E_{VB}}} \cos \iota_{1/E_{VB}}).$$

Examining Figure 5.7 one immediately sees that for any leg, the direction of the fixed line in the VB frame, E_{VB}, is determined by the angle

$$\begin{aligned} \iota_{1/E_{VB}} &= (\iota_{1/2} + \iota_{2/E}) + \vartheta_{E/E_{VB}}, \\ &= \iota_{1/E} - \vartheta_{E_{VB}/E}. \end{aligned} \tag{5.27}$$

The data in Table 5.5 can now be used to compute the univariate coefficients. The FK solutions obtained from the roots of the univariate give the pose of the base frame, Σ, expressed in the VB frame, E_{VB}:

$$\begin{bmatrix} a' \\ b' \\ \varphi' \end{bmatrix} = \begin{bmatrix} O_{x_{\Sigma/E_{VB}}} \\ O_{y_{\Sigma/E_{VB}}} \\ \varphi_{\Sigma/E_{VB}} \end{bmatrix}. \tag{5.28}$$

However, what is required is the pose of the platform frame, E, expressed in the fixed base frame, Σ.

The orientation of frame E in Σ is easily determined (see Figure 5.7):

$$\varphi_{E/\Sigma} = -\varphi_{\Sigma/E} = -(\vartheta_{E_{VB}/E} + \varphi_{\Sigma/E_{VB}}), \tag{5.29}$$

where $\vartheta_{E_{VB}/E}$ is computed from the variable joint inputs and design constants, as in Equation (5.24), and $\varphi_{\Sigma/E_{VB}}$ is computed from the univariate output.

Next, the origin of Σ expressed in E, $O_{\Sigma/E}$, is determined with the transformation:

$$\begin{bmatrix} a_{\Sigma/E} \\ b_{\Sigma/E} \\ 1 \end{bmatrix} = \begin{bmatrix} O_{x_{\Sigma/E}} \\ O_{y_{\Sigma/E}} \\ 1 \end{bmatrix} = \begin{bmatrix} \cos\vartheta_{E_{VB}/E} & -\sin\vartheta_{E_{VB}/E} & O_{x_{E_{VB}/E}} \\ \sin\vartheta_{E_{VB}/E} & \cos\vartheta_{E_{VB}/E} & O_{y_{E_{VB}/E}} \\ 0 & 0 & 1 \end{bmatrix} \begin{bmatrix} a' \\ b' \\ 1 \end{bmatrix}, \tag{5.30}$$

where $O_{x_{E_{VB}/E}} = d_{3_A}\cos\alpha_{2/E}$ and $O_{y_{E_{VB}/E}} = d_{3_A}\sin\alpha_{2/E}$.

Transformation Equation 5.30 is derived analogously to Equation (5.19). Its validity can be confirmed with a close examination of Figure 5.7. Finally, the desired pose of the moving platform frame E in the fixed base frame Σ is computed using the transformation given in Equation 5.8, reproduced here as Equation 5.31:

$$\begin{bmatrix} a_{E/\Sigma} \\ b_{E/\Sigma} \\ \varphi_{E/\Sigma} \end{bmatrix} = \begin{bmatrix} -\cos\varphi_{\Sigma/E} & -\sin\varphi_{\Sigma/E} & 0 \\ \sin\varphi_{\Sigma/E} & -\cos\varphi_{\Sigma/E} & 0 \\ 0 & 0 & -1 \end{bmatrix} \begin{bmatrix} a_{\Sigma/E} \\ b_{\Sigma/E} \\ \varphi_{\Sigma/E} \end{bmatrix}. \tag{5.31}$$

5.1.4. Virtual Platform FK Solution Procedure. The virtual platform (VP), like the VB, is formed by the triangle whose vertices are the points of intersection of the links directly connected to the base and those directly connected to the platform. The difference being that for a given set of joint inputs the virtual platform points (VPP) are fixed points in the moving frame. The moving frame is E for RR- and PR-type platforms and is frame Σ for RP-type platforms. VPP are required for

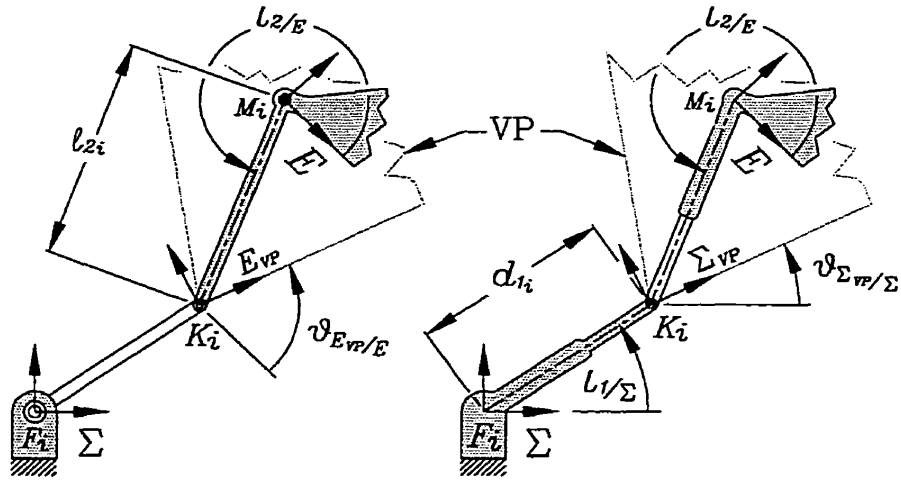

(i) $RR\underline{R}$ *(ii)* $\underline{P}RP$

FIGURE 5.8. VP parameters for *(i)* an $RR\underline{R}$ and *(ii)* a $\underline{P}RP$ platform.

$RR\underline{R}$, $RR\underline{P}$, $PR\underline{R}$, $PR\underline{P}$, $\underline{P}RP$ and $\underline{R}RP$ platforms. The main difference from the VB is that here certain types of *platform* joints are active.

***RRR* and *RRP* Platforms.** For these platforms, as well as for the PR-type, the VP reference frame is indicated by E_{VP}, because its pose is known with respect to the platform frame, E. It is similar to the VP illustrated in Figure 5.8. The origin of this frame, $O_{E_{VP}}$, is on the knee joint in leg A, K_A. The orientation of E_{VP} is defined so that K_B is on the positive $x_{E_{VP}}$-axis. The position of $O_{E_{VP/E}}$ is determined by the input of leg A. Analogous to the determination of the VB orientation, vector arguments are used to obtain:

$$\overrightarrow{K_AK_B} = (\overrightarrow{M_AM_B} + \overrightarrow{M_BK_B}) - \overrightarrow{M_AK_A}. \tag{5.32}$$

The orientation can be determined with the two argument inverse tangent function using the components of Equation (5.32), yielding

$$\vartheta_{E_{VP}/E} = \text{atan2}(y, x), \tag{5.33}$$

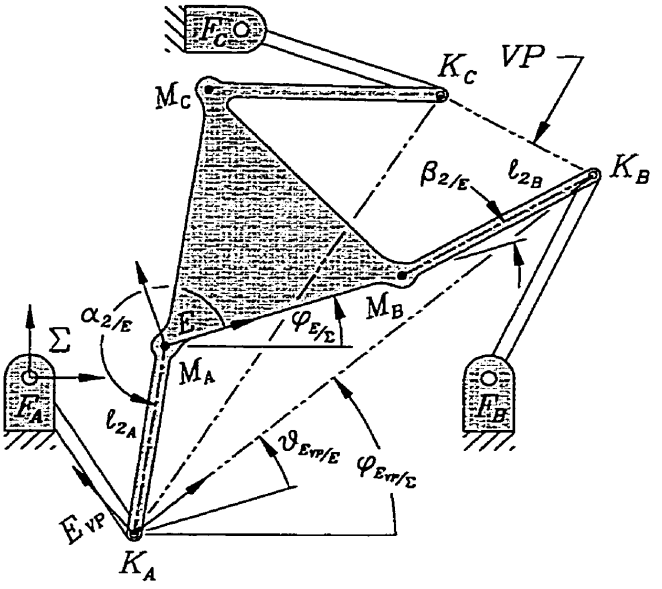

FIGURE 5.9. Determining the VP for *PR*-type platforms.

where

$$\begin{aligned} x &= M_{B_{x_{/E}}} + \ell_{2_B}\cos\beta_{2/E} - \ell_{2_A}\cos\alpha_{2/E}, \\ y &= \ell_{2_B}\sin\beta_{2/E} - \ell_{2_A}\sin\alpha_{2/E}. \end{aligned}$$

The knee joint coordinates expressed in the VP frame are determined using this information in the transformation:

$$\boldsymbol{k}_{i/E_{VP}} = \boldsymbol{T}_{E/E_{VP}}\boldsymbol{k}_{i/E}, \tag{5.34}$$

where,

$$\boldsymbol{T}_{E/E_{VP}} = \begin{bmatrix} \cos\vartheta_{E_{VP}/E} & \sin\vartheta_{E_{VP}/E} & -(O_{x_{E_{VP}/E}}\cos\vartheta_{E_{VP}/E} + O_{y_{E_{VP}/E}}\sin\vartheta_{E_{VP}/E}) \\ -\sin\vartheta_{E_{VP}/E} & \cos\vartheta_{E_{VP}/E} & O_{x_{E_{VP}/E}}\sin\vartheta_{E_{VP}/E} - O_{y_{E_{VP}/E}}\cos\vartheta_{E_{VP}/E} \\ 0 & 0 & 1 \end{bmatrix}.$$

Next, the transformed knee joint coordinates are used, together with the rest of the information listed in Table 5.6, to evaluate the univariate coefficients and compute

Virtual Platform	$RR\underline{R}$ and $RR\underline{P}$ Platforms
Fixed frame	Σ
Moving frame	E_{VP}
$RR\underline{R}$ Active joint inputs	$\iota_{2/E}$
$RR\underline{P}$ Active joint inputs	d_{3_i}
Moving points on circle	$K_{i/E_{VP}}$
Circle centres	$F_{i/\Sigma}$
Circle radii	$r_i = \ell_{1_i}$
Circle coordinates	
$\mathcal{K}_{0_i}$	1
$\mathcal{K}_{1_i}$	$F_{x_{i/\Sigma}}$
$\mathcal{K}_{2_i}$	$F_{y_{i/\Sigma}}$
$\mathcal{K}_{3_i}$	$R_i - (K^2_{x_{i/E_{VP}}} + K^2_{y_{i/E_{VP}}})$, where $R_i = \mathcal{K}^2_{1_i} + \mathcal{K}^2_{2_i} - r_i^2 + \mathcal{K}_{0_i}(K^2_{x_{i/E_{VP}}} + K^2_{y_{i/E_{VP}}})$

TABLE 5.6. $RR\underline{R}$ and $RR\underline{P}$ reference frames and univariate constants.

the roots. The roots represent the FK solutions, but they yield the pose of the VP frame, E_{VP}, in the fixed base frame, Σ:

$$\begin{bmatrix} a' \\ b' \\ \varphi' \end{bmatrix} = \begin{bmatrix} O_{x_{E_{VP}/\Sigma}} \\ O_{y_{E_{VP}/\Sigma}} \\ \varphi_{E_{VP}/\Sigma} \end{bmatrix}. \tag{5.35}$$

However, what is required is

$$\begin{bmatrix} a \\ b \\ \varphi \end{bmatrix} = \begin{bmatrix} O_{x_{E/\Sigma}} \\ O_{y_{E/\Sigma}} \\ \varphi_{E/\Sigma} \end{bmatrix}. \tag{5.36}$$

Finally, the desired solution reveals itself upon examination of Figure 5.9. One may immediately deduce

$$a = a' + \ell_{2_A} \cos \alpha_{2/\Sigma}, \tag{5.37}$$

$$b = b' + \ell_{2_A} \sin \alpha_{2/\Sigma}, \tag{5.38}$$

$$\alpha_{2/\Sigma} = (\alpha_{2/E} - \pi) + \vartheta_{E_{VP}/\Sigma} + \vartheta_{E/E_{VP}}, \tag{5.39}$$

$$\varphi = \varphi' + \vartheta_{E/E_{VP}}$$

$$= \varphi' - \vartheta_{E_{VP}/E}. \tag{5.40}$$

***PRR* and *PRP* Platforms.** The FK solution procedure for these platforms is the same as for the *RRR* and *RRP* platforms just discussed, except that the information in Table 5.7 must be used. This is due to the fact that the constraint curves are lines and not circles. Other than that, all the equations for *RRR* and *RRP* platforms, from Equation (5.32) to (5.40) are used in the FK procedure.

Virtual Platform	*PR*-Type Platforms	*RP*-Type Platforms
Fixed frame	Σ	E
Moving frame	E_{VP}	Σ_{VP}
Active joint inputs	PRR : $\iota_{2/E}$	RRP : $\iota_{1/\Sigma}$
	PRP : d_{3_i}	PRP : d_{1_i}
Moving points on line	$K_{i/E_{VP}}$	$K_{i/\Sigma_{VP}}$
Circle coordinates:		
$\mathcal{K}_{0_i}$	0	0
$\mathcal{K}_{1_i}$	$\frac{1}{2} F_{z_{i/\Sigma}} \sin \iota_{1/\Sigma}$	$\frac{1}{2} M_{z_{i/E}} \sin \iota_{2/E}$
$\mathcal{K}_{2_i}$	$-\frac{1}{2} F_{z_{i/\Sigma}} \cos \iota_{1/\Sigma}$	$-\frac{1}{2} M_{z_{i/E}} \cos \iota_{2/E}$
$\mathcal{K}_{3_i}$	$(F_{x_{i/\Sigma}} \sin \iota_{1/\Sigma} - F_{y_{i/\Sigma}} \cos \iota_{1/\Sigma})$	$(M_{x_{i/E}} \sin \iota_{2/E} - M_{y_{i/E}} \cos \iota_{2/E})$

TABLE 5.7. *PR*- and *RP*-type reference frames and univariate constants.

***RRP* and *PRP* Platforms.** For these platforms the univariate requires the description of the displacement of Σ, the base-fixed frame, with respect to E, the platform-fixed frame. In these computations, Σ is considered to move relative to E. Here, the VP is an *extension of the base.* It is a bit confusing, which is unfortunate, but allows for the use of the univariate, which is fortunate! The VPP are the same as for the *RR*- and *PR*-type platforms, but the reference frame is different.

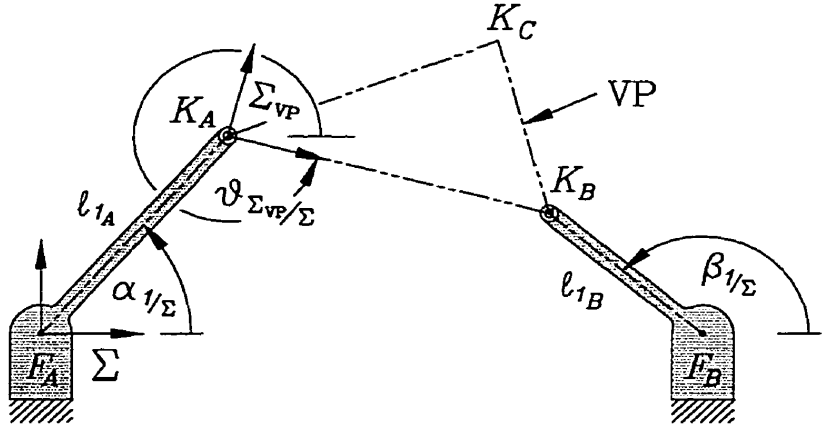

FIGURE 5.10. Determining the VP pose for *RP*-type platforms.

Analogous to *RRR* and *PRR* platforms using the VB (changing the virtual base to a virtual platform in Figure 5.4 gives Figure 5.10), the pose of the VP for *RRP* and *PRP* platforms is determined with Equation (5.15), with VB in the right-hand side changed to read VP, together with the base-fixed joint input for leg A. The vertices of the VP are the three knee joint centres described in the VP frame, Σ_{VP}. Consider Figure 5.10, the pose information obtained by using Equation (5.15) can be used to transform the the knee joint coordinates in the following way:

$$\boldsymbol{k}_{i/\Sigma_{VP}} = \boldsymbol{T}_{\Sigma/\Sigma_{VP}} \boldsymbol{k}_{i/\Sigma}, \tag{5.41}$$

where,

$$\boldsymbol{T}_{\Sigma/\Sigma_{VP}} = \begin{bmatrix} \cos\vartheta_{\Sigma_{VP}/\Sigma} & \sin\vartheta_{\Sigma_{VP}/\Sigma} & -(O_{x_{\Sigma_{VP}/\Sigma}}\cos\vartheta_{\Sigma_{VP}/\Sigma} + O_{y_{\Sigma_{VP}/\Sigma}}\sin\vartheta_{\Sigma_{VP}/\Sigma}) \\ -\sin\vartheta_{\Sigma_{VP}/\Sigma} & \cos\vartheta_{\Sigma_{VP}/\Sigma} & O_{x_{\Sigma_{VP}/\Sigma}}\sin\vartheta_{\Sigma_{VP}/\Sigma} - O_{y_{\Sigma_{VP}/\Sigma}}\cos\vartheta_{\Sigma_{VP}/\Sigma} \\ 0 & 0 & 1 \end{bmatrix}.$$

After the input data is suitably transformed, it can be used, together with the rest of the information listed in Table 5.7, to compute the univariate coefficients. The output from the roots of the univariate is the pose of Σ_{VP} in E,

$$\begin{bmatrix} a' \\ b' \\ \varphi' \end{bmatrix} = \begin{bmatrix} O_{x_{\Sigma_{VP}/E}} \\ O_{y_{\Sigma_{VP}/E}} \\ \varphi_{\Sigma_{VP}/E} \end{bmatrix}. \tag{5.42}$$

However, what is required is

$$\begin{bmatrix} a \\ b \\ \varphi \end{bmatrix} = \begin{bmatrix} O_{x_{E/\Sigma}} \\ O_{y_{E/\Sigma}} \\ \varphi_{E/\Sigma} \end{bmatrix}. \tag{5.43}$$

First, the pose of E with respect to Σ_{VP} is determined, using a transformation derived analogously to Equation (5.8):

$$\begin{bmatrix} O_{x_{E/\Sigma_{VP}}} \\ O_{y_{E/\Sigma_{VP}}} \\ 1 \end{bmatrix} = \begin{bmatrix} -\cos\varphi_{\Sigma_{VP}/E} & -\sin\varphi_{\Sigma_{VP}/E} & 0 \\ \sin\varphi_{\Sigma_{VP}/E} & -\cos\varphi_{\Sigma_{VP}/E} & 0 \\ 0 & 0 & 1 \end{bmatrix} \begin{bmatrix} a' \\ b' \\ 1 \end{bmatrix}. \tag{5.44}$$

These coordinates are then transformed to the base frame using

$$\begin{bmatrix} a \\ b \\ 1 \end{bmatrix} = \begin{bmatrix} \cos\vartheta_{\Sigma_{VP}/\Sigma} & -\sin\vartheta_{\Sigma_{VP}/\Sigma} & O_{x_{\Sigma_{VP}/\Sigma}} \\ \sin\vartheta_{\Sigma_{VP}/\Sigma} & \cos\vartheta_{\Sigma_{VP}/\Sigma} & O_{y_{\Sigma_{VP}/\Sigma}} \\ 0 & 0 & 1 \end{bmatrix} \begin{bmatrix} O_{x_{E/\Sigma_{VP}}} \\ O_{y_{E/\Sigma_{VP}}} \\ 1 \end{bmatrix}. \tag{5.45}$$

Finally, the orientation is computed, completing the solution procedure:

$$\varphi_{E/\Sigma} = \vartheta_{\Sigma_{VP}/\Sigma} - \varphi_{\Sigma_{VP}/E}. \tag{5.46}$$

5.2. Mixed-Leg Platforms

As mentioned in Chapter 4, some topologically asymmetric platforms can be analysed using the univariate. However, due to the limitation imposed by the derivation that $\mathcal{K}_0$ be the same for all legs (see Section 4.3), combinations must all belong to one of the three types: RR-, PR- or RP-type. For example the platform may be comprised of one $\underline{R}RR$ leg, one $R\underline{P}R$ leg, and one $RR\underline{P}$ leg. The procedure is simply a combination of the virtual base, regular and virtual platform procedures. A detailed example is given in Appendix A.7.

All combinations within a leg type are possible, the issue becomes a matter of keeping track of the transformations required to compute the univariate coefficients and, if needed, solutions in the base frame. As shown in the introduction to Chapter 4, this amounts to 168 different manipulators. The FK problem of the remaining 504 can not be solved by directly evaluating the univariate. The process instead involves computing the intersections of the three constraint surfaces, which requires the simultaneous solution of three quadratic equations. However, this procedure will not be further discussed, instead the reader is referred to [**2, 64, 69, 79, 130**].

5.3. Lower-Pair Jointed Platform Summary

The following three tables, 5.8, 5.9, and 5.10, provide a summary of the information needed to apply the univariate to the FK problem for any of the 168 manipulators, including the 18 PSGP, discussed earlier.

Platform	Geometric constraints	Circle and point coordinates
$RR\underline{R}$ 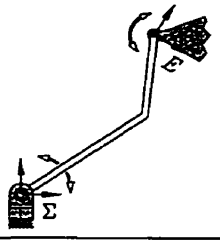	Hip points M_i, with fixed positions in E move on fixed circles centred on stationary ankle points, F_i, in Σ. The circle radii are determined by the intermediate R-pair angular inputs.	$\mathcal{K}_{0_i} = 1,$ $\mathcal{K}_{1_i} = F_{x_i/\Sigma},$ $\mathcal{K}_{2_i} = F_{y_i/\Sigma},$ $\mathcal{K}_{3_i} = \mathcal{K}_{1_i}^2 + \mathcal{K}_{2_i}^2 - r_i^2,$ where $r_i = [(\ell_{1_i} + \ell_{2_i}\cos\iota_{2/1})^2 + (\ell_{2_i}\sin\iota_{2/1})^2]^{\frac{1}{2}}.$ Note: $i \in \{A,B,C\}$ and $\iota \in \{\alpha,\beta,\gamma\}$.
$R\underline{P}R$ 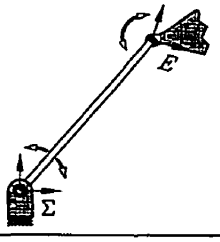	Kinematically isomorphic to the $R\underline{R}R$ platform.	$\mathcal{K}_{0_i} = 1,$ $\mathcal{K}_{1_i} = F_{x_i/\Sigma},$ $\mathcal{K}_{2_i} = F_{y_i/\Sigma},$ $\mathcal{K}_{3_i} = \mathcal{K}_{1_i}^2 + \mathcal{K}_{2_i}^2 - r_i^2,$ where $r_i = d_{2_i}.$
$\underline{R}RR$ 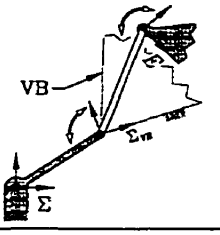	Hip points M_i, with fixed positions in E move on fixed circles centred on stationary knee points, $\mathcal{K}_i$, in Σ_{VB}. These circle centres, determined by the base R-pair inputs, are vertices of the VB.	$\mathcal{K}_{0_i} = 1,$ $\mathcal{K}_{1_i} = K_{x_i/\Sigma_{VB}},$ $\mathcal{K}_{2_i} = K_{y_i/\Sigma_{VB}},$ $\mathcal{K}_{3_i} = \mathcal{K}_{1_i}^2 + \mathcal{K}_{2_i}^2 - r_i^2,$ where $r_i = \ell_{2_i}$, $[K_{x_i/\Sigma} : K_{y_i/\Sigma} : K_{z_i/\Sigma}] =$ $[(F_{x_i/\Sigma} + \ell_{1_i}\cos\iota_{1/\Sigma}) : (F_{y_i/\Sigma} + \ell_{1_i}\sin\iota_{1/\Sigma}) : 1],$ and $\boldsymbol{k}_{i/\Sigma_{VB}} = \boldsymbol{T}_{\Sigma/\Sigma_{VB}}\boldsymbol{k}_{i/\Sigma}$, see Equation (5.16).
$\underline{P}RR$ 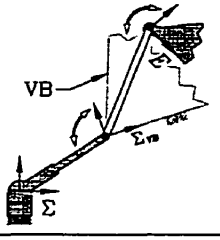	Kinematically isomorphic to $\underline{R}RR$ platforms.	See $\underline{R}RR$ platform and set $\ell_{1_i} = d_{1_i}$.
$RR\underline{R}$ 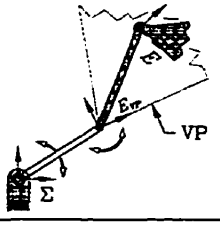	Knee points, K_i, with fixed positions in E_{VP}, determined by the platform R-pair inputs, move on fixed circles in Σ. The K_i are the vertices of the VP.	$\mathcal{K}_{0_i} = 1,$ $\mathcal{K}_{1_i} = F_{x_i/\Sigma},$ $\mathcal{K}_{2_i} = F_{y_i/\Sigma},$ $\mathcal{K}_{3_i} = \mathcal{K}_{1_i}^2 + \mathcal{K}_{2_i}^2 - r_i^2,$ where, $r_i = \ell_{1_i}$, $[K_{x_i/E} : K_{y_i/E} : K_{z_i/E}] =$ $[(M_{x_i/E} + \ell_{2_i}\cos\iota_{2/E}) : (M_{y_i/E} + \ell_{2_i}\sin\iota_{2/E}) : 1],$ and $\boldsymbol{k}_{i/E_{VP}} = \boldsymbol{T}_{E/E_{VP}}\boldsymbol{k}_{i/E}$, see Equation (5.34).
$RR\underline{P}$ 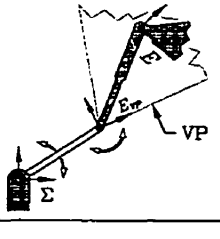	Kinematically isomorphic to $RR\underline{R}$ platforms.	See $RR\underline{R}$ platform and set $\ell_{2_i} = d_{3_i}$.

TABLE 5.8. RR-type platform constraints and parameters needed for the FK solution procedure. Frame E moves relative to Σ.

Platform	Geometric constraints	Circle and point coordinates
$PR\underline{R}R$ 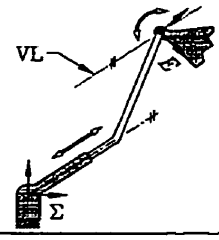	Hip points, M_i, with fixed positions in E move on fixed VL parallel to the translation direction of the grounded P-pairs.	$\mathcal{K}_{1_i} = \frac{1}{2}F_{z_i/\Sigma}\sin\iota_{1/\Sigma}$, $\mathcal{K}_{2_i} = -\frac{1}{2}F_{z_i/\Sigma}\cos\iota_{1/\Sigma}$, $\mathcal{K}_{3_i} = (F_{x_i/\Sigma} + \ell_{2_i}\cos\iota_{2/\Sigma})\sin\iota_{1/\Sigma} -$ $(F_{y_i/\Sigma} + \ell_{2_i}\sin\iota_{2/\Sigma})\cos\iota_{1/\Sigma}$. **Note:** $\mathcal{K}_{0_i} = 0$ for all PR-type platforms and $i \in \{A,B,C\}$ and $\iota \in \{\alpha,\beta,\gamma\}$.
$P\underline{P}R$ 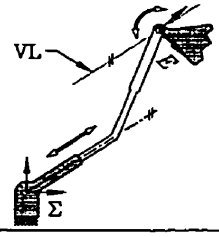	Kinematically isomorphic to $P\underline{R}R$ platforms.	See $P\underline{R}R$ platform and set $\ell_{2_i} = d_{3_i}$.
$\underline{R}PR$ 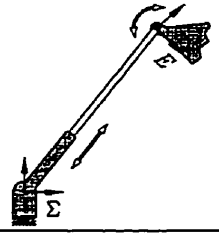	Hip points, M_i, with fixed positions in E move on fixed lines in Σ. The line coordinates for each leg are determined by the base R-pair inputs.	$\mathcal{K}_{1_i} = \frac{1}{2}F_{z_i/\Sigma}\sin\iota_{1/\Sigma}$, $\mathcal{K}_{2_i} = -\frac{1}{2}F_{z_i/\Sigma}\cos\iota_{1/\Sigma}$, $\mathcal{K}_{3_i} = F_{x_i/\Sigma}\sin\iota_{1/\Sigma} - F_{y_i/\Sigma}\cos\iota_{1/\Sigma}$.
$\underline{P}PR$ 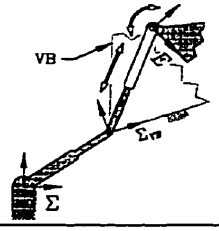	Hip points, M_i, with fixed positions in E move on fixed lines in Σ_{VB}. The three knee points, K_i, are the vertices of the VB. The line coordinates are determined by the grounded P-pair inputs.	$\mathcal{K}_{1_i} = \frac{1}{2}K_{x_i/\Sigma_{VB}}\sin\iota_{2/\Sigma_{VB}}$, $\mathcal{K}_{2_i} = -\frac{1}{2}K_{x_i/\Sigma_{VB}}\cos\iota_{2/\Sigma_{VB}}$, $\mathcal{K}_{3_i} = K_{x_i/\Sigma_{VB}}\sin\iota_{2/\Sigma_{VB}} - K_{y_i/\Sigma_{VB}}\cos\iota_{2/\Sigma_{VB}}$, where $[K_{x_i/\Sigma} : K_{y_i/\Sigma} : K_{z_i/\Sigma}] =$ $[(F_{x_i/\Sigma} + d_{1_i}\cos\iota_{1/\Sigma}) : (F_{y_i/\Sigma} + d_{1_i}\sin\iota_{1/\Sigma}) : 1]$, and $\boldsymbol{k}_{i/\Sigma_{VB}} = \boldsymbol{T}_{\Sigma/\Sigma_{VB}}\boldsymbol{k}_{i/\Sigma}$, see Equation (5.16).
$PR\underline{R}$ 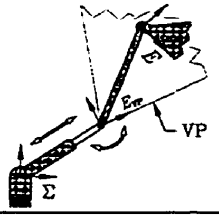	Knee points, K_i, with fixed positions in E_{VP}, determined by the platform R-pair inputs, move on fixed lines in Σ. The three knee points, K_i, are the vertices of the VP.	$\mathcal{K}_{1_i} = \frac{1}{2}F_{z_i/\Sigma}\sin\iota_{1/\Sigma}$, $\mathcal{K}_{2_i} = -\frac{1}{2}F_{z_i/\Sigma}\cos\iota_{1/\Sigma}$, $\mathcal{K}_{3_i} = F_{x_i/\Sigma}\sin\iota_{1/\Sigma} - F_{y_i\Sigma}\cos\iota_{1/\Sigma}$, with $[K_{x_i/E} : K_{y_i/E} : K_{z_i/E}] =$ $[(M_{x_i/E} + \ell_{2_i}\cos\iota_{2/E}) : (M_{y_i/E} + \ell_{2_i}\sin\iota_{2/E}) : 1]$, and $\boldsymbol{k}_{i/E_{VP}} = \boldsymbol{T}_{E/E_{VP}}\boldsymbol{k}_{i/E}$, see Equation (5.34).
$PR\underline{P}$ 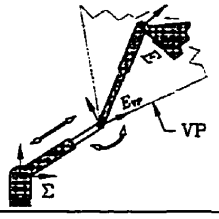	Kinematically isomorphic to $PR\underline{R}$ platforms.	See $PR\underline{P}$ platform and set $\ell_{2_i} = d_{3_i}$.

TABLE 5.9. PR-type platform constraints and parameters needed for the FK solution procedure. Frame E moves relative to Σ.

Platform	Geometric constraints	Circle and point coordinates
$\underline{RR}P$ 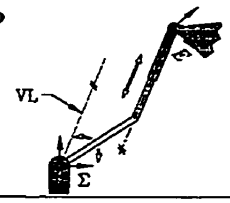	Ankle points, F_i, with fixed positions in Σ move on fixed VL parallel to the translation direction of the platform-fixed P-pairs.	$\mathcal{K}_{1_i} = \frac{1}{2} M_{z_i/E} \sin \iota_{2/E}$, $\mathcal{K}_{2_i} = -\frac{1}{2} M_{z_i/E} \cos \iota_{2/E}$, $\mathcal{K}_{3_i} = (M_{x_i/E} + \ell_{1_i} \cos \iota_{1/E}) \sin \iota_{2/E} -$ $(M_{y_i/E} + \ell_{1_i} \sin \iota_{1/E}) \cos \iota_{2/E}$. **Note:** $\mathcal{K}_{0_i} = 0$ for all RP-type platforms and $i \in \{A, B, C\}$ and $\iota \in \{\alpha, \beta, \gamma\}$.
$\underline{RP}P$ 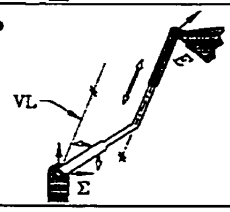	Kinematically isomorphic to $\underline{RR}P$ platforms.	See $\underline{RR}P$ platform and set $\ell_{1_i} = d_{1_i}$.
$RP\underline{R}$ 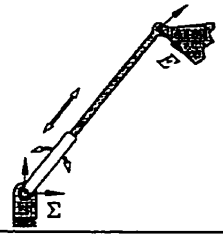	Ankle points, F_i, with fixed positions in Σ move on fixed lines in E. The line coordinates for each leg are determined by the platform-fixed R-pair inputs.	$\mathcal{K}_{1_i} = \frac{1}{2} M_{z_i/E} \sin \iota_{2/E}$, $\mathcal{K}_{2_i} = -\frac{1}{2} M_{z_i/E} \cos \iota_{2/E}$, $\mathcal{K}_{3_i} = M_{x_i/E} \sin \iota_{2/E} - M_{y_i/E} \cos \iota_{2/E}$.
$RP\underline{P}$ 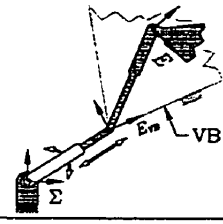	Ankle points, F_i, with fixed positions in Σ move on fixed lines in E_{VB}. The three knee points, K_i, are the vertices of the VB. The line coordinates are determined by the platform P-pair inputs.	$\mathcal{K}_{1_i} = \frac{1}{2} K_{z_i/E_{VB}} \sin \iota_{1/E_{VB}}$, $\mathcal{K}_{2_i} = -\frac{1}{2} K_{z_i/E_{VB}} \cos \iota_{1/E_{VB}}$, $\mathcal{K}_{3_i} = K_{x_i/E_{VB}} \sin \iota_{1/E_{VB}} - K_{y_i} \cos \iota_{1/E_{VB}}$, where $[K_{x_i/E} : K_{y_i/E} : K_{z_i/E}] =$ $[(M_{x_i/E} + d_{3_i} \cos \iota_{2/E}) : (M_{y_i/E} + d_{3_i} \sin \iota_{2/E}) : 1]$, and $\boldsymbol{k}_{i/E_{VB}} = \boldsymbol{T}_{E/E_{VB}} \boldsymbol{k}_{i/E}$, see Equation (5.25).
$\underline{RR}P$ 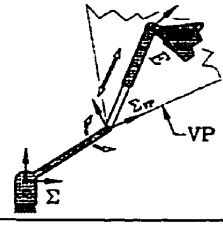	Knee points, K_i, with fixed positions in Σ_{VP}, determined by the base R-pair inputs, move on fixed lines in E. The three knee points, K_i, are the vertices of the VP.	$\mathcal{K}_{1_i} = \frac{1}{2} M_{z_i/E} \sin \iota_{2/E}$, $\mathcal{K}_{2_i} = -\frac{1}{2} M_{z_i/E} \cos \iota_{2/E}$, $\mathcal{K}_{3_i} = M_{x_i/E} \sin \iota_{2/E} - M_{y_i/E} \cos \iota_{2/E}$, with $[K_{x_i/\Sigma} : K_{y_i/\Sigma} : K_{z_i/\Sigma}] =$ $[(F_{x_i/\Sigma} + \ell_{1_i} \cos \iota_{1/\Sigma}) : (F_{y_i/\Sigma} + \ell_{1_i} \sin \iota_{1/\Sigma}) : 1]$, and $\boldsymbol{k}_{i/\Sigma_{VP}} = \boldsymbol{T}_{\Sigma/\Sigma_{VP}} \boldsymbol{k}_{i/\Sigma}$, see Equation (5.41).
$\underline{P}RP$ 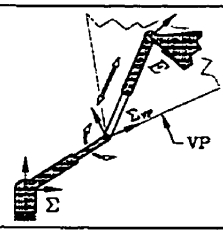	Kinematically isomorphic to $\underline{RR}P$ platforms.	See $\underline{P}RP$ platform and set $\ell_{1_i} = d_{1_i}$.

TABLE 5.10. RP-type platform constraints and parameters needed for the FK solution procedure. Roles of Σ and E reversed: Σ moves relative to E.

5.4. FK Solution Procedure for *RRG* Platforms

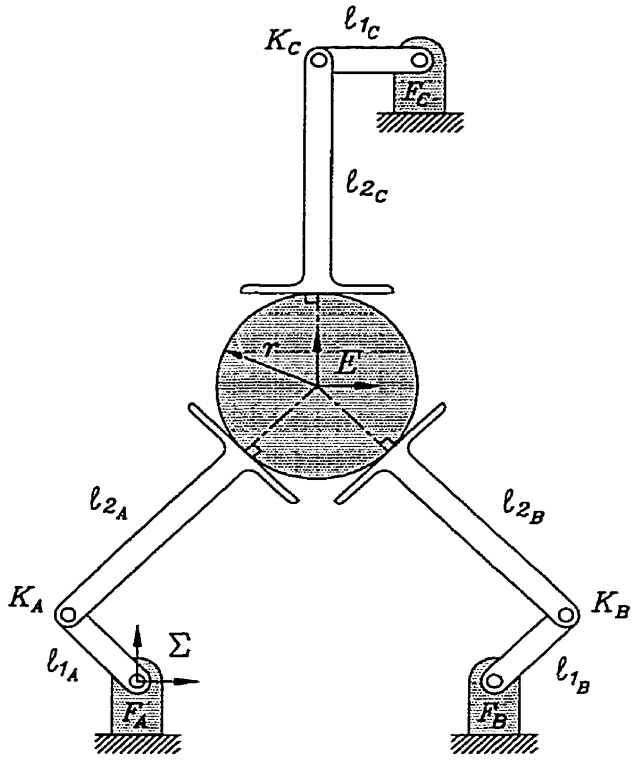

FIGURE 5.11. An *RRG* platform.

RRG platforms are quite different from those with only lower-pair jointed legs. Nevertheless, the two classes of platform may be considered as instantaneous computational equivalents because once the rack tangent angles are fixed, the higher-pair platform momentarily becomes an *RR*-type PSGP.

For the platform shown in Figure 5.11, the three variable joint input parameters are the change in rack tangent angles, due to the change in contact points measured along each of the three racks. They are given by the three numbers $\Delta d_i = r\Delta\tau_i$, $i \in \{A, B, C\}$, where the Δd_i are the changes in arclength, the radius of the pinion is r, and the $\Delta\tau_i$ are the change between the initial and final rack tangent angles. Since tangential contact between rack and pinion is always maintained, the change in tangent angle is the same as the change normal angle, $\Delta\eta_i$. This is illustrated in

Figure 5.12 (*i*). The parameters required to fix the pose of the i^{th} leg are illustrated in Figure 5.12 (*ii*).

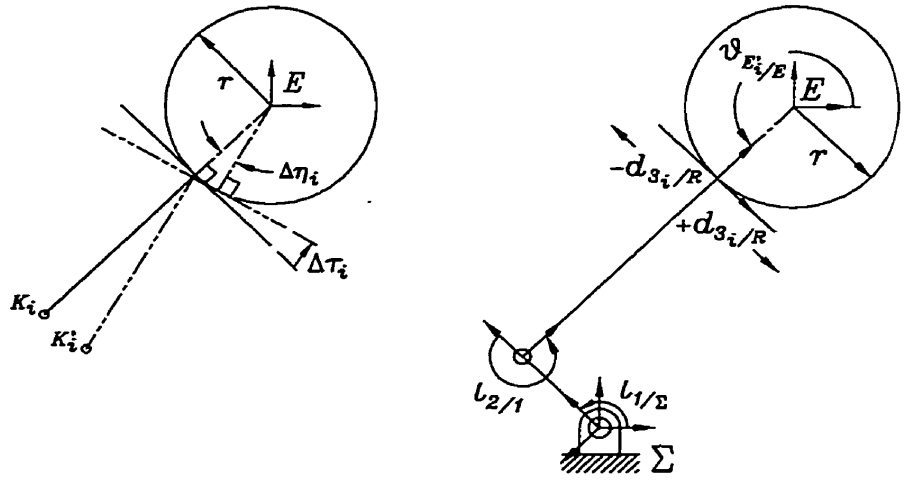

FIGURE 5.12. *(i)* $\Delta\tau_i = \Delta\eta_i$; *(ii)* parameters for the i^{th} leg.

When the active higher pairs are locked the platform may be temporarily considered an *RR*-type PSGP. The VP can be used in the solution procedure for the FK problem. The VP for a given set of input rack tangent angles is illustrated in Figure 5.13. It is important to emphasise that the pure rolling nature of the higher pairs make platforms of the type in Figure 5.11 markedly different from lower-pair-jointed SGP. The FK analysis cannot be directly reduced to the lower pair SGP case because of the contact point location ambiguity arising from the rolling constraints. Furthermore, there exists no such equivalent mechanism which can exactly reproduce a rack-and-pinion motion (see Hunt [**75**], p.106). Methods, such as those discussed in Gosselin and Sefrioui [**50**], Wohlhart [**142**], or Merlet [**100**] cannot be used unless suitably modified to account for the relative rolling. However, these procedures tend to be poorly suited to this platform type by virtue of the fact that the platform attachment points, *i.e.*, the points of contact between the pinion and racks, change relative to each other from pose to pose.

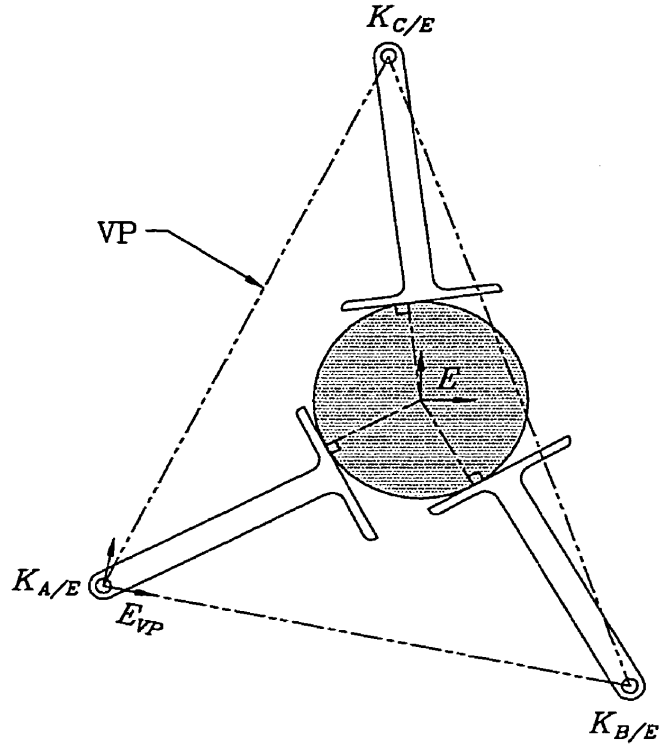

FIGURE 5.13. The VP for a given set of inputs.

5.4.1. Involute Inputs. Expressions for the VPP must be developed so they can be used as inputs to the kinematic mapping. We want the VPP in terms of the joint input variables so they can be used to evaluate the univariate coefficients. Consider, for now, only leg A in Figure 5.14 and observe that the knee joint K_A has a fixed position in the reference frame attached to the rack, R_A. We know it moves on a circle in Σ, but it also experiences motion relative to the moving disk frame E. What is required is a description of that motion in terms of the joint inputs. This turns out to be straightforward: if the pinion is fixed and the relative motion of the rack with respect to E is pure rolling then the original contact point on the rack moves on an involute of the pinion [82]. There is a bijective correspondence, that depends on the change in rack tangent angle, between positions of a given rack point on its involute and the knee joint positions. This gives a complete description of the motion of the

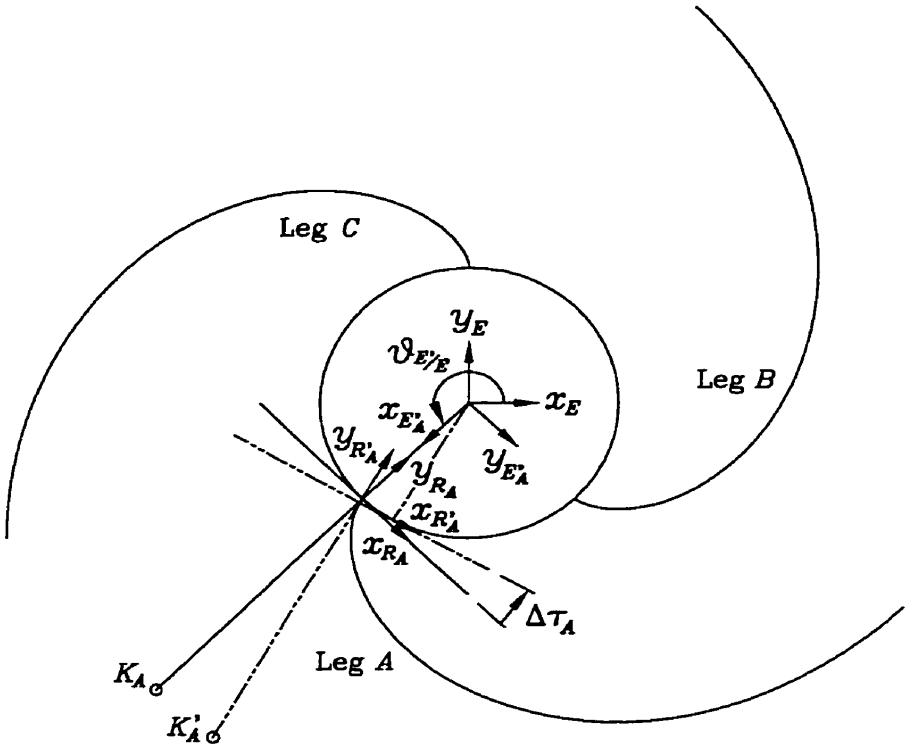

FIGURE 5.14. Reference systems in leg A after a rotation $\Delta\tau_A$.

knee joints in terms of the input variables. Due to their positional dependence on an involute, we call these one parameter sets of knee joint positions *involute inputs.*

The motion of the knee joints of the remaining two legs must be the same type as that of leg A relative to E, but the starting points of the involutes are different. Thus, for every set of three joint input parameters one obtains a set of three VPP expressed in E. With the VPP transformed as involute inputs the kinematic mapping can be used.

In what follows the involute inputs will be derived. Figure 5.14 shows the reference coordinate systems used to transform the position of the knee joint K_A from the moving rack reference frame, R_A, to the relatively fixed pinion reference frame, E. The origin of R_A moves along its involute and R'_A gives the new position of R_A after a change in tangent angle, $\Delta\tau_A$. The intermediate system accounting for the

location of the starting point and orientation of the involute, E'_A, is fixed relative to E. Examining Figure 5.14, it is easy to see that for each leg the required transformation to take the coordinates of the knee joint K_i from frame R'_i to frame E are the concatenation of transformations expressing points in frame R'_i relative to frame E'_i and those expressing points in frame E'_i relative to frame E:

$$\begin{aligned} \boldsymbol{T}_{R'_i/E} &= \boldsymbol{T}_{E'_i/E}\boldsymbol{T}_{R'_i/E'_i} \\ &= \begin{bmatrix} c\vartheta_{E'_i/E} & -s\vartheta_{E'_i/E} & 0 \\ s\vartheta_{E'_i/E} & c\vartheta_{E'_i/E} & 0 \\ 0 & 0 & 1 \end{bmatrix} \begin{bmatrix} -s\Delta\tau_i & -c\Delta\tau_i & r(c\Delta\tau_i + \Delta\tau_i s\Delta\tau_i) \\ c\Delta\tau_i & -s\Delta\tau_i & r(s\Delta\tau_i - \Delta\tau_i c\Delta\tau_i) \\ 0 & 0 & 1 \end{bmatrix}, \end{aligned}$$

where $c \equiv \cos$, and $s \equiv \sin$.

The geometrical significance of $\boldsymbol{T}_{R'_i/E'_i}$ is seen when each column is examined [**91**]. The first column is the direction of the disk tangent in E'_i (the direction of the x-axis of frame R'_i). The second column is the direction in E'_i, towards the centre of the pinion, of the normal at the new contact point (the direction of the y-axis of frame R'_i). The third column is the position of the origin of frame R'_i on the involute, also expressed in E'_i. The remaining transformation, $\boldsymbol{T}_{E'_i/E}$, depends on the angle between the x-axis of frame E and the rack normal in the home-position, indicated by $\vartheta_{E'_i/E}$.

The knee joints, shown in Figure 5.11, all have the same coordinates in their respective R_i and R'_i frames:

$$\boldsymbol{k}_{i/R_i} = \boldsymbol{k}_{i/R'_i} = \begin{bmatrix} 0 \\ -\ell_{2_i} \\ 1 \end{bmatrix}.$$

Once the changes in rack tangent angle (joint inputs), $\Delta\tau_i$, are specified the coordinates of the knee joints (involute inputs) in frame E, $\boldsymbol{k}_{i/E}$, are easily determined by

left multiplying the $\boldsymbol{k}_{i/R_i'}$ with the appropriate $\boldsymbol{T}_{R_i'/E}$,

$$\boldsymbol{k}_{i/E} = \boldsymbol{T}_{R_i'/E}\boldsymbol{k}_{i/R_i'}. \tag{5.47}$$

5.4.2. Remaining Computation Steps. The VPP expressed in the VP frame, E_{VP}, are needed to evaluate the univariate coefficients. We can not simply use the procedure for *RRR* or *RRP* platforms due to the nature of the higher pairs and because the platform frame moves with the centre of the pinion, not an attachment point.

We proceed in a slightly different way from Section 5.1.4. The first step is to compute the following for use in the transformation $\boldsymbol{T}_{E/E_{VP}}$, from Equation (5.34):

$$O_{x_{E_{VP}/E}} = K_{x_{A/E}}, \tag{5.48}$$

$$O_{y_{E_{VP}/E}} = K_{y_{A/E}}, \tag{5.49}$$

$$\vartheta_{E_{VP}/E} = \text{atan2}\left((K_{y_{B/E}} - K_{y_{A/E}}), (K_{y_{B/E}} - K_{y_{A/E}})\right). \tag{5.50}$$

The coordinates required to evaluate these equations are determined using Equation (5.47).

Now we have everything needed to compute the required transformation. The right-hand side of Equation (5.47) is pre-multiplied with the transformation from Equation (5.34), which is the following concatenation:

$$\boldsymbol{T}_{R_i'/E_{VP}} = \boldsymbol{T}_{E/E_{VP}}\boldsymbol{T}_{R_i'/E}, \tag{5.51}$$

$$= \boldsymbol{T}_{E/E_{VP}}\boldsymbol{T}_{E_i'/E}\boldsymbol{T}_{R_i'/E_i'}. \tag{5.52}$$

We can use the simplest expression of the VPP, $\boldsymbol{k}_{i/R_i'} = [0 : -\ell_{2_i} : 1]^T$, to obtain the required coordinates:

$$\boldsymbol{k}_{i/E_{VP}} = \boldsymbol{T}_{R_i'/E_{VP}}\boldsymbol{k}_{i/R_i'}. \tag{5.53}$$

With the VPP obtained from Equation (5.53), together with the base geometry and IAC, the univariate coefficients can be evaluated. The roots of the univariate yield the pose of E_{VP} with respect to the base frame, Σ:

$$\begin{bmatrix} a' \\ b' \\ \varphi' \end{bmatrix} = \begin{bmatrix} O_{x_{E_{VP}/\Sigma}} \\ O_{y_{E_{VP}/\Sigma}} \\ \varphi_{E_{VP}/\Sigma} \end{bmatrix}. \tag{5.54}$$

However, the required information is

$$\begin{bmatrix} a \\ b \\ \varphi \end{bmatrix} = \begin{bmatrix} O_{x_{E/\Sigma}} \\ O_{y_{E/\Sigma}} \\ \varphi_{E/\Sigma} \end{bmatrix}. \tag{5.55}$$

The solution is evident upon examination of Figure 5.13. The pinion displacement parameters, then, are given by:

$$a = a' + (l_{2_A} + r)\cos\alpha - d_{3_A}\sin\alpha, \tag{5.56}$$

$$b = b' + (l_{2_A} + r)\sin\alpha + d_{3_A}\cos\alpha, \tag{5.57}$$

$$\begin{aligned} \varphi &= \varphi' + \vartheta_{E/E_{VP}}, \\ &= \varphi' - \vartheta_{E_{VP}/E}, \end{aligned} \tag{5.58}$$

where,

$$\begin{aligned} \alpha &= \vartheta_{E'_A/E} + \Delta\tau_A - \pi, \\ d_{3_A} &= r\Delta\tau_A. \end{aligned}$$

A detailed numerical example is given in Appendix A.8.

CHAPTER 6

The Inverse Kinematics Problem

The inverse kinematics (IK) may be stated as: given the position and orientation of the platform frame E, determine the variable joint inputs and corresponding assembly modes required for the platform to attain the desired pose. It is generally acknowledged that the IK problem for PSGP is trivial. Closed form algebraic solutions can usually be found. As for the FK problem, the conventional Cartesian approaches are architecture and geometry specific. There is, as yet, no unified approach to the problem for the general case. While the kinematic mapping procedure offered here is not the desired unified approach, it does represent a step on the road towards this goal. The main thing to emphasise is that the kinematic mapping allows for the development of IK algorithms that are independent of the geometry of the platform and hence, provide solutions to the IK problem of $RR\underline{G}$-type platforms that remain unsolved by conventional Cartesian approaches [**3, 4, 63**]. It is mainly for this reason that the issue of the IK is broached.

To begin, one observes that the FK problem reduces to determining the intersection points of three constraint surfaces in the projective homogeneous image space. Each point of intersection represents a platform pose. It follows that the IK problem can be solved by working in the opposite direction: start with a given point in the image space which represents a feasible platform pose and extract a set of active joint

inputs from the corresponding pre-image. Because the mapping is not bijective (there is at most one pre-image for every point in the image space) there are points in this space that are not the image of a planar displacement.

With the use of kinematic mapping it is a simple matter to determine all IK solutions by considering the general constraint surface for each leg of the platform in question. Each leg of the platform can be considered separately because the solutions are decoupled from leg-to-leg. Hence, the IK problem of every lower pair jointed three-legged planar platform with three DOF can be solved by determining the joint input value from the image point satisfying the associated constraint surface equation. Moreover, the IK problem for *RRG*-type platforms are also easily determined. This is a new result, which is not possible with conventional Cartesian approaches due to the ambiguities introduced by the relative rolling between each rack and the pinion [**63, 67**].

6.1. Lower Pair Platforms

The solutions to the IK problem of a given three-legged planar platform with three DOF are uncoupled between legs [**49**]. That is, the value of the active joint input in each leg, given a desired platform pose, depends only on the geometry of the given leg and the pose. Thus, we can solve the IK problem for any of the 1140 possible platforms composed of combinations of the 18 characteristic chains taken 3 at a time using the kinematic mapping. Of course, it is easy to write the three independent equations for these platforms based on their Cartesian geometry. As a means-to-an-end this approach is complete. However, each distinct leg type requires a distinct equation. Solving the IK problem by finding the pre-image of an image point in the kinematic mapping image space ultimately lands one in the same pot of stew. However, it is to be hoped that adopting an approach that is independent of

the geometry of the base and platform will eventually lead to a unified IK solution procedure. For this reason the following material is presented.

Because of the trivial nature of the problem from a Cartesian point of view it is natural to expect that the kinematic mapping procedure be simple and straightforward. Indeed, this is the case. There are only two main groups of leg type to consider: RR-type and non-RR-type. Recall that the general constraint surface can be expressed by Equation (4.9), repeated here.

$$\begin{aligned}
&\mathcal{K}_0 z^2(X_1^2 + X_2^2) + (1/4)\left[\mathcal{K}_0(1-z^2)(x^2+y^2) + 2z(\mathcal{K}_1 x + \mathcal{K}_2 y) + Rz^2\right] X_3^2 + \\
&(1/4)\left[Rz^2 + \mathcal{K}_0(1-z^2)(x^2+y^2) - 2z(\mathcal{K}_1 x + \mathcal{K}_2 y)\right] X_4^2 - (\mathcal{K}_1 z^2 + \mathcal{K}_0 xz)X_1X_3 + \\
&(\mathcal{K}_2 z^2 - \mathcal{K}_0 yz)X_1X_4 - (\mathcal{K}_0 yz + \mathcal{K}_2 z^2)X_2X_3 + (\mathcal{K}_0 xz - \mathcal{K}_1 z^2)X_2X_4 + \\
&(\mathcal{K}_1 yz - \mathcal{K}_2 xz)X_3X_4) \;=\; 0. \qquad (6.1)
\end{aligned}$$

Because each platform leg is solved independently the subscripts indicating the leg to which a parameter belongs, $i \in \{A, B, C\}$, may be safely dropped. For a particular leg, Equation (6.1) contains only variables and constants associated with that leg. Thus, the homogeneous coordinates of points in the platform frame E are

$$p_{i/E} \;=\; (x : y : z).$$

Those of points in the fixed base frame Σ are

$$p_{i/\Sigma} \;=\; (X : Y : Z).$$

6.1.1. *RR*-type Platforms. For all characteristic passive sub-chains the active joint is either an R-pair or a P-pair. For RR-type platforms the joint input can always be characterised by the distance between the fixed base point and the moving platform point, regardless of active joint type. This quantity is the radius, r, of the constraint circle.

A given image point $[X_1 : X_2 : X_3 : X_4]$ represents a platform pose. But, it also represents a point of intersection of a family of constraint surfaces. The image point is uniquely fixed by the platform displacement parameters, (a, b, ϕ). Each constraint surface containing this point is a function of the image point itself $[X_1 : X_2 : X_3 : X_4]$, the moving platform points $(x : y : z)$, and the circle coordinates $(\mathcal{K}_0 : \mathcal{K}_1 : \mathcal{K}_2 : \mathcal{K}_3)$. Recall that for RR-type characteristic passive sub-chains the circle coordinates are defined as follows:

$$\begin{aligned}
\mathcal{K}_0 &= \text{arbitrary homogenising constant,} \\
\mathcal{K}_1 &= X_c, \\
\mathcal{K}_2 &= Y_c, \\
\mathcal{K}_3 &= R - \mathcal{K}_0(x^2 + y^2), \\
R &= \mathcal{K}_1^2 + \mathcal{K}_2^2 - r^2 + \mathcal{K}_0(x^2 + y^2).
\end{aligned}$$

Examining all these quantities together, it is to be seen that the only unknown is the radius r of the constraint circle. Note, this quantity represents the distance between corresponding base and platform points. After making the substitution $R = \mathcal{K}_1^2 + \mathcal{K}_2^2 - r^2 + \mathcal{K}_0(x^2 + y^2)$ in Equation (6.1) and expanding then collecting terms of r yields a quadratic with the form

$$Ar^2 + Br + C = 0, \tag{6.2}$$

where

$$\begin{aligned}
A &= -z^2(X_3^4 + X_4^4 + 2X_3^2X_4^2), \\
B &= 0, \\
C &= 4z^2X_1^2(X_3^2 + X_4^2) + 4zX_1[X_4(X_3^2 + X_4^2)(\mathcal{K}_2z - y) - X_3(X_3^2 + X_4^2)(x + \mathcal{K}_1z)] + \\
&\quad 4z^2X_2^2(X_3^2 + X_4^2) + 4zX_2[X_4(X_3^2 + X_4^2)(x - \mathcal{K}_1z) - X_3(X_3^2 + X_4^2)(y + \mathcal{K}_2z) + \\
&\quad X_3^4[x^2 + y^2 + z^2(\mathcal{K}_1^2 + \mathcal{K}_2^2) + 2z(\mathcal{K}_1x + \mathcal{K}_2y)] + 4z(X_4X_3^3 + X_4^3X_3)(\mathcal{K}_1y - \mathcal{K}_2x) + \\
&\quad 2X_3^2X_4^2[x^2 + y^2 + z^2(\mathcal{K}_1^2 + \mathcal{K}_2^2)] + X_4^4[x^2 + y^2 + z^2(\mathcal{K}_1^2 + \mathcal{K}_2^2) - 2z(\mathcal{K}_1x + \mathcal{K}_2y)].
\end{aligned}$$

This quadratic has a solution of the form:

$$r = \pm\frac{\sqrt{-AC}}{A}. \tag{6.3}$$

While this result means that there are two real solutions, only one is acceptable since the quantity represents the radius of a circle, which is, by convention, a positive non-zero number. Thus, there is but one solution for a given RR-type platform leg:

$$r = \left|\frac{\sqrt{-AC}}{A}\right|. \tag{6.4}$$

The fact that there is but one value for r does not, in general, mean that there is but one solution to the IK problem. This is only so for $R\underline{P}R$-type legs. The remaining RR-type legs all have *elbow-up* and *elbow-down* solutions, meaning there is a maximum of 2 solutions for each leg, $2^3 = 8$ for a PSGP. The input parameter for each leg required to attain the desired pose for these legs is easily obtained from the calculated r using plane trigonometry and the known design parameters, see the example in Appendix B.1. The upper bounds on the number of solutions for each RR-type PSGP are listed in Table 6.1. While for arbitrary mixed leg platforms there can be 1, 2, 4, or 8 solutions, depending on the architecture of the constituent legs.

RR-type PSGP	Maximum solutions
$R\underline{R}R$	8
$R\underline{P}R$	1
$\underline{R}RR$	8
$\underline{P}RR$	8
$RR\underline{R}$	8
$RR\underline{P}$	8

TABLE 6.1. Maximum number of IK solutions for RR-type PSGP.

6.1.2. *PR*- and *RP*-type Legs. Solving the IK for PR- and RP-type subchains is accomplished by solving the general constraint equation for a single variable:

the unknown direction of the line joining the F_i and the corresponding M_i. Thus, unlike the FK problem the two types do not have to be considered separately. The circle coordinates have the uniform definition:

$$\begin{aligned}
\mathcal{K}_0 &= 0, \\
\mathcal{K}_1 &= \frac{1}{2} Z \sin\iota, \\
\mathcal{K}_2 &= -\frac{1}{2} Z \cos\iota, \\
\mathcal{K}_3 &= R = X \sin\iota - Y \cos\iota,
\end{aligned}$$

where the $(X : Y : Z)$ are the homogeneous coordinates of the fixed base point.

Clearly, the unknown is the angle ι. Making the appropriate substitutions in Equation (6.1) gives an equation linear in the sines and cosines of ι. Solving for ι gives:

$$\iota = \text{atan2}(N, D), \tag{6.5}$$

where

$$\begin{aligned}
N &= 2z(X_1X_4 - X_2X_3) - 2xX_3X_4 + (zY + y)X_3^2 + (zY - y)X_4^2 \\
D &= 2yX_3X_4 - 2z(X_1X_3 + X_2X_4) + (zX + x)X_3^2 + (zX - x)X_4^2
\end{aligned}$$

The input parameter for each PR- or RP-type leg required to attain the given pose is easily obtained from the calculated value of ι using plane trigonometry and known design parameters. Two examples are given in Appendix B.2. As for the RR-type legs, there is one solution for this equation, but not, in general, to the IK problem for PR- and RP-type PSGP. The upper bounds on the number of solutions for these two types of PSGP are listed in Table 6.2. Of course, for arbitrary architectures there can be 1, 2, 4, or 8 solutions.

PR-type PSGP	Max. sol.	*RP*-type PSGP	Max. sol.
$PR\underline{R}$	8	$RR\underline{P}$	8
$PP\underline{R}$	1	$RP\underline{P}$	1
$\underline{R}PR$	1	$RP\underline{R}$	1
$\underline{P}PR$	1	$RP\underline{P}$	1
$PR\underline{R}$	8	$\underline{R}RP$	8
$PR\underline{P}$	1	$\underline{P}RP$	1

TABLE 6.2. Maximum number of IK solutions for *PR*- and*RP*-type PSGP.

6.2. Higher Pair $RR\underline{G}$ Platforms

A complicating factor in general plane displacement analysis of the $RR\underline{G}$ platform is the ambiguity that the rolling constraint introduces. That is, φ, the desired final disk orientation does not divulge how much of the new position was achieved by rotation of the grounded and non-grounded links and how much was achieved by pure rolling between the disk and the legs. By how much has the disk rolled on the racks and by how much has each rack rolled on the disk? Is there a combination, and if so, what is the ratio? These questions lead to difficulties in the determination of the joint inputs, $\Delta\tau$, if only the trigonometry in the Cartesian plane is considered. Furthermore, displacement analysis requires the presence of initial assembly conditions (IAC) in the kinematic closure equations. This dependency on the IAC means that analysis is not possible using only the techniques employed on lower pair jointed SG type platforms by [**50**], for instance.

Indeed, there exists no practical IK solution procedure for these manipulators. An algorithm is offered in [**3**], however, the authors fail to account for the orientation of the end-effector in the inertial reference frame. They use instead a relative angle which can change for certain displacements while the orientation of the end-effector remains constant. The only other algorithm, [**63**], is problematic because it leads to many spurious solutions.

6.2.1. Solution Procedure. The goal is to determine the inputs required to attain a desired feasible end-effector pose. As for the lower pair PSGP, the constraint hyperboloids for each leg are first examined. An image point $(X_1 : X_2 : X_3 : X_4)$ is fixed by the given pinion displacement parameters (a, b, φ). Furthermore, the constants $(\mathcal{K}_0 : \mathcal{K}_1 : \mathcal{K}_2 : \mathcal{K}_3)$ are known because the circle centres and radii are all specified. This leaves the three homogeneous VPP coordinates $(x : y : z)$ as unknowns. It is important to note that for the IK problem the VPP coordinates must be expressed in the pinion frame, E, and not in the VPP frame, E_{VP}. Thus, we have three hyperboloid equations and nine unknowns:

$$H_i = f_i(x_i, y_i, z_i), \qquad i \in \{A, B, C\}. \tag{6.6}$$

Since a detailed example is presented in Appendix B.3, the leg specific subscripts, $i \in \{A, B, C\}$, are again used.

Since no practical design requires the VP to have points on the line at infinity, $\mathcal{L}_\infty$, it is safe to set $z_i = 1$, reducing the quantity of unknowns to six:

$$H_i = f_i(x_i, y_i), \qquad i \in \{A, B, C\}. \tag{6.7}$$

At least three more equations are required. Consider the involute input Equations (5.47). With $z_i = 1$, these are a set of six equations expressing the knee joint coordinates in the moving frame, E, in terms of the three unknown rack tangent angle inputs, $\Delta\tau_i$. This gives nine equations and nine unknowns, coming in independent sets of three. That is, $x_i, y_i, \Delta\tau_i$ can be solved independently for each $i \in \{A, B, C\}$:

$$\left.\begin{aligned} H_i &= f_i(x_i, y_i) \\ x_i &= g_i(\Delta\tau_i) \\ y_i &= h_i(\Delta\tau_i) \end{aligned}\right\}, \qquad i \in \{A, B, C\} \tag{6.8}$$

where f_i is a function in the two variables x_i and y_i, which are themselves single variable functions g_i and h_i, respectively, in terms of $\Delta\tau_i$.

Substituting the expressions for $x_i = g(\Delta\tau_i)$ and $y_i = h(\Delta\tau_i)$ into H_i gives the univariate function

$$\begin{aligned} H_i(\Delta\tau_i) &= a_0 + a_1\Delta\tau_i + a_2(\Delta\tau_i)^2 + a_3\cos\Delta\tau_i + a_4\sin\Delta\tau_i + \\ &\quad \Delta\tau_i(a_5\cos\Delta\tau_i + a_6\sin\Delta\tau_i), \end{aligned} \tag{6.9}$$

where the a_i are coefficients in the field of real numbers:

$$\begin{aligned} a_0 &= X_1^2 + X_2^2 + \frac{1}{4}(X_3^2 + X_4^2)(2l_2r + l_2^2 + r^2 + \mathcal{K}_3) + \mathcal{K}_1(X_1X_3 + X_2X_4) + \\ &\quad \mathcal{K}_2(X_2X_3 - X_1X_4), \\ a_1 &= 0, \\ a_2 &= \frac{r^2}{4}(X_3^2 + X_4^2), \\ a_3 &= (l_2 + r)\left[\frac{1}{2}\mathcal{K}_1(X_4^2 - X_3^2) - X_1X_3 + X_2X_4 + \mathcal{K}_2X_3X_4\right], \\ a_4 &= (l_2 + r)\left[\frac{1}{2}\mathcal{K}_2(X_4^2 - X_3^2) - X_2X_3 - X_1X_4 - \mathcal{K}_1X_3X_4\right], \\ a_5 &= r\left[\frac{1}{2}\mathcal{K}_2(X_3^2 - X_4^2) + X_2X_3 + X_1X_4 + \mathcal{K}_1X_3X_4\right], \\ a_6 &= r\left[\frac{1}{2}\mathcal{K}_1(X_4^2 - X_3^2) + X_2X_4 - X_1X_3 + \mathcal{K}_2X_3X_4\right]. \end{aligned}$$

Solve $H_i(\Delta\tau_i)$ for $\Delta\tau_i$, and use this value to determine x_i and y_i from the g_i and h_i. This immediately yields the knee joint coordinates in the moving pinion frame. $H_i(\Delta\tau_i)$ represents a curve. The roots of this function, *i.e.*, the zero-crossings in the $\Delta\tau - H(\Delta\tau)$ plane, give the change in rack tangent angles, which are the solutions to the IK problem. The upper bound on the number of solutions depends on the number of roots. These will now be examined.

The curve is characterised as a *quadratically dominant oscillating curve.* That is, the curve $H(\Delta\tau)$ is the locus of points oscillating about the parabola

$$H_p \;=\; a_0 + a_2(\Delta\tau)^2. \tag{6.10}$$

Examining Figure 6.1, it is evident that the amplitude of the oscillations is minimum at $\Delta\tau = 0$. As $\Delta\tau$ moves away from zero, in either direction along the $\Delta\tau$-axis the amplitude increases and the frequency decreases. The *period* (the term is used even though this is not a periodic function, strictly speaking) is about 8 radians. If $a_0 < 0$ it is possible to have more than two zeros. If, however, the range of the change in rack tangent angles is restricted to a value smaller than 8 radians, more than two full rotations, the maximum number of zeros is 2. This gives the expected upper bound on the number of IK solutions for each leg.

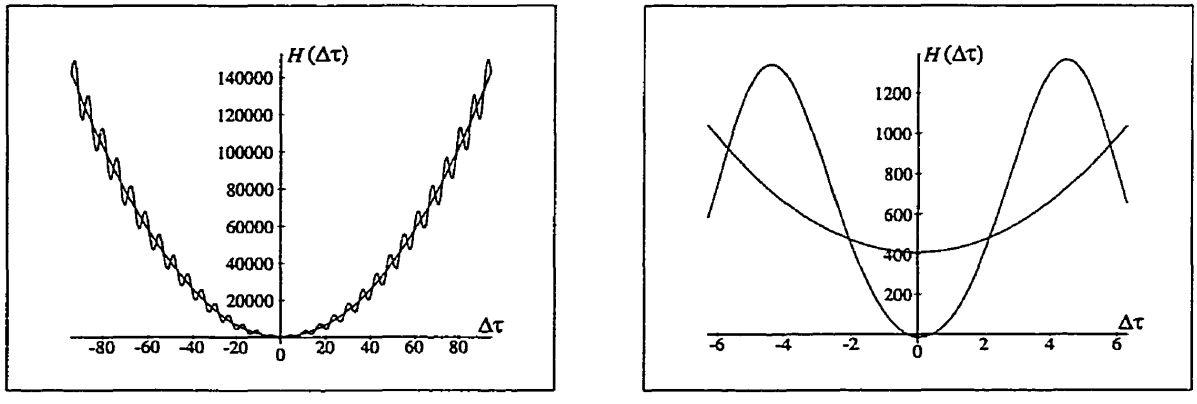

FIGURE 6.1. The one parameter curve $H(\Delta\tau)$ oscillating about a parabola in the $\Delta\tau - H(\Delta\tau)$ plane.

It is a simple matter of plane trigonometry to extract the assembly configuration(s) from the nine parameters, x_i, y_i, and $\Delta\tau_i$. The solutions are decoupled among legs and there is an upper bound on the number of solutions to the IK problem of $2^3 = 8$. A detailed numerical example can be found in Appendix B.3.

CHAPTER 7

Workspace and Singularities

One of the general drawbacks of parallel manipulators, as mentioned in Chapter 1, is the smaller workspace as compared to serial manipulators. Moreover, the relatively small workspace can be densely packed with singularities. These two issues are discussed in the following sections.

7.1. Workspace Analysis

Whether or not solutions to the IK problem of a manipulator exist raises the issue of its *workspace*. The total workspace of the manipulator, usually called the *reachable workspace*, is defined as the area, or volume within which a reference point on the end effector can be made to coincide with a given point [**92**]. There are various definitions of subsets of the reachable workspace. For instance, the *dextrous workspace* is defined as the set of points in the reachable workspace that the end effector can reach with any orientation [**92**].

The workspace of PSGP has received a large amount of attention and has been fully established by Gosselin [**49**], Pennock and Kassner [**112**], Merlet and Mouly [**98**]. Indeed, various interactive software packages for design, motion and trajectory

planning [**52, 99**] already exist. However, only recently has kinematic mapping been applied to workspace analysis by Husty [**80**]. By virtue of the ruled constraint surfaces which describe all possible positions of the end-effector it is a useful, informative and overlooked visualisation aid and design tool. Moreover, it facilitates computations when more than one end-effector reference point is considered [**80**].

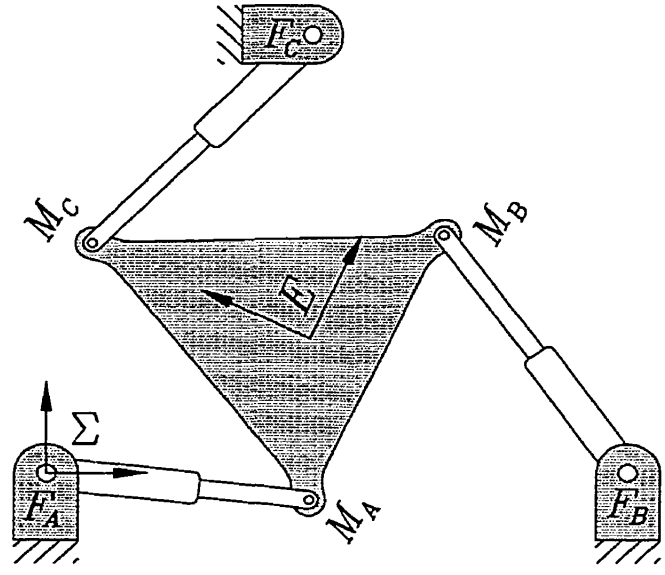

FIGURE 7.1. An $R\underline{P}R$ platform.

7.1.1. Reachable Workspace. Here an $R\underline{P}R$ platform is considered, as reported in [**80**], but the procedure may be adapted to any PSGP. The following is a summary of the procedure described by Husty [**80**]. The image of the reachable workspace can be obtained in the following way. The leg lengths, d_i, must be within the joint limits $d_{i_{min}} \leq d_i \leq d_{i_{max}}$, $i \in \{A, B, C\}$. This condition means that for each leg there correspond two coaxial constraint hyperboloids. They bound the region of all possible positions and orientations of the platform, assuming the platform attachment points of the other two legs have been disconnected. Performing the same procedure for each leg in turn yields three solid regions bounded by six hyperboloids, each pair

coaxial. Figure 7.2 shows the three solids for the platform illustrated in Figure 7.1. Note that the origin of frame E is located on the centroid of the platform.

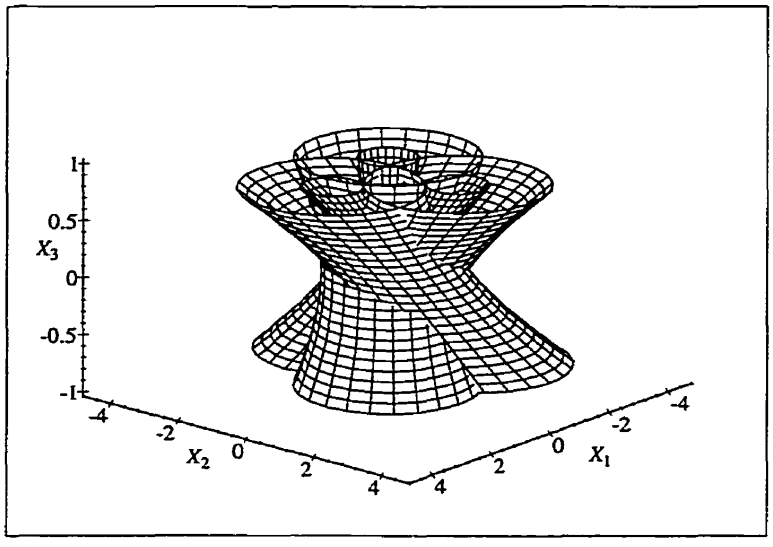

FIGURE 7.2. The kinematic image of the reachable workspace for an $R\underline{P}R$ platform.

The parametric equation for the constraint hyperboloid given by Equation (4.22) is reproduced, and modified by adding the subscript i to the radius r, here as Equation (7.1) representing the constraint solid:

$$\begin{bmatrix} X_1 \\ X_2 \\ X_3 \end{bmatrix} = \frac{1}{2} \begin{bmatrix} [(\mathcal{K}_1 + x)t - \mathcal{K}_2 + y] + (r_i\sqrt{t^2+1})\cos\zeta \\ [(\mathcal{K}_2 + y)t + \mathcal{K}_1 - x] + (r_i\sqrt{t^2+1})\sin\zeta \\ 2t \end{bmatrix}, \quad \begin{array}{l} \zeta \in \{0, \ldots, 2\pi\}, \\ t \in \{-\infty, \ldots, \infty\}, \\ i_{min} \leq i \leq i_{max}. \end{array} \tag{7.1}$$

Note that $r_{i_{min}} = d_{i_{min}}$ and $r_{i_{max}} = d_{i_{max}}$ and the parameter lines $t =$ constant correspond to those positions which belong to a constant orientation.

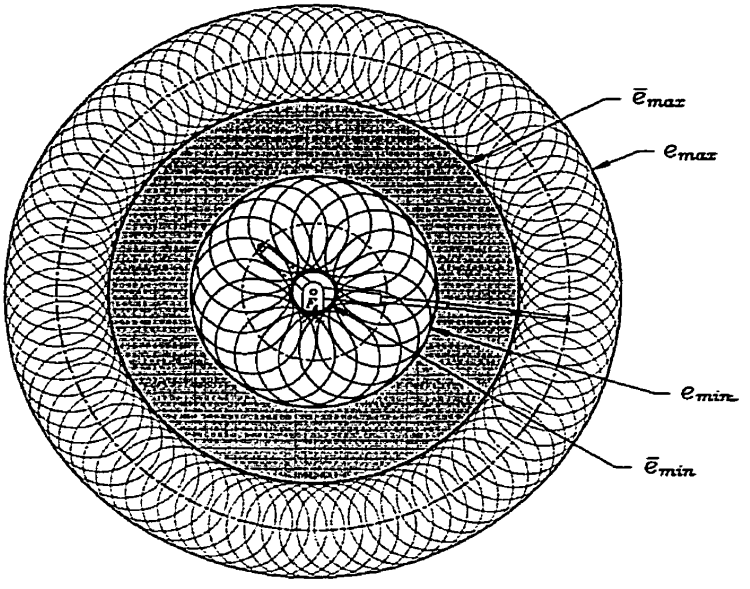

FIGURE 7.3. Pre-Image of a constraint solid for leg A.

The next step is to obtain the pre-image of the constraint solids. This is done by substituting Equation (7.1) into Equation (3.45). The pre-image depends on the platform reference point $(x : y : 1)$, which makes it relatively easy to compute different Cartesian workspaces for different points on the end-effector. Figure 7.3 shows the pre-image of the solid region bounded by the smallest hyperboloid H_{min}, determined with d_{min}, and by the largest H_{max}, corresponding to d_{max}. The envelopes of the one parameter families of circles represent the boundaries of the reachable workspace of the end-effector when the connections for legs B and C between base and platform have been removed.

For each constraint solid there are four envelops. The two belonging to $H_{i_{max}}$ are denoted by $e_{i_{max}}$ and $\bar{e}_{i_{max}}$, and those belonging to $H_{i_{min}}$ by $e_{i_{min}}$ and $\bar{e}_{i_{min}}$. To obtain a description of the workspace four cases must be distinguished:

(1) $\bar{e}_{i_{max}}$ and $\bar{e}_{i_{min}}$ both contain overlapping circles (*i.e.*, valid poses). The workspace is given by $W_i = e_{i_{max}} - e_{i_{min}}$.

(2) $\overline{e}_{i_{max}}$ consists of areas of overlapping circles, but not $\overline{e}_{i_{min}}$. The workspace is $W_i = e_{i_{max}} - (e_{i_{min}} - \overline{e}_{i_{min}})$.

(3) $\overline{e}_{i_{min}}$ consists of areas of overlapping circles, but not $\overline{e}_{i_{max}}$. The workspace is $W_i = (e_{i_{max}} - \overline{e}_{i_{min}}) - e_{i_{min}}$.

(4) Both $\overline{e}_{i_{max}}$ and $\overline{e}_{i_{min}}$ are devoid of overlapping circles. Then the workspace is $W_i = (e_{i_{max}} - \overline{e}_{i_{min}}) - (e_{i_{min}} - \overline{e}_{i_{min}})$.

The intersection of the workspaces W_i of the three legs gives the reachable workspace W:

$$W = W_A \cap W_B \cap W_C. \tag{7.2}$$

7.1.2. Dextrous Workspace. The dextrous workspace is defined by Kumar [**92**] as a set of points in the reachable workspace about which the end-effector can rotate through 360°. Husty [**80**] has shown that a necessary condition for the existence of a dextrous workspace is that the disk $\overline{D}_{i_{max}}$, which is the disk bound by $\overline{e}_{i_{max}}$, contain overlapping circles. Moreover, $\overline{D}_{i_{max}}$ should not be completely covered by any *hole* in the workspace. This condition can be expressed

$$\overline{e}_{i_{max}} \geq e_{i_{min}}. \tag{7.3}$$

Figure 7.3 is an example of a dextrous workspace for leg A. In this leg the dextrous workspace is located between $e_{i_{min}}$ and $\overline{e}_{i_{max}}$. The existence of a dextrous portion of the whole workspace depends on the intersection of the dextrous workspace of each leg.

7.1.3. *PR*- and *RP*-type Platforms. Figure 7.4 shows a $P\underline{P}R$ platform. The constraint surfaces for these, and for all PR- and RP-type platforms are hyperbolic paraboloids. The constraint solids consist of pairs of identically shaped, but displaced hyperbolic paraboloids. The left-hand side of Figure 7.5 illustrates the image

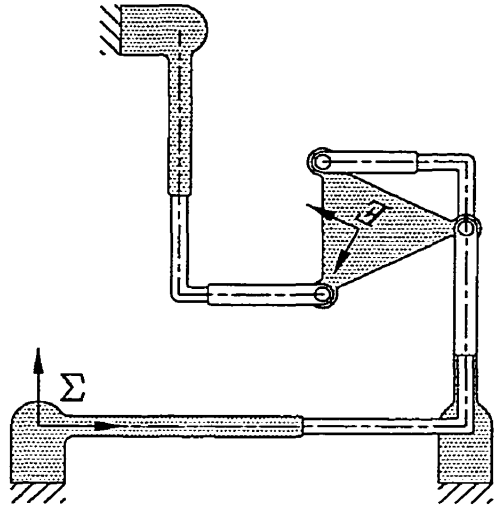

FIGURE 7.4. A $P\underline{P}R$ platform.

space solid corresponding to the reachable workspace of one leg of an $P\underline{P}R$ platform. The image of the reachable workspace is the solid bounded by the intersection of the three pairs of constraint solids representing the joint limits.

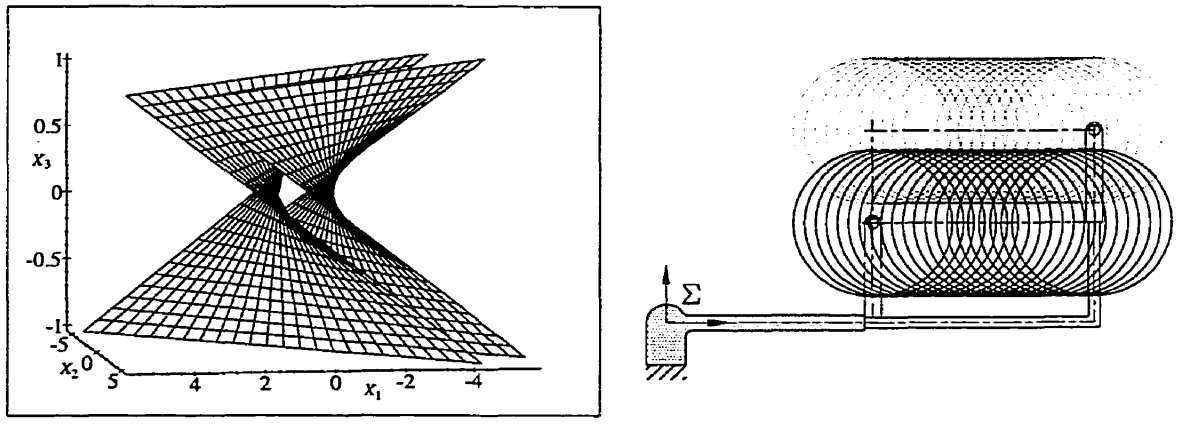

FIGURE 7.5. The kinematic image of the reachable workspace for a $P\underline{P}R$ platform and the corresponding pre-image.

The right-hand side of Figure 7.5 shows the pre-image of the solid bounded by the extreme hyperbolic paraboloids for leg A of the platform. As for the $R\underline{P}R$ platform analysed earlier, for each solid there are four envelops. To obtain a description of the workspace, the same four cases, as in Section 7.1.1, must be distinguished. Examining the four cases leads to an identical criteria for the existence of a dextrous workspace as expressed in Section 7.1.2

7.1.4. Workspace of $RR\underline{G}$ Platforms. The determination of the workspace of $RR\underline{G}$ platforms remains, essentially, an unsolved problem. It was attempted by Agrawal and Pandravada in 1993 [**4**], but the IK procedure upon which the workspace analysis is based is fraught with formulation singularities. This is because of the seemingly impossible task of modelling pinion displacements in E_2. A better approach remains elusive, but should be found in the kinematic mapping image space.

While no means of determining the constraint solid for these platforms has yet been found, it is worthwhile to study the effects of displacements on the hyperboloid axis. This is because the characterisation of the associated family of hyperboloids may be obtained by characterising the family of lines of their axes. Recall that a line in a 3D space is uniquely defined by four generalised coordinates. This means that there are ∞^4 unique lines in space.

If the line coordinates are related by one equation, then ∞^1 lines are excluded and the ∞^3 remaining lines constitute a *linear complex*[1] represented by the equation. A single equation may also represent a surface, or curve, for there are ∞^3 lines tangent to a given surface, or cutting a given curve. Such an equation is called the *line equation* of the surface or curve [**136**].

[1]The terms *complex* and *congruence*, used to indicate ∞^3 and ∞^2 systems of lines, were first introduced by Plücker in [**116**].

If the coordinates are related by two simultaneous linear equations then there are ∞^2 lines satisfying these equations, which constitute a *linear congruence* described by the set of equations. A congruence contains all congruent lines of two complexes, it may be regarded as their mutual intersection [**115**].

If three equations are simultaneously verified by the four coordinates the corresponding lines, ∞^1 in number, constitute a *ruled surface* (*Strahlenfläche* [**115**]), represented by the system of three equations. A ruled surface may be considered as the mutual intersection of three complexes, *i.e.*, as the geometric locus of lines belonging to all three complexes.

Four equations relating the four coordinates means that there are a finite number of lines, ∞^0, which satisfy the equations. In line geometric terms, such a system can be represented by the mutual intersection of four complexes, or two ruled surfaces [**116**]. Ordinarily, no line satisfies five conditions.

The parametric equation of the axis of the constraint hyperboloid for an *RR*-type leg is given by Equation (4.18), reproduced below as Equation (7.4):

$$\begin{bmatrix} X_1 \\ X_2 \\ X_3 \end{bmatrix} = \frac{1}{2}\begin{bmatrix} y - K_2 \\ K_1 - x \\ 0 \end{bmatrix} + \frac{t}{2}\begin{bmatrix} K_1 + x \\ K_2 + y \\ 2 \end{bmatrix}. \tag{7.4}$$

The radius of a circle in the plane $X_3 = \text{const.}$, Equation (4.15), is reproduced below:

$$R_{X_3} = \frac{r}{2}\sqrt{(1 + X_3^2)}, \tag{7.5}$$

where r is the constraint circle radius in E_2. In the image space plane $X_3 = 0$ this radius is simply $r/2$. Clearly, since r is the fixed length of the grounded link, the constraint hyperboloid striction curve and shape parameters are invariant under any feasible planar displacement associated with the corresponding leg.

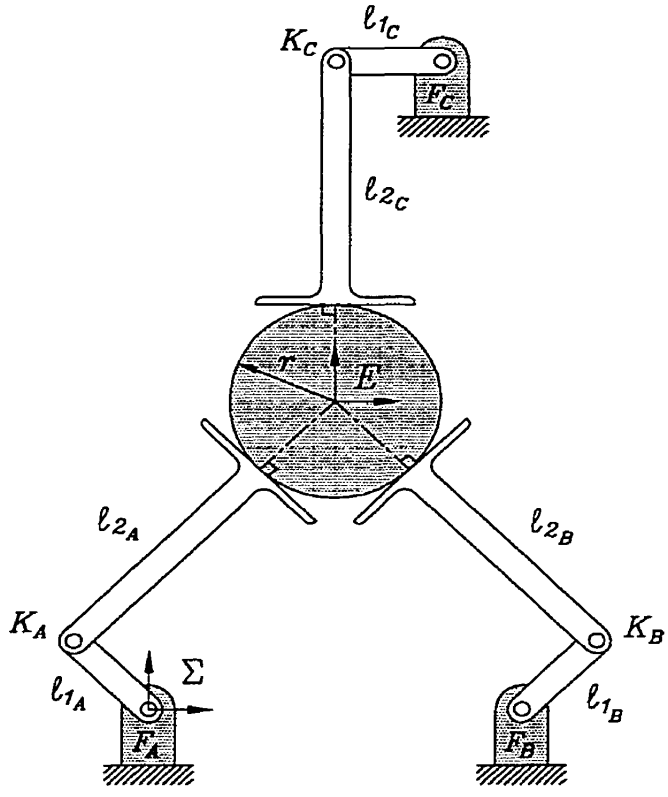

FIGURE 7.6. An $RR\underline{G}$ platform.

For the $RR\underline{G}$ platform, shown in Figure 7.6, $\mathcal{K}_1$ and $\mathcal{K}_2$ are design constants (the Cartesian coordinates for the base of the given leg expressed in the fixed frame Σ) and x and y are the knee joint locations with respect to the moving frame E, which are constants for each distinct displacement considered separately. Equation (7.4) is a representation of the line of the image circle centres in terms of parameter t: $-\infty < t < \infty$.

Let us now consider two distinct arbitrary poses of any leg of the platform. These poses are characterised by (x_1, y_1) for the first and (x_2, y_2) for the second. Let t and s be the parameters for first and second poses, respectively. Clearly, for each distinct pose the line coordinates of the axis will change. The significance of this is that the associated hyperboloids are not coaxial. Thus, the constraint solid can not be obtained as for lower pair PSGP. This is a direct result of the use of higher pair joints.

For each distinct set of rack tangent angles, the relative location of the pinion contact points change. In this sense, the platform geometry changes continuously during any motion. If the axes of the corresponding constraint hyperboloids intersect we obtain the following relation:

$$\begin{bmatrix} \mathcal{K}_2 + y_1 \\ -\mathcal{K}_1 - x_1 \\ 0 \end{bmatrix} + t \begin{bmatrix} x_1 - \mathcal{K}_1 \\ y_1 - \mathcal{K}_2 \\ 2 \end{bmatrix} = \begin{bmatrix} \mathcal{K}_2 + y_2 \\ -\mathcal{K}_1 - x_2 \\ 0 \end{bmatrix} + s \begin{bmatrix} x_2 - \mathcal{K}_1 \\ y_2 - \mathcal{K}_2 \\ 2 \end{bmatrix}. \quad (7.6)$$

These are three linearly independent equations. We see immediately from the third equations ($2t = 2s$) that a condition for the two lines to intersect is that $s = t$, *i.e.*, the point of intersection occurs when the two parameters take on identical values. From the first two equations in (7.6) we obtain after setting $s = t$:

$$t = \frac{y_2 - y_1}{x_1 - x_2} = \frac{x_1 - x_2}{y_1 - y_2}. \quad (7.7)$$

We can rearrange Equation (7.7) to read

$$-(y_1 - y_2)^2 = (x_1 - x_2)^2. \quad (7.8)$$

Clearly, there are no real values for the constants x_1, x_2, y_1, y_2 which satisfy Equation (7.8). We must conclude that all axes for a given leg are mutually skew and lie in a ruled surface. Substituting the involute inputs from Equation (5.47) into Equation (7.4) indicates that the surface is non-algebraic[2], indeed it is transcendental. Figure 7.7 shows the set of axes for a set of displacements of one leg of an $R\underline{P}R$ platform. While we have yet to determine the true nature of this surface, we are certain it is related to its associated involute.

[2]The equation of an *algebraic surface* can be reduced to a finite number of terms involving positive integer powers of its variables. If the equation contains variables that are the arguments of transcendental functions, it cannot be so expressed and is *non-algebraic*.

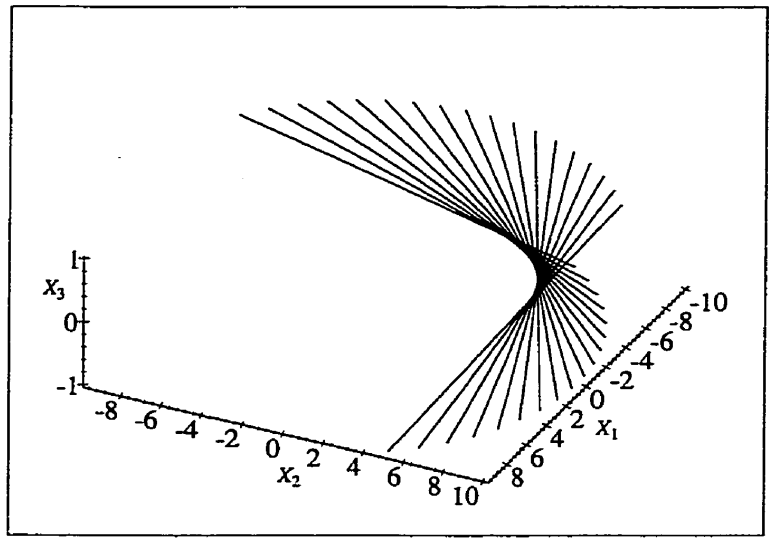

FIGURE 7.7. The set of axes for a set of displacements of one leg of an $R\underline{P}R$ platform.

7.2. Singularities

Manipulator singularities occur when different FK and/or IK solutions coincide [**49, 34**]. A singularity is defined algebraically as a rank deficiency of the associated *Jacobian*[3]. The geometric definition amounts to an instantaneous change in the DOF of the platform. That is, either one or more DOF is lost, or one or more uncontrollable DOF are gained. This means that when a platform approaches a singularity either the platform can undergo infinitesimal motions when the actuators are locked, or finite changes in the inputs produce no platform motion. Both situations are highly undesirable.

[3]The Jacobian has come to mean the matrix that maps the vector of *output rates* (*i.e.*, the time rate of change of the platforms generalised coordinates) to the vector of *input rates* (the time rate of change of the variable joint inputs).

Work in the area of singularity analysis of parallel platforms is extensive. Merlet [**96**] uses Plücker's *line geometry* (called *Grassmann geometry* by Merlet)[4] to give a comprehensive enumeration of the conditions on the position and orientation of the legs of planar and spatial SGP which lead to singular configurations of the platform. Mohamed and Duffy [**105**] classified singularities into three groups based on the nature of the rank deficiency of the Jacobian. These are *stationary configurations* where DOF are gained, *immovable structure* where DOF are lost, and *uncertainty configurations* where the Jacobian is indeterminate. Gosselin [**49**] presented a similar classification scheme. Ma and Angeles [**94**] introduced a somewhat different idea. Here they are classified as: *i*) *configuration singularity* which is an inherent manipulator property that occurs at some points within the workspace; 2) *architecture singularity*, which is caused by the manipulator architecture and can prevail over the entire workspace; 3) *formulation singularity*, caused by the failure of the kinematic model of the platform for certain configurations.

Singular assembly configurations of parallel platforms have the property that the set of joint inputs is not sufficient to define the pose. This is due to the gain, or loss of an infinitesimal, or even continuous DOF. Hartmann gives a comprehensive examination of singular SGP in [**62**]. Sefrioui and Gosselin [**131, 132**] examined the loci of singular positions in the platforms workspace for a fixed orientation. They observed that the loci are conic sections. Later, Collins and McCarthy [**26**] employed planar quaternions to obtain an algebraic, but implicit, expression of a quartic surface in a 3-D projective space that represents all singular poses of all possible $R\underline{P}R$ platforms. In the most general case, the singularity surface contains a double line at infinity. They further investigate special architectures where the quartic reduces to a quartic

[4]The subject of *line geometry* owes its origin to Plücker. Types of coordinates of the line were introduced by Cayley and Grassmann; Plücker line coordinates are a special form of these, but the discovery of line geometry itself is *entirely* Plücker's work [**87**]. So, it is appropriate to use the term coined by Plücker himself: *line geometry*.

ruled surface, two planes and an hyperboloid of one sheet, and pairs of hyperbolic paraboloids.

7.2.1. Self-Motions. Notwithstanding the LADD (linear actuation device) actuator [**86**], awareness of platforms with one (or more) DOF continuous motion while active joints are locked did not seem to exist until examples were revealed in 1994 by Husty and Zsombor-Murray [**78**]. In that paper, line geometry is used to show that when the six legs of a spatial SGP remain in a specific linear complex, congruence or hyperboloidal ruled surface then the platform will execute a finite one DOF motion while all legs remain at constant length. These motions are termed *self-motions*. Their existence was essentially identified, and classified to a certain extent, simultaneously but independently by Borel [**16**] and Bricard [**18**]. They were investigating continuous motions where some points on a rigid body are each constrained to remain on the surface of as many given fixed spheres, which is the case for spatial SGP. This was the topic of a competition conducted by L'Académie des Sciences de l'Institut National de France in 1903. The prize-winning papers were those of Borel and Bricard [**16, 18**]. Self-motions are uncontrollable in the context of P-pair actuated SGP and, one might imagine, would be most unwelcomed by pilots engaged in training exercises on board a flight simulator prone to such motions. Still, mechanisms that exhibit these motions may be useful. The LADD actuator is a good example [**86**].

Research in the area of self-motions is beginning to gain attention. See [**88, 93, 125**] for example. Nonetheless, it is unnerving that self-motions are only now being seriously considered because parallel manipulators have been commercially available since 1979 [**102**]. Moreover, there exists a patented design for a flight simulator [**55**] which has self-motions in every point of the workspace [**85**]. That means no matter how the platform is assembled with legs of given fixed length it is movable when it

is supposed to be a structure! It turns out that the associated Jacobian matrix is always rank deficient [85].

7.2.2. *RR*-Type PSGP Continuous Self-Motons. In [79], Husty shows that it is possible to construct planar RR-type platforms that exhibit self-motions in one assembly mode, but are structures in others. It is well known that two congruent rigid triangles whose corresponding vertices are joined by legs of equal fixed lengths can exhibit continuous relative motion. The relative motion is a curvilinear translation. The reason for this self-motion is that the three constraint hyperboloids all share a common circle which leads to a one parametric set of solutions. Additionally, however, this variety contains discrete solutions. Therefore, it is possible to construct platforms which are continuously movable in one assembly mode and rigid structures in others.

7.2.3. *PP*-Type PSGP Continuous Self-Motons. If the image space constraint surface corresponding to possible displacements of a PP-type leg is quadratic, it must be a degenerate quadric that splits into a real and an imaginary plane. This is because only curvilinear motion of the platform can result when the two of the platform attachment joints are disconnected. Once the angular input of the active R-pair is fixed no rotation of leg or platform is possible. Still, the image of a two parameter family of displacements must be a two parameter constraint manifold, but because φ is constant, the image space coordinates $X_3 = f(\varphi)$ and $X_4 = g(\varphi)$ must also be constant. Hence, the finite part of the two dimensional constraint manifold is linear and must be a hyper-plane.

Upon normalising the image space coordinates, by setting $X_4 = 1$, all planes corresponding to possible displacements of the PP-type leg still connected are parallel to $X_3 = 0$. There are three possibilities:

(1) All three planes are parallel and contain only one line in the plane at infinity in common. This situation represents ∞^1 solutions at infinity. The platform cannot be assembled with the given inputs.

(2) One plane is parallel to two that are incident. Again, this represents ∞^1 solutions at infinity. The platform cannot be assembled with the given inputs.

(3) All three planes are incident. This means that there are ∞^2 real solutions. The platform can be assembled, but it is free to translate when it should be a rigid structure. This type of unwanted, unexpected and uncontrollable motion is a self-motion [88].

From a line geometric perspective, these three cases mean that whenever the platform can be assembled given a set of active joint inputs the Jacobian matrix derived from the line equations for each of the three legs[5] is always rank deficient.

The inescapable conclusion is that there is no practical design merit associated with PP-type PSGP as a three DOF platform. This, however, does not preclude designs of topologically asymmetrical three legged planar platforms with at most one PP-type leg. On the other hand, the self-motion property provides possibilities to design very stiff one DOF planar platforms which are relatively easy to actuate, like the LADD actuator mentioned above.

7.2.4. Singularity Detection. Recall the rational factor in the special univariate, Equation (4.47), for PR- and RP-type platforms:

$$A_1B_2 - A_2B_1 - A_1C_2 + A_2C_1 + B_1C_2 - B_2C_1. \tag{7.9}$$

Equation (7.9) is a relation between the directions of the three lines connecting the fixed and moving platforms. It has the following geometric significance: if it equals

[5]Merlet [96] shows that the Jacobian matrix of a parallel platform in a given configuration is transpose of the matrix whose columns are the Plücker coordinates for each leg in the corresponding pose.

zero after the input joints are locked then the centre lines of the passive P-pairs form a planar linear pencil (*i.e.*, the family of all lines passing through one point in the plane). When the P-pairs are mutually parallel the apex of the pencil is at infinity. This stems from the fact that the expression is the determinant of the following homogeneous matrix

$$\begin{bmatrix} A_1 & A_2 & 1 \\ B_1 & B_2 & 1 \\ C_1 & C_2 & 1 \end{bmatrix}. \tag{7.10}$$

If the determinant of (7.10) is equal to zero, there is a linear dependence among the lines causing the rank deficiency. Either the three lines have a single point in common, or at least two are incident. If two of the directions are parallel while the leg forces exert a couple (*i.e.*, with $A_3 = B_3 = C_3 = 1$), then two of the lines are coincident and all three are still in a pencil.

The vanishing of the rational factor means the selected inputs place the platform in a singular configuration where the platform exhibits infinitesimal motions. If the pencil apex is finite the platform can resist no moment about this point and the platform experiences a transitory mobility. This means the platform can rotate about the intersection point. If the apex is at infinity, the platform can resist no force perpendicular to the direction of the passive prismatics and the platform acquires an uncontrollable translational DOF.

The above discussion suggests a simple way to detect such singularities in any planar three-legged platform, including $RR\underline{G}$ type. When active joint inputs are specified these joints may be taken to be locked. The eight links of the parallel mechanism are effectively reduced to five [**112**], two of which are the base and the moving platform. What remains are three links connecting fixed points to moving points. These three pairs of points define three lines in the plane of the platform.

Here we may, without loss in generality, call the fixed points F_i and the moving points M_i, $i \in \{A, B, C\}$, even though either the fixed or moving points may, depending on the leg architecture, be the knee joint K_i. Recall from Section 3.3 that the line coordinates for a line $\mathcal{L}$ in the plane are obtained from two points on the line. If the two points are $(x_1 : x_2 : x_3)$ and $(y_1 : y_2 : y_3)$ the line coordinates can be written as

$$\left[\begin{vmatrix} x_2 & x_3 \\ y_2 & y_3 \end{vmatrix} : \begin{vmatrix} x_3 & x_1 \\ y_3 & y_1 \end{vmatrix} : \begin{vmatrix} x_1 & x_2 \\ y_1 & y_2 \end{vmatrix} \right] = [\mathcal{L}_1 : \mathcal{L}_2 : \mathcal{L}_3].$$

The condition for the incidence of three lines, say one for each leg of the manipulator $\mathcal{L}_i$, can be expressed as

$$\begin{vmatrix} \mathcal{L}_{1_A} & \mathcal{L}_{2_A} & \mathcal{L}_{3_A} \\ \mathcal{L}_{1_B} & \mathcal{L}_{2_B} & \mathcal{L}_{3_B} \\ \mathcal{L}_{1_C} & \mathcal{L}_{2_C} & \mathcal{L}_{3_C} \end{vmatrix} = 0.$$

The vanishing of this determinant represents exactly the singularity given by the vanishing of Equation (7.9). The line geometric explanation is that the three lines lie in a planar linear pencil. It is worthwhile pointing out that these singularities are determined without calculating the Jacobian.

7.2.5. Singularity Quantification. The workspace of a given three-legged planar platform is likely to contain some points where the platform will be in the singular configuration described above. It is always of interest to know the proximity to these locations for trajectory and path planning tasks. A simple means to quantify this proximity is to compare the area of the triangle enclosed by the $\mathcal{L}_i$ lines on the vertices $V_i = \mathcal{L}_{i+1} \cap \mathcal{L}_{i+2}$, $i \in \{A = 1, B = 2, C = 3\}$ [**35**] with the average area of the fixed and moving triangles. The ratio A/A_{ave}, or its reciprocal can be used. The point coordinates of the V_i, indicated by $(v_{1_i} : v_{2_i} : v_{3_i})$, are obtained by expanding

the singular determinant representing three lines that intersect on the same point:

$$\begin{vmatrix} \mathcal{L}_1 & \mathcal{L}_2 & \mathcal{L}_3 \\ \mathcal{L}_{1_{i+1}} & \mathcal{L}_{2_{i+1}} & \mathcal{L}_{3_{i+1}} \\ \mathcal{L}_{1_{i+2}} & \mathcal{L}_{2_{i+2}} & \mathcal{L}_{3_{i+2}} \end{vmatrix} = 0.$$

This gives the following point coordinates:

$$\left(\begin{vmatrix} \mathcal{L}_{2_{i+1}} & \mathcal{L}_{3_{i+1}} \\ \mathcal{L}_{2_{i+2}} & \mathcal{L}_{3_{i+2}} \end{vmatrix} : \begin{vmatrix} \mathcal{L}_{3_{i+1}} & \mathcal{L}_{2_{i+1}} \\ \mathcal{L}_{3_{i+2}} & \mathcal{L}_{2_{i+2}} \end{vmatrix} : \begin{vmatrix} \mathcal{L}_{1_{i+1}} & \mathcal{L}_{2_{i+1}} \\ \mathcal{L}_{1_{i+2}} & \mathcal{L}_{2_{i+2}} \end{vmatrix} \right) = (v_{1_i} : v_{2_i} : v_{3_i}).$$

The area A of triangle V_A, V_B, V_C is given by the *Grassmannian volume* [**90**]

$$A = \frac{1}{2v_{1_A}v_{1_B}v_{1_C}} \begin{vmatrix} v_{1_A} & v_{2_A} & v_{3_A} \\ v_{1_B} & v_{2_B} & v_{3_B} \\ v_{1_C} & v_{2_C} & v_{3_C} \end{vmatrix}. \tag{7.11}$$

When A vanishes the legs are in a pencil, however when A becomes infinite the legs are parallel and are still in a pencil, but the apex is on the line at infinity. Figure 7.8 illustrates three possible singular configurations of $\underline{R}RR$ platforms. As a performance indicator, an extremely small area ratio mean the configuration is *close* to singular, but so does an extremely large area ratio.

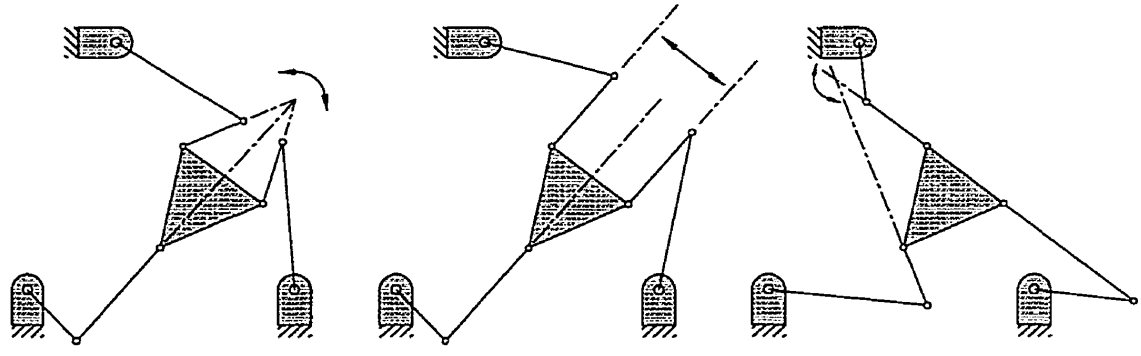

(i) *(ii)* *(iii)*

FIGURE 7.8. Three possible $\underline{R}RR$ platform singular configurations.

CHAPTER 8

Concluding Remarks

8.1. Conclusions

This thesis has presented a kinematic analysis of planar three-legged platforms in general, and PSGP in particular. This analysis involved the use of a kinematic mapping procedure to derive a univariate polynomial that can be applied to the FK problem of every PSGP. The univariate can also be applied to topologically asymmetric platforms provided the legs are all of one of three types: *RR*-, *PR*-, or *RP*-type. Furthermore, it can be used to solve the FK of PSGP-type manipulators with active holonomic higher pairs.

As a prelude to the study, a classification of planar three-legged platforms was reviewed, and PSGP were defined in that context. The holonomic higher pair architecture was detailed and special geometric properties were given. A detailed mobility analysis was performed.

Relevant geometric and algebraic tools and concepts were reviewed. Next, various representations of displacements were discussed, leading to derivations of the kinematic mapping employed in the subsequent kinematic analysis.

The application of kinematic mapping to the FK problem was then examined. First, the relevant kinematic constraints for RR-, PR- and RP-type platforms were described in the displacement space. Next, the images of these constraints in the kinematic mapping image space were examined and classified as either hyperboloids of one sheet, or hyperbolic paraboloids. The hyperboloids all contain the imaginary points $J_1(1 : -i : 0 : 0)$ and $J_2(1 : i : 0 : 0)$, while the hyperbolic paraboloids all have the the intersection of the hyper-planes $X_3 = 0$ and $X_4 = 0$, $(X_1 : X_2 : 0 : 0)$, as a common generator. The variety of the polynomial representation of three such image space quadrics leads directly to the univariate. It is obtained after eliminating two image space coordinates from three simultaneous constraint surface equations. The roots of the univariate yield all solutions to the given FK problem. Because the coefficients are determined symbolically, not numerically, the effects of design constants and joint inputs on solutions are immediately quantifiable. The upper bounds on the number of solutions to the FK problem were rationalised in terms of image space and Cartesian space representations of the relevant kinematic constraints.

Use of the univariate is limited to RR-, PR- and RP-type architectures. However, the FK problem of any 3-legged planar fully-parallel platform with 3 DOF, including those with active holonomic higher pairs, but excluding those with PR- and RP-type mixed legs, can be solved by solving three simultaneous quadric equations. There are 468 PR-RP-type mixed leg three DOF planar platforms jointed exclusively with R- and P-pairs. The FK of the remaining 672 lower-pair jointed planar platforms are solvable either by direct application of the univariate, or by locating the intersection points of the 3 constraint surfaces.

Not discussed were the possible platforms containing one PP-type leg. These are 513 in number. Such platforms would seem to be problematic from a design perspective, nonetheless, their inclusion beings the complete set of planar 3-legged

lower-pair platforms with 3 DOF to 1653. It would be ideal to reformulate the problem such that the FK problem of all 1653 platforms could be solved with a single univariate.

The IK problem for PSGP was detailed. Closed form solutions are obtained from the pre-image of points in the image space representing feasible displacements. Then a simple variation of the procedure was given for PSGP-type manipulators with holonomic higher pairs. This procedure, unlike the one in [**63**], yields all feasible solutions without generating spurious ones.

Finally, Husty's investigation of the workspace space analysis for $R\underline{P}R$ platforms was generalised to include all PSGP. This generalisation includes a simple criteria to test for the existence of a dextrous workspace. Additionally, some observations on the workspace analysis of PSGP-type manipulators with holonomic higher pairs using the kinematic mapping image space were discussed. Lastly, a simple test for self motions, and quantification of these singularities was proposed.

8.2. Suggestions for Future Research

Kinematic mapping is a valuable visualisation tool for complex problems in planar and spatial kinematics. It has proven to be useful in our solution procedure for the FK and IK problem of PSGP, as well as for workspace and singularity analysis. Clearly, it has potential as a mainstream tool in the formulation of manipulator control and analysis algorithms. It has not yet acquired wide acceptance because it is rooted in 19^{th} century geometry. Geometry is generally ignored in secondary, post-secondary, and advanced education curricula throughout most of the world. It still maintains a tenuous grip in central Europe, but this too is slipping. Solutions to current research problems in robot kinematics were solved by geometers of the 19^{th} century. For example, at the beginning of this century Borel [**16**] and Bricard [**18**] predicted self

motions of SGP. This type of singularity remained essentially hidden until 1994, when it was rediscovered by Husty and Zsombor-Murray [**78**]. The lesson is that a thorough understanding of geometry combined with some algebraic skill is required to understand and solve a broad range of kinematics problems. Skill at algebraic manipulation of symbols is not enough. Indeed, there exists an inverse relationship between the complexity of geometric and algebraic formulations of the same problem [**27**].

Having said that, what remains to complete the kinematic analysis of planar three-legged platforms is to formulate the FK problem in such a way that one symbolic univariate polynomial can be used to obtain solutions for all architectures. This univariate is likely to be found hiding somewhere in the kinematic image space. The same unified approach may also be brought to bear upon workspace and singularity analysis. Additionally, variations of the PSGP with holonomic higher pairs should be investigated. For example, it may be fruitful to examine $RP\underline{G}$, $\underline{R}RG$, or any of the three GGG architectures. Moreover, lower and higher pair mixed leg platforms, if feasible, are probably worth investigation.

APPENDIX A

FK Examples

In what follows several examples illustrating how to apply the univariate to the FK problem are examined in detail. They include procedures for regular PSGP, mixed leg, and $RR\underline{G}$-type platforms. The first two $R\underline{P}R$ examples demonstrate that the univariate exactly reproduces published results, thereby verifying the univariate polynomial algorithm.

A.1. Husty $R\underline{P}R$ Example

This example is taken from [**79**]. The base geometry and variable joint inputs listed in Table A.1, are used to compute the corresponding circle parameters. These $\mathcal{K}_i$ and R_i, needed to compute the univariate coefficients, are determined with the appropriate relations found in Table 5.1.

i	$F_{i/\Sigma}$	$M_{i/E}$	$r_i = d_{2_i}$	$(\mathcal{K}_{0_i} : \mathcal{K}_{1_i} : \mathcal{K}_{2_i} : \mathcal{K}_{3_i})$	R_i
A	$(0:0:1)$	$(0:0:1)$	1	$(1:0:0:-1)$	-1
B	$(3:0:1)$	$(2:0:1)$	2	$(1:3:0:5)$	9
C	$(1:3:1)$	$(1:2:1)$	2	$(1:1:3:6)$	11

TABLE A.1. Husty $R\underline{P}R$ geometry, joint inputs and circle parameters.

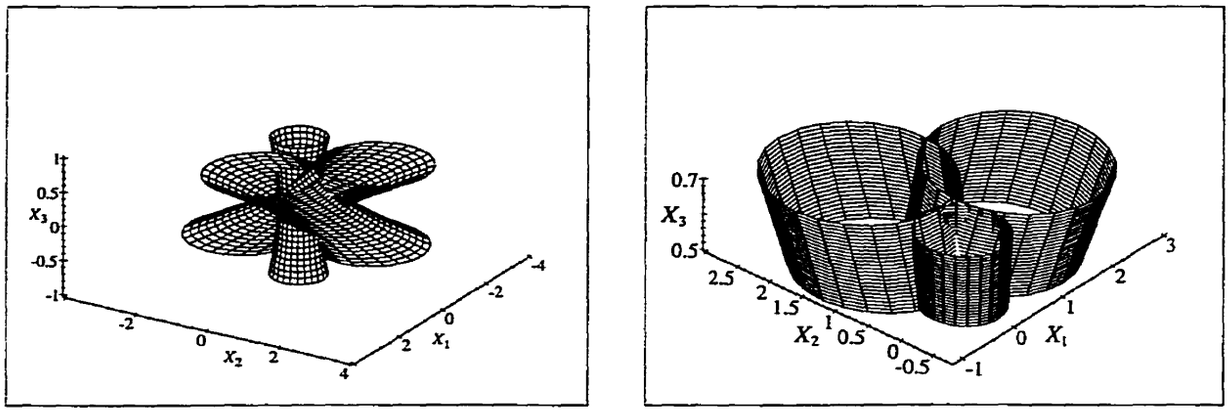

FIGURE A.1. The three constraint hyperboloids for the Husty *RPR* example where $-1 \leq t \leq 1$ and $0.5 \leq t \leq 0.7$, respectively.

Substituting these data into the equation for the general univariate yields the following:

$$4249X_3^6 - 1244X_3^5 - 1097X_3^4 + 200X_3^3 - 65X_3^2 + 4X_3 + 1 \;=\; 0. \qquad \text{(A.1)}$$

This equation has six distinct roots:

$$\begin{aligned}
(X_3)_1 &= -0.5120, \\
(X_3)_2 &= -0.0858, \\
(X_3)_3 &= 0.1608, \\
(X_3)_4 &= 0.6345, \\
(X_3)_5 &= 0.0476 + 0.2241i, \\
(X_3)_6 &= 0.0476 - 0.2241i.
\end{aligned} \qquad \text{(A.2)}$$

Back substitution of the four real solutions listed in Equations (A.2) into Equation

Solution	a	b	φ (deg.)
1	-0.0690	0.9976	-54.2255
2	-0.6290	-0.7773	-9.8079
3	-0.8916	-0.4529	18.2719
4	0.9829	-0.1841	64.7929

TABLE A.2. Husty $\underline{RP}R$: four real solutions.

(4.44) and Equation (4.45) gives two equations linear in X_1 and X_2. The values of X_1, X_2 and X_3, together with the unit homogenising coordinate, $X_4 = 1$, are the image of the FK solutions projected into the hyperplane $X_4 = 1$. The three constraint hyperboloids, each generated with Equation (4.22), are shown in Figure A.1. Two views of the three hyperboloids are shown, in the first $-1 \leq t \leq 1$ and in the second $-0.1 \leq t \leq 0.1$, respectively.

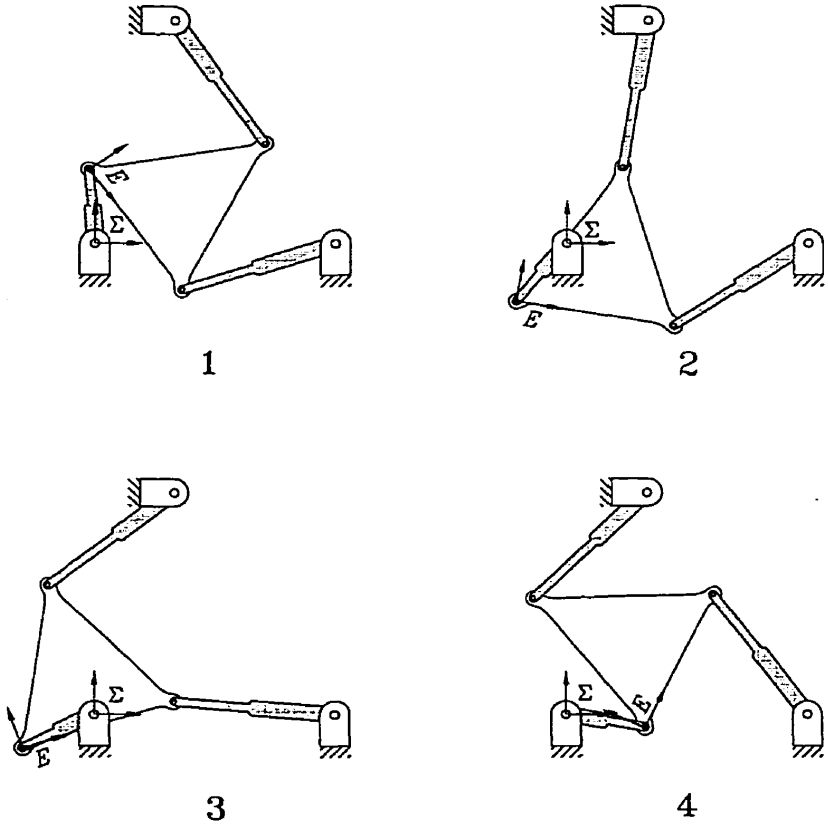

FIGURE A.2. The four real solutions for the Husty $\underline{RP}R$ example.

The preimages are found by repeated application of Equation (3.45). The four real solutions, *i.e.*, platform poses, are listed in Table A.2, and graphically illustrated in Figure A.2.

These results agree exactly with those in [**79**]. But, exactly the same equations are used to obtain the univariate, and hence agreement of the solutions is not a convincing validation of the procedure. For this reason, the next example is used because the methods for deriving the univariate are completely different.

A.2. Gosselin-Sefrioui $\boldsymbol{R\underline{P}R}$ Example

This example is taken from [**50**]. The kinematic parameters and links lengths from that example are used to extract the geometry data listed in Table A.3, while the circle parameters are determined with the appropriate relations found in Table 5.1.

i	$F_{i_{/\Sigma}}$	$M_{i_{/E}}$	$r_i = d_{2_i}$	$(\mathcal{K}_{0_i} : \mathcal{K}_{1_i} : \mathcal{K}_{2_i} : \mathcal{K}_{3_i})$	R_i
A	$(0:0:1)$	$(0:0:1)$	14.98	(1:0:0:-224.4004)	-224.4004
B	$(15.91:0:1)$	$(17.04:0:1)$	15.38	(1:15.91:0:16.58)	305.9238
C	$(0:10:1)$	$(13.24:16.10:1)$	12	(1:0:10:-44)	390.5076

TABLE A.3. Gosselin-Sefrioui $R\underline{P}R$ geometry, joint inputs & circle parameters.

Substituting these data into the equation for the general univariate gives:

$$1977.1359X_3^6 - 4401.4063X_3^5 + 948.1187X_3^4 + 1186.2945X_3^3 - 443.8786X_3^2 + 28.5790X_3 + 1 = 0. \quad \text{(A.3)}$$

The six distinct real roots are

$$\begin{aligned}
(X_3)_1 &= -0.5393, \\
(X_3)_2 &= -0.0248, \\
(X_3)_3 &= 0.1274, \\
(X_3)_4 &= 0.2977, \\
(X_3)_5 &= 0.5487, \\
(X_3)_6 &= 1.8164.
\end{aligned} \tag{A.4}$$

The preimages of the corresponding image points are found by repeated application of Equation (3.45). The six real solutions to the posed FK problem are listed in Table A.4. These solutions are in exact agreement with those reported in [**50**]. This represents a stronger validation for the procedure used here because the equations, and indeed the geometry, used are different from those used in [**50**].

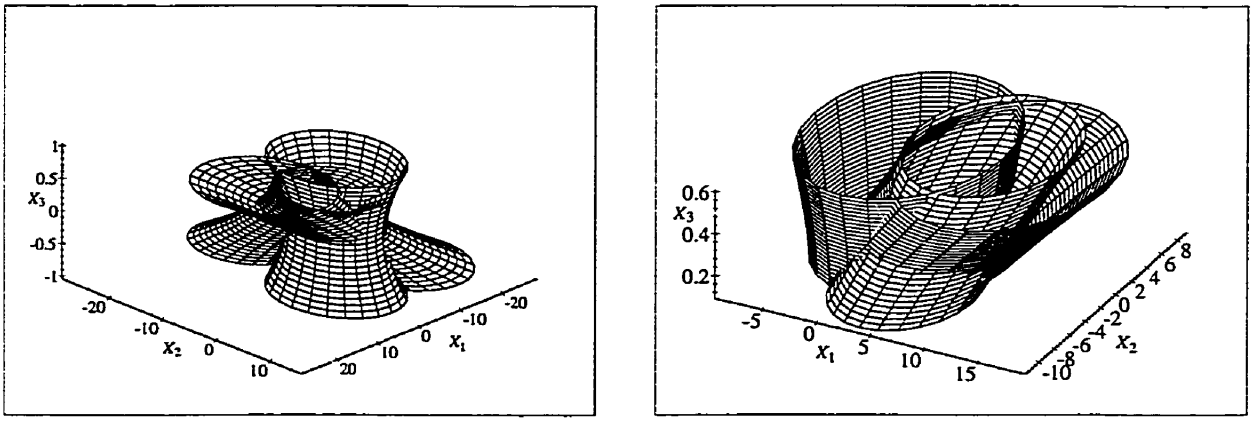

FIGURE A.3. The three constraint hyperboloids for the Gosselin-Sefrioui *RPR* example where $-1 \leq t \leq 1$ and $0.1 \leq t \leq 0.6$, respectively.

Solution	a	b	φ (deg.)
1	-8.7267	12.1756	-56.6729
2	-5.5442	-13.9163	-2.8424
3	-14.9136	1.4088	14.5208
4	-13.5050	-6.4820	33.1579
5	14.9234	-1.3011	57.5090
6	14.6830	-2.9682	122.3308

TABLE A.4. Gosselin-Sefrioui $R\underline{P}R$: six real solutions.

A.3. $\underline{R}RR$ Example

Without loss in generality, design parameters can be assigned to an $\underline{R}RR$ platform such that for one set of joint inputs the VB, defined by the inputs, has the same geometry as the base of the $R\underline{P}R$ platform in the Husty example. The intermediate links and the platform are dimensionally identical to those from the example. In this case the solutions to the FK problem, expressed in the VB frame, are identical to those from the example. This being the case, the constraint hyperboloids are also identical.

Therefore, the base geometry and base-fixed R-pair inputs are arbitrary, but must determine VBP identical to the F_i in the Husty example. The result is a platform with the design parameters and joint input angles listed in Table A.5.

i	$F_{i/\Sigma}$	$M_{i/E}$	ℓ_{1_i}	ℓ_{2_i}	ι	$\iota_{1/\Sigma}$ deg.
A	(0:0:1)	(0:0:1)	2	1	α	0
B	(6:0:1)	(2:0:1)	2	2	β	133.4325
C	(3:5:1)	(1:2:0)	2.4624	2	γ	230.1652

TABLE A.5. $\underline{R}RR$ geometry and joint input angles.

Solution	a	b	φ (deg.)
1	1.4567	0.8395	-25.2705
2	1.8260	-0.9847	19.1471
3	1.4391	-0.8279	47.2269
4	2.9492	0.3148	93.7479

TABLE A.6. $\underline{R}RR$: four real solutions.

This example is easily solved using the procedure described for $\underline{R}RR$ platforms in Chapter 5. However, we already know the solutions with respect to the VB frame; these are listed in Table A.2. What remains is to transform these solutions to the base frame, Σ. This is accomplished using Equation (5.17) and Equation (5.18). The solutions are enumerated in Table A.6 and illustrated in Figure A.4.

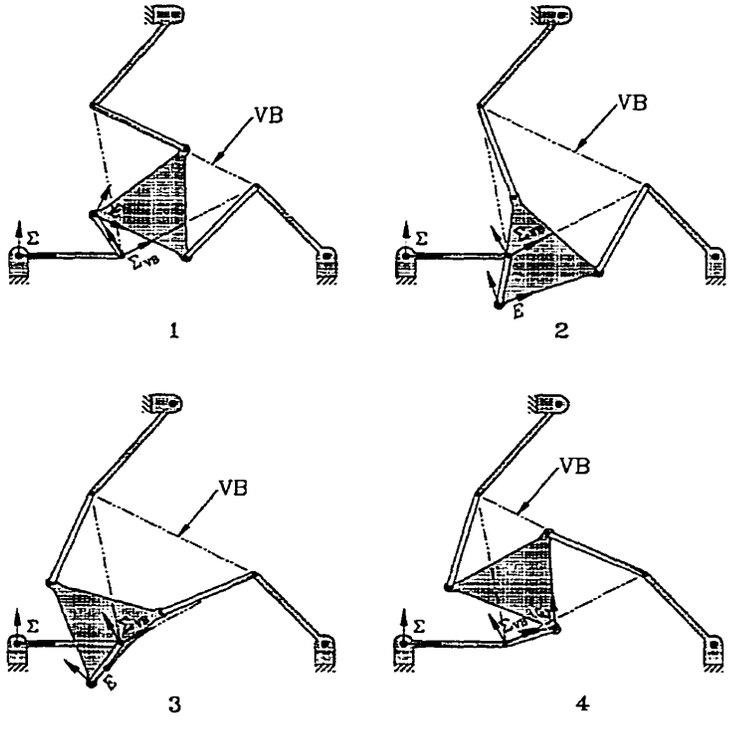

FIGURE A.4. The four real solutions for the $\underline{R}RR$ example.

A.4. $RR\underline{R}$ Example

In this example the platform geometry and fixed lengths of the platform-attached links and platform-fixed R-pair inputs are all selected so the resulting VP is dimensionally identical to the platform in the Husty $R\underline{P}R$ example. Moreover, the fixed base points and the fixed lengths of the base-attached links are identical to the same example. Thus, the base and platform geometry, link lengths, and inputs are listed in Table A.7

i	$F_{i/\Sigma}$	$M_{i/E}$	ℓ_{1_i}	ℓ_{2_i}	ι	$\iota_{2_{/E}}$ deg.
A	(0:0:1)	(0:0:1)	1	$\sqrt{13/16}$	α	213.6901
B	(3:0:1)	(1/2:0:1)	2	$\sqrt{13/16}$	β	326.3099
C	(1:3:1)	(1/4:1/2:1)	2	1	γ	90

TABLE A.7. $RR\underline{R}$ geometry and joint input angles.

The example can be solved with the procedure described for $RR\underline{R}$ platforms in Chapter 5. However, the poses of the VP frame, E_{VP}, are already known, and listed in Table A.2. What remains is to transform these solutions to give the pose of the platform frame E. This task is accomplished using Equation (5.19) and (5.40). Note, because the orientation of E_{VP} was contrived to be identical to E the orientations of the platform in this example agree exactly with the ones in the Husty $R\underline{P}R$ example. The four solutions are illustrated in Figure A.5.

Solution	a	b	φ (deg.)
1	0.6810	1.4976	-54.2255
2	0.1209	-0.2773	-9.8079
3	-0.1416	0.0471	18.2719
4	1.7329	0.3159	64.7929

TABLE A.8. $RR\underline{R}$: four real solutions.

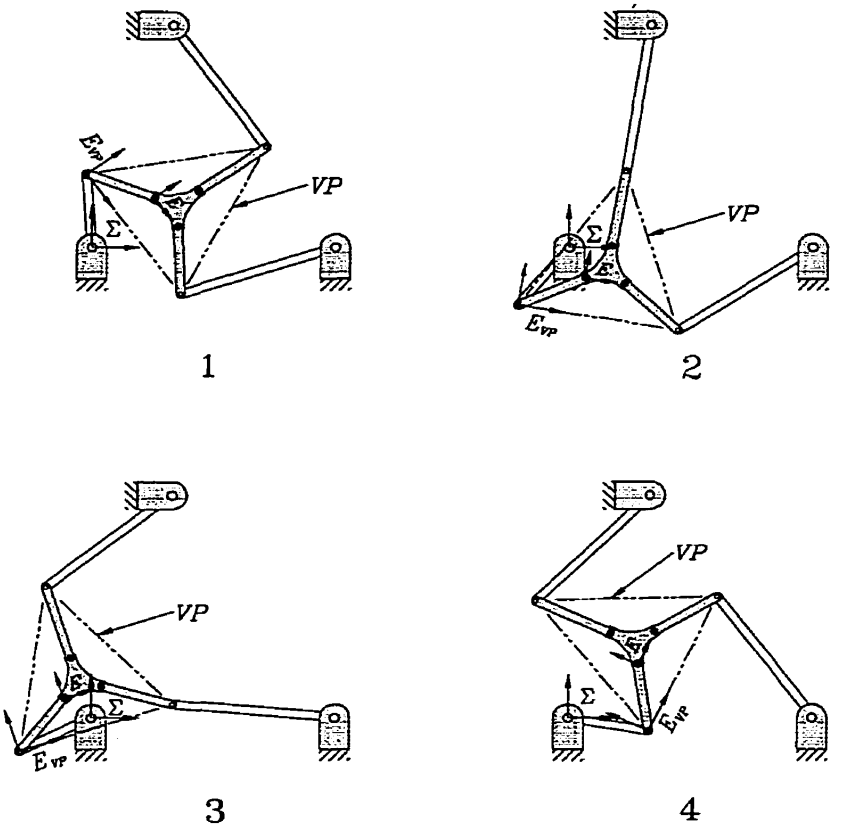

FIGURE A.5. The four real solutions for the $RR\underline{R}$ example.

A.5. $PP\underline{P}R$ Example

This example illustrates the use of the VL procedure. Here the fixed link angles were selected for convenience. The known design constants and P-pair inputs are listed in Table A.9.

i	$F_{i/\Sigma}$	$M_{i/E}$	d_{2_i}	ι	$\iota_{1_{/\Sigma}}$ deg.	$\iota_{2_{/1}}$	$\iota_{2_{/\Sigma}}$
A	(0:0:1)	(0:0:1)	3/2	α	0	90	90
B	(3:0:1)	$(\frac{\sqrt{5}}{2} : 0 : 1)$	1	β	90	90	180
C	(1:3:1)	$(\frac{3\sqrt{5}}{10} : \frac{2\sqrt{5}}{5} : 1)$	1	γ	270	90	0

TABLE A.9. $PP\underline{P}R$ geometry and joint input angles.

We proceed with the computations described for *PPR* platforms in Chapter 5. The circle coordinates are computed using Equation (5.13). Then, using these coordinates together with the M_i in Table A.9 the univariate coefficients are evaluated. The three hyperbolic paraboloids are illustrated in Figure A.6, showing one of the intersections.

Note that because the VL is used the coordinate $\mathcal{K}_{3_A}$ is, in general, not zero. Thus the 30 term univariate for *PR*-type platforms must be used. For this example the univariate takes the satisfying form:

$$X_3^2 - 4X_3 - 1 \;=\; 0.$$

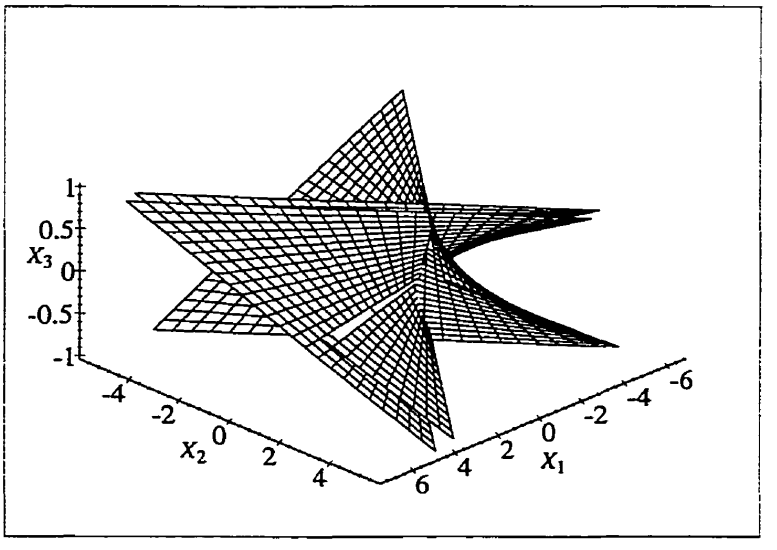

FIGURE A.6. A projection of the hyperbolic paraboloids where $-1 \leq t \leq 1$ and $-10 \leq s \leq 10$.

The preimage of the solutions the roots of this quadratic are the two real solutions listed in Table A.10.

Solution	a	b	φ (deg.)
1	1	1.5	-26.5651
2	3	1.5	153.4349

TABLE A.10. *PPR*: two real solutions.

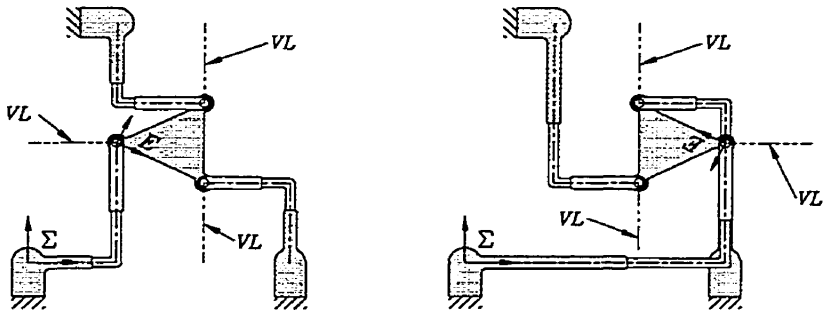

FIGURE A.7. The two real solutions for the *PPR* example.

A.6. *RPR* Example

This example is also based on the Husty *RPR* example presented earlier. Here, the inputs are based on solution 4 from that example. The procedure requires that Σ moves relative to E. Thus, the moving points are the F_i, while the fixed ones are the M_i. The variable joint inputs are the platform-fixed revolute angles, $\iota_{2/E}$. The circle coordinates are computed as

$$\begin{aligned}
\mathcal{K}_{0_i} &= 0, \\
\mathcal{K}_{1_i} &= \frac{1}{2} M_{z_i} \sin \iota_{2/E}, \\
\mathcal{K}_{2_i} &= -\frac{1}{2} M_{z_i} \cos \iota_{2/E}, \\
\mathcal{K}_{3_i} &= M_{x_i/E} \sin \iota_{2/E} - M_{y_i/E} \cos \iota_{2/E}.
\end{aligned}$$

The platform geometry, joint inputs and circle coordinates are given in Table A.11.

i	$F_{i/\Sigma}$	$M_{i/E}$	$\iota_{2/E}$ deg.	$(\mathcal{K}_{1_i} : \mathcal{K}_{2_i} : \mathcal{K}_{3_i})$
A	$(0:0:1)$	$(0:0:1)$	104.5980	$(0.4839 : 0.1260 : 0)$
B	$(3:0:1)$	$(2:0:1)$	240.8446	$(-0.4367 : 0.2436 : -1.7466)$
C	$(1:3:1)$	$(1:2:1)$	-19.2499	$(-0.1648 : -0.4720 : -2.2179)$

TABLE A.11. *RPR* geometry, joint inputs and circle parameters.

The data in Table A.11 determine the three image space constraint hyperbolic paraboloids. A projection of the three surfaces is illustrated in Figure A.8, which shows one of the intersection points. Substituting these data into the univariate

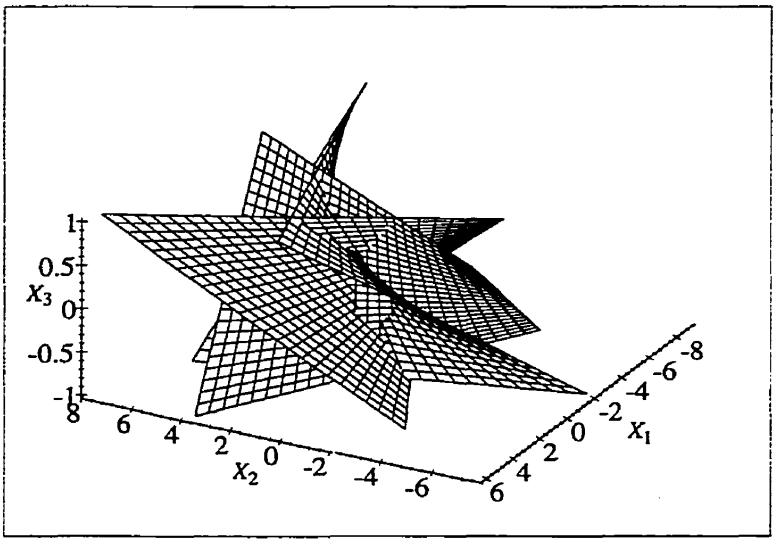

FIGURE A.8. A projection of the hyperbolic paraboloids where $-1 \leq t \leq 1$ and $-10 \leq s \leq 10$.

equation gives the following quadratic:

$$184.3861X_3^2 + 62.9298X_3 - 34.5792 \;=\; 0. \tag{A.5}$$

The roots of Equation (A.5) yield the pose of Σ with respect to E. These solutions are transformed, using Equation (5.8), to give the pose of E in Σ. Both sets of solutions are listed in Table A.12.

Solution	1	2	Solution	1	2
$a_{\Sigma/E}$	-0.2520	0.1248	$a_{E/\Sigma}$	0.9829	0.1559
$b_{\Sigma/E}$	0.9677	0.4793	$b_{E/\Sigma}$	-0.1841	0.4701
$\varphi_{\Sigma/E}$ (deg.)	-64.7929	32.9385	$\varphi_{E/\Sigma}$ (deg.)	64.7929	-32.9385

TABLE A.12. $RP\underline{R}$ FK solutions.

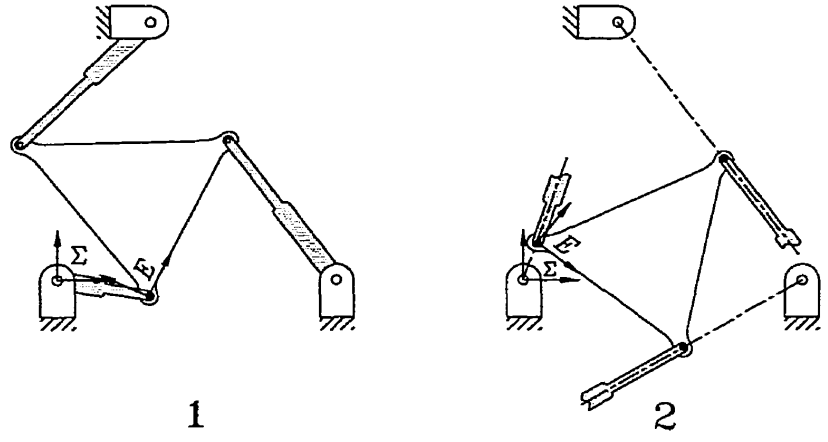

FIGURE A.9. The two real solutions for the $RP\underline{R}$ example.

Figure A.9 illustrates the two real solutions for this example. Clearly, solution 2 is not realizable. While the base points are on their respective lines, they violate the joint limits in that for the given input angles the solutions require the base points to be on the portion of the line unreachable by the prismatic joint. This illustrates that this procedure requires some extra verification that solutions are realizable.

A.7. *PR*-Type Mixed Leg Example

Mixed leg platforms are analysed using the same variety of procedures summarised in Tables 5.8, 5.9 and 5.10, however procedures can differ from leg to leg.

As mentioned earlier, platform legs must all belong to one of the three types. In the following example leg A is $\underline{R}PR$, leg B is $\underline{P}PR$, and leg C is $PR\underline{P}$, all belonging to the PR-type.

The base and platform points are listed in Table A.13, the fixed link angles in Table A.14, while the active joint inputs are in Table A.15.

i	$F_{i/\Sigma}$	$M_{i/E}$
A	(0:0:1)	(0:0:1)
B	(3:0:1)	(2:0:1)
C	(1:3:1)	(1:2:0)

TABLE A.13. Mixed PR-type leg base and platform points.

Angle	deg.
$\beta_{1_{/\Sigma}}$	225
$\beta_{2/1}$	225
$\gamma_{1_{/\Sigma}}$	350
$\gamma_{2_{/E}}$	120

TABLE A.14. Mixed PR-type leg fixed link angles.

Joint input	Value
$\alpha_{1_{/\Sigma}}$	67.5107 deg.
d_{1_B}	1.9083
d_{2_C}	1.2003

TABLE A.15. Mixed PR-type leg active joint inputs.

Consulting Table 5.9 the regular procedure can be used by leg A, the virtual base is required by leg B, and the virtual platform by leg C. The platform is illustrated in Figure A.10, showing the fixed joint angles together with the virtual components. Note that the architecture simplifies computations by virtue of the fact that the platform and VP frames, E and E_{VP}, are coincident. Meanwhile, the origins of Σ and Σ_{VB} are coincident, but the basis directions are different.

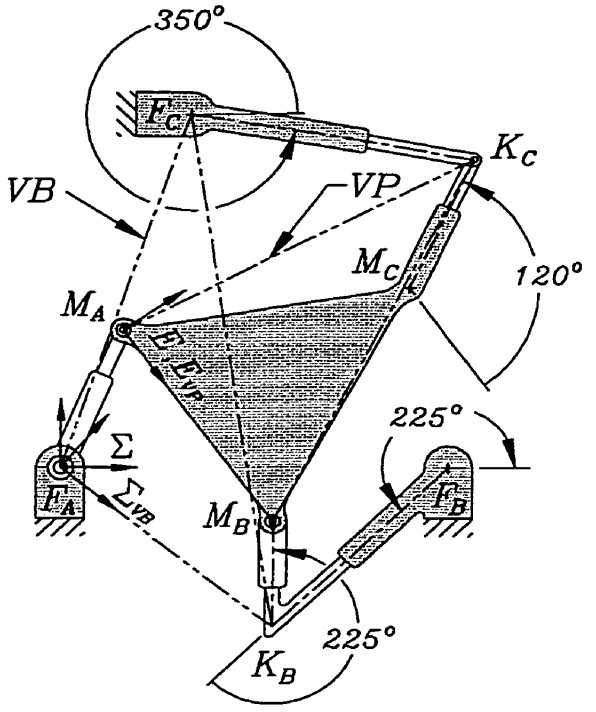

FIGURE A.10. The mixed *PR*-type leg platform.

Examining Figure A.10, one sees the vertices of the VB are the points F_A, K_B and F_C, while the vertices of the VP are M_A, M_B and K_C. Determining the orientation of $\vartheta_{\Sigma_{VB}/\Sigma}$ requires some additional observation. Equation (5.14) and (5.15) can not be used outright as the length d_{2_A} is not known *a priori*. However, this quantity is the distance between O_Σ and $O_{\Sigma_{VB}}$. Since the origins are coincident, this length vanishes, and Equation (5.14) is rewritten as Equation (A.6)

$$\overrightarrow{F_A K_B} = \overrightarrow{F_A F_B} + \overrightarrow{F_B K_B}, \tag{A.6}$$

while Equation (5.15) becomes Equation (A.7)

$$\vartheta_{\Sigma_{VB}/\Sigma} = \text{atan2}(y, x), \tag{A.7}$$

where

$$\begin{aligned} x &= F_{B_{x/\Sigma}} + d_{1_B} \cos \beta_{1/\Sigma}, \\ y &= d_{1_B} \sin \beta_{1/\Sigma}. \end{aligned}$$

Using the data from Tables A.14 and A.15 we obtain

$$\vartheta_{\Sigma_{VB}/\Sigma} = 320.7343 \text{ (deg.)}.$$

The next step is to compute the circle coordinates and VPP required to evaluate the univariate coefficients. For leg A we have

$$\mathcal{K}_{0_A} = 0, \tag{A.8}$$

$$\mathcal{K}_{1_A} = \frac{1}{2} \sin \alpha_{1_{/\Sigma_{VB}}}, \tag{A.9}$$

$$\mathcal{K}_{2_A} = -\frac{1}{2} \cos \alpha_{1_{/\Sigma_{VB}}}, \tag{A.10}$$

$$\mathcal{K}_{3_A} = 0, \tag{A.11}$$

where

$$\alpha_{1_{/\Sigma_{VB}}} = \alpha_{1_{/\Sigma}} - \vartheta_{\Sigma_{VB}/\Sigma} = 106.7764 \text{ (deg.)}. \tag{A.12}$$

For leg B the coordinates of $K_{B/\Sigma_{VB}}$ are required. First, $K_{B/\Sigma}$ are computed from the given inputs and design constants. These are transformed to $K_{B/\Sigma_{VB}}$ with Equation (5.16). Then the circle coordinates can be evaluated with

$$\mathcal{K}_{0_B} = 0, \tag{A.13}$$

$$\mathcal{K}_{1_B} = \frac{1}{2} \sin \beta_{2_{/\Sigma_{VB}}}, \tag{A.14}$$

$$\mathcal{K}_{2_B} = -\frac{1}{2} \cos \beta_{2_{/\Sigma_{VB}}}, \tag{A.15}$$

$$\mathcal{K}_{3_B} = K_{x_{B/\Sigma_{VB}}} \sin \beta_{2_{/\Sigma_{VB}}}, \tag{A.16}$$

where

$$\beta_{2_{/\Sigma_{VB}}} = \beta_{2_{/\Sigma}} - \vartheta_{\Sigma_{VB}/\Sigma} = 129.2657 \text{ (deg.)}. \tag{A.17}$$

For leg C the coordinates of $F_{C/\Sigma_{VB}}$ are needed. We simply transform $F_{C/\Sigma}$ with the transformation matrix from Equation (5.16). The coordinates of $K_{C/E_{VP}}$ must also be determined. But, because of the coincidence of E and E_{VP}, these coordinates are obtained directly from the input for leg C and the fixed angle $\gamma_{2/E}$. Then,

$$\mathcal{K}_{0_C} = 0, \tag{A.18}$$

$$\mathcal{K}_{1_C} = \frac{1}{2}\sin\gamma_{1_{/\Sigma_{VB}}}, \tag{A.19}$$

$$\mathcal{K}_{2_C} = -\frac{1}{2}\cos\gamma_{1_{/\Sigma_{VB}}}, \tag{A.20}$$

$$\mathcal{K}_{3_C} = F_{x_C/\Sigma_{VB}}\sin\gamma_{1_{/\Sigma_{VB}}} - F_{y_C/\Sigma_{VB}}\cos\gamma_{1_{/\Sigma_{VB}}}, \tag{A.21}$$

where

$$\gamma_{1_{/\Sigma_{VB}}} = \gamma_{1_{/\Sigma}} - \vartheta_{\Sigma_{VB}/\Sigma} = 29.2657 \text{ (deg.)}. \tag{A.22}$$

The above information, required to evaluate the univariate coefficients, is tabulated as the circle coordinates and VPP in Tables A.16 and A.17.

i	$\mathcal{K}_{1_i}$	$\mathcal{K}_{2_i}$	$\mathcal{K}_{3_i}$
A	0.4787	0.1443	0
B	0.3871	0.3165	1.6496
C	0.2444	-0.4362	-3.1281

TABLE A.16. Mixed PR-type leg circle coordinates.

Substituting the data from Tables A.16 and A.17 into the univariate equation gives the following quadratic:

$$24.6417X_3^2 - 26.7045X_3 - 3.9568 = 0. \tag{A.23}$$

i	$VPP_{x_i/E_{VP}}$	$VPP_{y_i/E_{VP}}$
A	$a_1 = 0$	$a_2 = 0$
B	$b_1 = 2.000$	$b_2 = 0$
C	$c_1 = 0.3999$	$c_2 = 3.0395$

TABLE A.17. Mixed *PR*-type VPP.

The roots yield the image points of the FK solutions in the VB frame. A projection of the three image space constraint hyperbolic paraboloids is shown in Figure A.11. The coordinates of O_E must be transformed using the rotation from Σ_{VB} to Σ, while

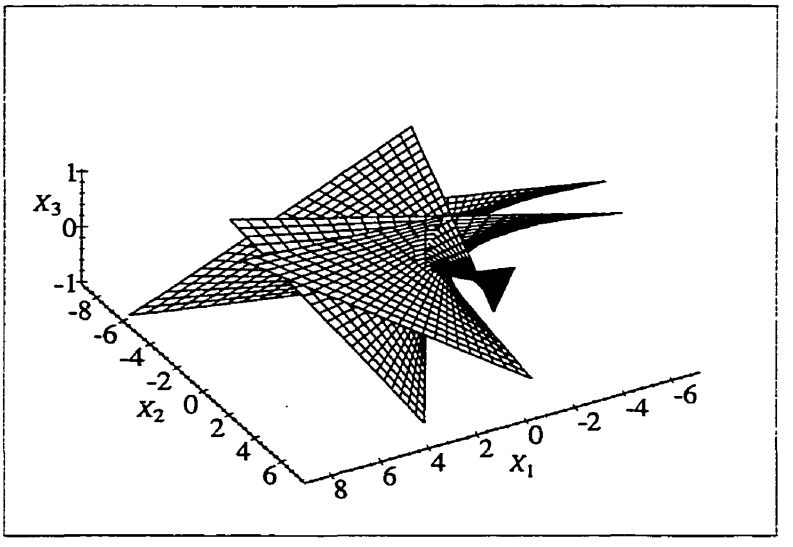

FIGURE A.11. A projection of the hyperbolic paraboloids where $-1 \leq t \leq 1$ and $-10 \leq s \leq 10$.

the orientation of E is

$$\varphi = \varphi_{E/\Sigma_{VB}} + \vartheta_{\Sigma_{VB}/\Sigma}. \tag{A.24}$$

The final FK solutions are illustrated in Figure A.12, while Table A.18 lists both sets of solutions.

Solution	1	2	Solution	1	2
$a_{\Sigma_{VB}}$	-0.3643	-0.5326	a	0.4829	0.7060
$b_{\Sigma_{VB}}$	1.2086	1.7670	b	1.1663	1.7052
$\varphi_{\Sigma_{VB}}$ (deg.)	-15.0474	101.1244	φ (deg.)	-54.3131	61.8587

TABLE A.18. Mixed *PR*-type FK solutions.

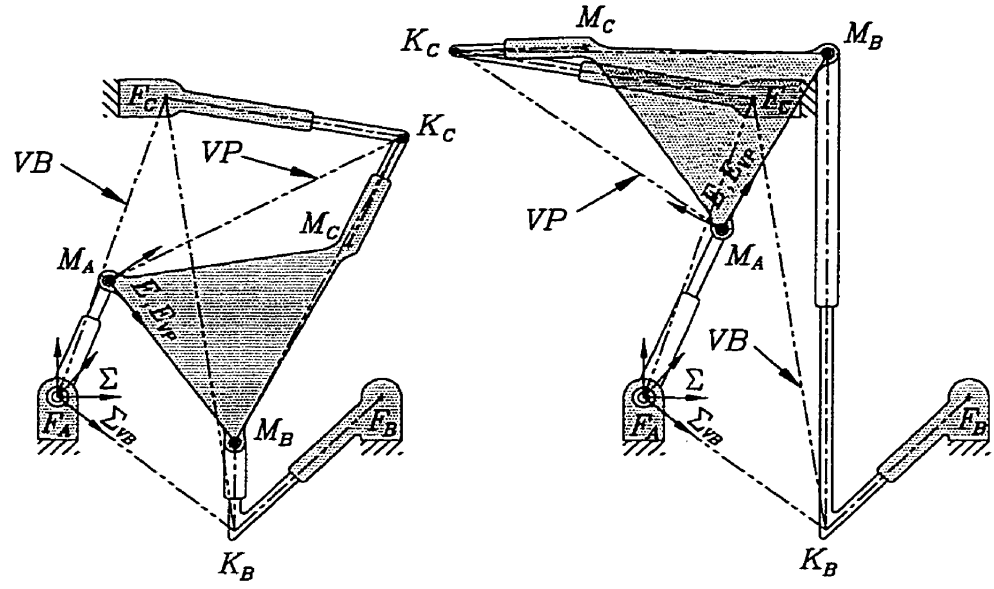

FIGURE A.12. The two real solutions for the mixed *PR*-type leg example.

Note that the two solutions illustrated in Figure A.12 represent two different platforms because of the difference in the direction of increasing d_{3_C} for each one. Thus, only one assembly configuration is realizable; the result of the fact that joint limits are not taken into account by the FK solution algorithm. This presents no practical difficulty in implementation of the algorithm because the workspace of a given platform is known *a priori* and solutions can be quickly checked to see if they fall within bounds.

A.8. *RRG* Example

This example deals with the FK of an *RR*-type platform with active holonomic higher pairs. For these platforms the initial assembly configuration (IAC) must be specified. Thus, the IAC is enumerated in Table A.19. Whereas Table A.20 gives the coordinates of the base points F_A, F_B, F_C in the fixed frame Σ, the change in rack tangent angles, and the corresponding knee joint positions in E, as well as E_{VP} (the VPP determined by their positions on their respective involutes), given by Equations (5.47) and (5.53), respectively. The link lengths, in generic units, are: $r = 4$, $\ell_{1_i} = 4$, $\ell_{2_i} = 10$.

i	$d_{3_{i/R}}$	$\vartheta_{E'_{i/E}}$ (deg.)	ι	$\iota_{1/\Sigma}$ (deg.)	$\iota_{2/1}$ (deg.)
A	0	225	α	135	270
B	0	315	β	45	90
C	0	90	γ	180	90

TABLE A.19. IAC for the *RRG* platform.

i	$F_{x_{i/\Sigma}}$	$F_{x_{i/\Sigma}}$	$\Delta\tau_i$ (deg.)	$K_{x_{i/E}}$	$K_{y_{i/E}}$	$K_{x_{i/E_{VP}}}$	$K_{y_{i/E_{VP}}}$
A	0	0	-17.5	-11.8540	-7.5482	0	0
B	$10\sqrt{2}$	0	-15	7.9069	-11.6008	20.1222	0
C	$5\sqrt{2}+4$	$9\sqrt{2}+14$	7.5	-1.3082	13.9486	6.0121	23.1771

TABLE A.20. Fixed base points, joint inputs, and VPP in E and E_{VP}.

The three inputs, $\Delta\tau_i$, determine the geometry of the VP. The VPP are computed using Equation (5.47). Substituting the VPP from Table A.20 into Equation (4.40) determines the three constraint hyperboloids illustrated in Figure A.13, showing one of the intersections. The circle coordinates are calculated for each leg using the relations found in Table 5.6. Then the circle coordinates, together with the IAC and $\boldsymbol{k}_{i_{/E_{VP}}}$ from Tables A.19 and A.20 are substituted into the univariate, Equation

(4.46), giving the following sixth degree polynomial:

$$8944.3066X_3^6 + 5225.3803X_3^5 + 1218.8858X_3^4 + 219.8942X_3^3 + 40.5995X_3^2 + 4.3567X_3 + 0.15898 = 0.$$

The roots consist of two real and two pairs of complex conjugate values for X_3:

$$\begin{aligned} (X_3)_1 &= -0.1538, \\ (X_3)_2 &= -0.0688, \\ (X_3)_3 &= -0.2238 + 0.0068i, \\ (X_3)_4 &= -0.2238 - 0.0068i, \\ (X_3)_5 &= 0.0429 + 0.1779i, \\ (X_3)_6 &= 0.0429 - 0.1779i. \end{aligned} \tag{A.25}$$

The real values are used to compute the corresponding values of X_1 and X_2. The preimage of these coordinates yield the pose of E_{VP} in Σ. Transforming these displacement parameters using Equation (5.58) gives the required FK solutions. Both sets of solutions, corresponding to the real value of X_3 are listed in Table A.21.

Solution	1	2	Solution	1	2
$a_{E_{VP}/\Sigma}$	-2.9833	-1.9109	$a_{E/\Sigma}$	9.5830	9.4289
$b_{E_{VP}/\Sigma}$	2.6647	3.5141	$b_{E/\Sigma}$	8.9561	11.8146
$\varphi_{E_{VP}/\Sigma}$ (deg.)	-17.4823	-7.8731	$\varphi_{E/\Sigma}$ (deg.)	-5.8927	3.7165

TABLE A.21. *RRG* FK solutions.

The rack tangent angle inputs, $\Delta\tau_i$, in Table A.20, expressed relative to the disk frame E, reveal the geometry of the VP. The origin of E is on the disk centre. Once the orientation and position of the VP, and hence E, are obtained as a triple of displacement parameters $(a, b; \varphi)$, it is a simple matter of plane trigonometry to

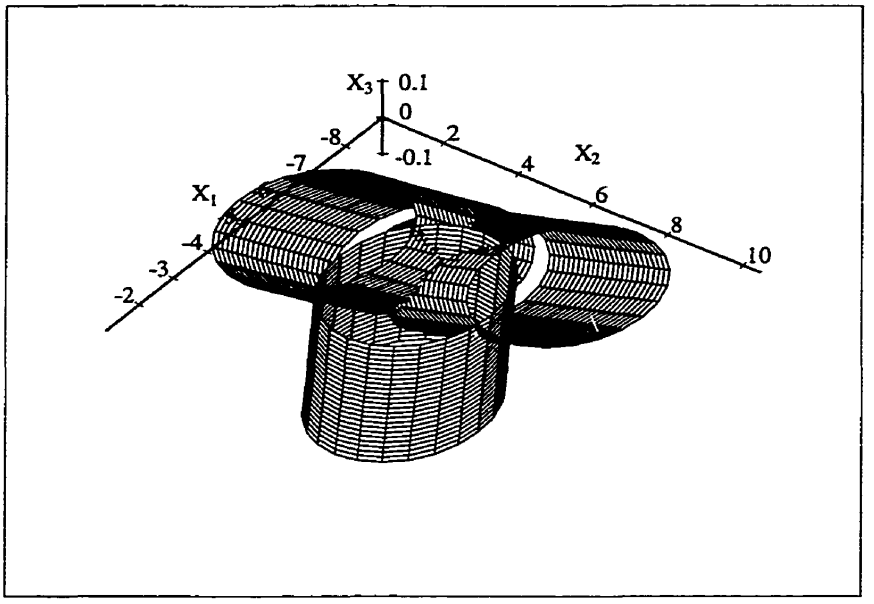

FIGURE A.13. The constraint hyperboloids in the $X_4 = 1$ projection of the image space.

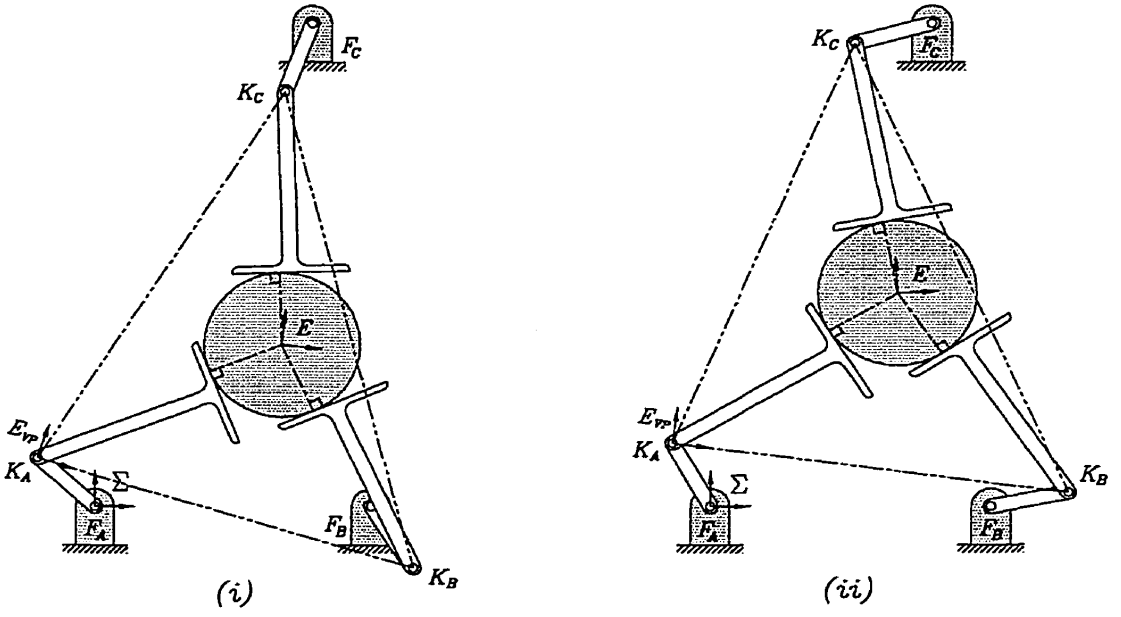

FIGURE A.14. The two real solutions: (*i*) solution 1; (*ii*) solution 2.

determine the relative link angles for the assembly configuration that correspond to the solution. Figure A.14 illustrates the two real assembly configurations, where the vertices of the VP are on their respective circles.

APPENDIX B

IK Examples

B.1. *RR*-Type Legs

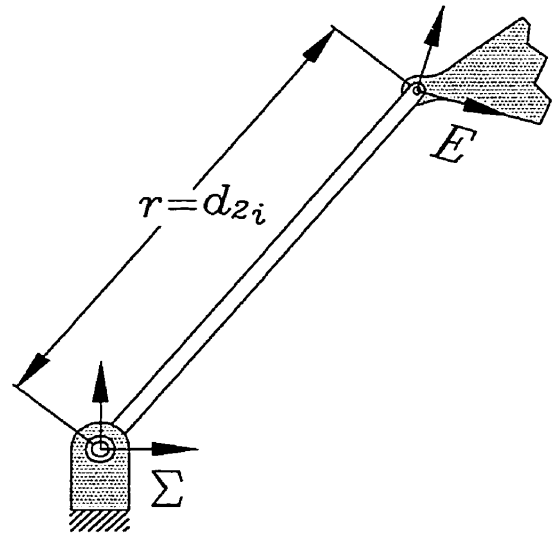

FIGURE B.1. IK problem for $R\underline{P}R$ legs.

Solving the IK problem for $R\underline{P}R$ legs, see Figure B.1, involves a straightforward application of Equation (6.4), reproduced below.

$$r \;=\; d_{2_i} \;=\; \left|\frac{\sqrt{-AC}}{A}\right|. \tag{B.1}$$

B.2. Non-*RR*-Type Legs

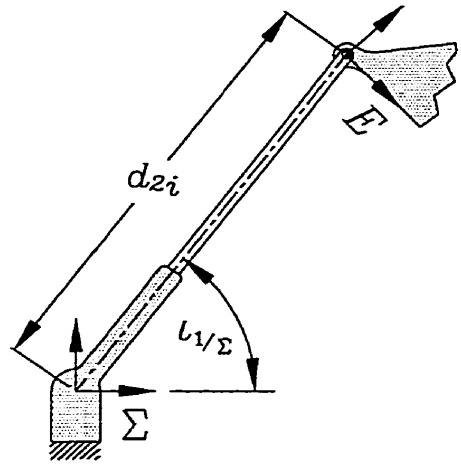

FIGURE B.2. IK problem for $\underline{R}PR$ legs.

B.2.1. $\underline{R}PR$ Legs. Solving the IK problem for $\underline{R}PR$ legs, see Figure B.2, involves a straightforward application of Equation (6.5), reproduced below.

$$\iota = \iota_{1/\Sigma} = \text{atan2}(N, D). \tag{B.2}$$

B.2.2. $RP\underline{P}$ Legs. For $RP\underline{P}$ legs, the IK problem involves some additional computation. The desired input parameter is d_{2_i}, whereas the output from the IK algorithm is the angle ι. Simple trigonometric analysis of Figure B.3 reveals, after application of the *law of sines*:

$$\begin{aligned}
\iota_{2/E} \quad &\text{and} \quad \iota_{1/2} \text{ are design constants.} \\
\iota &= \text{atan2}(N, D). \\
\iota_{/E} &= \iota + \pi - \varphi. \\
\rho &= |\iota_{2/E} - \iota_{/E}|. \\
d_{2_i} &= r\frac{\sin\rho}{\sin\iota_{1/2}}.
\end{aligned}$$

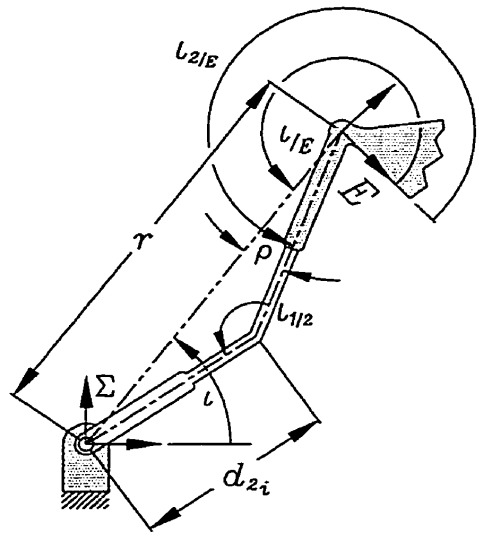

FIGURE B.3. IK problem for *RPP* legs.

B.3. *RRG* Example

Table B.3 gives the manipulator's initial assembly configuration (IAC). The $F_{x_{i/\Sigma}}$ and $F_{y_{i/\Sigma}}$ are the coordinates of the base of each leg expressed in the fixed frame, Σ. The initial rack normal angles in the moving frame, E, are $\eta_{i/E}$. The relative angles between the first link and base, and between the second and first links are $\iota_{1/\Sigma}$ and $\iota_{2/1}$, respectively. The location of the contact point along a rack measured in the corresponding rack frame, R_i, is $d_{3_{i/R_i}}$. The link lengths, in generic units, are: $r = 4$; $\ell_{1_i} = 4$; $\ell_{2_i} = 10$.

i	$F_{x_{i/\Sigma}}$	$F_{y_{i/\Sigma}}$	$\eta_{i/E}$	$\iota_{1/\Sigma}$	$\iota_{2/1}$	$d_{3_{i/R_i}}$
A	0	0	225°	135°	270°	0
B	$10\sqrt{2}$	0	315°	45°	90°	0
C	$5\sqrt{2}+4$	$9\sqrt{2}+14$	90°	180°	90°	0

TABLE B.1. Initial assembly configuration (IAC).

The desired pose of the end-effector and the corresponding image point are one of the solutions from the FK example in Appendix A.8:

$$\begin{bmatrix} a \\ b \\ \varphi \text{ (deg.)} \end{bmatrix} = \begin{bmatrix} 9.429 \\ 11.845 \\ 3.716° \end{bmatrix}, \quad \begin{bmatrix} X_1 \\ X_2 \\ X_3 \\ X_4 \end{bmatrix} = \begin{bmatrix} -11.503 \\ 9.807 \\ 0.065 \\ 1.999 \end{bmatrix}.$$

After making the appropriate substitutions, the following three univariate functions are obtained.

$$\begin{aligned} H_A(\Delta\tau_A) &= 408.489 + 16(\Delta\tau_A)^2 - 422.777\cos\Delta\tau_A - 19.875\sin\Delta\tau_A + \\ &\quad \Delta\tau_A(5.678\cos\Delta\tau_A - 120.793\sin\Delta\tau_A), \\ H_B(\Delta\tau_B) &= 341.710 + 16(\Delta\tau_B)^2 - 317.434\cos\Delta\tau_B + 161.514\sin\Delta\tau_B - \\ &\quad \Delta\tau_B(46.147\cos\Delta\tau_B + 90.694\sin\Delta\tau_B), \\ H_C(\Delta\tau_C) &= 405.104 + 16(\Delta\tau_C) - 413.715\cos\Delta\tau_C + 72.949\sin\Delta\tau_C - \\ &\quad \Delta\tau_C(20.843\cos\Delta\tau_C + 118.204\sin\Delta\tau_C). \end{aligned}$$

The values of $\Delta\tau_i$ from each solution are used to evaluate Equations (5.47), giving the corresponding knee joint coordinates (x_i, y_i). These are listed in Table B.3. The relative link angles for each assembly configuration are determined using plane trigonometry and the given position and orientation of the pinion end-effector (*i.e.*, the moving frame, E). Note that the solution in the first row of Table B.3 is in exact agreement from the corresponding FK example in Section A.8. Figure B.4 illustrates one of the eight real assembly configurations.

$\Delta\tau_A$	$K_{x_{A/E}}$	$K_{y_{A/E}}$	$\Delta\tau_B$	$K_{x_{B/E}}$	$K_{y_{B/E}}$	$\Delta\tau_C$	$K_{x_{C/E}}$	$K_{y_{C/E}}$
-17.5°	-11.845	-7.548	-15°	7.907	-11.601	7.5°	-1.308	13.949
25.04°	-6.422	-12.563	-55.07°	0.783	-14.554	-35.46°	6.106	12.839

TABLE B.2. Change in rack tangent angle and corresponding knee joint coordinates for each leg.

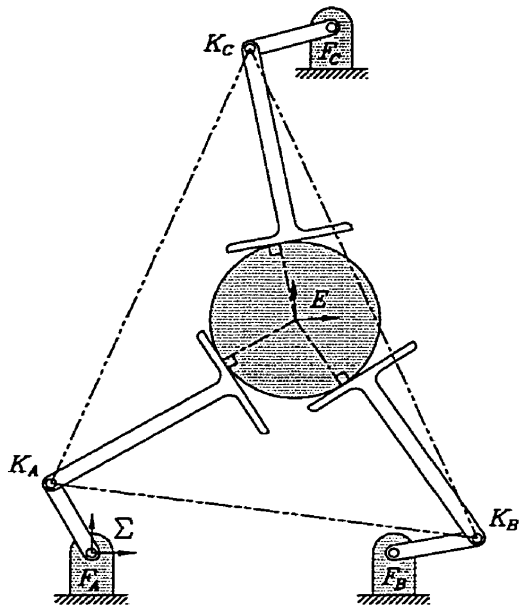

FIGURE B.4. One of the eight real solutions.

APPENDIX C

Maple V Worksheet: Univariate Derivations

In this Appendix the *Maple V* worksheet used to derive the general univariate is listed. There are a couple of points to note. First, The image space coordinates in the worksheet are those used in the Study kinematic mapping and not the Grünwald-Blaschke mapping (the one used in derivations in the text of this thesis), see Equation (3.44). Second, because it is difficult, if not impossible, to use subscripted variables in *Maple V* none are used. As a result equations in the worksheet appear somewhat different, for instance ($2C_2B_1b_1$) appear as (*2 C2 B1 b1*). Finally, only the coefficients of the 694 and 30 term versions of the univariate are listed. The 3613 term version produced the following error message when the version that included these terms was LaTeX'ed:

```
TeX capacity exceeded, sorry [main memory size=262141].
```

File: GenUni3.mws

Last updated: May 13, 1999

This worksheet shows how to determine the one univariate polynomial that can be used to solve the FK of ANY symmetrical (with respect to leg type) 3-legged planar SGP. It is based on Manfred Husty's approach for 3-legged RPR planar platforms. We start with Study's linear transformation representing general spatial displacements. The elements in the transformation matrix are the soma coordinates. The kinematic mapping is defined by the relationship between the following 8-tuples (the second being Study's soma coordinates): [x1:x2:x3:x0:y1:y2:y3:y0]=[c1:c2:c3:c0:g1/2:g2/2:g3/3:g0/2], where the ci and gi are defined as in THEORETICAL KINEMATICS, by Bottema and Roth (see pp. 150-151). (Note, the European representation is used to agree with Manfred's worksheet):

```
> restart;
> with(linalg):
```

```
Warning, new definition for norm
```

```
Warning, new definition for trace
```

```
> S:=matrix(4,4,[x0^2+x1^2+x2^2+x3^2,0,0,0,2*(- y1*x0+y0*x1-y3*x2+y2*x3),
x0^2+x1^2-x2^2-x3^2,2*(x1*x2-x0*x3),2*(x1*x3+ x0*x2),2*(-y2*x0+y0*x2-y1*x3+
y3*x1),2*(x1*x2+x0*x3),x0^2-x1^2+x2^2-x3^ 2,2*(x2*x3-x0*x1),2*(-y3*x0+y0*x3-
y2*x1+y1*x2),2*(x1*x3-x0*x2),2*(x2*x 3+x0*x1),x0^2-x1^2-x2^2+x3^2]);
```

$$S :=$$
$$[x0^2 + x1^2 + x2^2 + x3^2,\ 0,\ 0,\ 0]$$
$$[-2\,y1\,x0 + 2\,y0\,x1 - 2\,y3\,x2 + 2\,y2\,x3,\ x0^2 + x1^2 - x2^2 - x3^2,\ 2\,x1\,x2 - 2\,x0\,x3,$$
$$2\,x1\,x3 + 2\,x0\,x2]$$
$$[-2\,y2\,x0 + 2\,y0\,x2 - 2\,y1\,x3 + 2\,y3\,x1,\ 2\,x1\,x2 + 2\,x0\,x3,\ x0^2 - x1^2 + x2^2 - x3^2,$$
$$2\,x2\,x3 - 2\,x0\,x1]$$
$$[-2\,y3\,x0 + 2\,y0\,x3 - 2\,y2\,x1 + 2\,y1\,x2,\ 2\,x1\,x3 - 2\,x0\,x2,\ 2\,x2\,x3 + 2\,x0\,x1,$$
$$x0^2 - x1^2 - x2^2 + x3^2]$$

Now we restrict the displacement to the y-z principle plane in the fixed space. It is easy to verify that this condition requires x2=x3=y0=y1=0:

```
> S2:=subs(x2=0,x3=0,y0=0,y1=0,op(S));
```

$$S2 := \begin{bmatrix} x0^2 + x1^2 & 0 & 0 & 0 \\ 0 & x0^2 + x1^2 & 0 & 0 \\ -2\,y2\,x0 + 2\,y3\,x1 & 0 & x0^2 - x1^2 & -2\,x0\,x1 \\ -2\,y3\,x0 - 2\,y2\,x1 & 0 & 2\,x0\,x1 & x0^2 - x1^2 \end{bmatrix}$$

We can eliminate the second row and column for the following reason. The only non-zero element in the second row and column is multiplied by x=0.

```
> S3:=delrows(S2,2..2);
```

$$S3 := \begin{bmatrix} x0^2 + x1^2 & 0 & 0 & 0 \\ -2\,y2\,x0 + 2\,y3\,x1 & 0 & x0^2 - x1^2 & -2\,x0\,x1 \\ -2\,y3\,x0 - 2\,y2\,x1 & 0 & 2\,x0\,x1 & x0^2 - x1^2 \end{bmatrix}$$

Hence, the planar reduction of S is:

```
> Syz:=delcols(S3,2..2);
```

$$Syz := \begin{bmatrix} x0^2 + x1^2 & 0 & 0 \\ -2\,y2\,x0 + 2\,y3\,x1 & x0^2 - x1^2 & -2\,x0\,x1 \\ -2\,y3\,x0 - 2\,y2\,x1 & 2\,x0\,x1 & x0^2 - x1^2 \end{bmatrix}$$

```
> inverse(Syz);
```

$$\begin{bmatrix} \frac{1}{x0^2 + x1^2} & 0 & 0 \\ 2\,\frac{y2\,x0 + y3\,x1}{\%1} & \frac{x0^2 - x1^2}{\%1} & 2\,\frac{x0\,x1}{\%1} \\ 2\,\frac{y3\,x0 - y2\,x1}{\%1} & -2\,\frac{x0\,x1}{\%1} & \frac{x0^2 - x1^2}{\%1} \end{bmatrix}$$

$$\%1 := x0^4 + 2\,x0^2\,x1^2 + x1^4$$

```
> factor(x0^4+2*x0^2*x1^2+x1^4);
```

$$(x0^2 + x1^2)^2$$

In linear algebra terms, Syz is non-singular as long as x0^2+x1^2 is non-zero.

```
> Vr:=vector([1,x,y]);
```

$$Vr := [1, x, y]$$

```
> Vl:=multiply(Syz,Vr);
```

$$Vl := [x0^2 + x1^2,\ -2\,y2\,x0 + 2\,y3\,x1 + (x0^2 - x1^2)\,x - 2\,x0\,x1\,y,$$
$$-2\,y3\,x0 - 2\,y2\,x1 + 2\,x0\,x1\,x + (x0^2 - x1^2)\,y]$$

Next, we want a general expression for the image space hyperboloid representing displacements with one point constrained to move on a fixed circle in the fixed reference frame:

```
> Circle:=K0*(X1^2+X2^2)-2*K1*X0*X1-2*K2*X0*X2+ K3*X0^2;
```

$$Circle := K0\,(X1^2 + X2^2) - 2\,K1\,X0\,X1 - 2\,K2\,X0\,X2 + K3\,X0^2$$

The four Ki are the homogeneous coordinates of the circle (kreis), while the Xi are those of points on the circle. Four circle coordinates are required since three parameters are required to determine a circle, whereas two parameters determine a point.

The LHS of the equation X=Syz*x, where the vectors X and x are given by Vl and Vr, respectively, is then substituted into the circle equation...

```
> Cir1:=subs(X0=Vl[1],X1=Vl[2],X2=Vl[3],Circle) ;
```

$$Cir1 := K0((-2\,y2\,x0 + 2\,y3\,x1 + (x0^2 - x1^2)\,x - 2\,x0\,x1\,y)^2$$
$$+ (-2\,y3\,x0 - 2\,y2\,x1 + 2\,x0\,x1\,x + (x0^2 - x1^2)\,y)^2)$$
$$- 2\,K1\,(x0^2 + x1^2)\,(-2\,y2\,x0 + 2\,y3\,x1 + (x0^2 - x1^2)\,x - 2\,x0\,x1\,y)$$
$$- 2\,K2\,(x0^2 + x1^2)\,(-2\,y3\,x0 - 2\,y2\,x1 + 2\,x0\,x1\,x + (x0^2 - x1^2)\,y) + K3\,(x0^2 + x1^2)^2$$

```
> Cir:=factor(Cir1);
```

$$Cir := (x0^2 + x1^2)(-2\,x0^2\,K2\,y + x0^2\,K3 + x0^2\,K0\,x^2 - 2\,x0^2\,K1\,x + x0^2\,K0\,y^2$$
$$- 4\,x0\,K0\,y2\,x + 4\,x0\,K2\,y3 - 4\,x0\,K0\,y3\,y + 4\,x0\,K1\,x1\,y + 4\,x0\,K1\,y2 - 4\,x0\,K2\,x1\,x$$
$$- 4\,K0\,y3\,x1\,x + K3\,x1^2 + 4\,K0\,y2^2 + K0\,x1^2\,y^2 + K0\,x^2\,x1^2 + 4\,K0\,y2\,x1\,y + 4\,K0\,y3^2$$
$$- 4\,K1\,y3\,x1 + 4\,K2\,x1\,y2 + 2\,x1^2\,K2\,y + 2\,x1^2\,K1\,x)$$

The desired expression is the second of the two factors above. The first factor may be eliminated because it design parameter independent, as long as x0^2+x1^2 is non-zero.

```
> Hgen:=op(2,Cir);
```

$$Hgen := -2\,x0^2\,K2\,y + x0^2\,K3 + x0^2\,K0\,x^2 - 2\,x0^2\,K1\,x + x0^2\,K0\,y^2 - 4\,x0\,K0\,y2\,x$$
$$+ 4\,x0\,K2\,y3 - 4\,x0\,K0\,y3\,y + 4\,x0\,K1\,x1\,y + 4\,x0\,K1\,y2 - 4\,x0\,K2\,x1\,x - 4\,K0\,y3\,x1\,x$$
$$+ K3\,x1^2 + 4\,K0\,y2^2 + K0\,x1^2\,y^2 + K0\,x^2\,x1^2 + 4\,K0\,y2\,x1\,y + 4\,K0\,y3^2 - 4\,K1\,y3\,x1$$
$$+ 4\,K2\,x1\,y2 + 2\,x1^2\,K2\,y + 2\,x1^2\,K1\,x$$

```
> nops(Hgen);
```

22

```
> coeff(Hgen,x0,2);
```

$$-2\,K2\,y + K3 + K0\,x^2 - 2\,K1\,x + K0\,y^2$$

```
> coeff(Hgen,x1,2);
```

$$K3 + K0\,y^2 + K0\,x^2 + 2\,K2\,y + 2\,K1\,x$$

```
> H:=expand(subs(K3=R-K0*(x^2+y^2),Hgen));
```

$$H := 4\,x0\,K2\,y3 - 4\,K1\,y3\,x1 + 4\,K2\,x1\,y2 + 2\,x1^2\,K2\,y + 2\,x1^2\,K1\,x - 2\,x0^2\,K2\,y$$
$$- 2\,x0^2\,K1\,x + 4\,x0\,K1\,y2 + 4\,K0\,y2^2 + 4\,K0\,y3^2 + 4\,K0\,y2\,x1\,y - 4\,K0\,y3\,x1\,x$$
$$- 4\,x0\,K0\,y2\,x - 4\,x0\,K0\,y3\,y + 4\,x0\,K1\,x1\,y - 4\,x0\,K2\,x1\,x + x0^2\,R + x1^2\,R$$

```
> nops(H);
```

18

```
> Ha:=subs(K1=A1,K2=A2,R=R1,x=0,y=0,z=1,x0=1,y3 =X1,y2=-X2,x1=X3,H);
```

$$Ha :=$$
$$4\,A2\,X1 - 4\,A1\,X1\,X3 - 4\,A2\,X3\,X2 - 4\,A1\,X2 + 4\,K0\,X2^2 + 4\,K0\,X1^2 + R1 + X3^2\,R1$$

```
> Hb:=subs(K1=B1,K2=B2,R=R2,x=b1,y=0,z=1,x0=1,y 3=X1,y2=-X2,x1=X3,H);
```

$$Hb := 4\,B2\,X1 - 4\,B1\,X1\,X3 - 4\,B2\,X3\,X2 + 2\,X3^2\,B1\,b1 - 2\,B1\,b1 - 4\,B1\,X2 + 4\,K0\,X2^2$$
$$+ 4\,K0\,X1^2 - 4\,K0\,X1\,X3\,b1 + 4\,K0\,X2\,b1 - 4\,B2\,X3\,b1 + R2 + X3^2\,R2$$

```
> Hc:=subs(K1=C1,K2=C2,R=R3,x=c1,y=c2,z=1,x0=1, y3=X1,y2=-X2,x1=X3,H);
```

$$Hc := 4\,C2\,X1 - 4\,C1\,X1\,X3 - 4\,C2\,X3\,X2 + 2\,X3^2\,C2\,c2 + 2\,X3^2\,C1\,c1 - 2\,C2\,c2 - 2\,C1\,c1 - 4\,C1\,X2 + 4\,K0\,X2^2 + 4\,K0\,X1^2 - 4\,K0\,X2\,X3\,c2 - 4\,K0\,X1\,X3\,c1 + 4\,K0\,X2\,c1 - 4\,K0\,X1\,c2 + 4\,C1\,X3\,c2 - 4\,C2\,X3\,c1 + R3 + X3^2\,R3$$

```
> Hab:=Ha-Hb;
```

$$Hab := 4\,A2\,X1 - 4\,A1\,X1\,X3 - 4\,A2\,X3\,X2 - 4\,A1\,X2 + R1 + X3^2\,R1 - 4\,B2\,X1 + 4\,B1\,X1\,X3 + 4\,B2\,X3\,X2 - 2\,X3^2\,B1\,b1 + 2\,B1\,b1 + 4\,B1\,X2 + 4\,K0\,X1\,X3\,b1 - 4\,K0\,X2\,b1 + 4\,B2\,X3\,b1 - R2 - X3^2\,R2$$

```
> Hac:=Ha-Hc;
```

$$Hac := -4\,K0\,X2\,c1 + 2\,C2\,c2 + R1 - R3 + 4\,A2\,X1 - 4\,A1\,X2 + X3^2\,R1 - 4\,C2\,X1 + 4\,C1\,X2 - X3^2\,R3 - 4\,A1\,X1\,X3 - 4\,A2\,X3\,X2 + 2\,C1\,c1 + 4\,K0\,X1\,c2 - 2\,X3^2\,C2\,c2 + 4\,C2\,X3\,X2 + 4\,C1\,X1\,X3 - 2\,X3^2\,C1\,c1 - 4\,C1\,X3\,c2 + 4\,C2\,X3\,c1 + 4\,K0\,X2\,X3\,c2 + 4\,K0\,X1\,X3\,c1$$

```
> collect((Ha/4),[X1,X2,X3]);
```

$$K0\,X1^2 + (-A1\,X3 + A2)\,X1 + K0\,X2^2 + (-A2\,X3 - A1)\,X2 + \frac{1}{4}\,X3^2\,R1 + \frac{1}{4}\,R1$$

```
> collect((Hb/4),[X1,X2,X3]);
```

$$K0\,X1^2 + ((-B1 - K0\,b1)\,X3 + B2)\,X1 + K0\,X2^2 + (-B1 - B2\,X3 + K0\,b1)\,X2 + (\frac{1}{2}\,B1\,b1 + \frac{1}{4}\,R2)\,X3^2 - B2\,X3\,b1 - \frac{1}{2}\,B1\,b1 + \frac{1}{4}\,R2$$

```
> collect(Hc/4,[X1,X2,X3]);
```

$$K0\,X1^2 + ((-C1 - K0\,c1)\,X3 - K0\,c2 + C2)\,X1 + K0\,X2^2 + ((-C2 - K0\,c2)\,X3 + K0\,c1 - C1)\,X2 + (\frac{1}{2}\,C2\,c2 + \frac{1}{2}\,C1\,c1 + \frac{1}{4}\,R3)\,X3^2 + (C1\,c2 - C2\,c1)\,X3 + \frac{1}{4}\,R3 - \frac{1}{2}\,C2\,c2 - \frac{1}{2}\,C1\,c1$$

```
> collect(Hab/4,[X1,X2,X3]);
```

$$((-A1 + B1 + K0\,b1)\,X3 - B2 + A2)\,X1 + ((B2 - A2)\,X3 - K0\,b1 - A1 + B1)\,X2 + (-\frac{1}{4}\,R2 + \frac{1}{4}\,R1 - \frac{1}{2}\,B1\,b1)\,X3^2 + B2\,X3\,b1 + \frac{1}{4}\,R1 - \frac{1}{4}\,R2 + \frac{1}{2}\,B1\,b1$$

```
> collect(Hac/4,[X1,X2,X3]);
```

$$((C1 - A1 + K0\,c1)\,X3 + K0\,c2 + A2 - C2)\,X1 + ((K0\,c2 + C2 - A2)\,X3 - A1 + C1 - K0\,c1)\,X2 + (-\frac{1}{4}\,R3 + \frac{1}{4}\,R1 - \frac{1}{2}\,C1\,c1 - \frac{1}{2}\,C2\,c2)\,X3^2 + (-C1\,c2 + C2\,c1)\,X3 + \frac{1}{2}\,C1\,c1 + \frac{1}{2}\,C2\,c2 + \frac{1}{4}\,R1 - \frac{1}{4}\,R3$$

```
> Seq1:=solve({Hab,Hac},{X1,X2}):
> Seq2:=subs(Seq1[1],Seq1[2],Hc):
> Seq3:=factor(Seq2):
> Uni:=op(2,Seq3):
> Uni1:=collect(Uni,[X3]):
> Uni2:=sort(Uni1,[X3]):
> nops(Uni);
```

3613

```
> degree(Uni,X3);
```

6

The univariate can be simplified for platforms with three RR-type legs. It is obtained with the following substitutions in the general constraint manifold equation given by Hgen. HC indicates that at least one point in the moving plane moves on a circle in the fixed plane...the C stands for circle, the H for constraint Hyperboloid. Note that the constants are now: K0, B1, C1, C2, R1,R2,R3,b1, c1,c2. Here, K0=1.

```
> HCa:=subs(K0=1,K1=0,K2=0,x=0,y=0,R=R1,x0=1,y3 =X1,y2=-X2,x1=X3,H);
```

$$HCa := 4\,X2^2 + 4\,X1^2 + R1 + X3^2\,R1$$

```
> HCb:=subs(K0=1,K1=B1,K2=0,x=b1,y=0,R=R2,x0=1, y3=X1,y2=-X2,x1=X3,H);
```

$$HCb := -4\,B1\,X1\,X3 + 2\,X3^2\,B1\,b1 - 2\,B1\,b1 - 4\,B1\,X2 + 4\,X2^2 + 4\,X1^2 - 4\,X1\,X3\,b1 + 4\,X2\,b1 + R2 + X3^2\,R2$$

```
> HCc:=subs(K0=1,K1=C1,K2=C2,x=c1,y=c2,R=R3,x0= 1,y3=X1,y2=-X2,x1=X3,H);
```

$$HCc := 4\,C2\,X1 - 4\,C1\,X1\,X3 - 4\,C2\,X3\,X2 + 2\,X3^2\,C2\,c2 + 2\,X3^2\,C1\,c1 - 2\,C2\,c2 - 2\,C1\,c1 - 4\,C1\,X2 + 4\,X2^2 + 4\,X1^2 - 4\,X2\,X3\,c2 - 4\,X1\,X3\,c1 + 4\,X2\,c1 - 4\,X1\,c2 + 4\,C1\,X3\,c2 - 4\,C2\,X3\,c1 + R3 + X3^2\,R3$$

```
> HCab:=HCa-HCb;
```

$$HCab := R1 + X3^2\,R1 + 4\,B1\,X1\,X3 - 2\,X3^2\,B1\,b1 + 2\,B1\,b1 + 4\,B1\,X2 + 4\,X1\,X3\,b1 - 4\,X2\,b1 - R2 - X3^2\,R2$$

```
> HCac:=HCa-HCc;
```

$$HCac := R1 + X3^2\,R1 - 4\,C2\,X1 + 4\,C1\,X1\,X3 + 4\,C2\,X3\,X2 - 2\,X3^2\,C2\,c2 - 2\,X3^2\,C1\,c1 + 2\,C2\,c2 + 2\,C1\,c1 + 4\,C1\,X2 + 4\,X2\,X3\,c2 + 4\,X1\,X3\,c1 - 4\,X2\,c1 + 4\,X1\,c2 - 4\,C1\,X3\,c2 + 4\,C2\,X3\,c1 - R3 - X3^2\,R3$$

```
> eqC1:=solve({HCab,HCac},{X1,X2}):
> eqC2:=subs(eqC1[1],eqC1[2],HCc):
> eqC3:=factor(eqC2):
> UniCir:=op(2,eqC3):
> UniCir1:=collect(UniCir,[X3]):
> UniCir2:=sort(UniCir1,[X3]);
```

$$
\begin{aligned}
UniCir2 := (&-2\,C2^2\,R1\,R2 + 4\,b1^2\,C2^2\,B1^2 + 2\,R3^2\,B1\,b1 + 4\,c1^2\,B1^2\,b1^2 + 2\,R1^2\,B1\,b1 \\
&+ 2\,R1\,B1\,c1\,R2 - 2\,R1^2\,B1\,c1 + 4\,R1\,B1^2\,c1\,b1 + 4\,b1\,C2^2\,B1\,R2 + C2^2\,R1^2 \\
&- 2\,R1^2\,B1\,C1 - 2\,R1\,B1^2\,R3 + 4\,C1^2\,c1^2\,B1^2 + 4\,C1^2\,B1^2\,b1^2 + C2^2\,R2^2 - 2\,c2^2\,R2\,R1 \\
&+ 4\,c2^2\,B1^2\,b1^2 + 2\,C2\,R2^2\,c2 + 2\,C2\,R1^2\,c2 - 2\,R3\,B1\,c1\,R2 - 2\,C1\,R1^2\,b1 \\
&- 2\,C1^2\,R1\,R2 - 2\,R1\,b1^2\,R3 - 2\,R1^2\,b1\,c1 + 4\,c1^2\,B1\,b1\,R2 - 4\,R1\,b1^2\,C1\,c1 \\
&+ 2\,C1\,R2^2\,c1 + 2\,R1\,b1\,c1\,R2 - 4\,C1^2\,R2\,c1\,b1 + R1^2\,b1^2 - 4\,C1\,R1\,c1\,R2 \\
&+ 4\,C1^2\,R1\,c1\,b1 + 2\,C1\,R1^2\,c1 + 4\,R1\,B1^2\,C2^2 + 4\,R1\,b1^2\,c2^2 - 4\,C2\,R1\,c2\,R2 \\
&+ 8\,b1^2\,C2\,B1^2\,c2 - 4\,C1\,c1^2\,b1\,R2 + 4\,C1^2\,c1^2\,b1^2 + 8\,b1\,C2\,B1\,c2\,R2 - 2\,c1^2\,R2\,R1 \\
&+ c1^2\,R1^2 + R3^2\,b1^2 + 2\,c1\,R1\,R3\,b1 + c1^2\,R2^2 - 2\,c1\,R2\,R3\,b1 + 4\,c2^2\,B1\,b1\,R1 \\
&+ 4\,c2^2\,B1\,b1\,R2 + 4\,C1^2\,B1\,b1\,R2 - 4\,C1\,B1^2\,b1\,R3 - 4\,C1^2\,B1\,b1\,R1 \\
&+ 4\,C1\,B1^2\,b1\,R1 - 8\,C1^2\,B1^2\,b1\,c1 - 2\,R3\,B1\,C1\,R2 + 2\,R3\,B1\,C1\,R1 + 2\,R1\,B1\,C1\,R2 \\
&- 4\,C1^2\,c1\,B1\,R2 + 4\,C1^2\,c1\,B1\,R1 + 4\,C1\,c1\,B1^2\,R3 - 4\,C1\,c1\,B1^2\,R1 + c2^2\,R2^2 \\
&+ c2^2\,R1^2 + 4\,C1\,B1\,b1^2\,R1 - 4\,C1\,B1\,b1^2\,R3 - 8\,C1^2\,B1\,b1^2\,c1 + 8\,C1\,B1^2\,b1^2\,c1 \\
&- 4\,C1\,c1^2\,B1\,R2 + 8\,C1^2\,c1^2\,B1\,b1 - 8\,C1\,c1^2\,B1^2\,b1 + 4\,C1\,c1^2\,B1\,R1 \\
&- 4\,R3\,B1^2\,c1\,b1 + 4\,R1\,b1^2\,C2^2 + 4\,C2^2\,c2^2\,B1^2 + 4\,C2^2\,c2^2\,b1^2 - 4\,R1\,B1\,R3\,b1 \\
&+ R3^2\,B1^2 + 2\,C1\,R2\,R1\,b1 + 2\,C1\,R1\,R3\,b1 + R1^2\,B1^2 + 8\,C2\,C1\,c1\,b1^2\,c2 \\
&- 8\,C2\,C1\,B1\,b1^2\,c2 - 4\,C2\,c1\,R2\,c2\,B1 + 4\,C2\,R1\,B1^2\,c2 + 4\,C2\,c1\,R1\,c2\,b1 \\
&+ 4\,C2\,c1\,R1\,c2\,B1 + 16\,C2\,C1\,c1\,B1\,c2\,b1 + 8\,C2\,C1\,c1\,B1^2\,c2 - 8\,C2\,C1\,B1^2\,b1\,c2 \\
&+ 8\,C2\,R3\,B1\,c2\,b1 + 4\,C2\,R1\,b1^2\,c2 + 4\,C2\,C1\,R1\,c2\,b1 + 4\,C2\,C1\,R1\,c2\,B1 \\
&- 4\,C2\,C1\,R2\,c2\,b1 - 4\,C2\,C1\,R2\,c2\,B1 + 4\,C2\,R3\,B1^2\,c2 + 2\,R3\,B1\,c1\,R1 \\
&- 8\,C2\,c1\,B1\,b1^2\,c2 - 8\,C2\,c1\,B1^2\,b1\,c2 - 2\,C1\,R2\,R3\,b1 + 4\,R1\,b1^2\,c1\,B1 + C1^2\,R1^2 \\
&+ C1^2\,R2^2 - 4\,c1\,B1\,b1^2\,R3 - 4\,c1^2\,B1\,b1\,R1 - 8\,c1^2\,B1\,b1^2\,C1 - 16\,C1\,B1\,b1\,c1\,R1 \\
&+ 8\,C1\,B1\,b1\,c1\,R2 + 8\,C1\,c1\,B1\,R3\,b1 + 4\,C1\,c1\,b1^2\,R3 + 4\,C1\,c1^2\,b1\,R1 \\
&+ 4\,R1\,B1^2\,c2^2 + 4\,R1\,B1\,C2^2\,b1 + 8\,C2^2\,c2^2\,B1\,b1 - 4\,C2\,c1\,R2\,c2\,b1 + 4\,C2\,R3\,b1^2\,c2 \\
&)X3^6 + (8\,C1^2\,R1\,c2\,b1 - 8\,C1^2\,R2\,c2\,b1 + 8\,C2^2\,R2\,c2\,b1 - 16\,c1\,R1\,B1^2\,c2 \\
&- 16\,C2^2\,c2\,B1^2\,c1 - 16\,C1^2\,B1\,b1^2\,c2 - 16\,C2\,b1\,c2^2\,B1^2 + 16\,b1^2\,C1\,B1^2\,c2 \\
&+ 32\,C2\,C1\,c2^2\,B1\,b1 + 16\,C2^2\,b1^2\,B1\,c2 - 4\,C2\,R2^2\,c1 - 4\,C2\,R1^2\,c1 + 4\,C2\,R1^2\,b1 \\
&+ 8\,R3\,B1^2\,C1\,c2 - 32\,C1\,c1\,B1^2\,b1\,c2 - 4\,C2\,R1\,R3\,b1 + 4\,C2\,R2\,R3\,b1 \\
&- 4\,C2\,R2\,R1\,b1 - 4\,B1\,R1^2\,c2 + 4\,c2\,R2^2\,C1 - 4\,R3\,B1\,c2\,R2 + 4\,R3\,B1\,c2\,R1 \\
&+ 4\,c2\,R1^2\,C1 - 8\,C1\,c2\,B1^2\,R1 + 8\,C1^2\,c2\,B1\,R1 - 8\,C1^2\,c2\,B1\,R2 + 16\,c1^2\,B1\,b1^2\,C2 \\
&- 8\,b1^2\,C2\,B1\,R1 + 8\,b1^2\,C2\,B1\,R3 - 16\,b1\,C2\,B1\,c1\,R2 + 8\,R1\,b1^2\,C2\,c1 \\
&+ 16\,b1\,C1\,B1\,c2\,R2 - 16\,b1^2\,C2\,B1^2\,c1 + 8\,C2\,R1\,c1\,R2 + 8\,b1\,C2\,c1^2\,R2 \\
&- 8\,b1^2\,C2\,c1\,R3 - 8\,b1\,C2\,c1^2\,R1 - 16\,b1^2\,C2\,c1^2\,C1 - 8\,R3\,B1^2\,c2\,b1 \\
&- 16\,c1\,R1\,c2\,B1\,b1 - 8\,R1\,C1\,c2\,R2 + 4\,B1\,R1\,c2\,R2 + 8\,B1^2\,R1\,c2\,b1 \\
&- 8\,C2\,R3\,B1^2\,c1 - 8\,C2\,c2^2\,R2\,B1 + 16\,C2\,b1^2\,C1\,c2^2 - 16\,C1\,c1\,B1\,b1^2\,c2 \\
&+ 8\,C1\,R1\,b1^2\,c2 - 16\,b1^2\,C2^2\,c1\,c2 - 8\,C2^2\,R1\,c2\,b1 - 32\,C2^2\,c1\,B1\,c2\,b1 \\
&- 16\,C2\,R3\,b1\,c1\,B1 - 16\,C2\,c1\,R1\,C1\,b1 + 16\,C2\,c1\,R2\,C1\,b1 - 8\,C2\,c1^2\,R1\,B1 \\
&+ 8\,C2\,c1^2\,R2\,B1 - 32\,C2\,C1\,c1^2\,b1\,B1 + 16\,C2\,C1\,c2^2\,B1^2 - 16\,C2\,C1\,c1^2\,B1^2 \\
&+ 16\,C2\,C1\,B1^2\,b1\,c1 + 8\,C2\,R1\,c2^2\,B1 + 16\,C2\,c1^2\,B1^2\,b1 + 16\,C2\,R1\,b1^2\,C1 \\
&+ 8\,C1\,b1^2\,R3\,c2 + 8\,C2\,C1\,R2\,c1\,B1 + 16\,C2\,R1\,b1\,c1\,B1 - 8\,C2\,C1\,R1\,c1\,B1
\end{aligned}
$$

$$+32\,C2\,c1\,B1\,b1^2\,C1 - 8\,C2\,R1\,B1^2\,c1 + 16\,C2\,R1\,B1\,C1\,b1 - 8\,C1\,c1\,R2\,c2\,b1$$
$$- 16\,C1\,c1\,R2\,c2\,B1 + 16\,C1^2\,c1\,B1^2\,c2 + 16\,C1\,c1\,R1\,c2\,B1 + 8\,C1\,c1\,R1\,c2\,b1$$
$$+ 32\,C1^2\,c1\,B1\,c2\,b1 - 16\,C1^2\,B1^2\,b1\,c2 + 16\,C1^2\,c1\,b1^2\,c2 - 16\,C1\,R1\,B1\,c2\,b1$$
$$+ 16\,C1\,R3\,B1\,c2\,b1)X3^5 + (-6\,C2^2\,R1\,R2 - 4\,b1^2\,C2^2\,B1^2 + 2\,R3^2\,B1\,b1$$
$$- 4\,c1^2\,B1^2\,b1^2 + 2\,R1^2\,B1\,b1 + 2\,R1\,B1\,c1\,R2 - 2\,R1^2\,B1\,c1 - 4\,R1\,B1^2\,c1\,b1$$
$$+ 4\,b1\,C2^2\,B1\,R2 + 3\,C2^2\,R1^2 - 6\,R1^2\,B1\,C1 - 6\,R1\,B1^2\,R3 - 4\,C1^2\,c1^2\,B1^2$$
$$- 4\,C1^2\,B1^2\,b1^2 + 3\,C2^2\,R2^2 - 6\,c2^2\,R2\,R1 - 4\,c2^2\,B1^2\,b1^2 + 2\,C2\,R2^2\,c2 + 2\,C2\,R1^2\,c2$$
$$- 2\,R3\,B1\,c1\,R2 - 2\,C1\,R1^2\,b1 - 6\,C1^2\,R1\,R2 - 6\,R1\,b1^2\,R3 - 6\,R1^2\,b1\,c1$$
$$+ 4\,c1^2\,B1\,b1\,R2 - 4\,R1\,b1^2\,C1\,c1 + 2\,C1\,R2^2\,c1 + 6\,R1\,b1\,c1\,R2 + 4\,C1^2\,R2\,c1\,b1$$
$$+ 3\,R1^2\,b1^2 - 4\,C1\,R1\,c1\,R2 - 4\,C1^2\,R1\,c1\,b1 + 2\,C1\,R1^2\,c1 + 12\,R1\,B1^2\,C2^2$$
$$+ 12\,R1\,b1^2\,c2^2 - 4\,C2\,R1\,c2\,R2 - 24\,b1^2\,C2\,B1^2\,c2 - 4\,C1\,c1^2\,b1\,R2$$
$$- 32\,c1\,B1\,b1^2\,C2^2 - 4\,C1^2\,c1^2\,b1^2 - 8\,b1\,C2\,B1\,c2\,R2 - 6\,c1^2\,R2\,R1 + 3\,c1^2\,R1^2$$
$$+ 3\,R3^2\,b1^2 + 6\,c1\,R1\,R3\,b1 + 3\,c1^2\,R2^2 - 6\,c1\,R2\,R3\,b1 + 4\,c2^2\,B1\,b1\,R1$$
$$+ 4\,c2^2\,B1\,b1\,R2 + 4\,C1^2\,B1\,b1\,R2 - 4\,C1\,B1^2\,b1\,R3 - 4\,C1^2\,B1\,b1\,R1$$
$$+ 4\,C1\,B1^2\,b1\,R1 + 8\,C1^2\,B1^2\,b1\,c1 - 6\,R3\,B1\,C1\,R2 + 6\,R3\,B1\,C1\,R1 + 6\,R1\,B1\,C1\,R2$$
$$+ 16\,b1^2\,C2^2\,c1^2 - 4\,C1^2\,c1\,B1\,R2 + 4\,C1^2\,c1\,B1\,R1 + 4\,C1\,c1\,B1^2\,R3 - 4\,C1\,c1\,B1^2\,R1$$
$$+ 3\,c2^2\,R2^2 + 3\,c2^2\,R1^2 - 4\,C1\,B1\,b1^2\,R1 + 4\,C1\,B1\,b1^2\,R3 + 24\,C1^2\,B1\,b1^2\,c1$$
$$- 24\,C1\,B1^2\,b1^2\,c1 + 4\,C1\,c1^2\,B1\,R2 - 24\,C1^2\,c1^2\,B1\,b1 + 24\,C1\,c1^2\,B1^2\,b1$$
$$- 4\,C1\,c1^2\,B1\,R1 - 16\,c1\,R2\,C2^2\,b1 + 16\,c1\,R1\,C2^2\,b1 + 4\,R3\,B1^2\,c1\,b1 - 4\,R1\,b1^2\,C2^2$$
$$- 4\,C2^2\,c2^2\,B1^2 - 4\,C2^2\,c2^2\,b1^2 - 4\,R1\,B1\,R3\,b1 + 3\,R3^2\,B1^2 + 2\,C1\,R2\,R1\,b1$$
$$+ 2\,C1\,R1\,R3\,b1 + 3\,R1^2\,B1^2 - 40\,C2\,C1\,c1\,b1^2\,c2 + 56\,C2\,C1\,B1\,b1^2\,c2$$
$$+ 20\,C2\,c1\,R2\,c2\,B1 + 4\,C2\,R1\,B1^2\,c2 + 4\,C2\,c1\,R1\,c2\,b1 - 20\,C2\,c1\,R1\,c2\,B1$$
$$- 112\,C2\,C1\,c1\,B1\,c2\,b1 - 40\,C2\,C1\,c1\,B1^2\,c2 + 8\,C2\,C1\,B1^2\,b1\,c2$$
$$+ 32\,C2\,R1\,B1\,c2\,b1 - 8\,C2\,R3\,B1\,c2\,b1 + 4\,C2\,R1\,b1^2\,c2 - 20\,C2\,C1\,R1\,c2\,b1$$
$$+ 4\,C2\,C1\,R1\,c2\,B1 + 20\,C2\,C1\,R2\,c2\,b1 - 4\,C2\,C1\,R2\,c2\,B1 + 4\,C2\,R3\,B1^2\,c2$$
$$+ 2\,R3\,B1\,c1\,R1 + 8\,C2\,c1\,B1\,b1^2\,c2 + 56\,C2\,c1\,B1^2\,b1\,c2 - 2\,C1\,R2\,R3\,b1$$
$$+ 4\,R1\,b1^2\,c1\,B1 + 3\,C1^2\,R1^2 + 3\,C1^2\,R2^2 + 16\,C1\,c2^2\,R1\,B1 - 32\,C1\,c2^2\,B1^2\,b1$$
$$- 16\,C1\,c2^2\,R2\,B1 + 16\,C1^2\,R1\,b1^2 + 16\,C1^2\,c2^2\,B1^2 - 4\,c1\,B1\,b1^2\,R3 + 16\,c1^2\,R1\,B1^2$$
$$- 4\,c1^2\,B1\,b1\,R1 + 8\,c1^2\,B1\,b1^2\,C1 - 16\,C1\,B1\,b1\,c1\,R1 - 8\,C1\,B1\,b1\,c1\,R2$$
$$+ 32\,C1^2\,c2^2\,B1\,b1 + 16\,C2^2\,c1^2\,B1^2 + 32\,b1\,C2^2\,c1^2\,B1 + 16\,C1^2\,b1^2\,c2^2$$
$$- 8\,C1\,c1\,B1\,R3\,b1 + 4\,C1\,c1\,b1^2\,R3 + 4\,C1\,c1^2\,b1\,R1 - 4\,R1\,B1^2\,c2^2 + 4\,R1\,B1\,C2^2\,b1$$
$$- 24\,C2^2\,c2^2\,B1\,b1 - 4\,C2\,c1\,R2\,c2\,b1 + 4\,C2\,R3\,b1^2\,c2)X3^4 + (32\,C1^2\,B1\,b1^2\,c2$$
$$+ 32\,C2\,b1\,c2^2\,B1^2 - 32\,b1^2\,C1\,B1^2\,c2 - 64\,C2\,C1\,c2^2\,B1\,b1 - 32\,C2^2\,b1^2\,B1\,c2$$
$$- 8\,C2\,R2^2\,c1 - 8\,C2\,R1^2\,c1 + 8\,C2\,R1^2\,b1 + 16\,R3\,B1^2\,C1\,c2 + 64\,C1\,c1\,B1^2\,b1\,c2$$
$$- 8\,C2\,R1\,R3\,b1 + 8\,C2\,R2\,R3\,b1 - 8\,C2\,R2\,R1\,b1 - 8\,B1\,R1^2\,c2 + 8\,c2\,R2^2\,C1$$
$$- 8\,R3\,B1\,c2\,R2 + 8\,R3\,B1\,c2\,R1 + 8\,c2\,R1^2\,C1 - 16\,C1\,c2\,B1^2\,R1 + 16\,C1^2\,c2\,B1\,R1$$
$$- 16\,C1^2\,c2\,B1\,R2 + 16\,R1\,b1^2\,C2\,c1 + 32\,b1^2\,C2\,B1^2\,c1 + 16\,C2\,R1\,c1\,R2$$
$$+ 16\,b1\,C2\,c1^2\,R2 - 16\,b1^2\,C2\,c1\,R3 - 16\,b1\,C2\,c1^2\,R1 - 32\,c1\,R1\,c2\,B1\,b1$$
$$- 16\,R1\,C1\,c2\,R2 + 8\,B1\,R1\,c2\,R2 - 16\,C2\,R3\,B1^2\,c1 + 16\,C1\,R1\,b1^2\,c2$$

$$+64\,C2^2\,c1\,B1\,c2\,b1+64\,C2\,C1\,c1^2\,b1\,B1-32\,C2\,c1^2\,B1^2\,b1+16\,C1\,b1^2\,R3\,c2$$
$$+16\,C2\,C1\,R2\,c1\,B1-16\,C2\,C1\,R1\,c1\,B1-64\,C2\,c1\,B1\,b1^2\,C1-16\,C2\,R1\,B1^2\,c1$$
$$+32\,C2\,R1\,B1\,C1\,b1-16\,C1\,c1\,R2\,c2\,b1+16\,C1\,c1\,R1\,c2\,b1-64\,C1^2\,c1\,B1\,c2\,b1)$$
$$X3^3+(-6\,C2^2\,R1\,R2-4\,b1^2\,C2^2\,B1^2-2\,R3^2\,B1\,b1-4\,c1^2\,B1^2\,b1^2-2\,R1^2\,B1\,b1$$
$$-2\,R1\,B1\,c1\,R2+2\,R1^2\,B1\,c1-4\,R1\,B1^2\,c1\,b1-4\,b1\,C2^2\,B1\,R2+3\,C2^2\,R1^2$$
$$-6\,R1^2\,B1\,C1-6\,R1\,B1^2\,R3-4\,C1^2\,c1^2\,B1^2-4\,C1^2\,B1^2\,b1^2+3\,C2^2\,R2^2-6\,c2^2\,R2\,R1$$
$$-4\,c2^2\,B1^2\,b1^2-2\,C2\,R2^2\,c2-2\,C2\,R1^2\,c2+2\,R3\,B1\,c1\,R2+2\,C1\,R1^2\,b1$$
$$-6\,C1^2\,R1\,R2-6\,R1\,b1^2\,R3-6\,R1^2\,b1\,c1-4\,c1^2\,B1\,b1\,R2+4\,R1\,b1^2\,C1\,c1$$
$$-2\,C1\,R2^2\,c1+6\,R1\,b1\,c1\,R2+4\,C1^2\,R2\,c1\,b1+3\,R1^2\,b1^2+4\,C1\,R1\,c1\,R2$$
$$-4\,C1^2\,R1\,c1\,b1-2\,C1\,R1^2\,c1+12\,R1\,B1^2\,C2^2+12\,R1\,b1^2\,c2^2+4\,C2\,R1\,c2\,R2$$
$$+24\,b1^2\,C2\,B1^2\,c2+4\,C1\,c1^2\,b1\,R2+32\,c1\,B1\,b1^2\,C2^2-4\,C1^2\,c1^2\,b1^2$$
$$-8\,b1\,C2\,B1\,c2\,R2-6\,c1^2\,R2\,R1+3\,c1^2\,R1^2+3\,R3^2\,b1^2+6\,c1\,R1\,R3\,b1+3\,c1^2\,R2^2$$
$$-6\,c1\,R2\,R3\,b1-4\,c2^2\,B1\,b1\,R1-4\,c2^2\,B1\,b1\,R2-4\,C1^2\,B1\,b1\,R2+4\,C1\,B1^2\,b1\,R3$$
$$+4\,C1^2\,B1\,b1\,R1-4\,C1\,B1^2\,b1\,R1+8\,C1^2\,B1^2\,b1\,c1-6\,R3\,B1\,C1\,R2$$
$$+6\,R3\,B1\,C1\,R1+6\,R1\,B1\,C1\,R2+16\,b1^2\,C2^2\,c1^2+4\,C1^2\,c1\,B1\,R2-4\,C1^2\,c1\,B1\,R1$$
$$-4\,C1\,c1\,B1^2\,R3+4\,C1\,c1\,B1^2\,R1+3\,c2^2\,R2^2+3\,c2^2\,R1^2-4\,C1\,B1\,b1^2\,R1$$
$$+4\,C1\,B1\,b1^2\,R3-24\,C1^2\,B1\,b1^2\,c1+24\,C1\,B1^2\,b1^2\,c1+4\,C1\,c1^2\,B1\,R2$$
$$+24\,C1^2\,c1^2\,B1\,b1-24\,C1\,c1^2\,B1^2\,b1-4\,C1\,c1^2\,B1\,R1-16\,c1\,R2\,C2^2\,b1$$
$$+16\,c1\,R1\,C2^2\,b1+4\,R3\,B1^2\,c1\,b1-4\,R1\,b1^2\,C2^2-4\,C2^2\,c2^2\,B1^2-4\,C2^2\,c2^2\,b1^2$$
$$+4\,R1\,B1\,R3\,b1+3\,R3^2\,B1^2-2\,C1\,R2\,R1\,b1-2\,C1\,R1\,R3\,b1+3\,R1^2\,B1^2$$
$$-40\,C2\,C1\,c1\,b1^2\,c2-56\,C2\,C1\,B1\,b1^2\,c2+20\,C2\,c1\,R2\,c2\,B1-4\,C2\,R1\,B1^2\,c2$$
$$-4\,C2\,c1\,R1\,c2\,b1-20\,C2\,c1\,R1\,c2\,B1+112\,C2\,C1\,c1\,B1\,c2\,b1-40\,C2\,C1\,c1\,B1^2\,c2$$
$$+8\,C2\,C1\,B1^2\,b1\,c2+32\,C2\,R1\,B1\,c2\,b1-8\,C2\,R3\,B1\,c2\,b1-4\,C2\,R1\,b1^2\,c2$$
$$-20\,C2\,C1\,R1\,c2\,b1-4\,C2\,C1\,R1\,c2\,B1+20\,C2\,C1\,R2\,c2\,b1+4\,C2\,C1\,R2\,c2\,B1$$
$$-4\,C2\,R3\,B1^2\,c2-2\,R3\,B1\,c1\,R1+8\,C2\,c1\,B1\,b1^2\,c2-56\,C2\,c1\,B1^2\,b1\,c2$$
$$+2\,C1\,R2\,R3\,b1-4\,R1\,b1^2\,c1\,B1+3\,C1^2\,R1^2+3\,C1^2\,R2^2+16\,C1\,c2^2\,R1\,B1$$
$$+32\,C1\,c2^2\,B1^2\,b1-16\,C1\,c2^2\,R2\,B1+16\,C1^2\,R1\,b1^2+16\,C1^2\,c2^2\,B1^2$$
$$+4\,c1\,B1\,b1^2\,R3+16\,c1^2\,R1\,B1^2+4\,c1^2\,B1\,b1\,R1+8\,c1^2\,B1\,b1^2\,C1$$
$$-16\,C1\,B1\,b1\,c1\,R1-8\,C1\,B1\,b1\,c1\,R2-32\,C1^2\,c2^2\,B1\,b1+16\,C2^2\,c1^2\,B1^2$$
$$-32\,b1\,C2^2\,c1^2\,B1+16\,C1^2\,b1^2\,c2^2-8\,C1\,c1\,B1\,R3\,b1-4\,C1\,c1\,b1^2\,R3$$
$$-4\,C1\,c1^2\,b1\,R1-4\,R1\,B1^2\,c2^2-4\,R1\,B1\,C2^2\,b1+24\,C2^2\,c2^2\,B1\,b1$$
$$+4\,C2\,c1\,R2\,c2\,b1-4\,C2\,R3\,b1^2\,c2)X3^2+(-8\,C1^2\,R1\,c2\,b1+8\,C1^2\,R2\,c2\,b1$$
$$-8\,C2^2\,R2\,c2\,b1+16\,c1\,R1\,B1^2\,c2+16\,C2^2\,c2\,B1^2\,c1-16\,C1^2\,B1\,b1^2\,c2$$
$$-16\,C2\,b1\,c2^2\,B1^2+16\,b1^2\,C1\,B1^2\,c2+32\,C2\,C1\,c2^2\,B1\,b1+16\,C2^2\,b1^2\,B1\,c2$$
$$-4\,C2\,R2^2\,c1-4\,C2\,R1^2\,c1+4\,C2\,R1^2\,b1+8\,R3\,B1^2\,C1\,c2-32\,C1\,c1\,B1^2\,b1\,c2$$
$$-4\,C2\,R1\,R3\,b1+4\,C2\,R2\,R3\,b1-4\,C2\,R2\,R1\,b1-4\,B1\,R1^2\,c2+4\,c2\,R2^2\,C1$$
$$-4\,R3\,B1\,c2\,R2+4\,R3\,B1\,c2\,R1+4\,c2\,R1^2\,C1-8\,C1\,c2\,B1^2\,R1+8\,C1^2\,c2\,B1\,R1$$
$$-8\,C1^2\,c2\,B1\,R2-16\,c1^2\,B1\,b1^2\,C2+8\,b1^2\,C2\,B1\,R1-8\,b1^2\,C2\,B1\,R3$$
$$+16\,b1\,C2\,B1\,c1\,R2+8\,R1\,b1^2\,C2\,c1-16\,b1\,C1\,B1\,c2\,R2-16\,b1^2\,C2\,B1^2\,c1$$

$$+8\,C2\,R1\,c1\,R2+8\,b1\,C2\,c1^2\,R2-8\,b1^2\,C2\,c1\,R3-8\,b1\,C2\,c1^2\,R1$$
$$+16\,b1^2\,C2\,c1^2\,C1+8\,R3\,B1^2\,c2\,b1-16\,c1\,R1\,c2\,B1\,b1-8\,R1\,C1\,c2\,R2$$
$$+4\,B1\,R1\,c2\,R2-8\,B1^2\,R1\,c2\,b1-8\,C2\,R3\,B1^2\,c1+8\,C2\,c2^2\,R2\,B1$$
$$-16\,C2\,b1^2\,C1\,c2^2+16\,C1\,c1\,B1\,b1^2\,c2+8\,C1\,R1\,b1^2\,c2+16\,b1^2\,C2^2\,c1\,c2$$
$$+8\,C2^2\,R1\,c2\,b1-32\,C2^2\,c1\,B1\,c2\,b1+16\,C2\,R3\,b1\,c1\,B1+16\,C2\,c1\,R1\,C1\,b1$$
$$-16\,C2\,c1\,R2\,C1\,b1+8\,C2\,c1^2\,R1\,B1-8\,C2\,c1^2\,R2\,B1-32\,C2\,C1\,c1^2\,b1\,B1$$
$$-16\,C2\,C1\,c2^2\,B1^2+16\,C2\,C1\,c1^2\,B1^2-16\,C2\,C1\,B1^2\,b1\,c1-8\,C2\,R1\,c2^2\,B1$$
$$+16\,C2\,c1^2\,B1^2\,b1-16\,C2\,R1\,b1^2\,C1+8\,C1\,b1^2\,R3\,c2+8\,C2\,C1\,R2\,c1\,B1$$
$$-16\,C2\,R1\,b1\,c1\,B1-8\,C2\,C1\,R1\,c1\,B1+32\,C2\,c1\,B1\,b1^2\,C1-8\,C2\,R1\,B1^2\,c1$$
$$+16\,C2\,R1\,B1\,C1\,b1-8\,C1\,c1\,R2\,c2\,b1+16\,C1\,c1\,R2\,c2\,B1-16\,C1^2\,c1\,B1^2\,c2$$
$$-16\,C1\,c1\,R1\,c2\,B1+8\,C1\,c1\,R1\,c2\,b1+32\,C1^2\,c1\,B1\,c2\,b1+16\,C1^2\,B1^2\,b1\,c2$$
$$-16\,C1^2\,c1\,b1^2\,c2+16\,C1\,R1\,B1\,c2\,b1-16\,C1\,R3\,B1\,c2\,b1)X3-2\,C2^2\,R1\,R2$$
$$-2\,R3^2\,B1\,b1+4\,c1^2\,B1^2\,b1^2+4\,b1^2\,C2^2\,B1^2-4\,b1\,C2^2\,B1\,R2+2\,R1^2\,B1\,c1$$
$$+4\,R1\,B1^2\,c1\,b1-2\,R1\,B1^2\,R3+4\,C1^2\,c1^2\,B1^2+C2^2\,R1^2+C2^2\,R2^2-2\,c2^2\,R2\,R1$$
$$-2\,R1^2\,B1\,b1+4\,C1^2\,B1^2\,b1^2-2\,C2\,R1^2\,c2+2\,R3\,B1\,c1\,R2+2\,C1\,R1^2\,b1$$
$$-2\,C1^2\,R1\,R2-2\,R1\,b1^2\,R3-2\,R1^2\,B1\,C1-4\,c1^2\,B1\,b1\,R2+4\,R1\,b1^2\,C1\,c1$$
$$-2\,C1\,R2^2\,c1+2\,R1\,b1\,c1\,R2-4\,C1^2\,R2\,c1\,b1+4\,c2^2\,B1^2\,b1^2-2\,R1\,B1\,c1\,R2$$
$$+4\,C1^2\,R1\,c1\,b1-2\,C1\,R1^2\,c1+4\,R1\,B1^2\,C2^2+4\,R1\,b1^2\,c2^2+4\,C2\,R1\,c2\,R2$$
$$-8\,b1^2\,C2\,B1^2\,c2+4\,C1\,c1^2\,b1\,R2+4\,C1^2\,c1^2\,b1^2+8\,b1\,C2\,B1\,c2\,R2-2\,c1^2\,R2\,R1$$
$$+c1^2\,R1^2+R3^2\,b1^2-2\,C2\,R2^2\,c2+c1^2\,R2^2-2\,c1\,R2\,R3\,b1-4\,c2^2\,B1\,b1\,R1$$
$$-4\,c2^2\,B1\,b1\,R2-4\,C1^2\,B1\,b1\,R2+4\,C1\,B1^2\,b1\,R3+4\,C1^2\,B1\,b1\,R1$$
$$-4\,C1\,B1^2\,b1\,R1-8\,C1^2\,B1^2\,b1\,c1-2\,R3\,B1\,C1\,R2+2\,R3\,B1\,C1\,R1+2\,R1\,B1\,C1\,R2$$
$$+2\,c1\,R1\,R3\,b1-4\,C1^2\,c1\,B1\,R1-4\,C1\,c1\,B1^2\,R3+4\,C1\,c1\,B1^2\,R1+c2^2\,R2^2$$
$$+c2^2\,R1^2+4\,C1\,B1\,b1^2\,R1-2\,R1^2\,b1\,c1+8\,C1^2\,B1\,b1^2\,c1-8\,C1\,B1^2\,b1^2\,c1$$
$$-4\,C1\,c1^2\,B1\,R2-8\,C1^2\,c1^2\,B1\,b1+8\,C1\,c1^2\,B1^2\,b1+4\,C1^2\,c1\,B1\,R2$$
$$+4\,C1\,R1\,c1\,R2-4\,R3\,B1^2\,c1\,b1+4\,R1\,b1^2\,C2^2+4\,C2^2\,c2^2\,B1^2+4\,C2^2\,c2^2\,b1^2$$
$$+4\,R1\,B1\,R3\,b1+R3^2\,B1^2-2\,C1\,R2\,R1\,b1-2\,C1\,R1\,R3\,b1+R1^2\,B1^2$$
$$+8\,C2\,C1\,c1\,b1^2\,c2+8\,C2\,C1\,B1\,b1^2\,c2-4\,C2\,c1\,R2\,c2\,B1-4\,C2\,R1\,B1^2\,c2$$
$$-4\,C2\,c1\,R1\,c2\,b1+4\,C2\,c1\,R1\,c2\,B1-16\,C2\,C1\,c1\,B1\,c2\,b1+8\,C2\,C1\,c1\,B1^2\,c2$$
$$-8\,C2\,C1\,B1^2\,b1\,c2+8\,C2\,R3\,B1\,c2\,b1-4\,C2\,R1\,b1^2\,c2+4\,C2\,C1\,R1\,c2\,b1$$
$$-4\,C2\,C1\,R1\,c2\,B1-4\,C2\,C1\,R2\,c2\,b1+4\,C2\,C1\,R2\,c2\,B1-4\,C2\,R3\,B1^2\,c2$$
$$-2\,R3\,B1\,c1\,R1-8\,C2\,c1\,B1\,b1^2\,c2+8\,C2\,c1\,B1^2\,b1\,c2+2\,C1\,R2\,R3\,b1$$
$$-4\,R1\,b1^2\,c1\,B1+C1^2\,R1^2+C1^2\,R2^2-4\,C1\,B1\,b1^2\,R3+4\,c1\,B1\,b1^2\,R3$$
$$+4\,c1^2\,B1\,b1\,R1-8\,c1^2\,B1\,b1^2\,C1-16\,C1\,B1\,b1\,c1\,R1+8\,C1\,B1\,b1\,c1\,R2+R1^2\,b1^2$$
$$+4\,C1\,c1^2\,B1\,R1+8\,C1\,c1\,B1\,R3\,b1-4\,C1\,c1\,b1^2\,R3-4\,C1\,c1^2\,b1\,R1+4\,R1\,B1^2\,c2^2$$
$$-4\,R1\,B1\,C2^2\,b1-8\,C2^2\,c2^2\,B1\,b1+4\,C2\,c1\,R2\,c2\,b1-4\,C2\,R3\,b1^2\,c2$$

```
> nops(UniCir);
```

694

```
> degree(UniCir,X3);
```

6

The univariate may be further simplified for platforms with three PR-type or three RP-type legs. It is obtained with the following substitutions in the general constraint manifold equation given by Hgen. HL indicates that at least one point in the moving plane moves on a line in the fixed plane...the L stands for Line, the H for constraint hyperbolic paraboloid. PR-type and RP-type platforms may be viewed as inversions. In this way, the same polynomial may be used to solve the FK of each, except the results for the type 3 platform will be in the moving platform reference frame, E. So, these results must be transformed back to the fixed frame, Sigma. Note that the constants are now: K0, A1, A2, B1, B2, B3, C1, C2, C3, b1, c1,c2. For both platforms, the point in the moving frame moves on a real degenerate circle (a line) in the fixed frame. Hence, K0=0 and the other uppercase constants are now planar line coordinates. Note that the K3 components are still K3=R-K0*(x^2+y^2), Hence, this coordinate is now the moment of the given line about the origin.

```
> HLa:=subs(K0=0,K1=A1,K2=A2,R=A3,x=0,y=0,x0=1, y3=X1,y2=-X2,x1=X3,H);
```

$$HLa := 4\,A2\,X1 - 4\,A1\,X1\,X3 - 4\,A2\,X3\,X2 - 4\,A1\,X2 + A3 + X3^2\,A3$$

```
> HLb:=subs(K0=0,K1=B1,K2=B2,R=B3,x=b1,y=0,x0=1 ,y3=X1,y2=-X2,x1=X3,H);
```

$$HLb := 4\,B2\,X1 - 4\,B1\,X1\,X3 - 4\,B2\,X3\,X2 + 2\,X3^2\,B1\,b1 - 2\,B1\,b1 - 4\,B1\,X2 - 4\,B2\,X3\,b1 + B3 + X3^2\,B3$$

```
> HLc:=subs(K0=0,K1=C1,K2=C2,R=C3,x=c1,y=c2,x0= 1,y3=X1,y2=-X2,x1=X3,H);
```

$$HLc := 4\,C2\,X1 - 4\,C1\,X1\,X3 - 4\,C2\,X3\,X2 + 2\,X3^2\,C2\,c2 + 2\,X3^2\,C1\,c1 - 2\,C2\,c2 - 2\,C1\,c1 - 4\,C1\,X2 + 4\,C1\,X3\,c2 - 4\,C2\,X3\,c1 + C3 + X3^2\,C3$$

```
> HLab:=HLa-HLb;
```

$$HLab := 4\,A2\,X1 - 4\,A1\,X1\,X3 - 4\,A2\,X3\,X2 - 4\,A1\,X2 + A3 + X3^2\,A3 - 4\,B2\,X1 + 4\,B1\,X1\,X3 + 4\,B2\,X3\,X2 - 2\,X3^2\,B1\,b1 + 2\,B1\,b1 + 4\,B1\,X2 + 4\,B2\,X3\,b1 - B3 - X3^2\,B3$$

```
> HLac:=HLa-HLc;
```

$$HLac := 4\,A2\,X1 - 4\,A1\,X1\,X3 - 4\,A2\,X3\,X2 - 4\,A1\,X2 + A3 + X3^2\,A3 - 4\,C2\,X1 + 4\,C1\,X1\,X3 + 4\,C2\,X3\,X2 - 2\,X3^2\,C2\,c2 - 2\,X3^2\,C1\,c1 + 2\,C2\,c2 + 2\,C1\,c1 + 4\,C1\,X2 - 4\,C1\,X3\,c2 + 4\,C2\,X3\,c1 - C3 - X3^2\,C3$$

```
> eqL1:=solve({HLab,HLac},{X1,X2}):
> eqL2:=subs(eqL1[1],eqL1[2],HLc):
> eqL3:=factor(eqL2);
```

$$eqL3 := -(-2\,A2\,X3^2\,C2\,c2\,B1 - 2\,A2\,X3^2\,C1\,c1\,B1 - A2\,X3^2\,C3\,B1 + A2\,X3^2\,C1\,B3 + 2\,B1\,A2\,C1\,c1 + 2\,B1\,A2\,C2\,c2 + 4\,B1\,A2\,C2\,X3\,c1 - 2\,B1\,b1\,C1\,A2 - B1\,C3\,A2 - A3\,C1\,X3^2\,B2 - A3\,C1\,B2 + A3\,X3^2\,C2\,B1 + 4\,A1\,B2\,C2\,X3\,b1 + A3\,C2\,B1 - 2\,A1\,b1\,X3^2\,C2\,B1 + 2\,A1\,X3^2\,C1\,c1\,B2 + 2\,A1\,b1\,C2\,B1 + 2\,A1\,X3^2\,C2\,c2\,B2 + 4\,A1\,B2\,C1\,X3\,c2 + A1\,X3^2\,C3\,B2 - A1\,C2\,X3^2\,B3 + A1\,C3\,B2 - 2\,A1\,B2\,C2\,c2 - 2\,A1\,B2\,C1\,c1 - 4\,A1\,B2\,C2\,X3\,c1 - A1\,C2\,B3 + 2\,A2\,X3^2\,b1\,C1\,B1 + B3\,C1\,A2 - 4\,B2\,X3\,b1\,C1\,A2 - 4\,B1\,A2\,C1\,X3\,c2)/(A2\,B1 - C1\,A2 - A1\,B2 - C2\,B1 + C1\,B2 + C2\,A1)$$

```
> UniLine:=op(2,eqL3);
```

$$UniLine := -2\,A2\,X3^2\,C2\,c2\,B1 - 2\,A2\,X3^2\,C1\,c1\,B1 - A2\,X3^2\,C3\,B1 + A2\,X3^2\,C1\,B3 + 2\,B1\,A2\,C1\,c1 + 2\,B1\,A2\,C2\,c2 + 4\,B1\,A2\,C2\,X3\,c1 - 2\,B1\,b1\,C1\,A2 - B1\,C3\,A2 - A3\,C1\,X3^2\,B2 - A3\,C1\,B2 + A3\,X3^2\,C2\,B1 + 4\,A1\,B2\,C2\,X3\,b1 + A3\,C2\,B1 - 2\,A1\,b1\,X3^2\,C2\,B1 + 2\,A1\,X3^2\,C1\,c1\,B2 + 2\,A1\,b1\,C2\,B1 + 2\,A1\,X3^2\,C2\,c2\,B2 + 4\,A1\,B2\,C1\,X3\,c2 + A1\,X3^2\,C3\,B2 - A1\,C2\,X3^2\,B3 + A1\,C3\,B2 - 2\,A1\,B2\,C2\,c2 - 2\,A1\,B2\,C1\,c1 - 4\,A1\,B2\,C2\,X3\,c1 - A1\,C2\,B3 + 2\,A2\,X3^2\,b1\,C1\,B1 + B3\,C1\,A2 - 4\,B2\,X3\,b1\,C1\,A2 - 4\,B1\,A2\,C1\,X3\,c2$$

```
> nops(UniLine);
```

30

```
> degree(UniLine,[X3]);
```

2

```
> UniLine1:=collect(UniLine,[X3]):
> UniLine2:=sort(UniLine1,[X3]);
```

$$UniLine2 := (-2\,B1\,A2\,C2\,c2 - 2\,B1\,A2\,C1\,c1 - B1\,C3\,A2 + B3\,C1\,A2 - A3\,C1\,B2 + A3\,C2\,B1 - 2\,A1\,b1\,C2\,B1 + 2\,A1\,B2\,C1\,c1 + 2\,A1\,B2\,C2\,c2 + A1\,C3\,B2 - A1\,C2\,B3 + 2\,B1\,b1\,C1\,A2)X3^2 + (-4\,B2\,b1\,C1\,A2 + 4\,B1\,A2\,C2\,c1 + 4\,A1\,B2\,C1\,c2 - 4\,A1\,B2\,C2\,c1 - 4\,B1\,A2\,C1\,c2 + 4\,A1\,B2\,C2\,b1)X3 + A3\,C2\,B1 + B3\,C1\,A2 - A3\,C1\,B2 + 2\,A1\,b1\,C2\,B1 + 2\,B1\,A2\,C1\,c1 + 2\,B1\,A2\,C2\,c2 - 2\,B1\,b1\,C1\,A2 - B1\,C3\,A2 - 2\,A1\,B2\,C2\,c2 - 2\,A1\,B2\,C1\,c1 - A1\,C2\,B3 + A1\,C3\,B2$$

REFERENCES

[1] Abhyankar, S.S., 1990, *Algebraic Geometry for Scientists and Engineers*, American Mathematical Society, Mathematical Surveys and Monographs, Vol. 35.

[2] Adams, W., Loustaunau, P., 1994, *An Introduction to Gröbner Bases*, American Mathematical Society, Graduate Studies in Mathematics, Vol. 3.

[3] Agrawal, S.K., Pandravada, R., 1992, "Inverse Kinematic Solutions of a Rolling Disk Between Two Planar Manipulators", *Robotics, Spatial Mechanisms, and Mechanical Systems, ASME*, DE-vol. 45, pp. 473-478.

[4] Agrawal, S.K., Pandravada, R., 1993, "Kinematics and Workspace of a Rolling Disk Between Planar Manipulators", *Proc. Am. Control Conf.*, San Francisco, Cal., U.S.A., pp. 741-745.

[5] Akivis, M.A., Rosenfeld, B.A., 1993, *Élie Cartan (1869-1951)*, American Mathematical Society, Translations of Mathematical Monographs, Vol. 123.

[6] Angeles, J., 1982, *Spatial Kinematic Chains: Analysis, Synthesis, Optimization*, Springer-Verlag, New York, N.Y., U.S.A..

[7] Angeles, J., 1988, *Rational Kinematics*, Springer Tracts in Natural Philosophy, Springer-Verlag, New York, N.Y., U.S.A..

[8] Angeles, J., 1997, *Fundamentals of Robotic Mechanical Systems: Theory, Methods, and Algorithms*, Springer-Verlag, New York, N.Y., U.S.A..

[9] Anton, H., 1987, *Elementary Linear Algebra, 5th Ed.*, Wiley, New York, N.Y., U.S.A..

[10] Arnold, V.I., 1989, *Mathematics Methods of Classical Mechanics*, 2nd ed., translated from original 1974 Russian edition by K. Vogtmann and A. Weinstein, Springer-Verlag, New York, N.Y., U.S.A..

[11] Ayres, F., 1967, *Projective Geometry*, Schaum's Outline Series in Mathematics, McGraw-Hill Book Company, New York, N.Y., U.S.A..

[12] Becker, T., Weispfenning, V., 1993, *A Computational Approach to Commutative Algebra*, Graduate Texts In Mathematics, Springer-Verlag, Berlin, Germany.

[13] Biggs, N.L., 1989, *Discrete Mathematics*, revised edition, Clarendon Press, Oxford, England.

[14] Blaschke, W., 1911, "Euklidische Kinematik und nichteuklidische Geometrie", *Zeitschr. Math. Phys.*, Vol. 60, pp. 61-91 and 203-204:

[15] Blaschke, W., 1960, *Kinematik und Quaternionen*, Deutscher Verlag der Wissenschaften, Berlin, Germany.

[16] Borel, E., 1908, "Mémoire sur les désplacements à trajectoires sphériques", *Mém. présentés par divers savantes*, Vol. 33. No. 1, pp.1-128, Paris, France.

[17] Bottema, O., Roth, B., 1990, *Theoretical Kinematics*, Dover Publications, Inc., New York, N.Y., U.S.A..

[18] Bricard, R., 1906, "Mémoire sur les désplacements à trajectoires sphériques", *Journal de l'Ecole Polytechnique*, Vol. 11, pp. 1-96.

[19] Bumcrot, R.J., 1969, *Modern Projective Geometry*, Holt, Rinehart & Winston, Inc., New York, N.Y., U.S.A..

[20] Cauchy, A., 1813, " Deuxième Mémoire sur les Polygones et les Polyèdres", *Journal de l'Ecole Polytechnique*, XVIeme cahier, pp. 87-98.

[21] Cayley, A., 1859, "A Sixth Memoir Upon Quantics", *Philosophical Transactions of the Royal Society of London*, Vol. 155, pp. 725-791.

[22] Chari, V., Pressley, A., 1994, *A Guide to Quantum Groups*, Cambridge University Press, London, England.

[23] Chen, W., Kumar, V., 1995, "Workspace of Planar Cooperating Robots with Rolling Contacts", *Advanced Robotics*, The Int'l J. of the Robotics Soc. of Japan, Vol. 9, No. 5, pp. 483-504.

[24] Clark, A., 1971, *Elements of Abstract Algebra*, Dover Publications, Inc., New York, N.Y., U.S.A..

[25] Cole, A., Hauser, J., Sastry, S., 1988, "Kinematics and Control of Multifingered Hands with Rolling Contact", *Proc. of IEEE Int. Conf. Rob. Aut.*, pp. 228-233.

[26] Collins, C.L., McCarthy, J.M., 1998, "The Quartic Singularity Surface of Planar Platforms in the Clifford Algebra of the Projective Plane", *Mech. Mach. Theory*, Vol. 33, No. 7, pp. 931-944.

[27] Cox, D., Little, J., O'Shea, D., 1997, *Ideals, Varieties, and Algorithms: an Introduction to Computational Algebraic Geometry and Commutative Algebra*, second edition, Springer-Verlag, Berlin, Germany.

[28] Coxeter, H.S.M., 1954, *The Real Projective Plane*, second edition, Cambridge at the University Press, Cambridge, England.

[29] Coxeter, H.S.M., 1965, *Non-Euclidean Geometry*, fifth edition, University of Toronto Press, Toronto, On., Canada.

[30] Coxeter, H.S.M., 1969, *Introduction to Geometry*, second edition, John Wiley & Sons, Inc., Toronto, On., Canada.

[31] Coxeter, H.S.M., 1974, *Projective Geometry*, second edition, University of Toronto Press, Toronto, On., Canada.

[32] Coxeter, H.S.M., Moser, W.O.J., 1980, *Generators and Relations for Discrete Groups*, fourth edition, Springer-Verlag, Berlin, Germany.

[33] Craig, J.J., 1989, *Introduction to Robotics, Mechanics and Control*, second edition, Addison-Wesley Publishing Co., Reading, Mass., U.S.A..

[34] Daniali, H.R.M., 1995, *Contributions to the Kinematic Synthesis of Parallel Manipulators*, Ph.D. thesis, Dept. of Mech. Eng., McGill University, Montréal, Qc., Canada.

[35] Daniali, H.R.M., Zsombor-Murray, P.J., 1999, *Singularity Detection in Planar 3-Legged RRR Platforms*, private communication.

[36] De Sa, S., 1979, *Classification and Properties of Planar Motion Using Kinematic Mappings*, Dissertation, Stanford University, Stanford, Ca., U.S.A..

[37] De Sa, S., Roth, B., 1981, "Kinematic Mappings. Part 1: Classification of Algebraic Motions in the Plane", *ASME, J. of Mech. Design*, Vol. 103, pp. 585-591.

[38] De Sa, S., Roth, B., 1981, "Kinematic Mappings. Part 2: Rational Algebraic Motions in the Plane", *ASME, J. of Mech. Design*, Vol. 103, pp. 712-717.

[39] Denavit, J., Hartenberg, R.S., 1955, "A Kinematic Notation for Lower-Pair Mechanisms Based on Matrices", *J. of Applied Mechanics*, pp. 215-221.

[40] Dietmaier, P., 1998, "The Stewart-Gough Platform of General Geometry can Have 40 Real Postures", *Recent Advances in Robotic Kinematics*, eds. Lenarčič, Husty, M.L., Kluwer Academic Publishers, Dordrecht, The Netherlands, pp. 7-16..

[41] Dolciani, P., Berman, S., Wooton, W., 1963, *Modern Algebra and Trigonometry*, Thomas Nelson & Sons (Canada) Ltd., Don Mills, On., Canada.

[42] Fekete, A.E., 1985, *Real Linear Algebra*, Marcel Dekker, Inc., New York, N.Y., U.S.A..

[43] Fichter, E.F., 1988, "A Stewart Platform-Based Manipulator: General Theory and Practical Construction", *J. Robotics Research*, Vol. 5, No. 3, pp. 354-360.

[44] Fishback, W. T., 1969, *Projective and Euclidean Geometry*, John Wiley & Sons, Inc., New York, N.Y., U.S.A..

[45] Gans, D., 1969, *Transformations and Geometries*, Appelton-Century-Crofts, New York, N.Y., U.S.A..

[46] Gans, D., 1973, *An Introduction to Non-Euclidean Geometry*, Academic Press, New York, N.Y., U.S.A..

[47] Gemignani, M.C., 1990, *Elementary Topology*, second edition, Dover Publications, Inc., New York, N.Y., U.S.A..

[48] Ginsberg, J.H., 1988, *Advanced Engineering Dynamics*, Harper & Row, Publishers, New York, N.Y., U.S.A..

[49] Gosselin, C., 1988, *Kinematic Analysis, Optimization and Programming of Parallel Robotic Manipulators*, Ph.D. thesis, Dept. of Mech. Eng., McGill University, Montréal, Qc., Canada.

[50] Gosselin, C., Sefrioui, J., 1991, " Polynomial Solutions For the Direct Kinematic Problem of Planar Three-Degree-of Freedom Parallel Manipulators", *Proc. 5th Int. Conf. on Adv. Rob. (ICAR)*, Pisa, Italy, pp. 1124-1129.

[51] Gosselin, C., Sefrioui, J., Richard, M., 1992, "On The Direct Kinematics of General Spherical Three-Degree-of-Freedom Parallel Manipulators", *Robotics, Spatial Mechanisms, and Mechanical Systems, ASME*, DE-vol. 45, pp. 7-11.

[52] Gosselin, C., Lavadière, S., Côté, J., 1992, "SIMPA: A Graphic Simulator for the CAD of Parallel Manipulators", *Proc. of the ASME Comp. and Eng. Conf.*, Vol. 1, San Francisco, Ca., U.S.A., pp. 465-471.

[53] Gough, V.E., 1956, "Discussion in London: Automobile Stability, Control, and Tyre Performance", *Proc. Automobile Division, Institution of Mech. Engrs.*, pp. 392-394.

[54] Grassmann, H., 1844, *A New Branch of Mathematics*, English translation 1995 by Kannenberg, L. C., Open Court, Chicage, Ill., U.S.A..

[55] Griffis, M.W., Duffy, J., 1993 (Jan. 12), *Method and Apparatus for Controlling Geometrically Simple Parallel Mechanisms with Distinctive Connections*, United States Patent, Patent Number 5,179,525.

[56] Guggenheimer, H.W., 1977, *Differential Geometry*, Dover Publications, Inc., New York, N.Y., U.S.A..

[57] Grünwald, J., 1911, "Ein Abbildungsprinzip, welches die ebene Geometrie und Kinematik mit der räumlichen Geometrie verknüpft", *Sitzber. Ak. Wiss. Wien*, Vol. 120, pp. 677-741.

[58] Haaser, N.B., Sullivan, J.A., 1990, *Real Analysis*, Dover Publications, Inc., New York, N.Y., U.S.A..

[59] Harris, J., 1992, *Algebraic Geometry*, Graduate Texts In Mathematics, Springer-Verlag, Berlin, Germany.

[60] Harms, E., Kounias, S., Vroomen, L., Zsombor-Murray, P., 1991, "A Binary-Decision/Transputer Network For The Control of a Planar Three Drgree of Freedom Parallel Robotic Manipulator", *Microprocessing and Microprogramming, North-Holland*, pp 137-142.

[61] Hartenberg, R.S., Denavit, J., 1964, *Kinematic Synthesis of Linkages*, McGraw-Hill, Book Co., New York, N.Y., U.S.A..

[62] Hartmann, D., 1995, *Singular Stewart-Gough Platforms*, M.Eng. thesis, Dep't. of Mech. Eng., McGill University, Montréal, Qc., Canada.

[63] Hayes, M.J.D., Zsombor-Murray, P., 1996, "A Planar Parallel Manipulator with Holonomic Higher Pairs: Inverse Kinematics", *Proc. CSME Forum 1996, Symposium on the Theory of Machines and Mechanisms*, Hamilton, On., Canada., pp. 109-116.

[64] Hayes, M.J.D., Zsombor-Murray, P., 1996, "Kinematic Mapping of 3-legged Planar Platforms With Holonomic Higher Pairs ", *Recent Advances in Robotic Kinematics*, eds. Lenarčič, J., Parenti-Castelli, V., Kluwer Academic Publishers, Dordrecht, The Netherlands, pp. 421-430.

[65] Hayes, M.J.D., 1996, *Kinematic Analysis of Planar Parallel Platforms With Holonomic Higher Pairs*, M.Eng. thesis, Dep't. of Mech. Eng., McGill University, Montréal, Qc., Canada.

[66] Hayes, M.J.D., Husty, M.L., Zsombor-Murray, P., 1997, "Solving the Forward Kinematics of a Planar 3-legged Platform With Holonomic Higher Pairs", *Computational Methods in Mechanisms*, eds. Angeles, J., Zakhariev, E., NATO Advanced Study Institute, Vol. 2, pp. 525-534.

[67] Hayes, M.J.D., Zsombor-Murray, P., 1998, "Inverse Kinematics of a Planar Manipulator with Holonomic Higher Pairs", *Recent Advances in Robotic Kinematics*, eds. Lenarčič, Husty, M.L., Kluwer Academic Publishers, Dordrecht, The Netherlands, pp. 59-68.

[68] Hayes, M.J.D., Parsa, K., Angeles, J., 1999, "The Effect of Data-Set Cardinality on the Design and Structural Errors of Four-Bar Function-Generators", *Proceedings of the Tenth World Congress on the Theory of Machines and Mechanisms*, Oulu, Finland, pp. 437-442.

[69] Hayes, M.J.D., Husty, M.L., Zsombor-Murray, P.J., 1999, "Kinematic Mapping of Planar Stewart-Gough Platforms", *Proc. 17th Canadian Congress of Applied Mechanics (CANCAM 1999)*, Hamilton, On., Canada, pp. 319-320.

[70] Hayes, M.J.D., Husty, M.L., Zsombor-Murray, P., 1999, "Solving the Forward Kinematics of a Planar 3-legged Platform With Holonomic Higher Pairs", *ASME Journal of Mechanical Design*, Vol. 121, No. 2, pp. 212-219.

[71] Hilbert, D., Cohn-Vossen, S., 1952, *Geometry and The Imagination*, English translation by Nemenyi, P., of *Anschauliche Geometrie*, 1932, Chelsea Publishing Company, New York, N.Y., U.S.A..

[72] Hilbert, D., 1959, *The Foundations of Geometry*, English translation by E.J. Townsend of *Grundlagen der Geometrie, 2d. ed.*, 1902, Open Court, La Salle, Ill., U.S.A..

[73] Hilbert, D., 1993, *Theory of Algebraic Invariants*, Cambridge University Press, Cambridge, England.

[74] Hui, R., Goldenberg, A.A., 1989, "Formulation of the Hybrid Control Architecture Using the Constrained Manipulator Model-Application to Rolling Manipulation of a Rigid Object Using a Dextrous Robotic Hand", *Second*

Workshop on Military Robotic Applications, Kingston, On., Canada, pp. 316-323.

[75] Hunt, K.H., 1978, *Kinematic Geometry of Mechanisms*, Clarendon Press, Oxford, England.

[76] Hunt, K.H., 1983, "Structural Kinematics of In-Parallel-Actuated Robot Arms", *ASME J. of Mech., Trans. and Automation in Design*, Vol. 105, No. 4, pp. 705-712.

[77] Hunt, K.H., Primrose, E.J.F., 1993, "Assembly Configurations of Some In-Parallel-Actuated Manipulators", *Mech. Mach. Theory*, Vol. 28, No. 1, pp. 31-42.

[78] Husty, M., Zsombor-Murray, P., 1994, "A Special Type of Singular Stewart-Gough Platform", *Advances in Robot Kinematics and Computational Geometry*, eds. Lenarčič, J. and Ravani, B., Kluwer Academic Publishers, Dordrecht, The Netherlands, pp. 449-458.

[79] Husty, M.L., 1995, "Kinematic Mapping of Planar Three-Legged Platforms", Proc. *15th Canadian Congress of Applied Mechanics (CANCAM 1995)*, Victoria, B.C., Canada, Vol. 2, pp. 876-877.

[80] Husty, M.L., 1996, "On The Workspace of Planar Three-legged Platforms", *Proc. World Automation Conf., 6th Int. Symposium on Rob. and Manuf. (ISRAM 1996)*, Montpellier, France, Vol. 3, pp. 339-344.

[81] Husty, M.L., 1996b, "An Algorithm for Solving the Direct Kinematics of General Stewart-Gough Platforms", *Mechanism and Machine Theory*, Vol. 31, No. 4, pp. 365-379.

[82] Husty, M.L., 1996c (September 23, 1996), *Knee Joint Positions Expressed Relative to Associated Pinion Involutes*, private communication.

[83] Husty, M.L., Karger, A., Sachs, H., Steinhilper, W., 1997, *Kinematik und Robotik*, Springer-Verlag, Berlin, Germany.

[84] Husty, M.L., 1998a (August 20, 1998), *Vorwärtkinematik einer 3-RPR Platform*, private communication.

[85] Husty, M.L., 1999 (May 19, 1999), *A Patented Flight Simulator that is Singular in Every Assembly Configuration*, private communication.

[86] Jacobsen, S.C., 1975, "1-Oz 'Rope Ladder' Actuator Pulls 60-Lb Loads", News Report in *Electro Mechanical Design*, Vol. 19, No. 5.

[87] Jessop, C.M., 1903, *A Treatise on the Line Complex*, Cambridge University Press, also 1969, Chelsea, New York, N.Y., U.S.A..

[88] Karger, A., Husty, M.L., 1996, "On Self Motions of a Class of Parallel Manipulators", *Recent Advances in Robotic Kinematics*, eds. Lenarčič, J., Parenti-Castelli, V., Kluwer Academic Publishers, Dordrecht, The Netherlands, pp. 339-348.

[89] Klein, F., 1872, *Vergleichende Betrachiungen über neuere geometrische Forschungen*, Erlangen, reprinted in 1893, *Mathematische Annalen*, Vol. 43, pp. 63-100.

[90] Klein, F., 1939, *Elementary Mathematics from an Advanced Standpoint: Geometry*, Dover Publications, Inc., New York, N.Y., U.S.A..

[91] Kreyszig, E., 1964, *Differential Geometry*, University of Toronto Press, Toronto, On., Canada.

[92] Kumar, V., 1992, "Characterization of Workspaces of Parallel Manipulators", *ASME Journal of Mechanical Design*, Vol. 114, pp. 368-375.

[93] Lenarčič, J., 1998, " The Self Motion of an Anthropomorphic Manipulator", *Recent Advances in Robotic Kinematics*, eds. Lenarčič, Husty, M.L., Kluwer Academic Publishers, Dordrecht, The Netherlands, pp. 571-578.

[94] Ma, O., Angeles, J., 1992, "Architecture Singularities of Parallel Manipulators", *The Int. J. of Robotics and Automation*, Vol. 7, No. 1, pp. 23-29.

[95] McCarthy, J.M., 1990, *An Introduction to Theoretical Kinematics*, The M.I.T. Press, Cambridge, Mass., U.S.A..

[96] Merlet, J-P., 1989, "Singular Configurations of Parallel Manipulators and Grassmann Geometry", *The Int. J. of Robotics Research*, Vol. 8, No. 5, pp. 45-56.

[97] Merlet, J-P., 1990, *Les Robots Parallèles*, Hermès Publishers, Paris, France.

[98] Merlet, J-P., Mouly, N., 1994, *Espaces de Travail et Planification de Trajectoire des Robots Parallèles Plans*, Research Report 2291, Inst. Nat. de Rech. en Inf. et en Auto, France.

[99] Merlet, J-P., 1995, "Espace: Espace de Travail de Robot Parallèlle Plan", http://www-sop.inria.fr/saga/logiciels/RP/catalogue_eng.html, Inst. Nat. de Rech. en Inf. et en Auto, France.

[100] Merlet, J-P., 1996, "Direct Kinematics of Planar Parallel Manipulators", *IEEE Int. Conf. on Robotics and Automation*, Minneapolis, U.S.A., pp. 3744-3749.

[101] Merlet, J-P., 1998, "Determination of the Presence of Singularities in 6-D Workspace of a Gough Parallel Manipulator", *Advances in Robot Kinematics: Analysis and Control*, eds. Lenarčič, J., Husty, M.L., Kluwer Academic Publishers, Dordrecht, The Netherlands, pp. 39-48.

[102] Merlet, J-P., 1999, *Parallel Manipulators: State of the Art and Perspectives*, http://www-sop.inria.fr/saga/personnel/merlet/merlet.html, Inst. Nat. de Rech. en Inf. et en Auto, France.

[103] Minkowski, H., 1909, "Space and Time", *Bulletin of the Calcutta Mathematical Society*, Vol. 1, pp. 135-141.

[104] Mimura, N., Funahashi, Y., 1992, "Kinematics of Planar Multifingered Robot Hand with Displacement of Contact Points", *JSME International Journal*, Series 3, Vol. 35, No. 3, pp. 462-469.

[105] Mohamed, M.G., Duffy, J., 1985, "A Direct Determination of the Instantaneous Kinematics of Fully-Parallel Robot Manipulators, *Trans. of the ASME, J. of Mechanisms, Transmissions, and Automation in Design*, Vol. 207, pp. 226-229.

[106] Morgan, A., 1987, *Solving Polynomial Systems Using Continuation for Engineering and Scientific Problems*, Prentice-Hall, Inc., Englewood Cliffs, N.J., U.S.A..

[107] Murray, A.P., Pierrot, F., 1998, "N-Position Synthesis of Parallel Planar RPR Platforms", *Advances in Robot Kinematics: Analysis and Control*, eds. Lenarčič, J., Husty, M.L., Kluwer Academic Publishers, Dordrecht, The Netherlands, pp. 69-78.

[108] Nielsen, J., Roth, B., 1996, "The Direct Kinematics of the General 6-5 Stewart-Gough Mechanism", *Recent Advances in Robotic Kinematics*, eds. Lenarčič, J., Parenti-Castelli, V., Kluwer Academic Publishers, Dordrecht, The Netherlands, pp. 7-16.

[109] O'Neill, B., 1966, *Elementary Differential Geometry*, Academic Press, Inc., Boston, Mass., U.S.A..

[110] Paul, B., 1979, *Kinematics and Dynamics of Planar Machinery*, Prentice-Hall, Inc., N.J., U.S.A..

[111] Pennock, G.R., Kassner, D.J., 1992, "Kinematic Analysis of a Planar Eight-Bar Linkage: Application to a Platform-Type Robot", *ASME, J. of Mech. Des.*, Vol. 114, No. 1, pp. 87-95.

[112] Pennock, G.R., Kassner, D.J., 1993, "The Workspace of a General Geometry Planar Three-Degree-of-Freedom Platform-Type Manipulator", *ASME, J. of Mech. Des.*, Vol. 115, pp. 269-276.

[113] Peysah, E.E., "Determination of the Position of the Member of Three-Joint and Two-Joint Four Member Assur Groups with Rotational Pairs" (in Russian), *Maschinowedenie*, No. 5, pp. 55-61, 1985.

[114] Pierrot, F., Dauchez, P., Fournier, A., 1991, "Towards a Fully-Parallel 6 D.O.F. Robot for High Speed Applications", *IEEE Int. Conf. on Robotics and Automation*, Sacramento, CA, U.S.A., pp. 1288-1293.

[115] Plücker, J., 1830, "Über ein neues Coordinatensystem", *Journal für die reine und angewandte Mathematik (Crelle's Journal)*, 1830, Vol. 5, pp. 1-36.

[116] Plücker, J., 1865, "On a New Geometry of Space", *Philosophical Transactions of the Royal Society of London*, Vol. 155, pp. 725-791.

[117] Plücker, J., 1868, *Neue Geometrie des Raumes, gegründet auf die Betrachtung der geraden Linie als Raumelement*, Vol. 1, Teubner, Leipzig, Germany.

[118] Plücker, J., 1869, *Neue Geometrie des Raumes, gegründet auf die Betrachtung der geraden Linie als Raumelement*, Vol. 2, Teubner, Leipzig, Germany.

[119] Ravani, B., 1982, *Kinematic Mappings as Applied to Motion Approximation and Mechanism Synthesis*, Dissertation, Stanford University, Stanford, Ca., U.S.A..

[120] Ravani, B., Roth, B., 1983, "Motion Synthesis Using Kinematic Mappings", ASME, *J. of Mechanisms, Transmissions, & Automation in Design*, Vol. 105, pp. 460-467.

[121] Ravani, B., Roth, B., 1984, "Mappings of Spatial Kinematics", ASME, *J. of Mechanisms, Transmissions, & Automation in Design*, Vol. 106, pp. 341-347.

[122] Rooney, J., Earle, C.F., 1983, "Manipulator Postures and Kinematics Assembly Configurations", *6th World Congress on Theory of Machines and Mechanisms*, New Delhi, pp. 1014-1020.

[123] Roth, B., 1993, "Computations in Kinematics", in *Computational Kinematics*, eds. Angeles, J., Hommel, G., Kovács, P., Kluwer Academic Publishers, Dordrecht, The Netherlands, pp. 3-14.

[124] Roth, B., 1994, "Computational Advances in Robot Kinematics", in *Advances in Robot Kinematics and Computational Geometry*, eds. Lenarčič, J. and Ravani, B., Kluwer Academic Publishers, Dordrecht, The Netherlands, pp. 7-16.

[125] Royer, L., Bidard, C., Androit, C., 1998, " Determination of Singularities and Self Motion of a 7-DOF Anthropomorphic Manipulator", *Recent Advances in Robotic Kinematics*, eds. Lenarčič, Husty, M.L., Kluwer Academic Publishers, Dordrecht, The Netherlands, pp. 533-542.

[126] Sachs, H., et. al., 1993, *Comett II, Modul II: Linengeometrie*, Manuscript, Graz, Austria.

[127] Saha, S.K., Angeles, J., 1989, "Kinematics and Dynamics of 3-wheeled 2-DOF AGV", *Proc. of IEEE Int. Conf. Rob. Aut*, Scottsdale, Ariz., pp. 1572-1577.

[128] Salisbury, J.K., Roth, B., 1983, "Kinematic and Force Analysis of Articulated Mechanical Hands", *J. of Mech., Trans., and Aut. in Design, ASME*, Vol. 105, pp. 35-41.

[129] Salmon, G., 1879, *A Treatise on Conic Sections*, sixth edition, Longmans, Green, and Co., London, England.

[130] Salmon, G., 1885, *Lessons Introductory to the Modern Higher Algebra*, fourth edition, Hodges, Foster, and Figgis, Dublin, Rep. of Ireland.

[131] Sefrioui, J., Gosselin, C.M., 1992, "Singularity Analysis and Representation of Planar Parallel Manipulators", *Robotics and Autonomous Systems*, Vol. 10, pp. 209-224.

[132] Sefrioui, J., Gosselin, C.M., 1995, "On the Quadric Nature of the Singularity Curves of Planar Three-Degree-of-Freedom Parallel Manipulators", *Mech. Mach. Theory*, Vol. 30, No. 4, pp. 533-551.

[133] Shirkhodaie, A.H., Soni, A.H., 1987, "Forward and Inverse Synthesis for a Robot with Three Degrees of Freedom", *19th Summer Computation Simulation Conference*, Montréal, Qué, Canada, pp. 851-856.

[134] Sommerville, D.M.Y., 1910, "Classification of Geometries with Projective Metrics", *Proceedings of the Edinburgh Mathematical Society*, Vol. 28, pp. 25-41.

[135] Sommerville, D.M.Y., 1914, *The Elements of Non-Euclidean Geometry*, G. Bell and Sons, Ltd., London, England.

[136] Sommerville, D.M.Y., 1934, *Analytical Geometry of Three Dimensions*, Cambridge University Press, London, England.

[137] Stewart, D., 1965, "A Platform With Six Degrees of Freedom", *Proc. Instn. Mech. Engr.*, Vol. 180, Part 1, No. 15, pp. 371-378.

[138] Study, E., 1903,*Geometrie der Dynamen*, Teubner Verlag, Leipzig, Germany.

[139] Study, E., 1912, "Grundlagen und Ziele der analytischen Kinematik", *Sitzungsberichte der Berliner Mathematischen Gesellschaft*, 104, Sitzung, 21, Dec. 1912, pp. 36-60.

[140] Tarnai, T., Makai, E., 1989, "A Movable Pair of Tetrahedra", *Proc. Royal Society of London*, Vol. A423, pp. 423-442.

[141] Waldron, K.J., Hunt, K.H., 1991, "Series-Parallel Dualities in Actively Coordinated Mechanisms", *The Int. J. of Robotics Research*, Vol. 10, No. 2, pp. 473-480.

[142] Wohlhart, K., 1992, "Direct Kinematic Solution of the General Planar Stewart Platform", *Proc. of the Int. Conf. on Computer Integrated Manufacturing*, Zakopane, Poland, pp. 403-411.

[143] Yaglom, I.M., 1968, *Complex Numbers in Geometry* (translated by E.J.F. Primrose), Academic Press, New York, N.Y., U.S.A..

[144] Yaglom, I.M., 1988, *Felix Klein and Sophus Lie, Evolution of the Idea of Symmetry in the Nineteenth Century* (translated by Sergei Sossinsky), Birkhäuser, Boston, Mass., U.S.A..

[145] Yun, X., Kumar, V., Sarkar, N., Paljug, E., 1992, "Control of Multiple Arms with Rolling Constraints", *Proc. of IEEE Int. Conf. Rob. Aut.*, Nice, France, pp. 2193-2198.

[146] Zamanov, V.B., Sotirov, Z.M., 1991, "A Contribution to the Serial and Parallel Manipulator Duality", 8^{th} *World Congress on the Theory of Machines and Mechanisms*, Prague, pp. 517-520.

[147] Zsombor-Murray, P.J., Hyder, A., 1992, "An Equilateral Tetrahedral Mechanism", *Robotics and Autonomous Systems*, pp. 227-236.

[148] Zsombor-Murrary, P.J., Husty, M.L., 1994, "Engineering Graphics, Computational Geometry and Geometric Thinking", *Proc of ASEE Annual Conf.*, Edmonton, Canada, Vol. 1, pp. 437-443.

[149] Zsombor-Murrary, P.J., 1996, "Points, Planes and Lines", *ASEE/EDG J.*, Vol. 60, No. 2, pp. 5-14.

[150] Zsombor-Murrary, P.J., Hayes, M.J.D., 1999, "Grassmannian Reduction of Quadratic Forms", *Proc. 17th Canadian Congress of Applied Mechanics (CANCAM 1999)*, Hamilton, On., Canada, pp. 313-314.